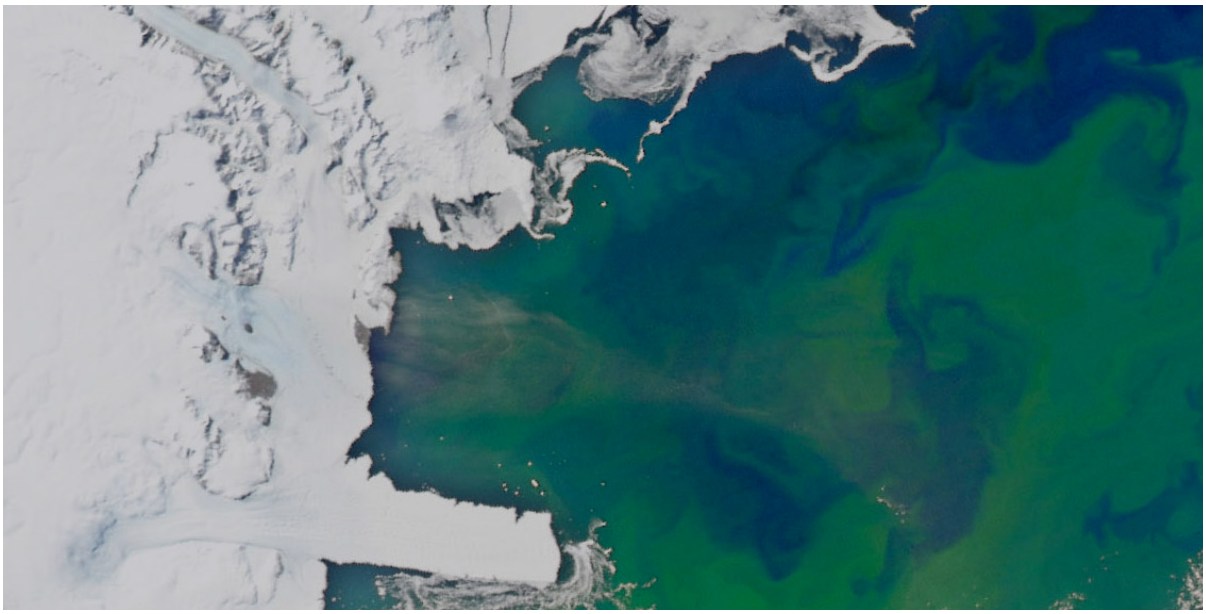

Role of sea ice as a biogeochemically active reservoir of iron and other trace metals

by

Luis Paulo Duprat
B.Sc., M.Sc.

Submitted in partial fulfilment of the requirements for the Degree of Doctor of Philosophy in Quantitative Antarctic Science

University of Tasmania (UTAS)
Institute for Marine and Antarctic Studies (IMAS)
Australian Antarctic Division (AAD)
Antarctic Climate & Ecosystems Cooperative Research Centre (ACE CRC)
Antarctic Gateway Partnership (AGP)

March 2021

Role of sea ice as a biogeochemically active reservoir of iron and other trace metals

by

Luis Paulo Duprat
B.Sc., M.Sc.

Under the supervision of Dr. Delphine Lannuzel, Dr. Klaus Meiners, Dr. Andrew Martin and Dr. Andrew McMinn

Submitted in partial fulfilment of the requirements for the Degree of Doctor of Philosophy in Quantitative Antarctic Science

University of Tasmania (UTAS)
Institute for Marine and Antarctic Studies (IMAS)
Australian Antarctic Division (AAD)
Antarctic Climate & Ecosystems Cooperative Research Centre (ACE CRC)
Antarctic Gateway Partnership (AGP)

March 2021

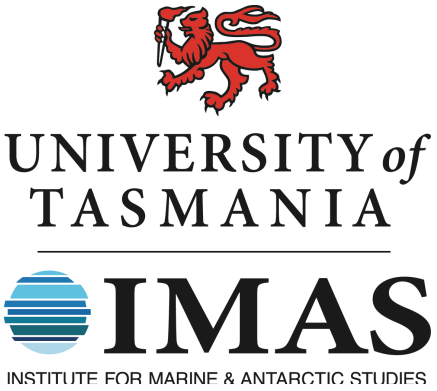

Declaration of originality

I declare that this thesis contains no material which has been accepted for a degree or diploma by the University or any other institution, except by way of background information and duly acknowledged in the thesis, and to the best of my knowledge and belief no material previously published or written by another person except where due acknowledgement is made in the text of the thesis, nor does the thesis contain any material that infringes copyright.

Signed:

Luis Paulo Duprat

Date: December 10th, 2020

Authority of access statement

The publisher of the papers comprising Chapter 2 and 3 holds the copyright for their content, and access to the material should be sought from the journal. The remaining non-published content of this thesis may be made available for loan and limited copying in accordance with the *Copyright Act 1968*.

Signed:

Luis Paulo Duprat

Date: December 10th, 2020

Acknowledgments

First, I would like to thank my supervisors, Dr. Delphine Lannuzel, Dr. Klaus Meiners, Dr. Andrew McMinn and Dr. Andrew Martin for all the guidance and support given during my PhD. A special thanks go to Delphine and Klaus who showed themselves prompt to assist me at any time. Thank you for giving me continuous feedback during this work. All the pertinent comments over the chapters were essential to enhance my critical sense. Delphine, thank you a lot for your close support and encouragement over the past four years.

I would also like to thank Dr. Pier van der Merwe, Dr Katrin Wuttig and Dr. Ashley Townsend for the support with the SeaFast and ICP analysis, crucial for generating the data described in this work. I could not leave behind my recognition for all you folks onboard Sipex-2, Davis and AAV2 expedition who collected and processed the samples used to write chapter 2, 3 and 4 of this thesis, namely, among others: Delphine Lannuzel, Klaus Meiners, Julie Janssens, Cristina Genovese, Mathew Corkill, Sebastian Moreau and Lavy Ratnarajah. Thank you for all your efforts! Similar credit applies to all collaborators who made these voyages possible. I would also like to thank the Gateway partnership and UTAS/IMAS for the essential financial and administrative support which made this work possible.

Finally, I would like to thank all my colleagues from IMAS who directly or indirectly contributed to this work and to those who made my PhD experience here a joyful one. I also want to express my gratitude to all my friends made during this journey. My super special thanks go to my family back in Brazil. *Muito obrigado por toda torcida e suporte emocional, principalmente naqueles momentos que pensei em desistir. Pepe e Tchuco, obrigado por cada visita, risada e soriso que compartilharam comigo durante esse tempo. Voces sao a coisa mais importante na minha vida!! Bol, obrigado por ser a irma mais maravilhosa do mundo! Pais, obrigado por tudo.*

Statement of Co-authorship

The following collaborators contributed to the publication of the work undertaken as part of this thesis:

(1) ***Luis Paulo Duprat (PhD candidate)*** - Institute for Marine and Antarctic Studies (IMAS), University of Tasmania, Hobart, Australia; Antarctic Gateway Partnership (AGP), University of Tasmania, Hobart, Tasmania.

(2) ***Delphine Lannuzel*** - Institute for Marine and Antarctic Studies (IMAS), University of Tasmania, Hobart, Australia.

(3) ***Klaus M. Meiners*** – Department of Agriculture, Water and the Environment, Kingston, Tasmania, Australia; Australian Antarctic Program Partnership, Institute for Marine and Antarctic Studies, University of Tasmania, Hobart, Tasmania, Australia.

(4) ***Pier C. van der Merwe*** - Antarctic Climate and Ecosystems Cooperative Research Centre (ACE CRC), University of Tasmania, Hobart, Australia.

(5) ***Arnout Roukaerts*** - Analytical, Environmental & Geo-Chemistry, Vrije Universiteit van Brussel, Brussels, Belgium.

(6) ***Ashley T. Townsend*** - Central Science Laboratory, University of Tasmania, Hobart, Australia.

(7) ***Sebastien Moreau -*** Norwegian Polar Institute, Tromsø, Norway

(8) ***Matthew Corkill (PhD candidate) -*** Institute for Marine and Antarctic Studies (IMAS), University of Tasmania, Hobart, Tasmania.

(9) ***Cristina Genovese (PhD candidate) -*** Institute for Marine and Antarctic Studies (IMAS), University of Tasmania, Hobart, Australia; Antarctic Gateway Partnership (AGP), University of Tasmania, Hobart, Tasmania.

(10) ***Julie Janssens*** - CSIRO Oceans and Atmosphere, Hobart, Tasmania, Australia.

(11) ***Florian Deman -*** AMGC Department, Vrije Universiteit Brussel, Brussels, Belgium.

(12) ***Naoya Kanna*** - Arctic Research Center, Hokkaido University, Sapporo, Japan; Atmosphere and Ocean Research Institute, The University of Tokyo, Kashiwa, Japan

Chapters 2 and 3 of this thesis, have been prepared as manuscripts for submission to peer-reviewed journals, and were accepted and published. In these chapters, the design and implementation of the research, data analysis, interpretation of the results, and preparation of the manuscripts were the responsibility of the candidate but were carried out in consultation with supervisors and with the input of specialist contributors. These contributions are highlighted for each of these manuscripts below.

Contribution of work by co-authors for each paper:

Chapter 2 (paper 1): Enhanced Iron Flux to Antarctic Sea Ice via Dust Deposition From Ice-Free Coastal Areas.

Journal of Geophysical Research: Oceans, 124(12), 8538-8557 (2019). https://doi.org/10.1029/2019jc015221

by

Luis Duprat (L.P.), Naoya Kanna (N.K.), Julie Janssens (J.J), Arnout Roukaerts (A.R.), Florian Deman (F.D), Ashley Townsend (A.T), Klaus M. Meiners (K.M.), Pier van der Merwe (P.M) and Delphine Lannuzel (D.L)

Co-authors contribution:

Project design (D.L and K.M.); fieldwork (sampling and processing) (J.J., A.R., F.D., N.K, K.M. and D.L); laboratory analysis (L.D, J.J, F.D, A.R, A.T., P.M. and D.L.); processing (M.C., C.G., S.M. and D.L.); laboratory analysis (L.D., M.C., C.G., A.T. and D.L.); data analysis (L.D.); leading role in the manuscript preparation and reviews (L.D); assisting in the manuscript revision (J.J., N.K., A.R., F.D., A.T., K.M., P.M., and D.L.)

Chapter 3 (paper 2): Nutrient distribution in East Antarctic summer sea ice: a potential Iron contribution from glacial basal melt.

Journal of Geophysical Research: Oceans, 125, e2020JC016130 (2020). https://doi.org/10.1029/2020JC016130

by

Luis Duprat (L.P.), Matthew Corkill (M.C.), Cristina Genovese (C.G.), Ashley Townsend (A.T), Klaus M. Meiners (K.M.), Sebastien Moreau (S.M.) and Delphine Lannuzel (D.L)

Project design (D.L.); fieldwork (sampling and processing (M.C., C.G., S.M. and D.L.); laboratory analysis (L.D., M.C., C.G., A.T. and D.L.); data analysis (L.D.); leading role in the manuscript preparation and reviews (L.D.); assisting in the manuscript revision (D.L., K.M., M.C., C.G., S.M. and A.T.)

We, the undersigned, endorse the above stated contribution of work undertaken for each of the published (or submitted) peer-reviewed manuscripts contributing to this thesis:

Luis Paulo Duprat

PhD Candidate
Institute for Marine and Antarctic Studies (IMAS) University of Tasmania

Signed:

Date: 10.12.2020

Dr. Delphine Lannuzel

Primary Supervisor
Institute for Marine and Antarctic Studies (IMAS) University of Tasmania

Signed:

Date: 10.12.2020

Pr. Neil Holbrook

Head of Centre, Oceans and Cryosphere
Institute for Marine and Antarctic Studies (IMAS) University of Tasmania

Signed:

Date: 10.12.2020

Table of content

CHAPTER 3. IRON DISTRIBUTION IN EAST ANTARCTIC SUMMER SEA ICE: A POTENTIAL CONTRIBUTION FROM GLACIAL BASAL MELT

CHAPTER 4. DISTRIBUTION OF TRACE METALS IN ANTARCTIC SEA ICE FROM THREE DIFFERENT LOCATIONS AND SEASONS: FERTILIZATION, LIMITATION AND TOXICITY

CHAPTER 5. GENERAL DISCUSSION AND PERSPECTIVES

List of figures

List of Tables

ABSTRACT

An increasing body of work has underlined the importance of Antarctic sea ice as a reservoir and source of iron (Fe) to the Southern Ocean, boosting local primary production and carbon export during spring and summer. The impact of Fe in controlling sea-ice and ocean productivity is unequivocal, but other trace metals (TMs) can also regulate productivity. Nevertheless, considerable uncertainty with respect to the pathways, fate and bioavailability of TMs in the sea-ice environment prevents us to accurately model the impact of predicted future changes in sea-ice extent and thickness on Southern Ocean ecosystems and our global climate. The aim of this PhD is to bring new evidence to our present understanding of the biogeochemical cycling of Fe and other bioactive TMs (Cd, Co, Cu, Mn, Ni and Zn) in Antarctic coastal land-fast (i.e. sea ice fastened to the coastline, ice shelves or to grounded icebergs) and pack ice (free drifting) and their relationship with regional primary productivity. The main findings from the analyses of TM distributions in sea ice from three field campaigns (SIPEX-2, 2012; Davis, 2015 and AAV2, 2016/17) along the East Antarctic coast are as follows: 1) Primary production in coastal land-fast ice is not Fe-limited during late-spring/early summer, potentially due to the high input of Fe from suspended sediment entrapped during ice formation; 2) Windblown dust from ice-free coastal landmasses can significantly contribute to the total Fe pool in land-fast ice and could become an important source of Fe and potentially other TMs, considering the projected expansion of ice-free areas across the Antarctic landmass by the end of the century; 3) Primary production in East Antarctic (fast and pack) ice is also not Fe-limited during mid-summer. Instead, low concentrations of inorganic nitrogen sources could be the main nutrient limiting sea-ice algal growth at this time of the year; 4) The formation of Fe-rich platelet ice underneath pack ice in proximity to glacial systems with negative ice mass balance (Totten Glacier basin) indicates the potentially large contribution of glacial meltwater to Fe and TM pools in sea ice collected near the coast; and finally, 5) TMs other than Fe are enriched in sea ice relative to seawater from winter/spring to summer. However, this enrichment is not consistent across the TMs analysed. Zinc, Cu and Ni display higher enrichment than Mn, Co and Cd, potentially because of different levels of complexation with organic ligands. High concentrations of dissolved Zn and Cu in sea ice suggest both elements are unlikely to limit sea-ice algae growth. Contrary, their levels could be toxic if they are not appreciably chelated. Free Zn and Cu ion measurements are needed to confirm this hypothesis. This study shows that sea ice serves as a biogeochemically active reservoir not only for Fe but potentially for Zn as well.

CHAPTER 1. INTRODUCTION

1.1 Background

Every year, the seasonal Arctic and Antarctic sea ice expands throughout a major area of the polar oceans to form one of the largest biomes on Earth (Dieckmann & Hellmer, 2010). Nevertheless, for hundreds of years, this hostile environment represented not much more than a barrier to human navigation or at most an occasional ground for fishing and hunting for those who could benefit from its relative proximity. It was only during the last century that the perception of the sea ice as a much more complex and important environment in a global context has emerged (McGhee, 2006). During the last sixty years, modern icebreakers have significantly facilitated the access to and *in situ* studies of this environment. Airborne equipment and remote sensing technologies have brought complementary large-scale information about the behaviour and role of the sea-ice cover. It is now well established that the extensive area of global sea ice provides not only a platform for an array of animals like birds and mammals but also a unique habitat for primary producers. Sea ice serves as a sustained surface in the ocean, providing sufficient nutrients and light for microorganisms to thrive (Thomas & Dieckmann, 2010). There, microscopic algae are the base of a food-chain supporting higher trophic levels during times of low pelagic production, also seeding open waters with new stocks of cells throughout the sea-ice melt season. Ice-associated primary production is controlled by the thermo-physical processes related to the sea-ice formation and melting cycles and contributes significantly to ocean biogeochemical cycling and carbon export. Hence, the seasonal sea-ice zone plays a pivotal role in the Earth`s climate (Arrigo et al., 2008; Vancoppenolle et al., 2013). As polar regions are especially susceptible to climate change (Goosse et al., 2018; Rignot et al., 2019), a better understanding of the large-scale physical and biogeochemical processes within the sea ice is key to reliably predict the effect of anthropogenic interferences in Earth's climate and marine ecosystems.

1.2. General context

The increase of atmospheric greenhouse gases from human activities is the primary driver of ongoing climate change over the last century (IPCC, 2014). Since the industrial revolution, atmospheric CO_2 concentration has almost doubled with direct and indirect impacts to the

marine ecosystems, ocean temperature and chemical composition, as well as sea-ice extent (Comiso, 2010). At present, global oceans are absorbing around 40% of anthropogenic CO_2 emissions, largely through physical processes (Verdugoa et al., 2004). Thus, the ocean has an undeniable role in reducing human impacts on the climate.

Despite covering less than 10% of the global ocean surface, the Southern Ocean (SO) alone is responsible for absorbing 25% of the atmospheric carbon through a physical and biological mechanism known as the solubility and biological carbon pumps, respectively (Takahashi et al., 2009). The solubility pump is driven primarily by physicochemical processes of CO_2 dissolution and outgassing. The efficiency of this abiotic pump is of particular importance in the SO where the formation of the seasonal sea ice and brine rejection contributes to the formation of Antarctic Bottom Water, a forceful component that drives the global thermohaline circulation (Figure 1.1; Rintoul, 2001).

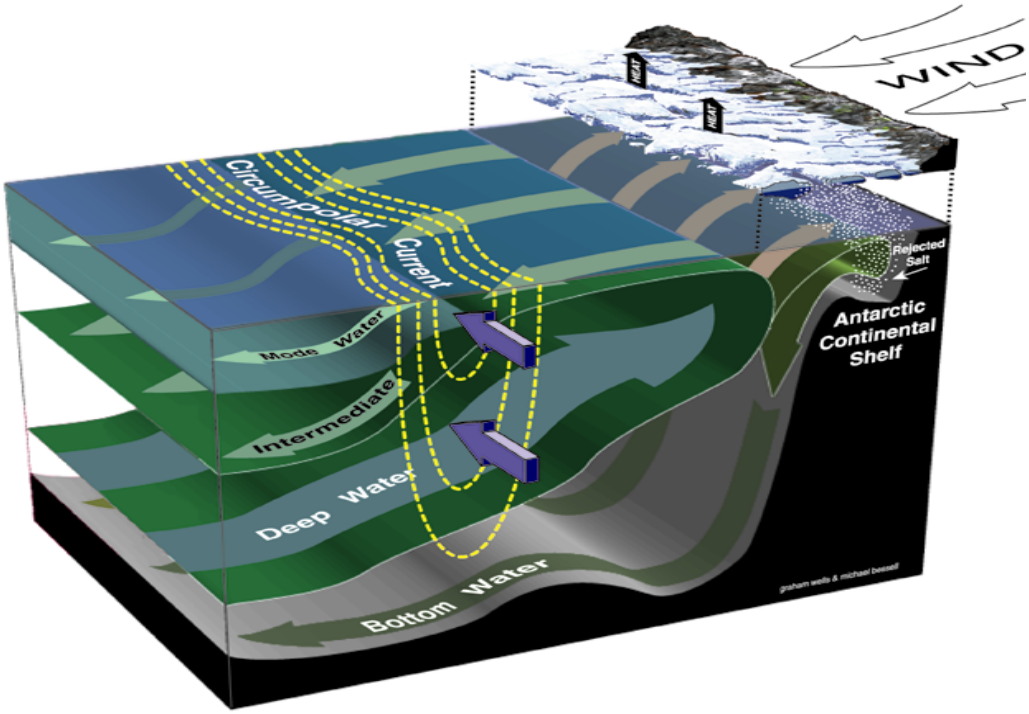

Figure 1.1 Illustration of the Antarctic Bottom Water formation (Rintoul and Sparrow, 2001).

On the other hand, the biological pump drives the natural carbon cycle through uptake and fixation of inorganic carbon into organic matter by autotrophic microorganisms called phytoplankton (Figure 1.2). These microorganisms represent only 1% of the total biomass on Earth but are capable of photosynthesizing organic carbon - net primary production (NPP) - at

values comparable to the world`s entire forests. The organic carbon they produce is eventually exported to the deep ocean by the sinking of the remaining plankton detritus (Blain et al., 2007; Sarmiento & Gruber, 2005). An estimated 16 gigatons of carbon are sequestered to the ocean depths every year through this process (Falkowski et al., 1998; Field et al., 1998). Studies have shown that the Antarctic seasonal sea-ice zone is a hotspot for primary production, fueling large algae blooms at retreating ice edges (Lizzotte, 2001), thus contributing to the biological pump in the south polar region (Moreau et al., 2016).

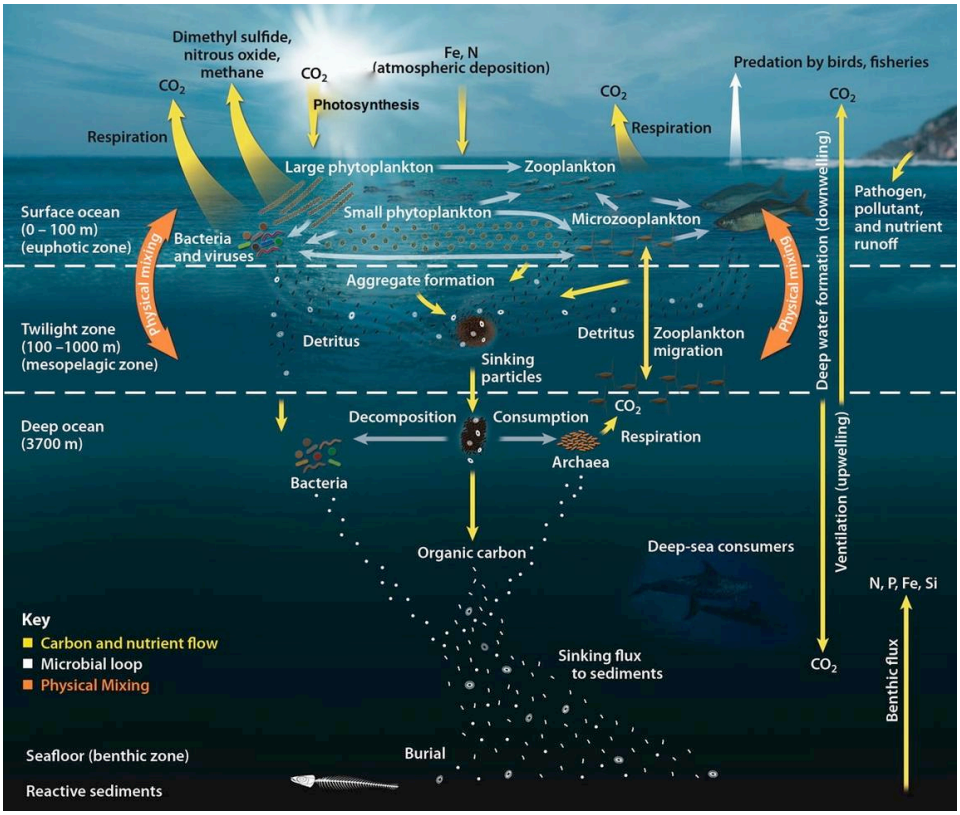

Figure 1.2 The oceanic carbon cycle. *Source*: Oak Ridge National Laboratory.

In addition to its contribution to the bottom water formation and carbon export, Antarctic sea ice has an important role in the ocean dynamics by controlling the heat exchange, mechanical mixing and light availability in the water column (Venables et al., 2013). Finally, the sea ice seasonal cycle can influence the atmospheric composition and its radiative properties via emission of climate-active gases (DMS, halogen elements) to the atmosphere, as well as the global radiative budget via its albedo effect (Ogura, 2004; Saiz-Lopez et al., 2015; Trevena & Jones, 2012). Paleo-climate studies demonstrated that major alterations in the polar ocean physicochemical characteristics led to changes in the rates of the carbon pump in the past with

consequent feedback responses in the atmospheric CO_2 concentration (Sigman et al., 2010). Although seasonal sea ice should still subsist by the end of the century in spite of an expected warmer climate, the future contribution of sea ice to the global carbon cycle and climate is difficult to predict due to a lack of a mechanistic understanding of coupled physical-biological processes, needed to inform models (Massom & Stammerjohn, 2010; Massom et al., 2013).

1.3 The iron hypothesis and the Antarctic paradox

High Nutrient Low Chlorophyll (HNLC) areas represent 20% of the global ocean where macronutrients are perennially available, yet phytoplankton biomass is relatively low. The SO is the largest HNLC area on Earth (figure 1.3), carrying high concentrations of macronutrients due to the upwelling of nutrient-rich deep waters (nitrate, phosphate, silicic acid) but a low concentration of chlorophyll-a (Chl*a*) (Kämpf & Chapman, 2016).

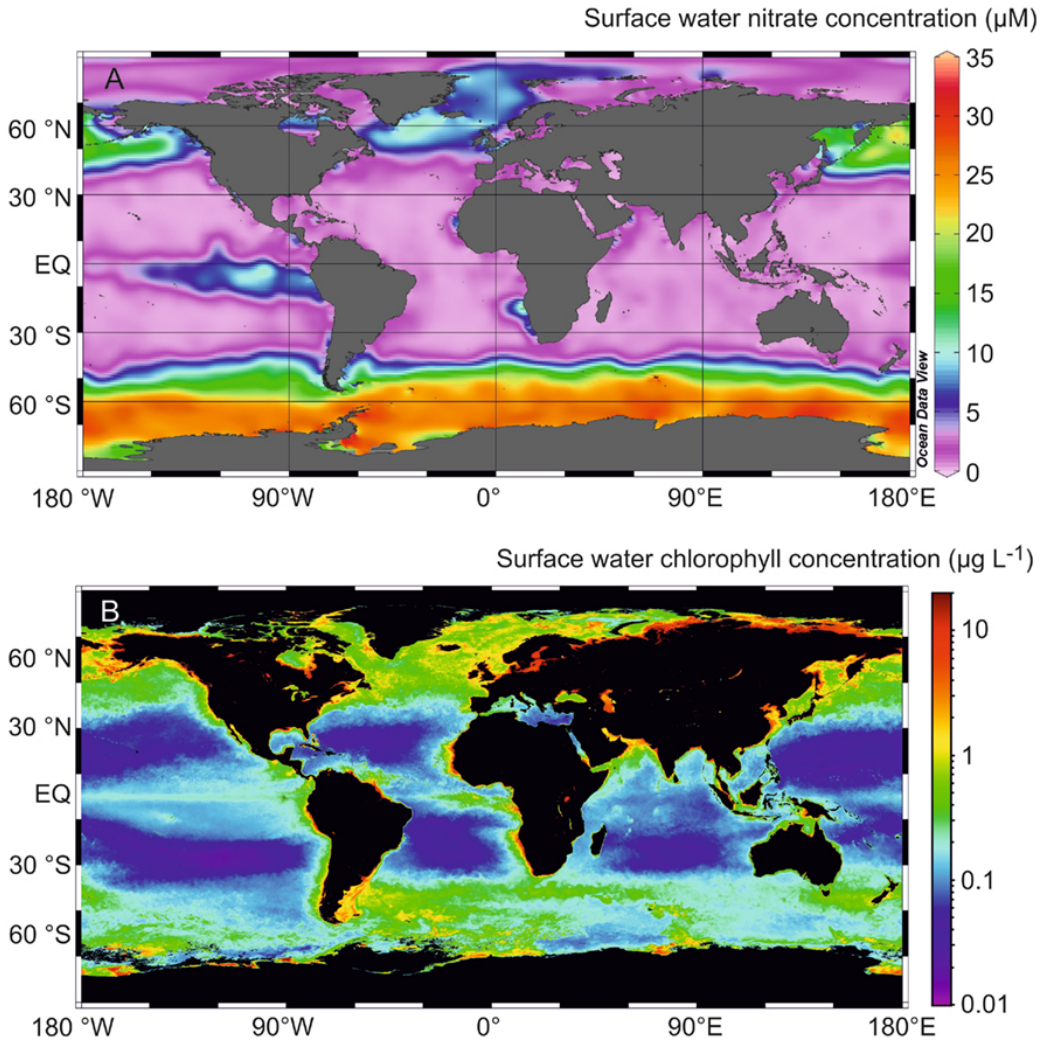

Figure 1.3 (Above) Annual average nitrate concentration (μM) and (below) composite chlorophyll-*a* (mg L^{-1}) distribution in surface waters of the global ocean. (NASA, 2010).

This paradox has been attributed to the limited presence of the micronutrient iron (Fe), an essential element for nitrogen fixation and amino acids synthesis, required by most autotrophic microorganisms (Boyd et al., 2000; de Baar et al., 1995). This theory was the basis of the "Iron hypothesis" first proposed by Martin (1990), which states that lower atmospheric CO_2 concentrations during glacial periods could be partially attributed to higher aeolian dust inputs to the oceans, therefore boosting primary productivity and carbon export during these periods (Figure 1.4).

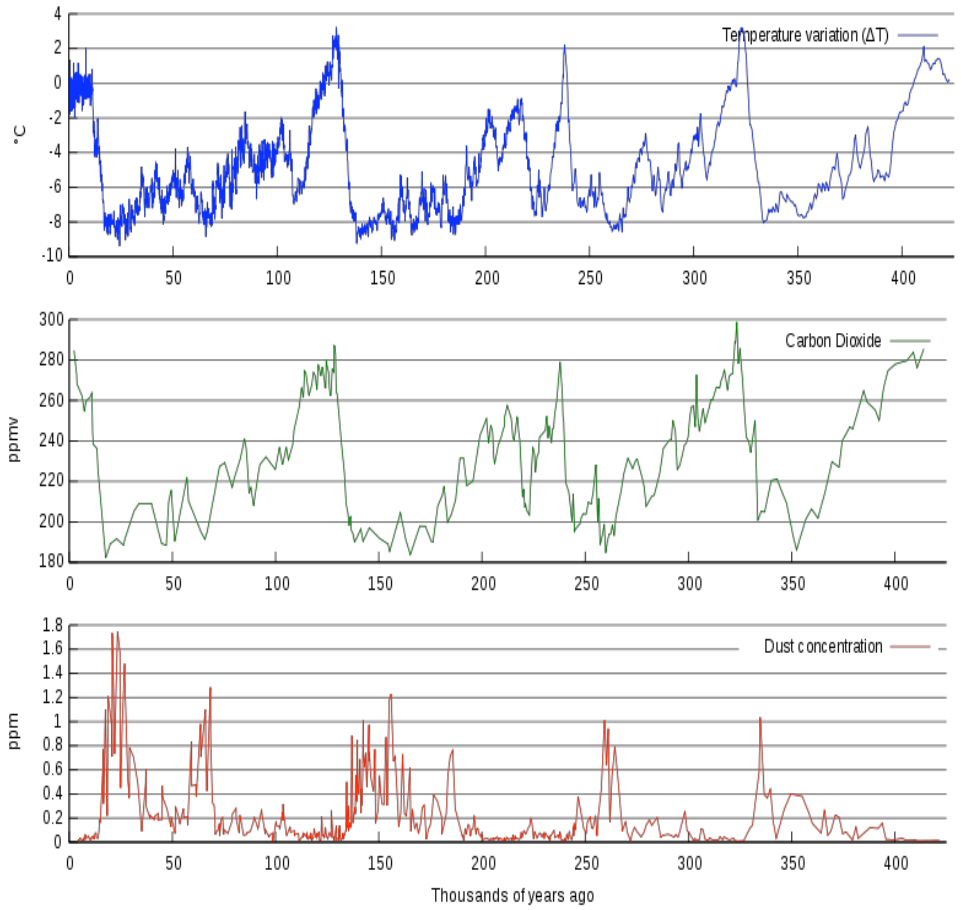

Figure 1.4 Graph of reconstructed temperature (blue), CO_2 (green), and dust (red) from the Vostok Station ice core for the past 420, 000 years (Petit et al., 1999).

Because of their distinctive nutritive properties, HNLC waters are characterized by low phytoplankton stocks and the presence of predominantly small flagellates which can cope better with low Fe availability due to their greater surface area to volume ratio (Deppeler & Davidson, 2017). In contradiction to that, near the sea ice edge around Antarctica, large phytoplankton blooms are commonly observed during spring and summer (Comiso et al., 1990)

mostly comprised of diatoms cells (*Fragilariopsis sp*) and *Phaeocystis antarctica* (Lizotte, 2001). Sea-ice cores obtained from a series of field expeditions during this last decade also revealed active biological and chemical processes with Fe concentrations within the sea ice markedly higher than in the oceanic surface waters (Lannuzel et al., 2007; Lannuzel et al., 2008; van der Merwe et al., 2011b). It has been suggested that growing sea ice incorporates and stores large amounts of Fe during its formation in winter (Janssens et al., 2016; Lannuzel et al., 2016b; Sedwick et al., 2000). Eventually, this Fe pool is released into surface waters during the melting season, triggering phytoplankton blooms at the retreating sea ice edges (Figure 1.5) and in opening polynyas (Arrigo, 2003; Grotti et al., 2001, 2005; Lannuzel et al., 2007; Lannuzel et al., 2008; Sedwick et al., 2000). This process can alleviate Fe limitation at a critical time, when light availability and water stratification favours phytoplankton growth, conferring to Antarctic sea ice an important status of a seasonal Fe reservoir in the Southern Ocean (Tagliabue & Arrigo, 2006). Considering that every winter an area of approximately 19 million km^2 is covered by sea ice in the Southern Hemisphere (Comiso, 2003), around 40% of the SO can be potentially fertilized by the annual formation and melting of ~80% of this ice cover. Although the role of Fe in controlling HNLC productivity is well established, other trace elements such as manganese (Mn), copper (Cu), zinc (Zn) and cobalt (Co) also have crucial ecological roles by co-limiting physiological processes in phytoplankton (Sunda et al., 2012) and possibly in sea-ice algae as well.

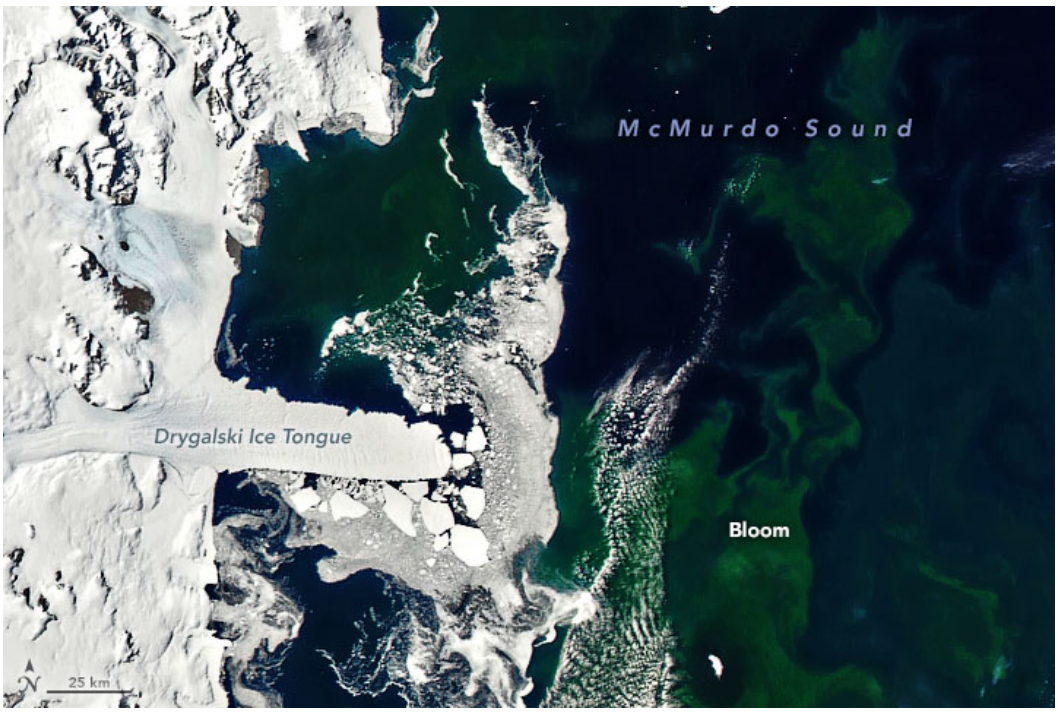

Figure 1.5 Decaying fast ice fertilizing a bloom of phytoplankton in East Antarctica. Image obtained on 21/01/2020 from Terra Modis satellite, NASA. *Image courtesy*: NASA Earth observatory.

1.4 External sources of trace metals to Antarctic waters

Iron, as well as other bioactive trace elements, can be supplied to the surface waters in many ways: upwelling/resuspension of shelf sediments to the mixed layer, hydrothermal vents, aeolian dust and glacial sources (Wadley et al. 2014). Although dust from arid deserts is an important source of trace elements such as Fe and Mn to oceans in the northern hemisphere (Figure 1.6), the direct atmospheric dust load to the Southern Ocean is extremely low. For Fe, this source represents only 15% of the total input (Maher et al., 2010).

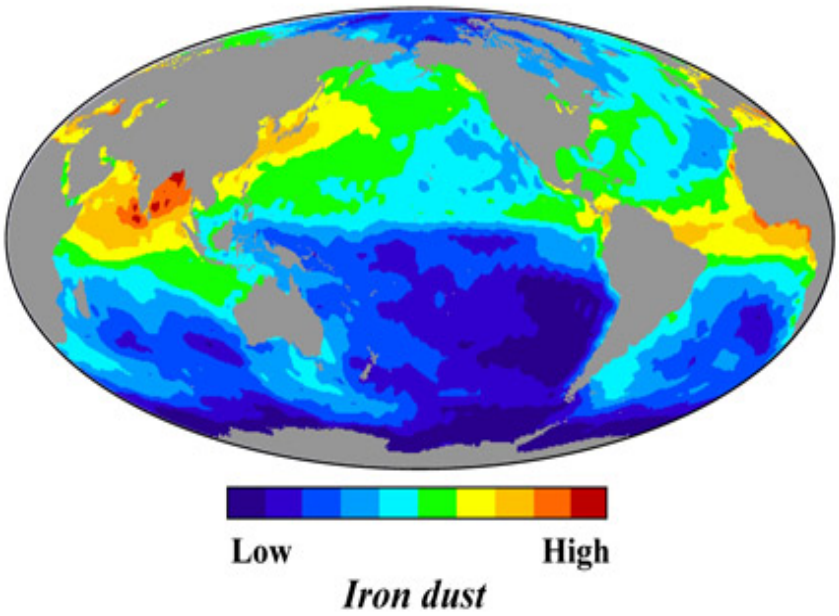

Figure 1.6 Aeolian dust input to the global ocean (Behrenfeld et al., 2006).

This low dust supply combined with the low solubility of Fe is mirrored by the overall low concentration of Fe in the SO open surface waters (Martin, 1990). While aeolian and glacial sources such as glaciers outflow, ice shelves, and free-drifting icebergs may be an important source for localized blooms (Figure 1.7), it is estimated that the majority of Fe input to the SO comes from local sediment resuspension on the continental shelves and shallow underwater plateaus surrounding the Antarctic continent and sub-Antarctic islands (Wadley et al., 2014).

In this context, although the sea ice is not a new source of Fe, it has the ability to store, recycle, transport, and release Fe at locations not constrained within the boundaries of the continental shelves, therefore acting as a pathway from coastal to open waters (Lannuzel et al., 2010). Katabatic winds can drive ice floes formed in coastal polynyas northwards, transporting Fe and other particles from lower latitudes further afield (Arrigo, 2003). Lateral transport of Fe-rich sediments, eddy shedding/sediment entrainment and bathymetric interactions with the Antarctic Circumpolar Current can further redistribute this limited nutrient across the Southern Ocean (Boyd & Ellwood, 2010). To which extent sea-ice formation and drift influence the spatial distribution of other trace elements is still not fully established. A preliminary survey indicates that the seasonal sea ice melt should not represent a significant source of bioactive metals, other than Fe, to Antarctic surface waters (Lannuzel et al., 2011). However, the lack of further of work on the topic hampers definite conclusions.

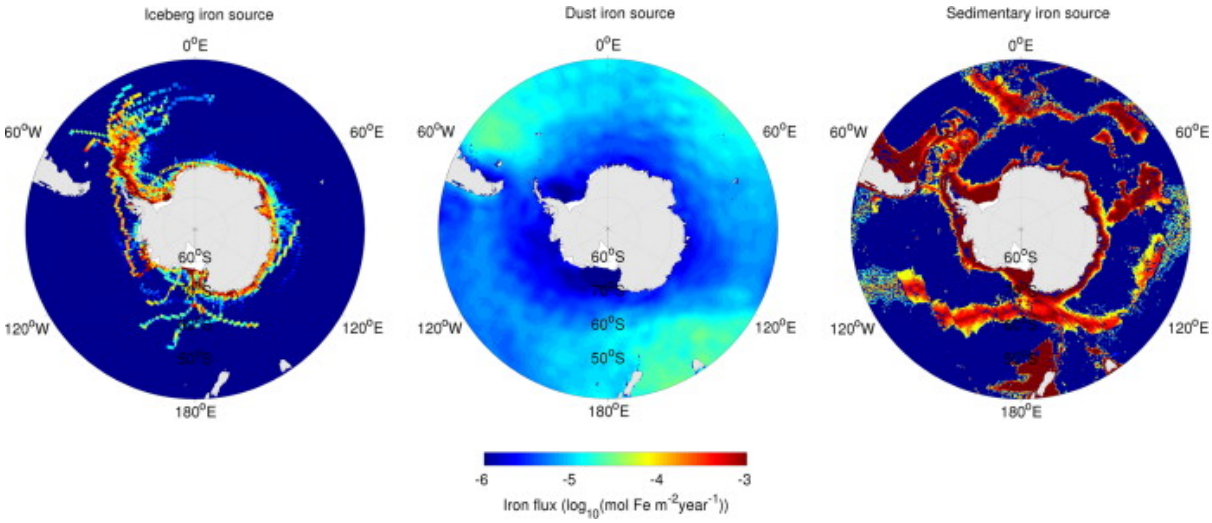

Figure 1.7 Iceberg, dust and sedimentary iron sources in the Southern Ocean (Boyd & Ellwood, 2010).

1.5 Biogeochemistry of macro and micronutrients in the sea ice.

The unique physical structure of sea ice and the processes influencing its formation and decay determine the biology and chemistry within the ice matrix. During spring and summer, the interior of sea ice is rarely isolated from seawater and exchanges between the ice and the ocean constantly occur. These exchanges are constrained by brine flushing, advection processes and

molecular diffusion across the diffusive boundary layer (Meiners & Michel, 2017; Thomas & Dieckmann, 2010; Tison et al., 2008; Vancoppenolle et al., 2010). Microorganisms are greatly influenced by the physics and chemistry of the medium surrounding them, and in turn, can modify it. A good example is the production of exopolysaccharides (EPS) by sea-ice algae and bacteria, a cryoprotective substance that can increase the habitability of sea ice (Krembs et al., 2011).

An analysis of vertical profiles of the most relevant biogeochemical tracers in the sea ice reveals contrasting behaviours. Concentrations of inorganic macronutrients such as nitrate, phosphate, and silicic acid, generally follow salinity in a conservative way, with concentrations in bulk sea ice being much smaller than in seawater. Significant deviations in nutrient concentrations as compared to salinity are associated with biological activity (Fripiat et al., 2017). Organic matter and dissolved Fe typically show higher concentrations in sea ice than in the underlying ocean. Mounting observations have highlighted the accumulation of Fe in the sea ice by up to two orders of magnitude when compared to the underlying seawater (Grotti et al., 2005; Lannuzel et al., 2007; Lannuzel et al., 2008; Lannuzel et al., 2010; van der Merwe et al., 2009, 2011a). First assessments of trace metals other than Fe show that most elements (Al, Cr, Mn, Ba, Cu, Zn, Cd, Mo and Mn) are not enriched in sea ice in the same way as Fe, with bulk concentrations comparable to those reported in the literature for Antarctic surface waters (Grotti et al., 2001, 2005; Lannuzel et al., 2011). The acknowledgement that these elements could behave conservatively with salinity and macronutrient nurture the odds that they might limit local primary production (Lannuzel et al., 2016).

1.6 Fe cycle in the sea ice environment

Sea ice has an important function in the ocean biogeochemistry by acting as a temporal reservoir of Fe, a key micronutrient which is known to limit primary production in large parts of the Southern Ocean (Lannuzel et al., 2016b; Schoffman et al., 2016). The enrichment of Fe driven by a decoupling behaviour from salinity and other macronutrients suggests different sources and/or incorporation mechanisms (Grotti et al., 2005; Lannuzel et al., 2016b). Although the importance of sea ice as a source of Fe to the Southern Ocean has extensively been described, the mechanisms leading to the high Fe levels in sea ice, its physicochemical dynamics, bioavailability and finally spatial and temporal distribution still need to be identified and, most importantly, quantified.

1.6.1 The incorporation of Fe into sea ice

The mechanism of Fe incorporation into sea ice has not yet been fully elucidated. Studies point towards a scavenging process of biogenic and lithogenic particles from seawater during sea-ice formation (de Jong et al., 2013; Janssens et al., 2016). When supercooled seawater freezes under turbulent conditions during strong wind events, so-called frazil ice form as small crystal-like needles and spicules which rise to the ocean surface and consolidate into granular ice (Leonard et al., 2011). It has been suggested that as they ascend towards the ocean surface, frazil ice crystals could scavenge particles suspended in the water column such as organic detritus, algae cells, sedimentary and terrestrial material. The newly formed ice layer could then also sieve particles from seawater and trap them into the existing ice matrix (Gradinger & Ikavalko, 1998). Ice nucleation on marine particles consolidating into the granular ice has also been reported as a potential mechanism of particle enrichment into newly forming sea ice (Lannuzel et al., 2016b). Beneath the granular ice layer, a columnar ice layer can grow under calmer conditions (Ackley & Sullivan, 1994; Jeffries et al., 1994). During this phase of ice formation, sea salts and other impurities such as Fe particles can be rejected from the ice matrix forming brine pockets that are connected through a web of brine channels.

The co-occurrence of high concentrations of Fe and organic matter in sea ice suggests a link between their incorporation processes. Recent *in situ* sea-ice growth experiments showed that enrichment of Fe and organic matter in sea ice relative to seawater occurs during the very first stages of the sea-ice formation (Janssens et al., 2016). The role of organic matter, especially EPS, in the mechanisms of Fe enrichment was further investigated in the laboratory using a cold finger apparatus to stimulate the ice growth under non-contaminating carbon and trace metal conditions (Janssens et al., 2018). Results indicated that the "quality" of the organic matter (i.e., freshly formed versus old EPS) played a crucial role in the rate of incorporation of Fe into sea ice (Janssens et al., 2018). When evaluating the fractionation of Fe between the dissolved and particulate phases (DFe and PFe, respectively), a preferential enrichment of PFe over DFe was observed. Ice algae from Davis station and desert dust from South Georgia were separately added to a seawater solution to evaluate the possible differences in the respective rates of incorporation of biogenic and lithogenic PFe into growing ice. Results from this experiment indicated the preferential enrichment of biogenic Fe over lithogenic Fe. Field studies have also shown a temporal decoupling between the PFe and DFe fractions during the sea-ice melting phase (Grotti et al., 2001; van der Merwe et al., 2011a). Van der Merwe et al.

(2011a) observed that only the dissolved fraction was present in the brine drained into sack holes indicating, therefore, the particulate fraction stayed somehow retained in the brine channel network, i.e. associated with the sea-ice matrix. Whether this retention is exclusively controlled by physical constraints of the brine network, the presence of organic ligands or a combination of both is still unclear. The studies suggest that organic ligands like EPS might not only control the incorporation of PFe in the sea ice, but also its retention in sea ice.

Once the sea ice is formed, Fe uptake and bioaccumulation by sea-ice algae and dust deposition can increase the sea-ice bulk Fe concentration, especially in the particulate form (de Jong et al., 2013; Fitzwater et al., 2000; Lannuzel et al., 2010; Sedwick et al., 2000; van der Merwe et al., 2011a). Dynamic processes such as rafting and ridging of ice floes can also create heterogeneous vertical profiles of Fe distribution in the sea ice. Finally, the incorporation of remaining biogenic material from the preceding productive season, recycling processes (remineralization from bacterial activity), grazing, and excretion from higher trophic levels can also be expected to influence the Fe concentration in sea ice (Lannuzel et al., 2016a; Ratnarajah et al., 2014).

1.6.2 Fe speciation and bioavailability in sea ice

The physical and chemical forms of Fe (i.e. speciation) present in sea ice have important implications for its fertilization potential and persistence in the ocean and can vary with location, type of ice and biological activity. Understanding the partitioning and dynamics between the different forms of Fe is crucial to quantify its bioavailability for autotrophic and heterotrophic microorganisms residing in sea ice and surrounding seawaters.

Although most studies have reported Fe using operational definitions of particulate (i.e. fraction retained on a 0.2 μm pore size filter) and dissolved fraction (fraction passing through a 0.2 μm pore size filter) to evaluate its bioavailability, Fe can span across a wide array of continuous size fractions, from soluble to particles of variable aggregates sizes (Figure 1.8) Lannuzel et al., 2016b; Worsfold et al., 2014). Dissolved Fe can naturally occur in its redox forms of Fe^{2+}, Fe^{3+}, free (Fe') or complexed with organic and inorganic ligands (Liu & Millero, 2002). Despite dissolved unchelated (free) inorganic Fe (Ferrous Fe(II)'/ferric Fe(III)') being the most readily available form of Fe to phytoplankton, modern oceans bear only picomolar to nanomolar concentrations of these species (Johnson et al., 1997). Notwithstanding, this

normally transient fraction is still an important pool contributing to meet microalgal requirements (Morel et al., 2008).

In seawater, DFe is most commonly found in its hydroxide complex $Fe(OH)^{3+}$ (aq) since the organic speciation of Fe(III) is thermodynamically favoured in the seawater pH natural range. Therefore, the availability of Fe in ocean waters is predominantly limited by the solubility of Fe(III). Although Fe(III) is only soluble in strong acidic solutions, natural processes can favour its reduction to Fe(II), thereby increasing Fe solubility (Worsfold et al., 2014). Besides carrying a positive charge, these Fe forms are prone to bind with organic ligands produced *in situ* by sea-ice algae and bacteria or supplied externally from sediment resuspension (Breitbarth et al., 2010; Kuma et al., 1996; Liu & Millero, 2002). Organic complexation is crucial for the maintenance of the DFe concentrations above the solubility threshold, retarding Fe adsorption onto sinking particles, increasing its solubility and extending the time microalgae can access this pool (Kuma et al., 1996; Morel et al., 2008).

Organic ligands have been classified into two major categories based on their stability and bond strength to Fe^{3+}: L1 (stronger siderophore-like molecules) and L2 class (weaker compounds derived from cellular degradation) (Hunter & Boyd, 2007). Lannuzel et al. (2015) showed that the vast majority (>99%) of Fe (dissolved and colloidal) in seawater is, in fact, bound to organic ligands. Similar observations were made in Antarctic fast ice (Lannuzel et al., 2015) and pack ice (Genovese et al., 2018). A compilation of all existing DFe concentrations in brines and bulk sea ice showed that 90% of the DFe is somehow attached or adsorbed to something inside the sea-ice matrix (Lannuzel et al., 2016b). High concentrations of EPS have been reported in sea ice and, together with being negatively charged, suggested as the main type of organic ligands in this medium (Verdugoa et al., 2004). Recent studies have found that the weakly bound EPS-Fe complex is highly available to diatoms and other phytoplankton assemblages due to the saccharide properties that can stabilize Fe in the dissolved and colloidal form (Hassler & Schoemann, 2009; Hassler et al., 2011a, b). On the other hand, while the adsorbent property of the EPS can 'wrap' microbial cells and aggregates creating a protective microenvironment that can store and prevent Fe diffusive losses (Krembs et al. 2011), the same isolating property may reduce concentration-dependent processes of new Fe acquisition from the surrounding environment (Shaked & Lis, 2012). Moreover, the same chemical properties of EPS are believed to induce the aggregate formation and particles export,

shortening its residence in the surface water (Decho & Gutierrez, 2017). Clearly, further investigation into the role of organic ligands, particularly, EPS, is needed.

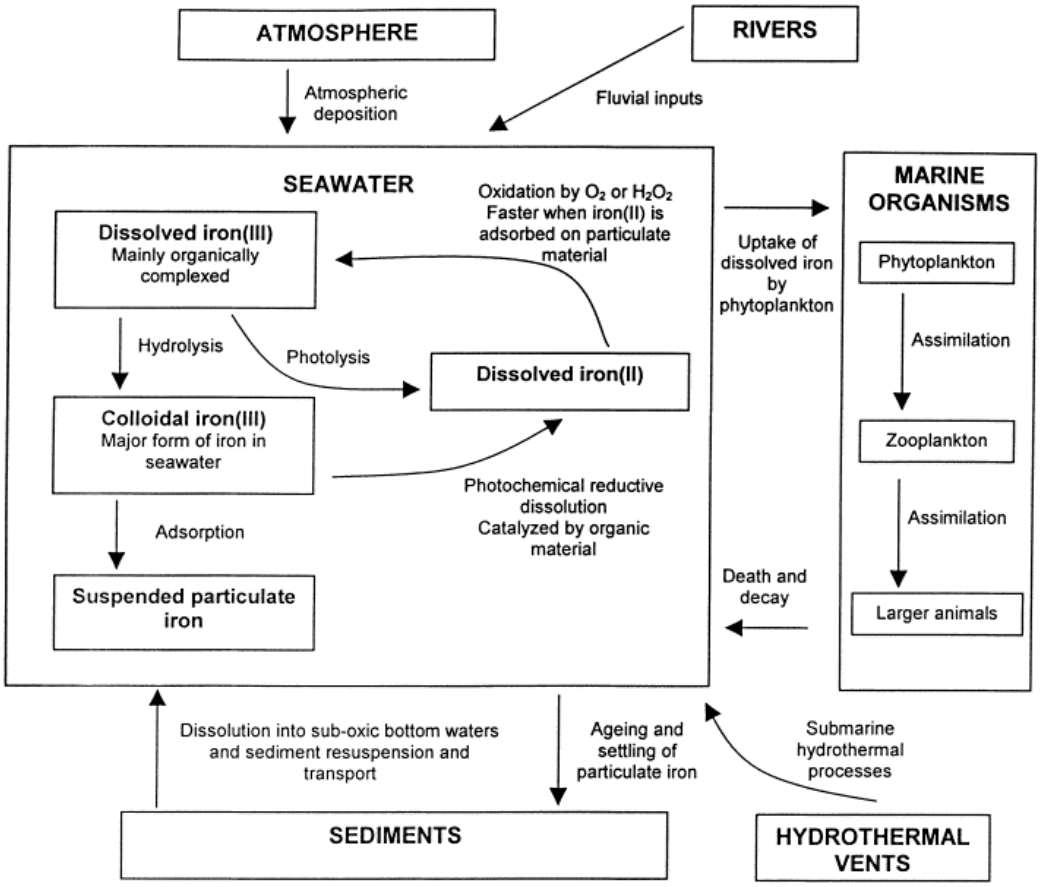

Figure 1.8 Schematic diagram of biogeochemical Fe cycling in the ocean (Achterberg et al., 2001).

Biological uptake and remineralization can also control the distribution and fractionation of Fe between the dissolved and particulate phases. A positive correlation of PFe with brine volume and associated biological parameters such as chlorophyll-a (Chl*a*) and particulate organic carbon (POC) was observed in previous sea-ice studies in East Antarctica (van der Merwe et al., 2011b). While autotrophic activity can reduce the concentration of DFe via uptake and induce bioaccumulation of biogenic PFe in sea ice during spring, DFe may also become bioavailable through seawater leaching process, protozoan grazing, bacterial remineralization and phytoplankton exudation (Lannuzel et al., 2016b; Tagliabue & Arrigo, 2006). Sea-ice EPS has been reported as a hotspot of bacterial activity, therefore potentially enhancing Fe recycling (Meiners et al., 2008).

It is important to highlight that Fe bioavailability is not a simple concept. Instead of an absolute bivalent yes/no attribute, in practice, a spectrum of bioavailability degrees can be expected due to the many interwoven facets of Fe speciation and kinetics, phytoplankton physiology, ecosystem processes and environmental circumstances that ultimately arbitrate the final Fe bioavailability. Iron uptake largely depends on the uptake machinery of the microorganism: siderophore mediated Fe acquisition, reductive Fe uptake pathway (eukaryotic microalgae), a combination of both, or other mechanisms yet to be described (Shaked & Lis, 2012). That being said, Fe bioavailability can be seen as a function of the chemical compatibility of a Fe-substrate with the specific cell transport system. To add complexity, environmental variables can change Fe kinetics and phytoplankton physiology. For instance, Fe(II) can be naturally produced in surface waters by photochemical and/or thermal reduction while low temperatures and pH can also delay the Fe(II) oxidation (Croot et al., 2001; Johnson et al., 1994; Roy & Wells, 2008). Iron limitation was also shown to upregulate high-affinity Fe acquisition systems (Kustka et al., 2007). Likewise, basic processes in the natural system such as the secretions of EPS, changes in O_2 via respiration and photosynthesis, enzymatic activity, production of bio-generated redox/superoxide agents, among others, can also modulate Fe speciation in complex ways, either beneficial or detrimental to the microorganism acquisition mechanism (Balzano et al., 2009; Barbeau, 2006; Rose, 2012). Finally, ecological interactions such as *in situ* recycling of cellular Fe through grazing and viral lysis and microbial reduction of faecal pellets can also exert influence on the redox state, bioavailability and fate of Fe (Shaked & Lis, 2012).

1.6.3 Distribution of Fe in Antarctic sea ice

Since practices and standardization of sea ice, brine and seawater sampling procedures have been developed for trace metal analysis, an increasing number of field surveys have been performed to investigate the role of sea ice in the Fe cycle (Lannuzel et al., 2016b). Nevertheless, due to the extensive logistics and arduous working conditions imposed by the polar environment, data are still very sparse when considering the vast area that sea ice covers. The majority of sea-ice cores obtained for Fe biogeochemical investigations were collected in the Australian sector of Antarctica (between 90°E and 150°E; Figure 1.9). Table 1.1 reports background information for each of these expeditions (Lannuzel et al., 2016b). In addition to the lack of spatial coverage, most studies were carried out in spring and summer, usually on undeformed sea ice. Only a few studies have focused on the temporal aspect of Fe distribution

in sea ice (de Jong et al., 2013; de Jong et al., 2015; Lannuzel et al., 2008; Janssens et al., 2016; van der Merwe et al., 2011b).

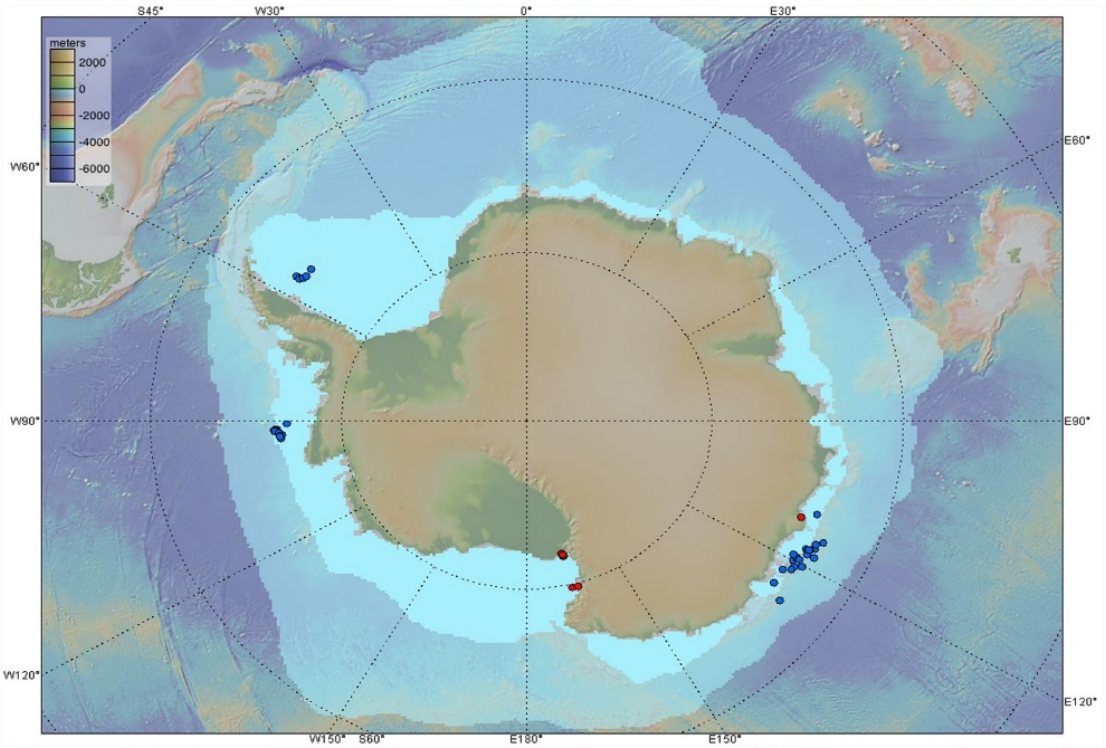

Figure 1.9 Map showing the locations of pack (blue) and fast (red) ice cores used for Fe analysis, with blue shades representing mean (1979–2007) maximal (September) and minimal (March) sea-ice extent. (Lannuzel et al., 2016b)

Table 1.1 List of sea-ice Fe data currently available in the literature. (Lannuzel et al, 2016 and references therein).

Ocean	Expedition	Sector	Year	Month	N. of cores	Type of ice	Water depth (m)	[DFe] (nM)	[Pfe] (nM)	[TDFe] (nM)
Southern Ocean	PNRA[a]	Ross Sea	1997, 1998	Nov	1	fast	430	n.a.	718–7,091	n.a.
	PNRA[b]	Ross Sea	2000, 2001	Nov–Dec	5	fast	430	1.07–5.98	26–1,162	n.a.
	CASEY[c]	South Pacific	2009	Nov	7	fast	17	2.1–81	40.2–6,828	33.8–4,240
	Scott Base[d]	Ross Sea	2003	Jan	6	fast	50–450	2.2–109	9–1,854	10–1,178
	ARISE[e]	South Pacific	2003	Sept–Oct	6	pack	> 1,000	2.6–26.0	n.a.	3.3–65.8
	ISPOL[f]	Weddell Sea	2004–2005	Nov–Jan	7	pack	> 500	0.7–36.8	2.0–141.2	2.3–97.8
	SIPEX[g]	South Pacific	2007	Sept–Oct	8	pack and fast	> 1,000	0.2–14.4	n.a.	1.2–378

	McMurdo[h]	Ross Sea	2009	Nov	3	fast	600	n.a.	12–9,318	n.a.
	SIPEX2[i]	South Pacific	2012	Sept–Nov	6	pack	> 1,000	0.9–17.4	0.04–990	n.a.
	SIMBA[j]	Bellingshausen Sea	2007	Oct	10	pack	> 1,000	1.1–30.2	n.a.	2.8–77.7
	AWECS[k]	Weddell Sea	2013	July	5	pack	500–4,000	1.0–3.2	20.1–254.1	n.a.

[a] Grotti et al. (2001)
[b] Grotti et al. (2005)
[c] van der Merwe et al. (2011b)
[d] de Jong et al. (2013)
[e] Lannuzel et al. (2007)
[f] Lannuzel et al. (2008)
[g] van der Merwe et al. (2011a)
[h] Noble et al. (2013)
[I] Lannuzel et al. (2016a)
[j] de Jong et al. (2015)
[k] Janssens et al. (2016)

Overall, higher concentrations (at least an order of magnitude) of all forms of Fe are found in both Antarctic fast and pack ice when compared to coastal and offshore seawater concentrations. Total dissolvable Fe (TDFe), defined as the fraction of the total iron dissolved at pH=1.8 after 6 months of storage, and PFe contribute to the majority of the Fe pool in sea ice. Nevertheless, Fe distribution and concentration in sea ice can be markedly heterogeneous, potentially reflecting the high variability of PFe concentrations observed between coastal and open waters in the Southern Ocean (Tagliabue et al., 2012). The dynamic interactions between autotroph and heterotrophs in the sea ice environment have direct implications for the temporal distribution of Fe since higher heterotrophic activity is expected during winter and higher autotrophic activity is expected in spring and summer (Riedel et al., 2007). A summary of the current Fe data available in sea ice is presented in Table 1.2.

Table 1.2 Summary statistics for Fe concentrations in Antarctic sea ice (Lannuzel et al, 2016b).

Parameter	DFe	TDFe	PFe
Number of cores with valid data	56 (11 fast, 45 pack)	50 (9 fast, 41 pack)	44 (14 fast, 30 pack)
Number of core sections with valid data	275	280	181
Mean fraction of core length sampled (%)	50	50	43
Concentration range (nmol L^{-1})	0.2–110	0.04–6,800	0.9–7,100
Mean concentration ± S.D. (nmol L^{-1})	9.8 ± 15.0	210 ± 660	310 ± 770
Median concentration (nmol L^{-1})	4.4	23	39

Mean inventory ± S.D. (μmol m^{-2})			
All	12 ± 21	250 ± 460	310 ± 480
Fast ice	22 ± 20	1,100 ± 500	930 ± 450
Pack ice	9.6 ± 20	70 ± 150	80 ± 220
Median inventory (μmol m^{-2})			
All	4.7	14	21
Fast ice	14	1,100	840
Pack ice	2.9	11	9.6

1.6.3.1 Land-fast ice

The relative abundance of Fe found in coastal seawater due to the proximity to landmass when compared to offshore areas (Martin, 1990) is reflected in the Fe concentrations observed in land-fast ice (Table 1.2). For example, significantly higher concentrations of PFe (0.96–214 nM) were found in fast ice compared to pack ice (0.87–77.7 nM) during a time series conducted in spring at the East Antarctica sector (van der Merwe et al., 2011b). Fast ice generally has a high lithogenic Fe fraction via sedimentary resuspension and lateral advection from the Antarctic continent (Lannuzel et al., 2016b). As a consequence, differences in depth and extent of the continental shelf might influence Fe distribution in sea ice (de Jong et al., 2013; Lannuzel et al., 2010). Tidal and winter vertical mixing influence would, therefore, assure the availability of bioactive micronutrients for coastal phytoplankton and sea-ice algae (Fitzwater et al., 2000; Lannuzel et al., 2010; Sedwick et al., 2000).

A high concentration of biogenic Fe content in land-fast ice is also observed due to extended light exposure at higher latitudes and biomass accumulation (Lannuzel et al., 2016b). Iron is generally more concentrated towards the bottom of the ice due to algae scavenging of Fe from seawater and/or brine drainage from upper layers, creating a characteristic fast-ice L-shape vertical profile for Fe and other biogeochemical parameters (Lannuzel et al., 2016b). However, the proximity to dust sources and active biomass can lead to a heterogeneous spatial and temporal distribution of Fe in land-fast ice. Nonetheless, the bioavailability of this (primarily lithogenic) Fe source for algal uptake is still not clear and further investigation is needed.

1.6.3.2 Pack ice

While the importance of sea ice as a reservoir of Fe in coastal waters can be deemed obsolete due to the close proximity to other Fe-rich sources, sea ice becomes prominent in open waters where other sources are less prevalent (Lannuzel et al., 2016a). Flux estimations suggest that most of Fe found in Antarctic pack ice come from marine sources, either via upwelling of Fe-rich waters or from the incorporation of biogenic material from the previous summer (Lannuzel et al., 2016a). The gradual solubilization of resuspended sediments during lateral transport from coastal waters could also influence the concentration of DFe in pack ice (Lannuzel et al., 2010). The highest concentrations of Fe in pack ice are normally found in the uppermost parts of the ice cover, presumably because of entrainment of Fe during frazil ice formation and/or due to snow-ice formation from flooding events, conferring a general C-shaped vertical profile distribution in pack ice. Although extremely high levels of Fe in the pack ice can occur as a result of advection of ice floes formed at higher latitudes, Lannuzel et al. (2010) showed that depth-averaged concentration of DFe in pack ice does not show significant large-scale spatial differences (e.g., East Antarctica versus Weddell sea).

Lastly, reported Fe:Al molar ratios indicate that Fe from biogenic origin dominates (>70%) the Fe pool in pack ice (Lannuzel et al., 2016a). Hosting communities with high production rates (Thomas & Dieckmann, 2010), pack ice might be an important spot of biotransformation of less bioavailable Fe fractions to more labile biogenic fractions. This suggests that the fertilization potential of PFe may have been previously underestimated due to the assumption that it is primarily lithogenic in composition (Lannuzel et al., 2014). A large fraction of the total Fe pool within sea ice might become bioavailable once released into seawater and therefore, effective in promoting primary productivity in the marginal ice zone during spring.

1.7 Distribution, speciation and bioavailability of other trace metals in sea ice.

Although Fe is the most limiting to phytoplankton in the SO and has the greatest effect on algal species diversity, other trace metal nutrients such as zinc (Zn), cobalt (Co), copper (Cu), and manganese (Mn) can also exert an important influence on the species abundance and composition of algal communities (Sunda et al., 2012). The distribution of metals other than Fe in sea ice has only recently started to be investigated. Pioneering work in Antarctic pack ice showed dissolved-to-total metal Mn Cu, Zn and Cd were found almost exclusively in the dissolved phase (Lannuzel et al., 2011). Still, concentrations of dissolved metals in bulk sea ice were comparable to those for oceanic waters. The dissolved-to-total ratio is significantly

reduced in fast ice compared to pack ice, possibly due to external inputs of both lithogenic and sedimentary material in the particulate phase (Grotti et al., 2005; Lannuzel et al., 2011). The speciation and bioavailability of bioactive elements, other than Fe, in the sea ice, however, remain unexplored.

In oceanic oxygenated seawater, dissolved Ni, Zn, and Cd (DNi, DZn and DCd) are present as soluble divalent cations or complexed to varying degrees by inorganic and/or organic chelators (Sunda et al., 2012). More than 98% of dissolved Zn is chelated by an unidentified strong organic ligand present at low concentrations in open waters (Bruland, 1989; Ellwood, 2004). Two distinct high and low-affinity Zn transport systems have been identified and are responsible for maintaining intracellular Zn concentrations in phytoplankton. Manganese, Cu and Co can be found in more than one oxidation state in oceanic waters, with different solubilities and binding strengths with organic ligands. Manganese exists in seawater as Mn(II), Mn(III), and Mn(IV), the last two as insoluble stable oxides in oxic waters. The particulate phase can be reduced chemically and photochemically to soluble Mn(II), which is not appreciably bound by organic ligands (Sunda & Huntsman, 1994). Dissolved Mn(II) can be taken up by phytoplankton by a single high-affinity transport system, which is controlled by a negative feedback regulation (Sunda & Huntsman, 1985, 1986). The thermodynamically stable form of Cu is Cu(II), which is found almost entirely chelated by strong organic ligands near-surface waters, although DCu stripped of ligands can be found in surface waters influenced by upwelled systems (Moffett & Dupont, 2007). Besides, photochemical reduction and re-oxidation cycles in surface waters can lead to a steady concentration of Cu(I), making up approximately 10% of the dissolved fraction (Moffett & Zika, 1988). Uptake of Cu is a function of the concentration of the dissolved free metal species. Finally, at seawater pH, Co co-exists as soluble Co(II), strongly chelated dissolved Co(III) or insoluble Co(III) oxides. Like Cd, uptake of Co occurs via an inducible transport system which can be down-regulated when environmental and intracellular Zn' are too high (Sunda, 2012).

1.8 Sea ice primary productivity and Fe fertilization

Sea ice provides a vast habitat for productive microbial communities of algae, bacteria, archaea, heterotrophic protists, fungi and viruses living at the base, in the interior and the surface layers of sea-ice floes (Thomas & Dieckmann, 2010). Diatoms dominate algal biomass during the bloom period (Ligowski et al., 2012). They are also the biggest contributors to global

primary production in the ocean and are important exporters of organic carbon and silica to the seafloor (Smetacek, 1999). Maximum carbon uptake rates recorded in land-fast sea ice exceed 1 g C m^{-2} d^{-1} (Arrigo et al., 1995, Grossi et al., 1987) whereas primary production in Antarctic pack ice shows much lower rates, with values reaching 60 mg C m^{-2} d^{-1} (Roukaerts et al., 2016).

Primary production via photosynthesis involves complex processes of light harvesting, electron transport and carbon fixation that have different sensitivities not only to cellular control but also to environmental conditions such as light intensity and quality, temperature, salinity and nutrient availability. Therefore, the type of sea ice and associated gradient of environmental conditions control sea-ice algal primary productivity. A major factor controlling Antarctic sea-ice algae growth is the presence of nutrients (Saenz & Arrigo 2014). Because of that, algae usually flourish in the lower-most 0.2m of the ice cover where it is most tightly coupled to the underlying seawater and conditions are usually more stable and favourable (Figure 1.10; Thomas & Dieckmann, 2010). Within the ice interior, sea-ice algae can be limited by high salinities, low temperatures, lack of space and low nutrients within the brine system. Internal communities are often subjected to the largest environmental fluctuations and often associated with the more porous frazil ice (Thomas & Dieckmann, 2010). Overall, autotrophic flagellates characterize surface communities, mixed microalgal populations form interior communities and pennate diatoms dominate bottom communities (van Leeuwe et al., 2018).

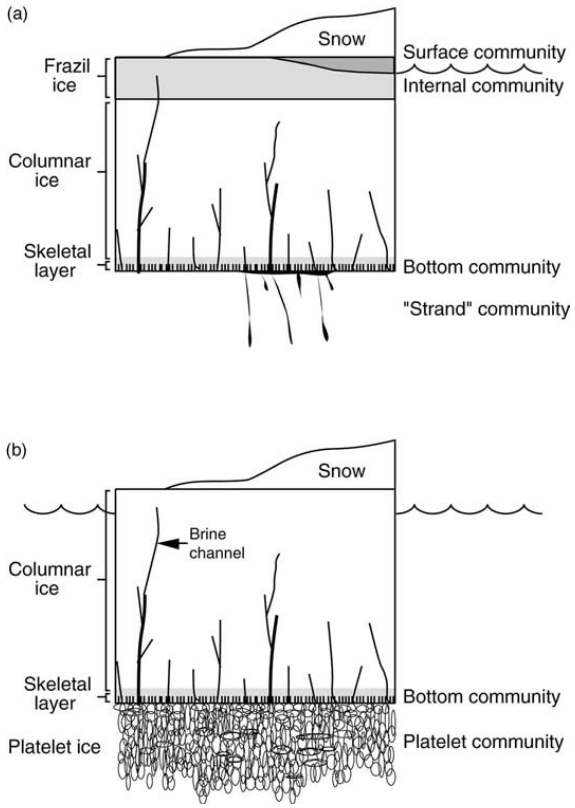

Figure 1.10 Illustration of the vertical distribution of sea ice communities in pack (a) and fast (b) sea ice. Pack ice sea algae normally grow at the bottom and near the sea surface in the porous frazil ice where light levels are high and the ice surface is commonly flooded with nutrients. In land-fast sea ice, the growth in the skeletal layer is determined primarily by the salinity and by the thickness of the overlying snow cover through its effect on vertical light attenuation. (Thomas & Dieckmann, 2010)

While during the early spring under-ice ocean productivity is limited by irradiance, later in spring when light conditions improve, pack ice starts to melt and releases Fe to the water column in a matter of days (70% Fe loss over 10 days) (Lannuzel et al., 2008; Smith Jr. et al., 2000). The fertilization potential of melting sea ice has been widely discussed, with measured Fe concentrations in under-ice seawater well above those generally measured in ice-free waters (de Jong et al., 2013). Based on *in situ* observation, van der Merwe et al. (2011b) showed that a square meter of sea ice has a fertilization potential for 419 m^3 of Southern Ocean water with total dissolvable Fe (TDFe) and 49 m^3 with DFe. Elevated concentrations of Fe coincide with increased productivity, phytoplankton biomass increase, and macronutrient drawdown. This indicates that Fe availability influences the uptake of N, P and Si by phytoplankton and, hence, controls the location, timing and duration of ice-edge blooms, and their contribution to the biological carbon pump (Arrigo et al., 2008a; Fitzwater et al., 2000; Sedwick & DiTullio, 1997).

Although numerous studies have addressed the importance of Fe in the Southern Ocean, there is still very limited information on the individual response of sea-ice algal species to Fe limitation. Models and field-based studies largely rely on experiments conducted on phytoplankton cultures. The Fe limitation has been shown to reduce photosynthetic pigment content, light absorption, storage of carbohydrates, growth and quantum yield (ratio between carbon assimilated to photons absorbed) in pelagic diatoms in the SO (Pankowski & McMinn, 2009; Timmermans et al., 2004). Considerable distinctions in Fe use efficiencies have been reported for different species of microalgae adapted to different habitats. The harsh conditions experienced by sea-ice algae might have exerted a significant evolutionary pressure on sea-ice algae to develop a unique Fe metabolism (Pankowski & McMinn, 2009). How changes to the physiology will change ice algae abundance and diversity, and therefore, the seeding potential of ice algae in the MIZ is unclear.

The assessment of the large-scale contribution of Antarctic sea ice to the SO primary production has been proven to be challenging with only a few estimates from direct and indirect techniques. Sea-ice primary productivity was estimated from extrapolation of *in situ* measurements and numerical models, ranging between ~10 to 70 Tg C yr^{-1} (Arrigo, 1997; Saenz & Arrigo, 2014, Jeffery et al., 2020) with a total Seasonal Sea Ice Zone productivity of ~140 – 180 Tg C yr^{-1} (Arrigo et al., 2008b; Deppeler & Davidson, 2017) including the marginal ice zone. Total primary production in the Southern Ocean (waters south of 50°S) was assessed by satellite colour imagery using a primary production algorithm parameterized for SO waters and was estimated at approximately 1,949 ± 70.1 Tg C yr^{-1} (Arrigo et al., 2008b). Therefore, up to 10% of the primary productivity of the Southern Ocean might be associated with the presence of sea ice. Nevertheless, these estimations carry lots of assumptions and uncertainties and they might have greatly underestimated total production in the ice. So far, models do not account for complex features like leads, pressure ridges, rafted ice and platelet ice. It is also possible that models underestimate the upper and freeboard communities notable because production there is sustained by processes such as surface flooding, snow loading and remineralization that are rather simply parameterized (Jeffery et al., 2020).

Satellite imagery has limited reach for evaluating phytoplankton blooms under the usually very cloudy circum-Antarctic waters, and it has no applicable use to assess sea-ice algae productivity in and under the refractive sea ice barrier. Finally, present data of sea-ice Chl*a* and other biochemical parameters are still very sparse (Fripiat et al. 2017; Meiners et al. 2012).

The expansion of *in situ* sea-ice data and/or the development of new remote sensing technologies could accelerate the characterization of the magnitude and variability of the horizontal distribution of sea-ice algae underneath the ice pack contributing, therefore, to more accurate estimations for primary productivity (Meiners et al. 2017).

1.9 Final remarks

In the last decades, a better understanding of the importance of sea ice in the polar ecosystem has been achieved. Notably, sea ice can harvest and recycle macro- and micronutrients, nurturing microorganism communities that are at the base of the marine Antarctic food web. Besides, sea ice regulates the ocean dynamics, biogeochemical cycles, carbon export, atmospheric composition and the global radiation budget. While physical interactions between ocean, atmosphere and sea ice are integrated into current Earth System Models biogeochemical processes have so far been left out sea ice. This is because uncertainties remain such as on the temporal and spatial distribution of Fe and other trace metals in ice-covered waters, their incorporation pathways, and the reciprocal interactions between trace metals and sea-ice biota. Under these circumstances, this PhD work aims to increase our understanding of the distribution of the key nutrients Fe, Cd, Co, Mn, Ni Cu and Zn in East Antarctica sea ice and how they shape sea-ice biology from winter to late summer.

1.10 References

Achterberg, E. P., T. W. Holland, A. R. Bowie, R. Fauzi, C. Mantoura, & P. J. W. (2001). Determination of iron in seawater. *Analytica Chimica Acta,* 442, 1–14. https://doi.org/10.1016/S0003-2670(01)01091-1

Ackley, S. F., & C. W. Sullivan (1994). Physical controls on the development and characteristics of Antarctic sea ice biological communities - A review and synthesis. *Deep Sea Research*, 41, 1583–1604. https://doi.org/10.1016/0967-0637(94)90062-0

Arrigo, K. R. (1997). Primary Production in Antarctic Sea Ice. *Science,* 276(5311), 394-397. https://doi.org/10.1126/science.276.5311.394

Arrigo, K. R. (2003). Phytoplankton dynamics within 37 Antarctic coastal polynya systems. *Journal of Geophysical Research,* 108(C8), 1-18. https://doi.org/10.1029/2002jc001739

Arrigo, K. R., G. van Dijken, & M. Long (2008a). Coastal Southern Ocean: A strong anthropogenic CO_2 sink. *Geophysical Research Letters,* 35(21). https://doi.org/10.1029/2008GL035624

Arrigo, K. R., G. van Dijken, & S. Bushinsky (2008b). Primary production in the Southern Ocean, 1997-2006. *Journal of Geophysical Research-Oceans,* 113(C8). https://doi.org/10.1029/2007jc004551

Balzano, S., P. J. Statham, R. D. Pancost, & J. R. Lloyd (2009). Role of microbial populations in the release of reduced iron to the water column from marine aggregates. *Aquatic Microbial Ecology,* 54, 291-303. https://doi.org/10.3354/ame01278

Barbeau, K. (2006). Photochemistry of Organic Iron(llI) Complexing Ligands in Oceanic Systems. *Photochemistry and Photobiology*, 82, 1505-1501. https://doi.org/10.1111/j.1751-1097.2006.tb09806.x

Blain, S., B. Queguiner, L. Armand, S. Belviso, B. Bombled, L. Bopp et al. (2007). Effect of natural iron fertilization on carbon sequestration in the Southern Ocean. *Nature*, 446(7139), 1070-1074. https://doi.org/10.1038/nature05700

Behrenfeld, M. J., O'Malley, R. T., Siegel, D. A., McClain, C. R., Sarmiento, J. L., Feldman, G. C. et al. (2006). Climate-driven trends in contemporary ocean productivity. *Nature*, 444(7120), 752-755. doi:10.1038/nature05317. https://doi.org/10.1038/nature05317

Boyd, P. W., & M. J. Ellwood (2010). The biogeochemical cycle of iron in the ocean. *Nature Geoscience* 3(10), 675-682. https://doi.org/10.1038/ngeo964

Boyd, P. W., A. J. Watson, C. S. Law, E. R. Abraham, T. Trull, R. Murdoch et al. (2000). A mesoscale phytoplankton bloom in the polar Southern Ocean stimulated by iron fertilization. *Nature*, 407(6805), 695-702. https://doi.org/10.1038/35037500

Breitbarth, E., R. J. Bellerby, C. C. Neill, M. V. Ardelan, M. Meyerhofer, E. Zollner et al. (2010). Ocean acidification affects iron speciation during a coastal seawater mesocosm experiment. *Biogeosciences*, 7(3), 1065-1073. https://doi.org/10.5194/bg-7-1065-2010

Bruland, K. W. (1989). Complexation of zinc by natural organic ligands in the central North Pacific. *Limnology and Oceanography*, 34(2), 269-285. https://doi.org/10.4319/lo.1989.34.2.0269

Comiso, J. (2003). Large-scale characteristics and variability of the global sea ice cover. *Sea Ice: An Introduction to Its Physics, Chemistry, Biology and Geology*. Oxford, Blackwell Scientific Publishing, 112 -142. https://doi.org/10.1002/9780470757161.ch4

Comiso, J. (2010). *Variability and trends of the global sea ice cover* In: *Sea Ice*. Oxford, UK, Wiley-Blackwell. https://doi.org/10.1002/2017JC012768

Comiso, J. C., N. G. Maynard, W. O. Smith, & C. W. Sullivan (1990). Satellite Ocean Color Studies of Antarctic Ice Edges in Summer and Autumn. *Journal of Geophysical Research-Oceans*, 95(C6), 9481-9496. https://doi.org/10.1029/JC095iC06p09481

Croot, P. L., A. R. Bowie, R. D. Frew, M. T. Maldonado, J. A. Hall, K. A. Safi et al. (2001). Retention of dissolved iron and FeII in an iron induced Southern Ocean phytoplankton bloom. *Geophysical Research Letters*, 28(18), 3425-3428. https://doi.org/10.1029/2001gl013023

de Baar, H., J. de Jong, D. Bakker, B. Löscher, C. Veth, U. Bathmann, & V. Smetacek (1995). Importance of iron for plankton blooms and carbon dioxide drawdown in the Southern Ocean. *Nature*, 373, 412-415.

de Jong, A., V. Schoemann, N. Maricq, N. Mattielli, L. Patricia, H. T., & J. L. Tison (2013). Iron in land-fast sea ice of McMurdo Sound derived from sediment resuspension and wind-blown dust

attributes to primary productivity in the Ross Sea, Antarctica. *Marine Chemistry*, 157, 24–40. https://doi.org/10.1016/j.marchem.2013.07.001

de Jong, J. T. M., S. E. Stammerjohn, S. F. Ackley, J. L. Tison, N. Mattielli, & V. Schoemann (2015). Sources and fluxes of dissolved iron in the Bellingshausen Sea (West Antarctica): The importance of sea ice, icebergs and the continental margin. *Marine Chemistry*, 177, 518-535. https://doi.org/10.1016/j.marchem.2015.08.004

Decho, A. W., & T. Gutierrez (2017). Microbial Extracellular Polymeric Substances (EPSs) in Ocean Systems. *Frontiers of Microbiology*, 8, 922. https://doi.org/10.3389/fmicb.2017.00922

Deppeler, S. L. and A. T. Davidson (2017). Southern Ocean Phytoplankton in a Changing Climate. *Frontiers in Marine Science*, 4. https://doi.org/10.3389/fmars.2017.00040

Dieckmann, G., & H. Hellmer (2010). *The Importance of Sea Ice: An Overview*. Oxford, UK., Wiley-Blackwell. https://doi.org/10.1002/9781444317145.ch1

Ellwood, M. J. (2004). Zinc and cadmium speciation in subantarctic waters east of New Zealand. *Marine Chemistry*, 87(1-2), 37-58. https://doi.org/10.1016/j.marchem.2004.01.005

Falkowski, P. G., R. T. Barber, & V. V. Smetacek (1998). Biogeochemical Controls and Feedbacks on Ocean Primary Production. *Science*, 281(5374), 200-207. https://doi.org/10.1126/science.281.5374.200

Field, C. B., M. J. Behrenfeld, J. T. Randerson, & P. Falkowski (1998). Primary production of the biosphere: integrating terrestrial and oceanic components. *Science*, 281(5374), 237-240. https://doi.org/10.1126/science.281.5374.237

Fitzwater, S. E., K. S. Johnson, R. M. Gordon, K. H. Coale, & W. O. Smith (2000). Trace metal concentrations in the Ross Sea and their relationship with nutrients and phytoplankton growth. *Deep Sea Research Part II: Topical Studies in Oceanography*, 47(15-16), 3159-3179. https://doi.org/10.1016/S0967-0645(00)00063-1

Fripiat, F., K. M. Meiners, M. Vancoppenolle, S. Papadimitriou, D. N. Thomas, S. F. Ackley et. al. (2017). Macro-nutrient concentrations in Antarctic pack ice: Overall patterns and overlooked processes. *Elementa-Science of the Anthropocene*, 5(13), 2-24. https://doi.org/10.1525/elementa.217

Genovese, C., M. Grotti, J. Janssens, K. Wutting, F. Ardini, S. Moreau, & D. Lannuzel (2018). Influence of organic complexation on dissolved iron distribution in East Antarctic pack ice. *Marine Chemistry*, 203, 28-37. https://doi.org/10.1016/j.marchem.2018.04.005

Goosse, H., J. E. Kay, K. C. Armour, A. Bodas-Salcedo, H. Chepfer, D. Docquier et al. (2018). Quantifying climate feedbacks in polar regions. *Nature Communications*, 9(1), 1919 https://doi.org/10.1038/s41467-018-04173-0

Gradinger, R. & J. Ikavalko (1998). Organism incorporation into newly forming Arctic sea ice in the Greenland Sea. *Journal of Plankton Research*, 20(5), 871-886. https://doi.org/10.1093/plankt/20.5.871

Grotti, M., F. Soggia, M. L. Abelmoschi, P. Rivaro, E. Magi, & R. Frache (2001). Temporal distribution of trace metals in Antarctic coastal waters. *Marine Chemistry*, 76(3), 189-209. https://doi.org/10.1016/s0304-4203(01)00063-9

Grotti, M., F. Soggia, C. Ianni, & R. Frache (2005). Trace metals distributions in coastal sea ice of Terra Nova Bay, Ross Sea, Antarctica. *Antarctic Science*, 17(2), 289-300. https://doi.org/10.1017/s0954102005002695

Hassler, C. S., E. Alasonati, M. Nichols, & V. I. Slaveykova (2011a). Exopolysaccharides produced by bacteria isolated from the pelagic Southern Ocean - Role in Fe binding, chemical reactivity, and bioavailability. *Marine Chemistry*, 123(1–4), 88-98. https://doi.org/10.1016/j.marchem.2010.10.003

Hassler, C. S., & V. Schoemann (2009). Bioavailability of organically bound Fe to model phytoplankton of the Southern Ocean. *Biogeosciences*, 6, 2281–2296. https://doi.org/10.5194/bg-6-2281-2009

Hassler, C. S., V. Schoemann, C. M. Nichols, E. C. Butler, & P. W. Boyd (2011b). Saccharides enhance iron bioavailability to Southern Ocean phytoplankton. *Proceedings of the National Acadamy of Sciences*, U S A 108(3), 1076-1081. https://doi.org/10.1073/pnas.1010963108

Hunter, K. A., & P. W. Boyd (2007). Iron-binding ligands and their role in the ocean biogeochemistry of iron. *Environmental Chemistry*, 4(4). https://doi.org/10.1071/En07012

IPCC (2014). Climate Change 2014: Synthesis Report. Contribution of Working Groups I, II and III to the Fifth Assessment Report of the Intergovernmental Panel on Climate Change. IPCC, Geneva, Switzerland., 151.

Janssens, J., K. M.Meiners, A. T. Townsend, & D. Lannuzel (2018). Organic matter controls iron incorporation in growing sea ice. *Frontiers in Earth Science*, 6. https://doi.org/10.3389/feart.2018.00022

Janssens, J., K. M. Meiners, J.-L. Tison, G. Dieckmann, B. Delille, & D. Lannuzel (2016). Incorporation of iron and organic matter into young Antarctic sea ice during its initial growth stages. *Elementa: Science of the Anthropocene*, 4, 000123. https://doi.org/10.12952/journal.elementa.000123

Jeffery, N., M. E. Maltrud, E. C. Hunke, S. Wang, J. Wolfe, A. K. Turner et al. (2020). Investigating controls on sea ice algal production using E3SMv1.1-BGC. *Annals of Glaciology*, 61(82), 51-72. https://doi.org/10.1017/aog.2020.7

Jeffries, M., A. Raymond, K. Morris, A. Veazey, & H. Krouse (1994). Crystal structure, stable isotopes (B 180), and development of sea ice in the Ross, Amundsen, and Bellingshausen seas, Antarctica. *Journal of Geophysical Research*, 99, 985-995. https://doi.org/10.1029/93JC02057

Johnson, K. S., K. H. Coale, V. A. Elrod, & N. W. Tindale (1994). Iron photochemistry in seawater from the equatorial Pacific. *Marine Chemistry*, 46(4), 319-334. https://doi.org/10.1016/0304-4203(94)90029-9

Johnson, K. S., R. M. Gordon, & C. K.H. (1997). What controls dissolved iron concentrations in the world ocean? *Marine Chemistry*, 57, 137-161. https://doi.org/10.1016/s0304-4203(97)00043-1

Kämpf, J., & P. Chapman (2016). *Upwelling Systems of the World: A Scientific Journey to the Most Productive Marine Ecosystems*, Springer. https://doi.org/10.1007/978-3-319-42524-5

Krembs, C., H. Eicken, & J. W. Deming (2011). Exopolymer alteration of physical properties of sea ice and implications for ice habitability and biogeochemistry in a warmer Arctic. *Proceedings of the National Academy of Sciences*, U S A, 108(9), 3653-3658. https://doi.org/10.1073/pnas.1100701108

Kuma, K., J. Nishioka, & K. Matsunaga (1996). Controls on iron(III) hydroxide solubility in seawater: The influence of pH and natural organic chelators. *Limnology and Oceanography*, 41(3), 396-407. https://doi.org/10.4319/lo.1996.41.3.0396

Kustka, A. B., A. Allen, & F. M. Morel (2007). Sequence analysis and transcriptational regulation of iron acquisition genes in two marine diatoms. *Journal of Phycology*. 43(4), 715-729 https://doi.org/10.1111/j.1529-8817.2007.00359.x

Lannuzel, D., A. R. Bowie, P. C. van der Merwe, A. T. Townsend, & V. Schoemann (2011). Distribution of dissolved and particulate metals in Antarctic sea ice. *Marine Chemistry*, 124(1-4), 134-146. https://doi.org/10.1016/j.marchem.2011.01.004

Lannuzel, D., F. Chever, P. van der Merwe, J. Janssens, A. Roukaerts, A. Cavagna et al. (2016a). Iron biogeochemistry in Antarctic pack ice during SIPEX-2. *Deep Sea Research Part II: Topical Studies in Oceanography*, 131, 111-122. https://doi.org/10.1016/j.dsr2.2014.12.003

Lannuzel, D., M. Grotti, M. L. Abelmoschi, & P. van der Merwe (2015). Organic ligands control the concentrations of dissolved iron in Antarctic sea ice. *Marine Chemistry*, 174, 120-130. https://doi.org/10.1016/j.marchem.2015.05.005

Lannuzel, D., V. Schoemann, J. de Jong, L. Chou, B. Delille, S. Becquevort, & J.-L. Tison (2008). Iron study during a time series in the western Weddell pack ice. *Marine Chemistry*, 108(1-2), 85-95. https://doi.org/10.1016/j.marchem.2007.10.006

Lannuzel, D., V. Schoemann, J. de Jong, B. Pasquer, P. van der Merwe, F. Masson et al. (2010). Distribution of dissolved iron in Antarctic sea ice: Spatial, seasonal, and inter-annual variability. *Journal of Geophysical Research*, 115: G03022. https://doi.org/0.1029/2009JG001031

Lannuzel, D., V. Schoemann, J. de Jong, J.-L. Tison, & L. Chou (2007). Distribution and biogeochemical behaviour of iron in the East Antarctic sea ice. *Marine Chemistry*, 106(1-2), 18-32. https://doi.org/10.1016/j.marchem.2006.06.010

Lannuzel, D., P. C. van der Merwe, A. T. Townsend and A. R. Bowie (2014). Size fractionation of iron, manganese and aluminium in Antarctic fast ice reveals a lithogenic origin and low iron solubility. *Marine Chemistry*, 161, 47-56. https://doi.org/10.1016/j.marchem2014.02.006

Lannuzel, D., M. Vancoppenolle, P. van der Merwe, J. de Jong, K. M. Meiners, M. Grotti et al. (2016b). Iron in sea ice: Review and new insights. *Elementa: Science of the Anthropocene*, 4, 000130. https://doi.org/10.12952/journal.elementa.000130

Leonard, G. H., P. J. Langhorne, M. J. M. Williams, R. Vennell, C. R. Purdie, D. E. Dempsey et al. (2011). Evolution of supercooling under coastal Antarctic sea ice during winter. *Antarctic Science*, 23(04), 399-409. https://doi.org/10.1017/S0954102011000265

Ligowski, R., R. W. Jordan, & P. Assmy (2012). Morphological adaptation of a planktonic diatom to growth in Antarctic sea ice. *Marine Biology*, 159(4), 817-827. https://doi.org/10.1007/s00227-011-1857-6

Liu, X., & F. J. Millero (2002). The solubility of iron in seawater. *Marine Chemistry*, 77(1), 43-54. https://doi.org/10.1016/S0304-4203(01)00074-3

Lizzotte, M. P. (2001). The Contributions of Sea Ice Algae to Antarctic Marine Primary Production. *American Zoologist*, 41, 57–73. https://doi.org/10.1668/0003-1569(2001)041[0057:Tcosia]2.0.Co;2

Maher, B. A., J. M. Prospero, D. Mackie, D. Gaiero, P. P. Hesse, & Y. Balkanski (2010). Global connections between aeolian dust, climate and ocean biogeochemistry at the present day and at the last glacial maximum. *Earth-Science Reviews*, 99(1-2), 61-97. https://doi.org/10.1016/j.earscirev.2009.12.001

Martin, J. H. (1990). Glacial-interglacial CO2 change: The Iron Hypothesis. *Paleoceanography*, 5(1), 1-13. https://doi.org/10.1029/PA005i001p00001

Massom, R., P. Reid, S. Stammerjohn, B. Raymond, A. Fraser, & S. Ushio (2013). Change and variability in East antarctic sea ice seasonality, 1979/80-2009/10. *PLoS One* 8(5), e64756. https://doi.org/10.1371/journal.pone.0064756

Massom, R., & S. Stammerjohn (2010). Antarctic sea ice change and variability – Physical and ecological implications. *Polar Science*, 4(2), 149-186. https://doi.org/10.1016/j.polar.2010.05.001

McGhee, R. (2006). The Last Imaginary Place: A Human History of the Arctic World. Oxford, Oxford University Press. https://doi.org/10.1111/j.1467-9655.2006.00359_4.x.

Meiners, K., C. Krembs, & R. Gradinger (2008). Exopolymer particles: microbial hotspots of enhanced bacterial activity in Arctic fast ice (Chukchi Sea). *Aquatic Microbial Ecology*, 52(2), 195-207. https://doi.org/10.3354/ame01214

Meiners, K. M., M. Vancoppenolle, S. Thanassekos, G. S. Dieckmann, D. N. Thomas, J. L. Tison, et al. (2012). Chlorophylla in Antarctic sea ice from historical ice core data. *Geophysical Research Letters*, 39(21), n/a-n/a. https://doi.org/10.1029/2012gl053478

Meiners, K. M., & C. Michel (2017). *Dynamics of nutrients, dissolved organic matter and exopolymers in sea ice.* In: *Thomas, DN (ed.), Sea Ice*. Oxford, UK: Wiley-Blackwell: Wiley-Blackwell. https://doi.org/10.1002/9781118778371.ch17

Moffett, J. W. & Dupont, C. (2007). Cu complexation by organic ligands in the sub-arctic NW Pacific and Bering Sea. *Deep Sea Research Part I: Oceanographic Research Papers*, 54(4), 586-595. https://doi.org/10.1016/j.dsr.2006.12.013

Moreau, S., M. Vancoppenolle, L. Bopp, O. Aumont, G. Madec, B. Delille et al. (2016). Assessment of the sea-ice carbon pump: Insights from a three-dimensional ocean-sea-ice biogeochemical model (NEMO-LIM-PISCES). *Elementa: Science of the Anthropocene*, 4. https://doi.org/10.12952/journal.elementa.000122

Morel, F. M., A. B. Kustka, & Y. Shaked (2008). The role of unchelated Fe in the iron nutrition of phytoplankton. *Limnology and Oceanography*, 53(1), 400-404. https://doi.org/10.4319/lo.2008.53.1.0400

Noble, A. E., D. M. Moran, A. E. Allen & M. A. Saito (2013). Dissolved and particulate trace metal micronutrients under the McMurdo Sound seasonal sea ice: Basal sea ice communities as a capacitor for iron. Frontiers in Chemistry, 1(25): 25. https://doi.org/10.3389/fchem.2013.00025

Ogura, T. (2004). Effects of sea ice dynamics on the Antarctic sea ice distribution in a coupled ocean atmosphere model. *Journal of Geophysical Research*, 109(C4). https://doi.org/10.1029/2003jc002022

Pankowski, A., & A. McMinn (2009). Iron availability regulates growth, photosynthesis, and production of ferredoxin and flavodoxin in Antarctic sea ice diatoms. *Aquatic Biology*, 4(3), 273-288. https://doi.org/10.3354/ab00116

Petit, J., J. Jouzel, D. Raynaud, N. Barkov, J.-M. Barnola, I. Basile et al. (1999). Climate and atmospheric history of the past 420,000 years from the Vostok ice core, Antarctica. *Nature*, 399, 429 - 436. https://doi.org/10.1038/20859

Ratnarajah, L., A. R. Bowie, D. Lannuzel, K. M. Meiners, & S. Nicol (2014). The biogeochemical role of baleen whales and krill in Southern Ocean nutrient cycling. *PLoS One*, 9(12), e114067. https://doi.org/10.1371/journal.pone.0114067

Riedel, A., C. Michel, & M. Gosselin (2007). Grazing of large-sized bacteria by sea-ice heterotrophic protists on the Mackenzie Shelf during the winter–spring transition. *Aquatic Microbial Ecology*, 50, 25-38. https://doi.org/10.3354/ame01155

Rignot, E., J. Mouginot, B. Scheuchl, M. van den Broeke, M. J. van Wessem, & M. Morlighem (2019). Four decades of Antarctic Ice Sheet mass balance from 1979–2017. *Proceedings of the National Academy of Sciences*, 116(4), 1095-1103. https://doi.org/10.1073/pnas.1812883116

Rintoul, S. & Sparrow, M. (2001). Re: The Role of Antarctica and the Southern Ocean in Past, Present and Future Climate: A Strategy for the International Polar Year

Rose, A. L. (2012). The influence of extracellular superoxide on iron redox chemistry and bioavailability to aquatic microorganisms. *Frontiers of Microbiology,* 3, 124. https://doi.org/10.3389/fmicb.2012.00124

Roy, E., & M. Wells (2008). Persistence of iron(II) in surface waters of the western subarctic Pacific. *Limnology and Oceanography*, 53(1), 89–98. https://doi.org/10.4319/lo.2008.53.1.0089

Saenz, B. T., & K. R. Arrigo (2014). Annual primary production in Antarctic sea ice during 2005-2006 from a sea ice state estimate. *Journal of Geophysical Research-Oceans*, 119(6), 3645-3678. https://doi.org/10.1002/2013jc009677

Saiz-Lopez, A., C. S. Blaszczak-Boxe, & L. J. Carpenter (2015). A mechanism for biologically induced iodine emissions from sea ice. *Atmospheric Chemistry and Physics*, 15(17), 9731-9746. https://doi.org/10.5194/acp-15-9731-2015

Sarmiento, J., & N. Gruber (2005). *Ocean Biogeochemical dynamics*. Princeton, New Jersey and Los Angeles, California, Princeton University Press. https://doi.org/10.1063/1.2754608

Schoffman, H., H. Lis, Y. Shaked, & N. Keren (2016). Iron-Nutrient Interactions within Phytoplankton. *Frontiers in Plant Science*, 7, 1223. https://doi.org/10.4319/lo.1998.43.7.1427

Sedwick, P. N., & G. R. DiTullio (1997). Regulation of algal blooms in Antarctic Shelf Waters by the release of iron from melting sea ice. *Geophysical Research Letters*, 24(20), 2515-2518. https://doi.org/10.1029/97gl02596

Sedwick, P. N., G. R. DiTullio, & D. J. Mackey (2000). Iron and manganese in the Ross Sea, Antarctica: Seasonal iron limitation in Antarctic shelf waters. *Journal of Geophysical Research-Oceans*, 105(C5), 11321-11336. https://doi.org/10.1029/2000jc000256

Shaked, Y., & H. Lis (2012). Disassembling iron availability to phytoplankton. *Frontiers of Microbiology*, 3, 123. https://doi.org/10.3389/fmicb.2012.00123

Sigman, D. M., M. P. Hain, & G. H. Haug (2010). The polar ocean and glacial cycles in atmospheric CO(2) concentration. *Nature*, 466(7302), 47-55. https://doi.org/10.1038/nature09149

Smetacek, V. (1999). Diatoms and the Ocean Carbon Cycle. *Protist*, 150, 25-32. 10.1016/S1434-https://doi.org/4610(99)70006-4

Smith Jr., W., J. Marra, M. Hiscock, & R. Barber (2000). The seasonal cycle of phytoplankton biomass and primary productivity in the Ross Sea, Antarctica. *Deep-Sea Research II*, 47, 3119-3140. https://doi.org/10.1016/S0967-0645(00)00061-8

Sunda, W. G. (2012). Feedback Interactions between Trace Metal Nutrients and Phytoplankton in the Ocean. *Frontiers of Microbiology*, 3, 204. https://doi.org/10.3389/fmicb.2012.00204

Sunda, W. G., & S. A. Huntsman (1985). Regulation of cellular manganese and manganese transport rates in the unicellular alga Chlamydomonas. *Limnology and Oceanography*, 30(1), 71-80 https://doi.org/10.4319/lo.1985.30.1.0071

Sunda, W. G., & S. A. Huntsman (1986). Relationships among Growth Rate, Cellular Manganese Concentrations and Manganese Transport Kinetics in Estuarine and Oceanic Species of the Diatom Thalassiodira. *Journal of Phycology*, 22(3), 259-270. https://doi.org/10.1111/j.1529-8817.1986.tb00022.x

Sunda, W. G., & S. A. Huntsman (1994). Photoreduction of manganese oxides in seawater. *Marine Chemistry*, 46(1-2), 133-152. https://doi.org/10.1016/0304-4203(94)90051-5

Tagliabue, A., & K. R. Arrigo (2006). Processes governing the supply of iron to phytoplankton in stratified seas. *Journal of Geophysical Research*, 111(C6). https://doi.org/10.1029/2005jc003363

Tagliabue, A., T. Mtshali, O. Aumont, A. R. Bowie, M. B. Klunder, A. N. Roychoudhury, & S. Swart (2012). A global compilation of dissolved iron measurements: focus on distributions and processes in the Southern Ocean. *Biogeosciences*, 9(6), 2333-2349. https://doi.org/10.5194/bg-9-2333-2012

Takahashi, T., S. C. Sutherland, R. Wanninkhof, C. Sweeney, R. A. Feely, D. W. Chipman et al. (2009). Climatological mean and decadal change in surface ocean pCO2, and net sea–air CO2 flux over the global oceans. *Deep Sea Research Part II: Topical Studies in Oceanography*, 56(8-10), 554-https://doi.org/577. 10.1016/j.dsr2.2008.12.009

Thomas, D., & G. Dieckmann (2010). *Sea Ice*. Wiley-Blackwell, Wiley-Blackwell. https://doi.org/10.1002/9781444317145

Timmermans, K. R., B. v. d. Wagt, & H. J. W. d. Baar (2004). Growth rates, half-saturation constants, and silicate, nitrate, and phosphate depletion inrelation to iron availability of four large, open-ocean diatoms from the Southern Ocean. *Limnology and.Oceanography*, 49(6), 2141–2151. https://doi.org/10.4319/lo.2004.49.6.2141

Tison, J. L., A. Worby, B. Delille, F. Brabant, S. Papadimitriou, D. Thomas et al. (2008). Temporal evolution of decaying summer first-year sea ice in the Western Weddell Sea, Antarctica. *Deep-Sea Research Part II-Topical Studies in Oceanography*, 55(8-9), 975-987. https://doi.org/10.1016/j.dsr2.2007.12.021

Trevena, A., & G. Jones (2012). DMS flux over the Antarctic sea ice zone. *Marine Chemistry*, 134-135, 47-58. https://doi.org/10.1016/j.marchem.2012.03.001

van der Merwe, P., D. Lannuzel, A. R. Bowie, C. A. Mancuso Nichols, & K. M. Meiners (2011a). Iron fractionation in pack and fast ice in East Antarctica: Temporal decoupling between the release of dissolved and particulate iron during spring melt. *Deep Sea Research Part II: Topical Studies in Oceanography*, 58(9-10), 1222-1236. https://doi.org/10.1016/j.dsr2.2010.10.036

van der Merwe, P., D. Lannuzel, A. R. Bowie, & K. M. Meiners (2011b). High temporal resolution observations of spring fast ice melt and seawater iron enrichment in East Antarctica. *Journal of Geophysical Research*, 116(G3). https://doi.org/10.1029/2010jg001628

van der Merwe, P., D. Lannuzel, C. A. M. Nichols, K. Meiners, P. Heil, L. Norman, D. N. Thomas, & A. R. Bowie (2009). Biogeochemical observations during the winter–spring transition in East Antarctic sea ice: Evidence of iron and exopolysaccharide controls. *Marine Chemistry*, 115(3-4), 163-175. https://doi.org/10.1016/j.marchem.2009.08.001

van Leeuwe, M. A., L. Tedesco, K. R. Arrigo, P. Assmy, K. Campbell, K. M. Meiners, et al. (2018). Microalgal community structure and primary production in Arctic and Antarctic sea ice: A synthesis. *Elementa: Science of the Anthropocene*, 6. https://doi.org/10.1525/elementa.267

Vancoppenolle, M., H. Goosse, A. de Montety, T. Fichefet, B. Tremblay, & J. Tison (2010). Modeling brine and nutrient dynamics in Antarctic sea ice: The case of dissolved silica. *Journal of Geophysical Research*, 115(C2). https://doi.org/10.1029/2009jc005369

Vancoppenolle, M., K. M. Meiners, C. Michel, L. Bopp, F. Brabant, G. Carnat et al. (2013). Role of sea ice in global biogeochemical cycles: emerging views and challenges. *Quaternary Science Reviews*, 79, 207-230. https://doi.org/10.1016/j.quascirev.2013.04.011

Venables, H. J., A. Clarke, & M. P. Meredith (2013). Wintertime controls on summer stratification and productivity at the western Antarctic Peninsula. *Limnology and Oceanography*, 58(3), 1035-1047. https://doi.org/10.4319/lo.2013.58.3.1035

Verdugoa, P., A. Alldredgeb, F. Azamc, D. Kirchmand, U. Passowe, & P. Santschif (2004). The oceanic gel phase: a bridge in the DOM–POM continuum. *Marine Chemistry*, 1–4, 67–85. https://doi.org/10.1016/j.marchem.2004.06.017

Wadley, M. R., T. D. Jickells, & K. J. Heywood (2014). The role of iron sources and transport for Southern Ocean productivity. *Deep-Sea Research Part I-Oceanographic Research Papers*, 87, 82-94. https://doi.org/10.1016/j.dsr.2014.02.003

Worsfold, P. J., M. C. Lohan, S. J. Ussher, & A. R. Bowie (2014). Determination of dissolved iron in seawater: A historical review. *Marine Chemistry*, 166, 25-35. https://doi.org/10.1016/j.marchem.2014.08.009

CHAPTER 2. ENHANCED IRON FLUX TO ANTARCTIC SEA ICE VIA DUST DEPOSITION FROM ICE-FREE COASTAL AREAS

L. Duprat[1], N. Kanna[2], J. Janssens[1,7], A. Roukaerts[3], F. Deman[3], A. T. Townsend[4], K.M. Meiners[5,6], P. van der Merwe[6] and D. Lannuzel[1, 5]

[1]Institute for Marine and Antarctic Studies, University of Tasmania, Hobart, Australia, [2] Arctic Research Center, Hokkaido University, Sapporo, Japan, [3]AMGC Department, Vrije Universiteit Brussel, Brussels, Belgium, [4]Central Science Laboratory, University of Tasmania, Hobart, Australia, [5]Australian Antarctic Division, Kingston, Tasmania, Australia, [6]Antarctic Climate and Ecosystems Cooperative Research Centre, Hobart, Tasmania, Australia.

Corresponding author: Luis Paulo Duprat (luis.duprat@utas.edu.au)

Key Points:

- Primary production in East Antarctic fast ice is not Fe-limited during late-spring/early summer.
- Iron in suspended sediment entrapped during ice formation supports primary production in the ice.
- Windblown dust from ice-free coastal landmasses in the Vestfold Hills contributes significantly to the total iron pool in Davis fast ice.

[7]Current affiliation: Commonwealth Scientific and Industrial Research Organisation (CSIRO), Hobart, Tasmania, Australia.

Abstract

Antarctic sea ice is an important temporal reservoir of iron which can boost primary production in the marginal ice zone during the seasonal melt. While studies have reported that Antarctic fast ice bears high concentrations of iron due to the proximity to coastal sources, less clear are the biogeochemical changes this iron pool undergoes during late spring. Here we describe a 3-week time series of physical and biogeochemical data, including iron, from first-year coastal fast ice sampled near Davis Station (Prydz Bay, East Antarctica) during late austral spring 2015. Our study shows that dissolved and particulate iron concentrations in sea ice were up to two orders of magnitude higher than in under-ice seawater. Furthermore, our results indicate a significant contribution of lithogenic iron from the Vestfold Hills (as deduced from the comparison with crustal element ratios) to the particulate iron pool in fast ice after a blizzard event halfway through the time series. Windblown dust represented approximately 75% of the particulate iron found in the ice and is a potential candidate for keeping concentrations of soluble iron stable during our observations. These results suggest that iron entrapped during ice formation, likely from sediments, as well as local input of coastal dust, support primary productivity in Davis fast ice. As ice-free land areas are likely to expand over the course of the century, this work highlights the need to quantify iron inputs from continental Antarctic dust and its bioavailability for ice algae and phytoplankton.

Plain summary

Oceanic single-celled algae are the base of the ocean food web and play an important role in the Earth climate. In the Southern Ocean, the growth of these microorganisms is limited by the naturally low concentration of iron in the seawater. Microalgae benefits from the presence of the Antarctic sea ice since iron is highly concentrated in sea ice relative to the seawater. Less clear though is the contribution of the potential sources of iron to the sea ice. We collected and analysed sea ice cores for a series of parameters, including iron, from first-year coastal sea ice sampled near Davis Station (Prydz Bay, East Antarctica) during late austral spring 2015. Our results suggest that iron entrapped during ice formation, likely from seafloor sediments, as well as dust blown by winds from the neighbouring Vestfold Hills, are the main sources of iron to Davis coastal sea ice. Since we can expect the expansion of ice-free areas and exposed grounds over the course of this century, our results highlight the need to quantify the amount of iron coming from continental Antarctic dust and to access if microalgae can use this form of iron for their basic physiological needs.

Keywords: Iron; sea ice, dust; Antarctica; coastal

2.1 Introduction

The ubiquitous scarcity of the key micro-nutrient iron (Fe) makes the Southern Ocean the largest High Nutrient Low Chlorophyll (HNLC) area on Earth (Martin, 1990; Martin et al., 1991). Photosynthetic microalgae require Fe to fix carbon dioxide and, ultimately, fuel ocean food webs (Benner, 2011). While the importance of Fe for marine primary production and carbon sequestration is well-recognized (Boyd et al., 2007; Martin & Fitzwater, 1988; Moore et al., 2001), less is known about the bioavailability of the different sources of Fe to phytoplankton. Iron can co-exist in a range of different sizes, forms and complexation states in the ocean. Direct uptake studies (Hudson & Morel, 1993; Morel et al., 2008) and general kinetic models (Hudson & Morel, 1990) have demonstrated that unchelated inorganic Fe is the most readily bioavailable form to microalgae. However, at ocean pH and oxic conditions, this unchelated form is hardly soluble and precipitates as ferric oxyhydroxide solid complexes ($Fe(OH)_x$), leading to extremely low concentrations of this Fe specie in seawater (Lis et al., 2015; Millero, 1998). Filtrations and analyses enable the categorization of Fe into particulate (>0.2 µm) and "dissolved" (<0.2 µm) fractions. Still, the chemical forms of Fe within these fractions remain largely speculative (Wells et al.,1995). Today there is evidence that Fe is present in seawater mostly in the small colloidal phase, which is included in the operationally defined "dissolved" fraction and almost entirely complexed by organic ligands (Gledhill & Buck, 2012; Wu & Luther, 1994; Wu et al., 2001). The bioavailability of dissolved Fe (DFe) depends in part on its chemical nature (Lis et al., 2015; Wells & Goldberg, 1991). On the other hand, the bioavailability of the particulate Fe (PFe) is a function of the thermodynamic stability and kinetic lability of this phase (Chen et al., 2003; Kuma & Matsunaga, 1995). Although relatively low as a percentage (Lannuzel & Schoemann, 2011), when abundant, PFe can become a significant source for phytoplankton. Many studies have now pointed towards the importance of the particulate fraction in replenishing the DFe pool via thermal, photochemical and ligand-mediated dissolution (Borer et al., 2005; Kraemer, 2004; Sulzberger et al., 1989).

Despite widespread Fe limitation, intense and regularly occurring springtime algal blooms are observed in the Southern Ocean marginal ice zones (Sullivan et al., 1993). This phenomenon has been linked to the melting of the seasonal sea ice, which promotes the release of Fe to the seawater and surface water stratification (Grotti et al., 2005; Lannuzel et al., 2007, 2008, 2010; van der Merwe et al., 2009). In contrast to pack ice, which relies on biological activity to actively concentrate Fe (Lannuzel et al., 2014), fast ice (i.e., sea ice fastened to the shore)

can incorporate high concentrations of Fe simply due to its proximity to lithogenic sources such as eroded continental rocks, sediments and dust (Lannuzel et al., 2016). Melting fast ice, therefore, has the potential to trigger local phytoplankton blooms, as previously observed near Casey and McMurdo stations in Antarctica (de Jong et al., 2013; Lannuzel et al., 2014; van der Merwe et al., 2011b). The geographic location of growing fast ice can also greatly influence the amount of Fe stored during the initial phase of sea-ice formation, partly dictating the magnitude and nature of the sea-ice Fe pool. Naturally Fe-fertilized biological hotspots other than sea ice include areas near melting glaciers (Gerringa et al., 2012; Herraiz-Borreguero et al., 2016; Raiswell et al., 2008), icebergs (Duprat et al., 2016), areas affected by sediment resuspension as well as downstream of windblown dust (de Jong et al., 2013). Importantly, some coastal environments are prone to the fastest climatic changes, those which could cause an expansion of up to 25% of ice-free areas across the Antarctic landmass by the end of the century (Lee et al., 2017). Exposed dust and rocks may subsequently increase the fertilization of the Southern Ocean due to its impact on the Fe distribution in coastal sea-ice and potentially further offshore (Lannuzel et al., 2016). Ice-free areas such as the McMurdo Dry Valleys in Antarctica have been identified as a source of Fe to the Ross Sea via airborne transport, potentially boosting local marine productivity (de Jong et al., 2013). Nevertheless, the magnitude and effectiveness of extended ice-free grounds on coastal fertilization and carbon sequestration carry large uncertainties given the predominant refractory nature of Fe content in the dust (Mahowald et al., 2009).

Here we present results from a time series undertaken at a coastal site in Prydz Bay to provide new insights into sea-ice Fe biogeochemistry during late spring to summer transition. The time series also encompasses a blizzard event halfway through our visit, allowing for a dichotomous comparison between these two periods. Our study site (Figure 2.1) is surrounded by important climate-sensitive features such as the Amery Ice Shelf (AIS) and nearby glaciers, year-round sea ice, and one of the largest ice-free zones on the East Antarctic coast (the Vestfold Hills). Our first hypothesis is that fast ice plays an important role by delivering potentially bioavailable Fe to the waters of Prydz Bay, the third most productive polynya area in Antarctica (Arrigo et al., 2015; Figure 2.1c). Our second hypothesis is that Vestfold Hills represent a significant source of aeolian Fe dust to Prydz Bay. Findings from this study will help to assess the response of coastal Antarctic productivity to Antarctica`s changing cryosphere.

2.2 Materials and Methods

2.2.1 Study site

The study site was located in the Abatus Bay, approximately 2 km north of Davis Station (68° 34′ 36″ S, 77° 58′ 03″ E), East Antarctica. The area is on the northeast side of the greater Prydz Bay area, bounded by the Breidnes Peninsula in the Vestfold Hills, O'Gorman Rocks, Anchorage Island, Trigwell Island and Flutter Island (Figure 2.1b). The site was situated 600 m north of O'Gorman Rocks (a small rocky outcrop) and 200 m southeast of Anchorage Island in an area of undeformed sea ice and with a maximum water depth of 20 m. The sampling area was located upwind from Davis station (prevailing winds) and other operations in the vicinity of the station and off-limits to unauthorized personnel. No sign of foot or vehicle prints or other human activity was present at the location during the sampling period.

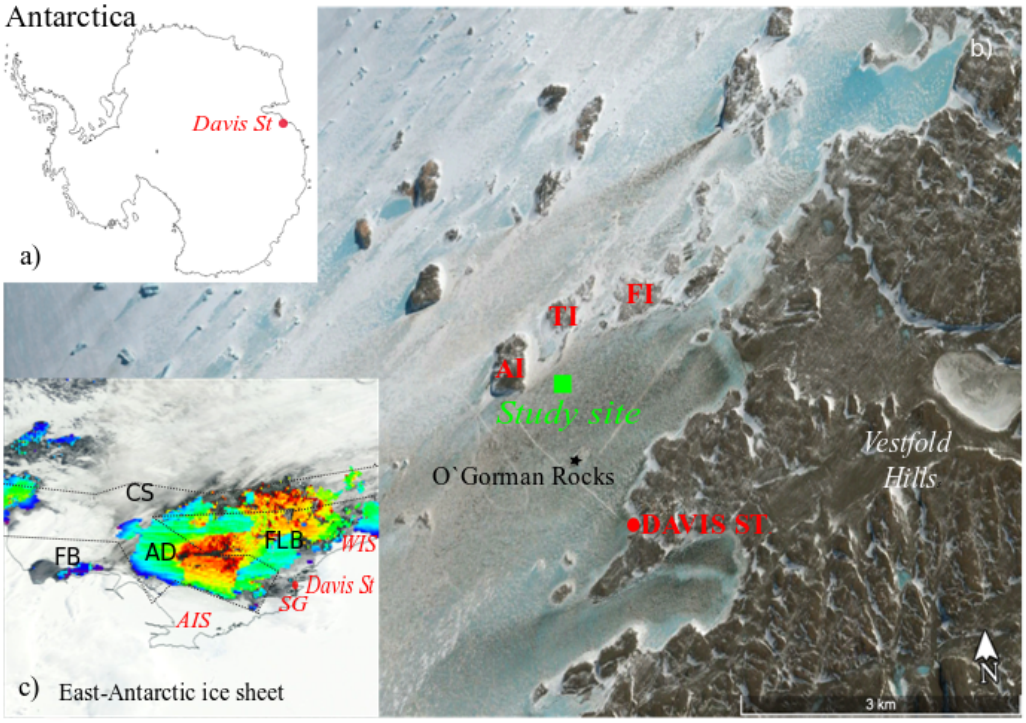

Figure 2.1 (a) Map of Davis Station location (68° 34′ 36″ S, 77° 58′ 03″ E), East Antarctica. Image is courtesy of Google Earth (Goggle Earth Pro V.3.2.5776, 2015). (b) Satellite image of Abatus Bay (Davis sea ice) obtained on the 10/13/2015 with geographic abbreviations: AI (Anchorage Island), TI (Trigwell Island) and FI (Flutter Island). (c) Chlorophyll colour image of Prydz Bay, late spring 2015 (NASA Earth Observing System Data and Information System, 2018). Dotted lines indicate the general geomorphology of the bay: AD (Amery depression), FB (Fram Bank), FLB (Four Ladies Bank) and CS (Continental slope). In red, the main glacial features of the area: AIS (Amery Ice Shelf), SG (Sørsdal Glacier) and WIS (West Ice Sheet).

2.2.2 Cleaning procedures

All plasticware including low-density polyethylene (LPDE) sampling bottles, polypropylene (PP) melting containers, and carboys, as well as all equipment used directly in contact with the samples, were cleaned according to the GEOTRACES protocols (Cutter et al., 2017) as follows: LDPE bottles were immersed in 2% (v:v) Decon90 for one week and then rinsed three times with reverse osmosis water and three times with ultra-high purity water (UHP water, Barnstead) before being soaked in 50% (v:v) HCl (analytical grade, Merck) for one month. After acid cleaning, bottles were rinsed five times with UHP water in a class-100 laminar flow hood. Bottles were then filled with 1% (v:v) HCl (ultrapure, Seastar Baseline) and stored in triple ziplock bags until use. During sampling, bottles were rinsed three times with the sample material immediately before collection. Between sampling days, all plastic equipment (Teflon® filtration sets, plastic tubing, plastic scoops, LDPE sampling bottles, PP melting containers) were rinsed with UHP water and soaked in an acid bath (10-20% (v:v) HCl, according to Nalgene® recommendations for each material) and then rinsed thoroughly before use. All glassware used for organic carbon and nitrogen filtrations were soaked in a 2% (v:v) HCl solution (analytical grade, Merck), rinsed with UHP water, wrapped in aluminium foil and combusted at 450 °C for 4 hours.

2.2.3 Sample collection

Snow, sea ice, “deep brine” and seawater were obtained on six different dates, converted to Julian days: 320, 325, 327, 330, 333, and 336. All samples were collected and analysed using trace metal clean protocols as described by Lannuzel et al. (2006) and van der Merwe et al. (2009). Samples were collected on consecutive dates upwind from each other to minimize cross-contamination, with an isolated zone allocated for the trace metal ice coring. Expeditioners wore cleanroom garments (Tyvek overall, overshoes and polyethylene gloves) over their warm clothing. Timeseries cores were spaced apart from one another by approximately 0.4 m, in a way to balance both the spatial heterogeneity and work disturbance effects. All items used for sample collection and storage were acid-cleaned and sealed in plastic bags.

On each sampling day, snow was collected from an area approximately 10 m away from the coring site using an acid-cleaned polyethylene (PE) hand shovel and stored in a 3.8-L wide

mouth Nalgene® PE bottle. The snow was left to melt at room temperature within the station laboratory where it was then processed for Fe and Chl*a* measurements. Four sea-ice cores were collected from each site: The first core was dedicated to temperature and salinity measurements, the second and third for Chl*a* and particulate organic matter (POC and PON) analyses, and the fourth core for trace metal analyses. Cores were sampled 0.1 m apart to minimize between-core spatial variability. They were drilled using an electric-powered, electro-polished stainless-steel corer of 0.14-m internal diameter (Lichtert Industrie, Belgium), previously shown to be noncontaminating for trace metals (Lannuzel et al., 2006; van der Merwe et al., 2009). Ice cores were sectioned in the field starting from the top using a medical-grade bone saw (Richards Analytical). Samples for salinity, POC and PON, were cut every 0.1 m along the whole ice core. For Chl*a* and Fe quantification, seven distinctive sections (here and after referred to S1-S7) were obtained by cutting two top sections of 0.2 m each (S1 and S2), two bottom sections of 0.05 m each (S6 and S7) and one middle section (S4) of 0.1 m starting 0.4 m away from the base of the ice. The remaining core length left between S2 and S4 and between S4 and S6 was designated S3 and S5, respectively. This provides a sequential top-bottom S1 to S7 core profile (Figure 2.2). Cores were kept in acid-cleaned plastic bags and stored frozen at −20 °C in the dark until further processing.

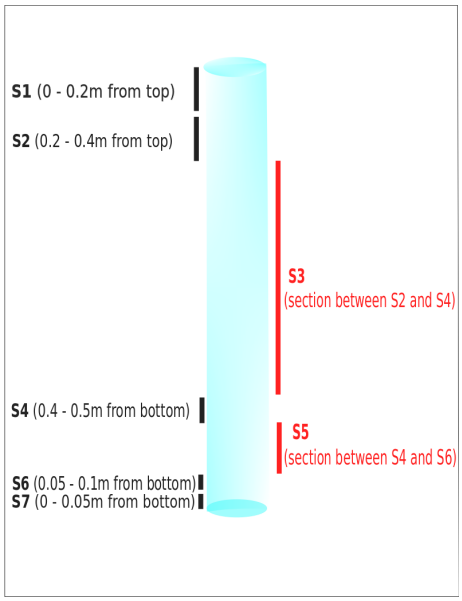

Figure 2.2 Schematic of the vertical sampling procedure for ice cores used for Fe and Chl*a* profile determination.

"Deep-brine" was collected after determination of the depth of the sea-ice -5 ºC isotherm. The core was drilled to the chosen depth and then removed, allowing the brine to drain and fill the

(sack) hole. During this process, the holes were covered with plastic plugs to avoid airborne contamination. The brine was then collected from the hole using a peristaltic pump (E/S Portable Sampler, Masterflex) and acid-cleaned Masterflex® tubing. Underlying seawater was collected at ~ 0-, 3- and 10-m depths (hereafter referred to as SW0, SW3, and SW10) using a custom-made polycarbonate 7-L Helmond-Byrne (H-B) water sampler suspended from a Kevlar line and triggered using a Teflon® messenger (Sedwick et al., 1997). The sampler was deployed through three holes drilled side by side on the first sampling day. Seawater and brine samples were distributed into several acid-washed 1-L LDPE Nalgene® bottles avoiding light exposure as much as possible until further processing for the suite of parameters described in the section below.

In the Davis station laboratories, sectioned cores were rinsed with UHP water, placed into individual acid-cleaned sealable PP buckets, and allowed to melt in the dark at room temperature. Melted samples were processed as soon as possible to avoid sample warming, limiting any further biological activity (Rintala et al., 2014). After each day, the saw, ice corer, and shovel were abundantly rinsed with UHP water, dried under a class-100 laminar flow hood and stored in triple plastic bags until next use.

2.2.4 Sample processing and analytical methods

2.2.4.1 Physical variables

Ice temperatures were measured using a Testo temperature probe (± 0.1 °C precision) following insertion into 4-mm holes freshly drilled into the ice core every 0.05 m. Bulk salinity of each 0.1-m melted ice sections and brines was measured using a Thermo Scientific Orion (Model 125A Plus) conductivity meter (± 0.1 precision). Brine volume fractions (V_b/V) were calculated according to Cox and Weeks (1988) using temperature and bulk salinity values. Where salinity and temperature profiles had different depth resolutions, the temperature was linearly interpolated to match the salinity. Since changes in the biogeochemical parameters can be explained by convective overturning, allowing nutrient supply from the seawater to the sea ice, the porous-medium mush-Rayleigh number (*Ra*) was calculated. The original set of parameters proposed by Notz and Worster (2008) for the *Ra* formulation was used, following recommendations in Vancoppenolle et al. (2013).

2.2.4.2 Particulate organic carbon and nitrogen

Snow, seawater, brines and melted ice samples for POC and PON quantification were gently homogenized before filtration (0.2–2.5 L). Particulate material was collected by filtration on preheated (450 °C, for 24 h) quartz filters (0.7 µm nominal porosity, MGF Sartorius). Samples were dried overnight at 60 °C and stored in the dark at room temperature (20 °C) in pre-combusted scintillation vials until further processing for isotopic composition at the Vrije Universiteit in Brussels, Belgium. Prior to analysis, inorganic carbon was removed from the filters by 24-h exposure to concentrated HCl fumes inside a closed glass container. Filters were packed in silver cups and analysed using an elemental analyzer (EuroEA3000, Eurovector) coupled online via a Con-Flo III interface to a Thermo Delta V isotope ratio mass spectrometer. POC and PON detection limits were calculated as 3× the standard deviation of the procedure blanks, determined as 3.3 and 2.2 µM, respectively (n = 4).

2.2.4.3 Chlorophyll-*a*

Ice cores for Chl*a* analysis were melted at room temperature in the dark (Rintala et al., 2014). Immediately after melting, ice core sections as well as brine and seawater samples were then filtered under low vacuum (<0.13 bar) onto GF/F filters. The filtered volume (0.1 – 1.5 L) depended on the visible organic content and care was taken not to clog the filter. Filters were stored individually in plastic holders at –80 ºC in the dark until analysis. Chl*a* concentrations were determined fluorometrically with a Turner Designs 10AU fluorometer (in vitro detection limit 0.02 µg/L) after extraction with 90% acetone for 12 hours. Fluorescence was measured at 750 nm for phaeopigment-corrected Chl*a* determination after acidification with 0.1 N HCl according to Arar and Collins (1997).

2.2.4.4. Iron

As soon as the snow and ice sections were melted, Fe size fractionation was obtained via filtration using a Teflon® perfluoroalkoxy (PFA) filtration apparatus (Savillex, USA) onto a 0.2-µm pore size 47-mm diameter polycarbonate (PC) membrane filter (Sterlitech) and under gentle vacuum (<0.13 bar) to avoid algal cell lysis. The process was repeated for the brine and seawater samples. In LDPE bottles, 60 ml of filtrate was collected for DFe analysis. A second (sub) filtrate was collected to obtain the sFe using 0.02-µm Whatman® Anotop® syringe filters

connected to Tygon® tubing mounted on a peristaltic pump set at 1 ml/min. The membrane was successively rinsed with 10% v:v ultrapure HCl (Seastar Baseline, choice Analytical) and UHP water for a combined time of 1 hour before circulating the DFe fraction onto the 0.02-µm membrane. The first 100 ml were discarded before the final collection of the sFe fraction. Filter blanks were also prepared following the same procedure, minus the addition of samples. Dissolved and sFe samples were then acidified to pH ~1.8 by adding 1% of 12-M ultrapure HCl (Seastar Baseline, choice Analytical) to the samples. Bottles were triple bagged and stored at room temperature until analyses. Polycarbonate filters with the retained particulate fraction (PFe > 0.2 µm) were placed into acid clean polystyrene petri dishes, triple bagged, and stored at –20°C in the dark until further processing and analyses in Australia.

2.2.4.4.1 Soluble and dissolved Fe analysis

An automated off-line sample system (seaFAST-pico™, Elemental Scientific; Nobias Chelate-PA1 resin) was used to preconcentrate trace metals and remove sea-ice and seawater filtrate matrices from our undiluted samples according to the method described by Wuttig et al. (2019). In-house testing proved the capability of the seaFAST system for accurate Fe determination over the large range of salinities encountered in this study. The method accuracy was evaluated through extensive analysis of a range of oceanographic standard reference where samples concentrations were found to agree with consensus values to within ± 6% and percentage recovery of 104 ± 9 (n = 33; salinity range 0 – 60 g/kg) for Fe (Wuttig et al., 2019). Preconcentration factors ranging from 10× (snow, bottom sea-ice and brines) to 40× (sea ice and seawater) were chosen to provide resultant analyte values. Concentrations of sFe and DFe were then determined at the Central Science Laboratory (Hobart, Australia) using a Sector Field Inductively Coupled Plasma Mass Spectrometer (SF-ICP-MS, Element 2) according to the methodology described by Wuttig et al. (2019).

The SF-ICP-MS was prepared for trace metal analysis with a clean sample introduction front end including sampler cones, torch, spray chamber, pump tubing, and nebulizer, with lengthy acid purging. During the period of analysis, the instrument was used exclusively for low-Fe level work. Before sample analysis, the instrument was purged with alternate 5% (v:v) HCl and 5% (v:v) HNO_3 solutions for 1 hour to ensure residual traces from previous analysis were not present. Then, the instrument was conditioned to match our sample matrix using a 10% (v:v) HNO_3 ultra-pure solution. A linear calibration curve was obtained each day using four

standards of Fe: 0ppb (0 nM), 1 ppb (17.9 nM), 5 ppb (89.5 nM) and 10 pbb (179. nM) prepared from mixed element solutions (QCD Analysts, MISA suite of solutions, VHG Labs, LGC Standards, Manchester, NH, USA), all in 10% (v:v) HNO_3. Indium (In) as an internal standard was added to all blanks, standards, and samples at a concentration of 10 ppb (87.1 nM). After calibration and rinsing, the calibration blank was analysed in triplicate to ensure a low instrument baseline prior to sample analysis. A 2.5-min rinse with 10% (v:v) HNO_3 was used between each sample. Furthermore, care was taken to run the samples in order of potential increasing concentrations to help minimize between sample carryover/memory effects (starting from snow followed by top/intermediate ice, seawater, brine and bottom ice). All samples were handled with care using standard trace metal work precautions (gloves and sleeves) inside a portable class-100 laminar flow hood under a flowing stream of HEPA-filtered air. Instrument drift was periodically monitored between each set of samples using the 5-ppb calibration standard as a quality control solution. Data were blank corrected by subtracting an average of at least three acidified UHP blanks. Finally, the average DFe detection limit from the five-day-instrument run was calculated as 0.001ppb (0.02 nM; n = 15; 3× the standard deviation of the acidified UHP blank for each day of analysis). Analysis of certified reference material prepared in 10% in-house seawater (NASS6, National Research Council Canada) was conducted in parallel with field samples. A mean Fe value of 0.423 ± 0.02 µg/L (n=3) was found, in good agreement with the certified (indicative) value of 0.493 ± 0.05 µg/L. Colloidal Fe fraction (cFe) was calculated as the difference between the DFe and sFe concentrations.

2.2.4.4.2 Particulate metals

Polycarbonate filters with retained PFe and procedural filter blanks were digested using strong ultrapure acids to ensure complete digestion of the most refractory particles (Bowie et al., 2010). Firstly, a mixture of 250-µl 12 M HCl, 250-µl 16 M HNO_3, and 500-µl 29 M HF (Seastar Baseline, Choice Analytical) was added to each 15 ml Teflon® PFA vial (Savillex, USA) containing sample filters or blank filters. Vials were immediately closed and heated to 120 ºC for 12 hours over a Teflon®-coated hot plate (SCP Science) inside a clean laboratory fume hood, followed by dry evaporation for 4 hours at 120ºC after the vials were opened. The dried residues were then resuspended in 9.9-ml ultrapure 10% (v:v) HNO_3 and 100 µl of In solution (final concentration of 10 ppb). Five-ml subsamples were then transferred to 10 ml PP tubes before PFe quantification using SF-ICP-MS following the same procedures as outlined in

Section 2.2.4.4.1. The mean value for procedural digested acid blanks (n = 3) was 0.01 ± 0.005 ppb (0.2 + 0.1 nM). The limit of detection was calculated as three times the standard deviation of the procedural blank, determined as 0.015 ppb (0.27 nM). The same procedure and quality control were run for determination of other metals which purpose is described in the following section, listed: aluminium (Al), barium (Ba), thorium (Th), strontium (Sr) and uranium (U).

2.2.5 Statistical Analysis

A linear mixed effects model was applied to the data set to investigate trends in the parameters of interest (DFe, sFe, cFe, PFe, PFe:DFe, Chl*a*, POC) over time. Before adjusting the model, a rank-based inverse transformation approach (rankit - Bishara & Hittner, 2012) was applied to reduce the asymmetry, variability and effects of discrepant observations; hence, normality could be assumed. The choice of a mixed model relies on the expected correlation between different ice sections, which was considered by a random effect of sections. Also included was the fixed effect of days, which was tested for significance in the regression models via a restricted maximum likelihood method. Potential correlations between sFe, cFe, DFe and PFe with other sea-ice physical and biogeochemical parameters were investigated using a Spearman correlation coefficient test due to the nonnormality observed in the data. For this test, two data sets were considered: all sections (S1 - S7) and only bottom sections (S6 and S7) along the whole study period. All analyses were performed using the R programming language (version 3.3.1). The molar elemental ratios Fe:Al, Ba:Sr and Th:U in the snow were used as a tracer of lithogenic sources (Sharaton & Collerson, 1984; Wedepohl, 1995) and were obtained by the average particulate fraction concentration of available samples.

2.2.6 Fe budget and demand calculation

Based on the measurements of Fe concentration and sea-ice thickness from the sampled cores, a depth-integrated DFe, PFe, and TFe (DFe +PFe) inventory was calculated for each sampling day. The DFe inventory (μmol/m^2) was determined by multiplying the concentrations of each ice core section by their section thickness and summing them up. In order to reduce a possible bias due to the inter-core variability and to obtain a conservative balance between the ongoing physical and biological mediated changes in the iron pool and the potential input of dust associated to the punctual blizzard event observed at day 329, the Fe budget during the period

under consideration was inferred by the following calculation. First, the inventory of the second half of the times series (median day 330-336) was subtracted by the inventory of the first half (median day 320-327). Next, this result was averaged with the budgets obtained from the median inventory of the first 2 days (320 and 325) and last 2 days (days 333 and 336) and from the first (320) and last day (336). The potential Fe demand by sea-ice algae during the spring season was estimated by considering the average of the three highest POC concentrations at S7 (where autotrophs usually dominate), which were found on days 325, 327 and 333. Since around 90% of the POC was present in the lowermost layer (S7), Fe demand calculations were restricted for this layer as a proxy for the entire ice cores. Therefore, the maximum Fe demand of the ice was calculated by multiplying the average of the highest S7 POC concentrations by the literature average Fe:C ratio for diatoms. Finally, the daily demand was determined by dividing the total demand by 90, that is, the number of days in spring.

2.3 Results

2.3.1 Sea-ice thermodynamics

Sea-ice temperatures increased with ice-core depths, and over time, consistent with increasing air temperatures over the study period (Figure 2.3a). Brine volume fractions above 5% during most of the time series indicate the permeable characteristic of the ice (Figure 2.3c). The highest *Ra* value (4.5) was observed on day 320 for the sea-ice top layer and values close to zero were found in the bottom ice sections across most sampling days (Figure 2.3d).

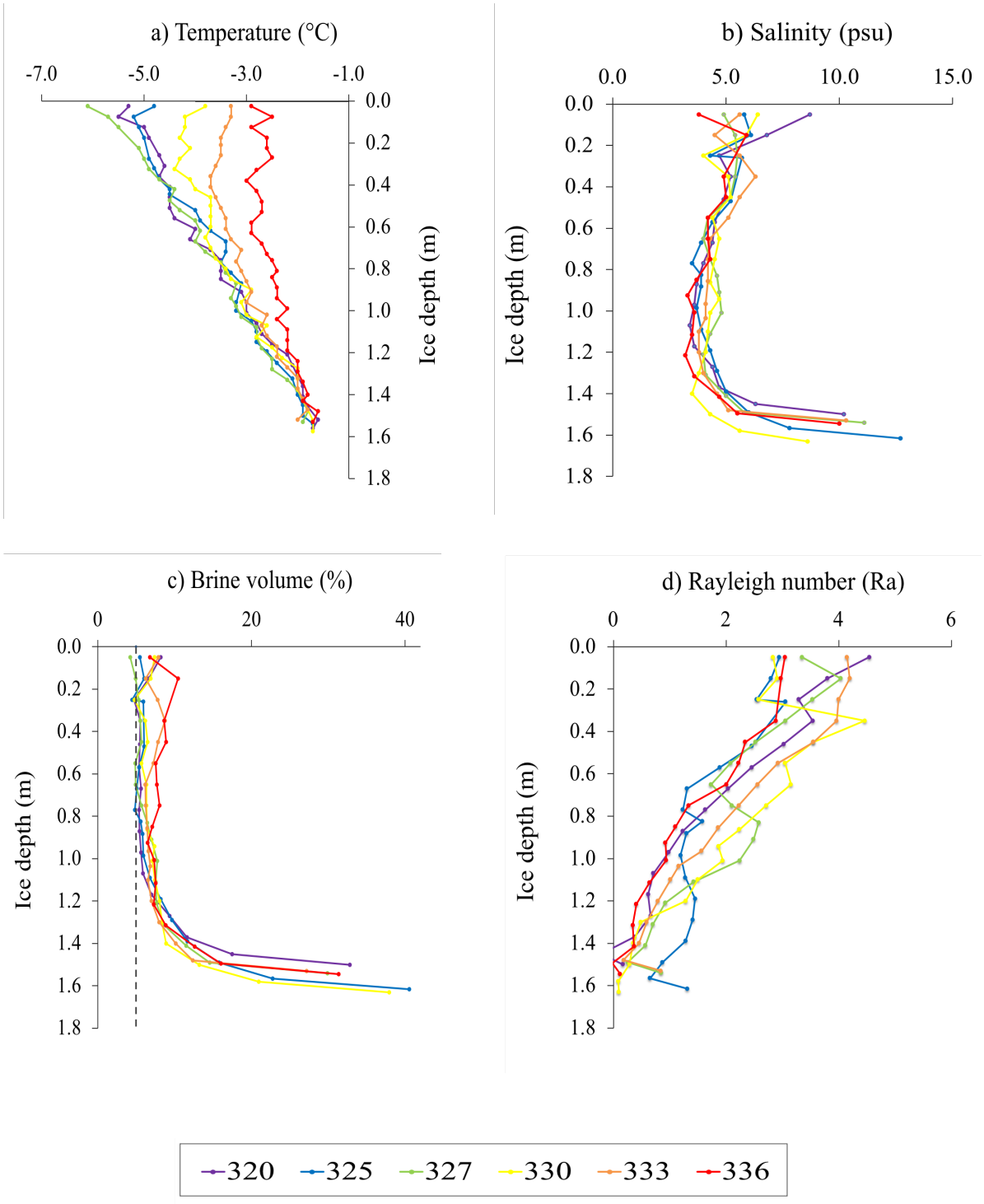

Figure 2.3 (a) Vertical profiles of sea-ice temperature, (b) bulk-salinity, (c) calculated brine volume with the theoretical 5% threshold for sea-ice permeability shown as dashed line and (d) Rayleigh numbers (*Ra*) for each sampling day. The *Ra* expresses the ratio between the negative buoyancy in the brines and dissipation. Greater *Ra* numbers indicate a higher propensity for brine convection to occur.

2.3.2 Vertical distribution of soluble, colloidal and particulate Fe

Despite the marked heterogeneity of the Fe distribution, DFe and PFe concentrations in sea ice were up to an order of magnitude higher than under ice water concentrations. Soluble, DFe and PFe concentrations measured in the snow, sea ice, brine, and seawater are summarized in Table 2.1. A detailed description of values for each day and ice section is available through the link in Section 2.6.

Table 2.1 Summary statistics for Fe fractions and biological parameters averaged for the whole time series.

Medium	**Iron fractions**						**Biology**		
	sFe (nM)	**cFe (nM)**	**DFe (nM)**	**PFe (nM)**	**PFe:DFe (nM)**	**Chl*a* (µg/L)**	**POC (µM)**	**PON (µM)**	**POC:PON (µM:µM)**
Snow	0.4 ± 0.4	19.1 ± 13.9	19.5 ± 13.6	1,630 ± 2,350	83.5 ± 136		10.0 ± 4.6	0.5 ± 0.3	19.3 ± 2.3
All sea ice (S1 – S7)									
Min.	0.1	0.6	1.0	2.1	0.1	0.1	13.7	1.0	6.2
Max.	17.1	46.8	63.8	416	30.9	240	3,270	435	45.1
Mean	2.1	5.5	7.5	47.2	7.9	36.4	303	31.6	11.5
SD	3.7	7.6	10.7	84.2	8.4	81.9	752	87.1	6.7
Sea ice without bottom ice	0.6 ± 0.4	3.3 ± 2.2	3.9 ± 2.1	20.6 ± 25.2	7.4 ± 8.9	1.0 ± 0.8	22.6 ± 5.8	2.2 ± 0.7	11.4 ± 4.5
S6 + S7 (Bottom sea ice)	5.3 ± 5.5	10.4 ± 12.0	15.7 ± 16.6	119 ± 130	9.0 ± 7.6	127 ± 114	1,000 ± 1,170	105 ± 142	11.7 ± 11.2
S7 (including skeletal layer)	9.5 ± 4.8	15.1 ± 16.0	24.5 ± 20.3	176 ± 163	7.1 ± 4.9	223 ± 38.4	1,950 ± 920	205 ± 141	7.2 ± 0.9
Deep brine	1.8 ± ± 0.54	6.9 ± 3.3	8.6 ± 3.7	12.5 ± 7.0	1.8 ± 1.4	1.4 ± 0.6	30.8 ± 23.8	65.8 ± 150	5.7 ± 3.1
Seawater 0m	1.3 ± 2.2	4.3 ± 2.2	5.6 ± 1.5	56.2 ± 80.3	10.7 ± 14.7	0.2 ± 0.1	14.0 ± 13.0	1.9 ± 2.1	8.1 ± 3.1
Seawater 3m	0.4 ± 0.2	3.6 ± 1.5	4.0 ± 1.6	5.6 ± 4.6	1.6 ± 1.2	0.2 ± 0.1	4.4 ± 1.8	0.7 ± 0.3	7.1 ± 1.7
Seawater 10m	0.4 ± 0.2	3.4 ± 0.6	4.3 ± 1.2	4.4 ± 4.3	1.3 ± 1.5	0.1 ± 0.1	4.3 ± 1.4	0.6 ± 0.3	6.9 ± 1.0

The average depth-integrated iron inventories (days 320 - 336) for DFe, sFe, cFe, and PFe were 8.4 ± 3.0, 1.8 ± 0.4, 6.6 ± 2.8 and 38.3 ± 29.0 μmol/m^2, respectively. The cFe fraction represented approximately 75% of the integrated dissolved fraction, accounting for roughly 20% of the integrated TFe. Soluble and DFe for S5 on days 327, 330 and 333 showed distinct high outlier values when compared to the neighbouring sections and all top and intermediate layer values. We suspect that possible contamination could have occurred during the melting process of the S5 sections on these days since the same bucket was used, therefore, they were discarded for statistical analysis. Dissolved and PFe concentrations were generally high in the snowpack (Table 2.1), with markedly high values (>1 μM) for PFe found on days 330, 333 and 336. Grey ash-like deposits were observed on the snow filters on these days. The average snow particulate Fe:Al, Ba:Sr and Th:U molar ratios were 0.48 (0.46 to 0.53, n=6), 1.84 (1.52 to 2.12, n=5) and 2.6 (1.0 to 2.99, n=5), respectively. Average concentrations for DFe, cFe, sFe and PFe in seawater (SW3 and SW10) from all stations were 2.1 ± 1.4, 2.3 ± 0.1, 5.5 ± 1.1 and 2.4 ± 4.3 nM, respectively. Values for SW0 were not considered here in order to obtain a more realistic picture of the Fe profile of the water column without the interference of localized fluctuations from the bottom ice.

2.3.3 Temporal distribution of soluble, colloidal and particulate Fe

Davis data show there was a decrease in bulk sea-ice DFe concentration from day 320 to 336 when all ice layers (S1 – S7) are considered ($p < 0.05$). Both soluble and colloidal fraction (and consequently, total DFe) had a similar behaviour over time, with increasing basal and decreasing surface and internal concentrations (Figure 2.4b, c and d). The mean sFe, cFe and DFe concentrations from the upper and intermediate ice layers (S1 – S5) declined from 1.2 ± 0.1, 10.3 ± 14.5 and 9.6 ± 1.5 nM on day 320 to 0.7 ± 0.3, 1.8 ± 0.2 and 2.2 ± 0.8 nM on day 336, respectively. Bottom ice (S6 – S7) sFe, cFe, and DFe concentrations rose from 3.6 ± 0.7, 4.6 ± 1.6 and 8.2 ± 2.6 nM on day 320 to 6.8 ± 8.7, 8.3 ± 8.8 and 15.1 ± 17.5 nM on day 336. In contrast, an increasing trend in the bulk sea-ice PFe (S1 – S7) was observed for day 325, 330, 333 and 336 in relation to the first day ($p < 0.01$). Mean PFe concentration increased from 8.9 nM on day 320 to 70.3 nM on day 336, peaking at day 330 (112 nM). There is evidence of an accumulation of PFe also in the upper-middle layers of the ice (S1 – S5) where the concentration increased from 4.5 ± 1.5 nM on the first day to 20.6 ± 17.5 nM on the last day. Overall, Davis sea ice lost 0.3 ± 0.1 μmol.m^{-2}.day^{-1} of DFe and 0.3 ± 0.1 μmol.m^{-2}.day^{-1} of cFe

while soluble Fe was kept relatively constant (0.004 ± 0.02 µmol.m^{-2}.day^{-1}). PFe increased by 2.6 ± 0.7 µmol.m^{-2}.day^{-1} over the same period (see Section 2.2.6 for budget calculation). The comparison between the first and second half of the time series (before and after the blizzard event) highlights the marked gain of PFe (Figure 2.5d). During this time, average seawater DFe concentration decreased from 5.2 ± 1.1 to 3.1 ± 0.6 nM (n = 12; p <0.01), while seawater PFe concentration increased from 3.4 ± 5.0 to 6.6 ± 3.0 nM (n = 12; no statistical difference).

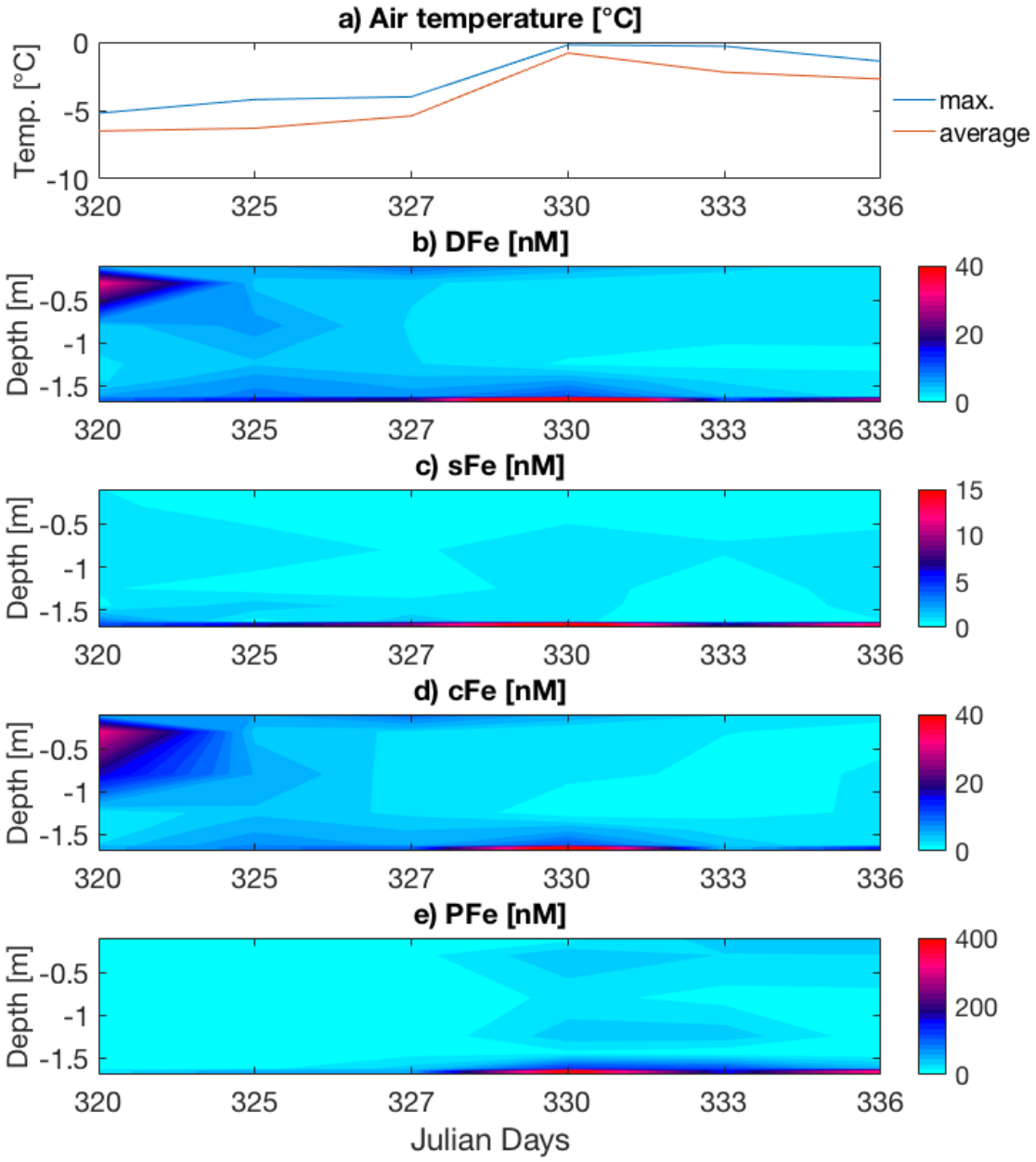

Figure 2.4 a) Maximum and average daily air temperatures. Contour maps showing the temporal evolution of b) dissolved (DFe), c) soluble (sFe), d) colloidal (cFe) and e) particulate (PFe) sea-ice iron fractions.

Finally, a significant increase in the PFe:DFe ratio (nM:nM) over time was also observed ($p < 0.01$). The mean PFe:DFe was 7.9 ± 8.4, increasing from 1.4 ± 0.8 on day 320 to 11.8 ± 7.6 on the last day. At day 320, PFe represented around 45% of the total Fe content in sea ice, increasing to over 90% on day 336. Both the soluble and colloidal fraction percentage decreased during the time series, with the reduction in the colloidal fraction more pronounced than in the soluble fraction.

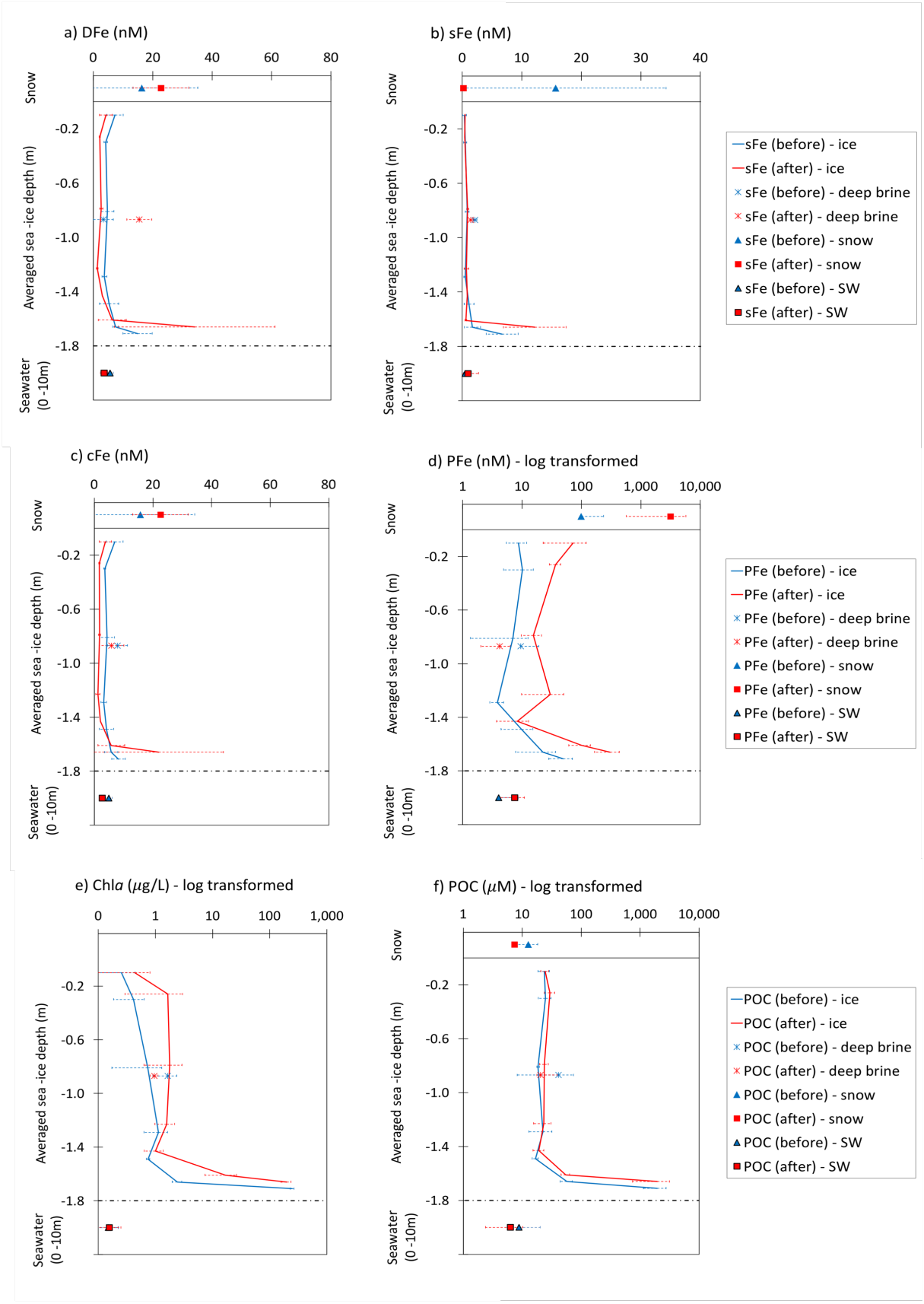
a) DFe (nM)
b) sFe (nM)
c) cFe (nM)
d) PFe (nM) - log transformed
e) Chl*a* (μg/L) - log transformed
f) POC (μM) - log transformed
Snow
Averaged sea -ice depth (m)
Seawater (0 -10m)
sFe (before) - ice
sFe (after) - ice
sFe (before) - deep brine
sFe (after) - deep brine
sFe (before) - snow
sFe (after) - snow
sFe (before) - SW
sFe (after) - SW
PFe (before) - ice
PFe (after) - ice
PFe (before) - deep brine
PFe (after) - deep brine
PFe (before) - snow
PFe (after) - snow
PFe (before) - SW
PFe (after) - SW
POC (before) - ice
POC (after) - ice
POC (before) - deep brine
POC (after) - deep brine
POC (before) - snow
POC (after) - snow
POC (before) - SW
POC (after) - SW

Figure 2.5 Vertical profiles of DFe, sFe, cFe, PFe, Chl*a,* and POC in sea ice before and after the blizzard event. Values were averaged for 320 – 327 (blue line) and 330 – 336 (red line). Standard deviations are represented by the horizontal bar. Also shown are values for snow, "deep brine" and under-ice seawater samples (expressed as mean values for SW0, SW1, and SW10 samples).

2.3.4 Sea-ice biogeochemistry and Correlations with Fe fractions

High concentrations of Chl*a* were maintained throughout the time series, particularly in S7, where values were up to three orders of magnitude higher than the mean Chl*a* concentration of the underlying seawater (Table 2.1). Although a statistically significant temporal trend in total Chl*a* could not be observed, an increase in Chl*a* is evidenced when both half-period averages are compared (Figure 2.5e). A significant increase in POC over time was detected for day 325, 330, 333 and 336 ($p < 0.01$). The POC and PON vertical profiles followed the same pattern as the Chl*a,* with higher values in the bottom sections (link to data available in Section 2.6).

A strong correlation of PFe with POC and PON ($\rho > 0.7$, $p < 0.01$) and a moderate correlation of sFe with Chl*a* was observed ($\rho = 0.6$, $p < 0.01$). A moderate correlation of sFe with temperature ($\rho = 0.7$), salinity ($\rho = 0.6$) and brine volume ($\rho = 0.6$) was also found. There was no evidence of a correlation between DFe and PFe for all the sections analysed together and only a moderate one for the bottom ice ($\rho = 0.6$, $p < 0.05$).

2.4 Discussion

2.4.1 How thermodynamics control Fe distribution in fast ice during late spring

During this study we could observe a transitional sea-ice stage characterized by temperatures evolving towards isothermal conditions and decreasing brine salinities (Figure 2.3). At the beginning of the time series (day 320), the lower air temperature maintained the ice surface colder than the bottom and a resulting C-shape salinity profile (Figure 2.3 a, b). The season progressed, and ice surface temperatures reached values above the threshold for bulk ice permeability (–5 °C) for the first time on day 325. Although the *Ra* number did not exceed any theoretical threshold for brine convection during this study (typically of 7; Notz & Worster, 2008), higher *Ra* numbers were observed in the top layers of the ice (where cold, salty and dense brine sits) on day 320 (Figure 2.3 d). This suggests a potential instability and propensity for brine convection to occur and could explain the transfer of most of the DFe pool from the

upper layers of the ice (S1, S2) to the bottom ice (S6, S7) between day 320 and 325 (Figure 2.4b). The loss of brine by convection was also evidenced by a decrease in sea-ice surface salinity. On day 325, the *Ra* gradient (the difference between top and bottom) was already the lowest of the time series; thus, gravity drainage and diffusion are expected to be the main process driving the vertical transfer of Fe from thereon.

The lack of correlation of PFe, DFe, and cFe with brine volume suggests that part of the Fe was retained in the ice despite the brine movement (Lannuzel et al*.,* 2016). This is further evidenced by the fact the Fe concentrations measured in sack-hole brines were much lower than the theoretical brine concentrations calculated for all Fe fractions ($[Fe]_{br} = [Fe]/ \Phi_{br}$, where [Fe] is the concentration of Fe in the bulk sea-ice sample and Φbr is the brine fraction). Interestingly, the mean ratio between theoretical and measured concentrations for the soluble fraction (5 nmol/nmol) was half of that obtained for the colloidal fraction (10 nmol/nmol), suggesting a distinct behaviour between these size fractions. Soluble Fe concentrations also exhibited a moderate correlation with temperature ($\rho = 0.7$), salinity ($\rho = 0.6$) and brine volume ($\rho = 0.6$), further indicating some conservative behaviour between this fraction and the ice thermodynamics. Particulate Fe was also impoverished in the sack-hole brine compared to bulk sea ice when theoretical brine PFe concentrations were calculated, with no correlation with salinity, brine volume, or DFe. Although the high contribution of lithogenic sources to the particulate fraction might have masked any possible correlation between PFe and DFe, this result corroborates previous field observations (van de Merwe et al., 2011) showing that the PFe and cFe fractions might be more susceptible to physical entrapment in the brine channel system than the truly sFe fractions.

2.4.2 Sea-ice biology: estimating the Fe demand by ice algae

The enhanced autotrophic activity in the internal layers of the ice, evidenced by increasing Chl*a* concentrations, combined with a peak of Chl*a* in the upper 3 m of the water column on day 330 (from 0.1 µg/L on day 327 to 0.3 µg/L on day 330), suggests that both sea-ice algae and phytoplankton benefited from the above supply of DFe from surface and interior ice layers. The high Chl*a* concentrations in the lowermost ice sections, where conditions of light, space and nutrient availability are favourable for growth, point toward the dominance of autotrophic activity at this time of the year (Arrigo et al. 2017, Meiners et al., 2018). Archer et al. (1996) reported heterotrophic protozoa were approximately twice as abundant in the sea-ice interior

than in bottom ice near Davis station during late spring-summer 1994. In our study, differences in the POC:PON and Chl*a*:POC ratios observed between S7 and the layers above also suggest a predominant autotrophic bottom and heterotrophic ice interior.

Assuming that the majority of POC in both seawater and bottom sea ice consist of autotroph cells (as inferred from the POC:PON ratios), and using the average Fe:C uptake ratio of 35 µmol:mol for marine diatoms (Sarthou et al., 2004), one can estimate the maximum biological Fe demand during spring. Up to 52 nmol m^{-2} day^{-1} of Fe is required to sustain Davis fast ice (and water column) productivity. During the study period, DFe concentration in seawater (1 - 10 m) decreased by approximately 2 µmol.m^{-2} day^{-1}. Even if we assume that bottom ice communities used Fe exclusively from the seawater via ice-seawater exchanges, the daily loss of seawater DFe greatly exceeded the ice biological demand (and negligible consumption from the phytoplankton). A higher Fe:C uptake ratio by ice algae compared to pelagic phytoplankton could partially explain this difference; sea-ice algae could have evolved to less efficiently use of the abundant Fe present in sea ice. In fact, it has been demonstrated that Fe and silicate colimit diatom growth in the Southern Ocean (Brzezinski et al., 2005; de La Rocha et al., 2000; Franck et al., 2000, 2003; Hoffmann et al, 2007). Considering the predominance of this type of algae group in the ice, a higher silicate requirement per unit of carbon synthesized could, consequently, mean a higher demand for Fe as well. This said, an unlikely much higher µmol:mol Fe:C biological uptake is needed to fully explain the total removal of DFe observed in the seawater, assuming the stability of this fraction in the water. A more plausible answer for the observed mismatch between the primary producers' Fe demand and the seawater DFe decrease could be related to the short residence time of DFe in seawater. The relatively high initial DFe concentration in the seawater on day 320 could come from the sea ice; the changes in sea-ice temperature and permeability observed can promote the flushing of salts and DFe (Lannuzel et al., 2013). Within the seawater, this new input of DFe can rapidly be converted to less soluble forms of Fe in the particulate range via binding with unsaturated algae-produced exopolymeric substances (EPS) favouring aggregation processes onto settling particles or directly precipitated as particulate oxides (Decho & Gutierrez, 2017; Schoemann et al., 1998). In contrast to the DFe trend in the seawater, there is evidence of an increase in the seawater PFe concentration indicating that part of the DFe drainaged to the water might have indeed been adsorbed/converted into PFe. The dominance of autotrophic over heterotrophic processes in the surface water, assumed by the POC:PON ratio (6.7) close to the Redfield ratio of 6.6 for algae uptake (Redfield et al., 1963) would keep the seawater DFe concentration low due to the

lack of conversion of PFe into DFe via recycling. It is worth mentioning that potential advection of new water masses (e.g., tidal cycles) with different physicochemical properties could also have affected the seawater results, masking a clear interaction between the sea-ice and seawater Fe pools (Smith et al., 1984).

2.4.3 Sources of iron to Davis fast ice

The fast ice off Davis lost approximately 0.3 ± 0.14 μmol m^{-2} day^{-1} of DFe during the time series (3.6 ± 1.1 μmol/m^2 over the entire period). This suggests the ice itself could potentially supply all the Fe needed (52 nmol m^{-2} day^{-1}) for the local sea-ice algae and phytoplankton to grow. On the other hand, during the same period, bulk-ice PFe and total Fe (TFe = DFe + PFe) in Davis fast ice increased on average by 2.6 ± 0.7 and 2.3 ± 0.6 μmol m^{-2} day^{-1}, respectively. This represents a ~ 50% increase in the TFe inventory during the time series. The conversion of DFe to PFe via biological uptake would only account for a maximum of 5% of this budget. Therefore, an external input of PFe must be considered. In the next paragraphs, potential sources of Fe to Davis land-fast ice are discussed.

2.4.3.1 Sediments and tides: the influence of coastal proximity on the distribution of iron in fast ice.

Benthic diffusion and resuspension of sediments has been associated with high productivity rates in coastal areas of Antarctica and is suggested as the main pathway to fuel marine productivity on the Antarctic shelf (de Jong et al., 2012). Micromolar DFe concentrations can be found in sediments due to the anoxic reduction and dissolution of the particulate phase (Sachs et al., 2009). The shallow bathymetry of the studied area and the labile characteristics of local surface sediments of predominant biogenic nature would also favour bacterial activity (Dunbar et al., 1989). De Jong et al. (2012) described the presence of a permanent nepheloid layer at the seafloor associated with resuspension processes enriched in leachable PFe which could represent an upfront source of high levels of bioavailable Fe. Even the lower range of marine sediment fluxes reported by the author (1.3 μmol m^{-2} day^{-1}; de Jong et al., 2012) could fully explain the DFe concentrations found in sea ice and seawater throughout the present study. During autumn, the mobilization of this source, driven by the presence of ocean surface winds and a deeper mixed layer, could favour the incorporation of Fe-rich sediments into the

ice. Convection driven by barotropic currents (tidal and density) and vertical diffusion could further pump sediments into the porous sections of the bottom sea ice at the ice-water interface (Hodgkinson, 1991; Vaz & Lennon, 1996). Eventually, this Fe pool can be supplied to the ice algae and phytoplankton communities in spring, when environmental conditions favour primary productivity, but surface mixing is weakened by the presence of sea ice.

Sea-ice DFe concentrations from this study were close to those reported from fast ice in the Ross Sea during summer (de Jong et al., 2013) and in East Antarctica during winter / spring (van der Merwe 2011b). Common to these sites was the proximity to the coast (less than 2 km). DFe reported here were generally higher than those observed by Grotti et al. (2005) in the Ross Sea during summer (Table 2.2), possibly due to the deeper bathymetry (~450 m) of their study site. Our DFe values were also higher than those measured in East Antarctic fast ice, collected approximately 75 km away from the coast (van der Merwe et al, 2011a). Interestingly, PFe concentrations at Davis were in general lower compared to the past studies. This discrepancy could result from a range of factors. Differences in the type of sea ice (columnar versus granular), timing of ice formation, presence or absence of platelet ice, age of the ice (first/multi-year ice), and the stage of the season (spring versus summer), for example, could all lead to different concentrations of PFe incorporated from sedimentary sources (de Jong et al., 2013).

Table 2.2 Reported Fe concentrations (nM) in land-fast ice, snow on sea ice, and under-ice seawater from different areas of the Southern Ocean/Antarctica.

Sample type	Season	DFe (nM)	PFe (nM)	Region	Reference
Snow					
	Spring/summer	5.2 - 37.7	9.0 - 6,090	Prydz Bay, East Antarctica	This study
	Spring	0.2 - 1.1	1.1 - 12.0	East Antarctica	van der Merwe et al. (2011a)
	Winter /spring	0.9 - 7.1	2.3 - 101	East Antarctica	van der Merwe et al. (2011b)
	Summer	112 – 2,410	243 - 10,900	Ross Sea, McMurdo Sound	de Jong et al. (2013)
	Winter/spring	1.0 - 6.5	2.1 - 15.0	East Antarctica	Lannuzel et al. (2007)
	Spring/summer	0.7 - 3.2	7.8 - 14.0	Weddell Sea	Lannuzel et al. (2008)
Fast ice					
	Spring/summer	1.0 - 63.8	2.1 - 416	Prydz Bay, East Antarctica	This study
	Spring	0.8 - 2.1	7.5 - 215	East Antarctica	van der Merwe et al. (2011a)
	Winter /spring	2.1 - 81.0	40.4 - 6,830	East Antarctica	van der Merwe et al. (2011b)
	Summer	2.2 - 109	9.0 - 1,850	Ross Sea, McMurdo Sound	de Jong et al. (2013)
	Summer	1.1 - 6.0	26.0 - 1,162	Terra Nova Bay, Ross Sea	Grotti et al. (2005)
Under ice seawater					
	Spring/summer	2.5 - 6.6	0.2 - 11.8	Prydz Bay, East Antarctica	This study
	Spring	0.1 - 2.6	0.1 - 2.9	East Antarctica	van der Merwe et al. (2011a)
	Winter /spring	1.5 - 3.7	11.0 – 60.0	East Antarctica	van der Merwe et al. (2011b)
	Summer	0.3 - 3.7	1.1 - 20.0	Ross Sea, McMurdo Sound	de Jong et al. (2013)
	Summer	0.7 - 1.5	28.0 - 45.0	Terra Nova Bay, Ross Sea	Grotti et al. (2005)
	Winter/spring	1.1–4.5	<dl-4.4	East Antarctica	Lannuzel et al. (2007)
	Spring/summer	0.7–1.7	0.4–4.0	Weddell Sea	Lannuzel et al. (2008)

2.4.3.2 Snow and dust: Can ice-free areas impact Fe concentrations in fast ice?

Snowpack PFe values measured during the first half of the time series at Davis (days 320 – 327; 9.0 – 255 nM) were similar to those previously observed off Casey Station (van der Merwe, 2011a, 2011b). However, snow PFe values observed during the second half of our study (days 330 – 336, 1.2 – 6.1 μM) are much higher and only comparable to those reported from McMurdo Sound, Ross Sea (de Jong et al., 2013). Snowfall and snowdrift associated with strong winds (see Figure S1) halfway through the time series led to PFe concentrations >1 μM in the snowpack at day 330, 333 and 336. Hourly recorded air temperature data from Davis Station showed positive air temperatures were reached for the first time on day 329 (Figure 2.4a). This surface warming may have led to the percolation of Fe-rich particles through the melting snowpack, leading to the sharp PFe increase observed in the ice below on day 330. This input can be translated into 80% of PFe added to the sea ice between the first and second half of the time series and could be explained by the percolation of only 5% of the snow PFe.

The question is: where is this high PFe in snow coming from? The proximity to extensive ice-free land as a common geographic characteristic could explain the high snow PFe observed near Davis and McMurdo (de Jong et al., 2013). The Davis sampling site was surrounded by ice-free rocks: Vestfold Hills in the south, the largest rocky ice-free land in East Antarctica, and three major islands (Anchorage, Trigwell, and Futtler island) in the north. A satellite image obtained during springtime shows the possible influence of this dust source to the area (Figure 2.1b), where north-easterly winds draw a dust plume onto the ice offshore from the Vestfold Hills and surrounding islands. To validate this satellite observation, elemental molar ratios measured in snow samples were compared to literature values from the continental crust and Vestfold Hills rock samples. The average snow Fe:Al molar ratio of 0.5 obtained from Davis snow is consistent with previous Fe:Al ratio estimates of ~0.4 for the upper continental crust obtained during different geological surveys (Gao et al., 1998; Taylor & McLannen, 1985; Wedepohl, 1995). Similarly, the snow Ba:Sr ratio of 1.8 from this study also falls within the range of 0.9 - 2.5 for the upper and bulk continental crust and is close to values found in the predominant rock composition of the Vestfold Hills, listed: felsic tonalite (0.9 to 1.4), mafic granulite (0.6 to 3.1) and biotite-garnet-quartz-feldspar gneisses (~2.0), which vary along the Vestfold Hills (Sharaton & Collerson, 1984). The observed Davis snow Th:U ratio (2.6) was also consistent with Th:U values from the abundant tonalities found in the Mossel and Crooked Lake gneisses (2.0 and 4.0), two major lithogenic units of the Vestfold Hills (Sharaton & Collerson, 1984). Therefore, assuming the absence of seawater infiltration into the snow (as indicated by the low snow salinity value) and disregarding any negligible contribution from

long-range atmospheric aerosol deposition during the period under consideration, the overall high concentration of PFe in the snow can be plausibly linked to natural dust input from the surrounding land, as also suggested by the satellite imagery. In this context, we can calculate the PFe flux from local dust sources. Coastal dust was responsible for a flux of 374 ± 146 μmol m^{-2} day^{-1} of PFe over the blizzard event. The same can be translated into an average flux of 8.3 ± 3.3 μmol m^{-2} day^{-1} of dust PFe into Davis land-fast sea ice, assuming 3 months of the spring season.

Dust is a lithogenic and therefore a highly refractory source of Fe. Once added to sea ice or seawater, lithogenic Fe can undergo photochemical and biologically mediated processes that increase its bioavailability (Frew et al., 2006; Hassler & Schoemann, 2009). These processes can become especially relevant considering the magnitude of the dust flux observed. Besides affecting the amount of Fe input to sea ice, snow PFe can supplement the Fe released from melting sea ice, potentially extending the duration of the Fe fertilization from the event. Global-scale biogeochemical models have assigned the fractional solubility of natural Fe aerosols within the range of 1-10% (Archer & Johnson, 2000; Fung et al., 2000; Gao et al., 2003; Gregg et al., 2003; Moore et al., 2004; Moore & Doney, 2007). Using this solubility range and dust flux of 8.3 μmol m^{-2} day^{-1}, wind-blown dust could deliver 0.08 to 0.8 μmol m^{-2} day^{-1} of DFe to the sea ice and seawater during springtime. It is worth noting that this flux could be lower or higher given that Fe solubility in dust particles is still a highly debated topic (Chen et al., 2006; Mackie et al., 2005; Mahowald et al., 2009; Zhu et al., 1997). Edwards and Sedwick (2001), for example, reported Fe solubility of 30% in Antarctic snow, while other researchers have argued that almost all aeolian Fe might be bioavailable, depending on the timescale, ligands complexation and acquisition mechanisms from the biological community (Gledhill & Buck, 2012; Mahowald et al., 2009; Weber et al., 2005). The dissolution of lithogenic PFe within the snow could explain why the ice sFe concentrations were maintained constant through time even considering evidence of brine movement. Part of this sFe is expected to be rapidly converted into cFe (Wu et al., 2001), which could then bind to EPS and be adsorbed onto cell surfaces. The concentration of cFe would still decrease, as observed here, not only due to the loss of this fraction to the seawater via gravity drainage but also because cell coated cFe-EPS is retained during filtration. Interestingly, the mean sFe:PFe ratio obtained in snow samples from the first half of the time series ($5 \times 10^{-2} \pm 7 \times 10^{-2}$), before the snowstorm on day 329, was three orders of magnitude greater than the mean sFe:PFe from the second half ($7.5 \times 10^{-5} \pm 5 \times 10^{-5}$). This indicates that the interaction between snow, which can carry atmospheric acids

such as sulphate and organic acids, and the dust may increase Fe solubility in snow, given enough time for this process to occur. The relevance of this symbiotic interaction is evidenced by studies which have shown that atmospheric aerosol particles have much higher Fe solubility (up to 80%; Baker et al., 2006; Johansen et al*.,* 2000) than soil purely. Once deposited onto the snowpack, the Fe dissolution from refractory particles could be further aided by photochemical reactions in the snowpack, taking advantage of its upfront exposition to the sunlight. Photoreduction of Fe^{+3} to Fe^{+2} can enhance its solubility and bioavailability (Barbeau & Moffett, 2000). Therefore, even though most of the Fe found in the Davis snowpack is likely from local dust and not from other types of atmospheric aerosol particles (desert dust/combustion) carried during wet deposition (snow), the sFe:PFe results suggest an important interaction between snow and dust (soil) favouring the solubilization of Fe. Although the processes discussed above are potentially relevant for the first part of the time series, the short observation window after day 329 restricted our chances to observe the same Fe solubilization in surface snow during the second part. Clearly, measurements using relevant sieving and chemical leaching techniques are needed to deliver a uniform assessment on Fe solubility from lithogenic sources under varying atmospheric conditions.

2.4.3.3 Flux from other sources

The average and range of under-ice seawater DFe concentrations in this study were higher than previously observed under land-fast and pack ice (Table 2.2). This could not only be related to the shallow bathymetry of the area (20 m) and contribution from sea ice but also to the proximity of nearby ice shelves, lateral transport, as well as recycling processes. When the sea ice starts to consolidate during autumn, convective processes driven by the brine rejection contribute to the vertical mixing of water. At this time of the year, seawater is also enriched in Fe from the melting of the surrounding AIS and WIS. Herraiz-Borreguero et al. (2016) found concentrations of DFe in the marine ice of the AIS up to four orders of magnitude higher than those typical of Southern Ocean surface waters, which could fertilize waters 300 km away from the meltwater source. The potential influx of bioavailable Fe into Prydz Bay waters due to the common presence of icebergs could also have an important impact on the mobilization of sediments and mechanical mixing/upwelling of the water column, also dragging considerable amount of terrigenous material (Arrigo et al., 2008; Duprat et al., 2016; Raiswell et al., 2008; Smith et al*.,*2007). Lateral advection associated with the westerly current along the coast and

deeper intrusive water masses originating from the Antarctic Circumpolar Current can also sustain a constant influx of new stock of Fe into the area (Vas & Lennon 1996). Finally, biotic mechanisms such as grazing by protozoa and recycling by higher trophic levels have been proposed to regenerate bioavailable Fe in the seawater providing a secondary source of Fe to coastal fast ice (Nicol et al., 2010; Ratnarajah et al., 2014; Schmidt et al., 2011).

2.4.4 Estimating the potential primary production in East Antarctica from fast-ice melting

The combined sea-ice and snow median inventory of 13.9 µmol/m^2 DFe and 252 µmol/m^2 PFe for the study period could represent a flux to the seawater of approximately 0.5 and 8.4 µmol m^{-2} day^{-1}, respectively; assuming a period of 30 days for the complete release of both fractions (Lannuzel et al., 2008). This ice DFe flux is higher than the estimate of 0.3 µmol m^{-2} day^{-1} for pack ice around East Antarctica (Lannuzel et al., 2010), 0.34 and 0.25 µmol m^{-2} day^{-1} for ice floes in the Bellingshausen Sea (de Jong et al., 2015), and 0.05 - 0.3 µmol m^{-2} day^{-1} obtained for land-fast sea ice in McMurdo Sound, Ross Sea (de Jong et al., 2013). Based on our Fe concentration measurements, and considering that a strip of approximately 20 km wide first-year fast ice along the ~ 1,200 km eastern shore of Prydz Bay (Ingrid Christensen to Queens Mary Coast) is formed every winter (Fraser et al., 2012), 0.6 ± 0.2 tons/day DFe is expected to be released on the east coast of Prydz Bay during the melting season. The transport of coastal ice floes into off-shore waters could represent, therefore, an important source of this essential element to Fe-depleted waters. Under favourable conditions of light and macronutrient availability, this "new" Fe input could potentially produce about 170 mgC m^{-2} day^{-1} of biomass (disregarding any regenerative DFe process associated with the microbial loop, recycling from higher trophic levels and/or other sources of DFe), which is comparable to the production estimated as 200 mgC m^{-2} day^{-1} for early December (Arrigo et al., 2008) for the whole of Antarctic shelf waters. Our estimate suggests that Fe does not limit primary production in the coastal areas of the South Indian sector of Antarctica.

2.5 Conclusions

Results from this study indicate that primary production in East Antarctic fast ice is not Fe-limited during late spring/early summer. The contribution of ice-free land areas on the fast ice Fe pool is also highlighted. The magnitude of this Fe source will become more pronounced as

we expect ice-free areas to increase in Antarctica. A higher input of dust to the major system of polynyas in Prydz Bay via fast ice melting, and associated ocean physics and biological dynamics, could represent an important vector of potentially bioavailable Fe to Antarctic open waters. Foreseen changes in the prevailing precipitation regime towards higher snowfall in coastal East Antarctica are also expected to impact the biogeochemical and physical properties of the fast ice. This could also lead to a phenological mismatch between nutrient availability and ideal light conditions if the timing and duration of Fe delivery relative to the nutrient uptake capacity of algae communities are altered. For all that, the potential fertilization of the Southern Ocean via sea-ice melting should be directly impacted by changes in the coastal areas. Further studies are needed to assess the impact of enhanced lithogenic Fe input to Antarctic fast ice and beyond.

2.6 Acknowledgements and Data

This work was co-funded by the Australian Government Cooperative Research Centre Programme through the Antarctic Climate & Ecosystems (ACE CRC), the Australian Antarctic Science (AAS) project no. 4291 and 4298, the Australian Research Council's Special Research Initiative for Antarctic Gateway Partnership (Project ID SR140300001) and the Vrije Universiteit Brussel internal funding in the framework of Strategic Research Plan "Tracers of Past and Present Global Changes". The authors thank the two reviewers for their comments which greatly improved the manuscript. Data supporting the analyses and conclusions here presented can be accessed at the Australian Antarctic Data Centre website (https://data.aad.gov.au/metadata/records/AAS_4291_2016_seaice).

2.7 References

Arar, E. J., & Collins, G. B. (1997). *Method 445.0 [electronic resource]:* in vitro determination of chlorophyll a and pheophytin a in marine and freshwater algae by fluorescence. [Cincinnati, OH]: United States Environmental Protection Agency, Office of Research and Development, National Exposure Research Laboratory, [1997].

Archer, D. E. and K. Johnson (2000). A model of the iron cycle in the ocean. *Global Biogeochemical Cycles,* 14(1): 269-279. https://doi.org/10.1029/1999GB900053

Archer, S. D., Leakey, R. J. G., Burkill, P. H., Sleigh, M. A., & Appleby, C. J. (1996). Microbial ecology of sea ice at a coastal Antarctic site: Community composition, biomass and temporal change. *Marine Ecology Progress Series*, 135(1-3): 179-195. https://doi.org/10.3354/meps135179

Arrigo, K. R., van Dijken, G. L., Alderkamp, A.-C., Erickson, Z. K., Lewis, K. M., Lowry, K. E. et al. (2017). Early Spring Phytoplankton Dynamics in the Western Antarctic Peninsula. *Journal of Geophysical Research: Oceans*, 122(12): 9350-9369. https://doi.org/10.1002/2017jc013281

Arrigo, K. R., van Dijken, G. L., & Bushinsky, S. (2008). Primary production in the Southern Ocean, 1997-2006. *Journal of Geophysical Research: Oceans*, 113(C8). https://doi.org/10.1029/2007jc004551

Arrigo, K. R., van Dijken, G. L., & Strong, A. L. (2015). Environmental controls of marine productivity hot spots around Antarctica. *Journal of Geophysical Research: Oceans*, 120(8): 5545-5565. https://doi.org/10.1002/2015jc010888

Arrigo, K. R., Worthen, D. L., Lizotte, M. P., Dixon P., & Dieckmann, G. (1997). Primary production in Antarctic sea ice. *Science*, 276(5311): 394-397. https://doi.org/10.1126/science.276.5311.394

Arrigo, K. R., Worthen, D. L., & Robinson, D. H. (2003). A coupled ocean-ecosystem model of the Ross Sea: 2. Iron regulation of phytoplankton taxonomic variability and primary production. *Journal of Geophysical Research: Oceans*, 108(C7). https://doi.org/10.1029/2001jc000856

Baker, A. R., & Jickells, T. D. (2006). Mineral particle size as a control on aerosol iron solubility. *Geophysical Research Letters*, 33(17). https://doi.org/10.1029/2006gl026557

Barbeau, K., & J. W. Moffett (2000), Laboratory and field studies of colloidal iron oxide dissolution as mediated by phagotrophy and photo- lysis, *Limnology and Oceanography,* 45, 827–835. https://doi.org/10.4319/lo.2000.45.4.0827

Benner, R. (2011). Loose ligands and available iron in the ocean. *Proc. Natl. Acad. Sci. (PNAS) USA*, 108(3): 893-894. https://doi.org/10.1073/pnas.1018163108

Bishara, A. J., & Hittner, J. B. (2012). Testing the significance of a correlation with nonnormal data: comparison of Pearson, Spearman, transformation, and resampling approaches. *Psychol. Methods,* 17(3): 399-417. https://doi.org/10.1037/a0028087

Blain, S., Queguiner, B., Armand, L., Belviso, S., Bombled, B., Bopp, L. et al. (2007). Effect of natural iron fertilization on carbon sequestration in the Southern Ocean. *Nature*, 446(7139): 1070-1074. https://doi.org/10.1038/nature05700

Borer, P. M., Sulzberger, B., Reichard, P., & Kraemer, S. M. (2005). Effect of siderophores on the light-induced dissolution of colloidal iron(III) (hydr)oxides. *Marine Chemistry*, 93(2-4): 179-193. https://doi.org/10.1016/j.marchem.2004.08.006

Bowie, A. R., Townsend, A. T., Lannuzel, D., Remenyi T. A., & van der Merwe, P. (2010). Modern sampling and analytical methods for the determination of trace elements in marine particulate material using magnetic sector inductively coupled plasma-mass spectrometry. *Analytica Chimica Acta*, 676(1-2): 15-27. https://doi.org/10.1016/j.aca.2010.07.037

Boyd, P. W., Jickells, T., Law, C. S., Blain, S., Boyle, E. A., Buesseler, K. O. et al. (2007). Mesoscale iron enrichment experiments 1993-2005: synthesis and future directions. *Science*, 315(5812): 612-617. https://doi.org/10.1126/science.1131669

Brzezinski, M. A., Jones, J. L., & Demarest, M. S. (2005). Control of silica production by iron and silicic acid during the Southern Ocean Iron Experiment (SOFeX). *Limnology and Oceanography*, 50(3): 810-824. https://doi.org/10.4319/lo.2005.50.3.0810

Chen, M., Dei, R. C. H., Wang, W. X., & Guo, L. D. (2003). Marine diatom uptake of iron bound with natural colloids of different origins. *Marine Chemistry*, 81(3-4): 177-189. https://doi.org/10.1016/S0304-4203(03)00032-X

Cox, G. F. N. & Weeks, W. F. (1988). Numerical simulations of the profile properties of undeformed first-year sea ice during the growth season. *Journal of Geophysical Research*, 93(C10). https://doi.org/10.1029/JC093iC10p12449

Cutter, G., Casciotti, K., Cullen, P., Geibert, W., Heimbürger, L.-E., Lohan, M. C. et al. (2017). *Sampling and Sample-handling Protocols for GEOTRACES Cruises*. Retrieved from https://geotracesold.sedoo.fr/images/Cookbook.pdf

de Jong, A., Schoemann, V., Maricq, N., Mattielli, N., Patricia, L., Haskell, T. et al. (2013). Iron in land-fast sea ice of McMurdo Sound derived from sediment resuspension and wind-blown dust attributes to primary productivity in the Ross Sea, Antarctica. *Marine Chemistry*, 157: 24–40. https://doi.org/0.1016/j.marchem.2013.07.001

de Jong, J., V. Schoemann, Lannuzel, D., Croot, P., de Baar, H., & Tison, J.-L. (2012). Natural iron fertilization of the Atlantic sector of the Southern Ocean by continental shelf sources of the Antarctic Peninsula. *Journal of Geophysical Research: Biogeosciences*, 117(G1). https://doi.org/10.1029/2011jg001679

De La Rocha, C. L., Hutchins, D. A., Brzezinski, M. A., & Zhang, Y. (2000). Effects of iron and zinc deficiency on elemental composition and silica production by diatoms. *Marine Ecology Progress Series*, 195: 71-79. https://doi.org/10.3354/meps195071

Decho, A. W. & Gutierrez, T. (2017). Microbial Extracellular Polymeric Substances (EPSs) in Ocean Systems. *Frontiers in Microbiology*, 8: 922. https://doi.org/10.3389/fmicb.2017.00922

Dunbar, R. B., Leventer, A. R., & Stockton, W. L. (1989). Biogenic Sedimentation in Mcmurdo Sound, Antarctica. *Marine Geology*, 85(2-4): 155-179. https://doi.org/10.1016/0025-3227(89)90152-7

Duprat, L. P. A. M., Bigg, G. R., & Wilton, D. J. (2016). Enhanced Southern Ocean marine productivity due to fertilization by giant icebergs. *Nature Geoscience*, 9(3): 219-221. https://doi.org/10.1038/ngeo2633

Edwards, R. & Sedwick, P. (2001). Iron in East Antarctic snow: Implications for atmospheric iron deposition and algal production in Antarctic waters. *Geophysical Research Letters*, 28(20): 3907-3910. https://doi.org/10.1029/2001gl012867

Franck, V. M., Bruland, K. W., Hutchins, D. A., & Brzezinski, M. A. (2003). Iron and zinc effects on silicic acid and nitrate uptake kinetics in three high-nutrient, low-chlorophyll (HNLC) regions. *Marine Ecology Progress Series*, 252: 15-33. https://doi.org/10.3354/meps252015

Fraser, A. D., Massom, R. A., Michael, K. J., Galton-Fenzi, B. K., & Lieser, J. L. (2012). East Antarctic Landfast Sea Ice Distribution and Variability, 2000-08. *Journal of Climate*, 25(4): 1137-1156. https://doi.org/10.1175/Jcli-D-10-05032.1

Frew, R. D., Hutchins, D. A., Nodder, S., Sanudo-Wilhelmy, S., Tovar-Sanchez, A., Leblanc, K. et al. (2006). Particulate iron dynamics during Fe Cycle in subantarctic waters southeast of New Zealand. *Global Biogeochemical Cycles*, 20(1). https://doi.org/10.1029/2005gb002558

Fung, I. Y., Meyn, S. K., Tegen, I., Doney, S. C., John, J. G., & Bishop, J. K. B. (2000). Iron supply and demand in the upper ocean. *Global Biogeochemical Cycles*, 14(1): 281-295. https://doi.org/10.1029/1999gb900059

Gao, Y. (2003). Aeolian iron input to the ocean through precipitation scavenging: A modeling perspective and its implication for natural iron fertilization in the ocean. *Journal of Geophysical Research*, 108(D7). https://doi.org/10.1029/2002JD002420

Gao, S., Luo, T.-C., Zhang, B.-R., Zhang, H.-F., Han, Y.-w., Zhao, Z.-D. et al. (1998). Chemical composition of the continental crust as revealed by studies in East China. *Geochimica et Cosmochimica Acta*, 62(11): 1959-1975. https://doi.org/10.1016/s0016-7037(98)00121-5

Gerringa, L. J. A., Alderkamp, A.-C., Laan, P., Thuróczy, C.-E., De Baar, H. J. W., Mills, M. M. et al. (2012). Iron from melting glaciers fuels the phytoplankton blooms in Amundsen Sea (Southern Ocean): Iron biogeochemistry. *Deep Sea Research Part II: Topical Studies in Oceanography,* 71-76: 16-31. https://doi.org/10.1016/j.dsr2.2012.03.007

Gledhill, M., & Buck, K. N. (2012). The organic complexation of iron in the marine environment: a review. *Frontiers in Microbiology,* 3: 69. https://doi.org/10.3389/fmicb.2012.00069

Google Earth Pro 7 V.3.2.5776 (December 31, 2015). Davis Station, Antarctica. 68° 34′ 36″ S, 77°58′ 03″ E, Eye alt 8.7 Km. Image Landsat / Copernicus. DigitalGlobe 2019. http://www.earth.google.com [July 20, 2019]

Gregg, W. W., P. Ginoux, P. S. Schopf and N. W. Casey (2003). Phytoplankton and iron: validation of a global three-dimensional ocean biogeochemical model. *Deep Sea Research Part II: Topical Studies in Oceanography*, 50(22-26): 3143-3169. https://doi.org/10.1016/j.dsr2.2003.07.013

Grotti, M., Soggia, F., Ianni, C., & Frache, R. (2005). Trace metals distributions in coastal sea ice of Terra Nova Bay, Ross Sea, Antarctica. *Antarctic Science*, 17(2): 289-300. https://doi.org/10.1017/S0954102005002695

Hassler, C. S., & Schoemann, V. (2009). Bioavailability of organically bound Fe to model phytoplankton of the Southern Ocean. *Biogeosciences Discussions*, 6(10): 2281-2296. https://doi.org/10.5194/bg-6-2281-2009

Herraiz-Borreguero, L., Lannuzel, D., van der Merwe, P., Treverrow, A., & Pedro, J. B. (2016). Large flux of iron from the Amery Ice Shelf marine ice to Prydz Bay, East Antarctica. *Journal of Geophysical Research: Oceans*, 121(8): 6009-6020. https://doi.org/10.1002/2016jc011687

Hodgkinson, R., Colman, R.S., Robb, M.S., & Williams, R. (1991). Current meter moorings in the region of Prydz Bay, Antarctica, 1987. *Research notes 81*, Antarctic Division, Kingston, Tasmania, Australia, p. 130.

Hoffmann, L. J., Peeken, I., & Lochte, K. (2007). Co-limitation by iron, silicate, and light of three Southern Ocean diatom species. *Biogeosciences Discussions*, 4(1): 209-247. https://doi.org/10.5194/bgd-4-209-2007

Hudson, R. J. M., & Morel, F. M. M. (1990). lron transport in marine phytoplankton: Kinetics of cellular and medium coordination reactions. *Limnology and Oceanography*, 35(5): 1002-1020. https://doi.org/10.4319/lo.1990.35.5.1002

Hudson, R. J. M., & Morel, F. M. M. (1993). Trace-Metal Transport by Marine Microorganisms - Implications of Metal Coordination Kinetics. *Deep-Sea Research Part I: Oceanographic Research Papers*, 40(1): 129-150. https://doi.org/10.1016/0967-0637(93)90057-A

Johansen, A. M., Siefert, R. L., & Hoffmann, M. R. (2000). Chemical composition of aerosols collected over the tropical North Atlantic Ocean. *Journal of Geophysical Research: Atmospheres*, 105(D12): 15277-15312. https://doi.org/10.1029/2000jd900024

Kraemer, S. M. (2004). Iron oxide dissolution and solubility in the presence of siderophores. *Aquatic Sciences - Research Across Boundaries*, 66(1): 3-18. https://doi.org/10.1007/s00027- 003-0690-5

Kuma, K., & Matsunaga, K. (1995). Availability of Colloidal Ferric Oxides to Coastal Marine-Phytoplankton. *Marine Biology*, **122**(1): 1-11. https://doi.org/10.1007/Bf00349272

Lannuzel, D., de Jong, J., Schoemann, V., Trevena, A., Tison, J. L., & Chou, L. (2006). Development of a sampling and flow injection analysis technique for iron determination in the sea ice environment. *Analytica Chimica Acta*, 556(2): 476-483. https://doi.org/10.1016/j.aca.2005.09.059

Lannuzel, D., Schoemann, V., de Jong, J., Chou, L., Delille, B., Becquevort, S. et al. (2008). Iron study during a time series in the western Weddell pack ice. *Marine Chemistry*, 108(1-2): 85-95. https://doi.org/10.1016/j.marchem.2007.10.006

Lannuzel, D., Schoemann, V., de Jong, J., Pasquer, B., van der Merwe, P., Masson, F. et al. (2010). Distribution of dissolved iron in Antarctic sea ice Spatial seasonal and interannual variability. *Journal of Geophysical Research*, 115: G03022. https://doi.org/0.1029/2009JG001031

Lannuzel, D., Schoemann, V., de Jong, J., Tison J. L., & Chou, L. (2007). Distribution and biogeochemical behavior of iron in the East Antarctic sea ice. *Marine Chemistry*, 106(1-2): 18-32. https://doi.org/10.1016/j.marchem.2006.06.010

Lannuzel, D., van der Merwe P., Townsend, A. T., & Bowie, A. R. (2014). Size fractionation of iron, manganese and aluminum in Antarctic fast ice reveals a lithogenic origin and low iron solubility. *Marine Chemistry*, 161: 47-56. https://doi.org/10.1016/j.marchem2014.02.006

Lannuzel, D., Vancoppenolle, M., van der Merwe, P., de Jong, J., Meiners, K. M., Grotti, M. et al. (2016). Iron in sea ice: Review and new insights. *Elementa: Science of the Anthropocene*, 4: 000130. https://doi.org/10.12952/journal.elementa.000130

Lee, J. R., Raymond, B., Bracegirdle, T. J., Chades, I., Fuller, R. A., Shaw, J. D. et al. (2017). Climate change drives expansion of Antarctic ice-free habitat. *Nature*, 547(7661): 49-54. https://doi.org/10.1038/nature22996

Lis, H., Shaked, Y., Kranzler, C., Keren, N., & Morel, F. M. (2015). Iron bioavailability to phytoplankton: an empirical approach. *ISME J*, 9(4): 1003-1013. https://doi.org/10.1038/ismej.2014.199

M. Franck, V., Brzezinski, M. A., Coale, K. H., & Nelson, D. M. (2000). Iron and silicic acid concentrations regulate Si uptake north and south of the Polar Frontal Zone in the Pacific Sector of the Southern Ocean. *Deep Sea Research Part II: Topical Studies in Oceanography*, 47(15-16): 3315-3338. https://doi.org/10.1016/s0967-0645(00)00070-9

Mackie, D. S., Peat, J. M., McTainsh, G. H., Boyd, P. W., & Hunter, K. A. (2006). Soil abrasion and eolian dust production: Implications for iron partitioning and solubility. *Geochemistry, Geophysics, Geosystems*, **7**(12). https://doi.org/10.1029/2006gc001404

Mahowald, N. M., Engelstaedter, S., Luo, C., Sealy, A., Artaxo, P., Benitez-Nelson, C. et al. (2009). Atmospheric iron deposition: global distribution, variability, and human perturbations. *Annual Review of Marine Science*, 1: 245-278. https://doi.org/10.1146/annurev.marine.010908.163727

Martin, J. H. (1990). Glacial-interglacial CO_2 change: The Iron Hypothesis. *Paleoceanography*, 5(1): 1-13. https://doi.org/10.1029/PA005i001p00001

Martin, J. H., & Fitzwater, S. E. (1988). Iron deficiency limits phytoplankton growth in the north-east Pacific subarctic. *Nature*, 331: 341–343. https://doi.org/ 10.1038/331341a0

Martin, J. H., Gordon, R. M., & Fitzwater, S. E. (1991). The Case for Iron. *Limnology and Oceanography*, 36(8): 1793-1802. https://doi.org/10.4319/lo.1991.36.8.1793

Meiners, K., Brinkmeyer, R., Granskog, M. A., & Lindfors, A. (2004). Abundance, size distribution and bacterial colonization of exopolymer particles in Antarctic sea ice (Bellingshausen Sea). *Aquatic Microbial Ecology*, 35: 283-296. https://doi.org/10.3354/ame035283

Meiners, K. M., Krembs, C., & Gradinger, R. (2008). Exopolymer particles: microbial hotspots of enhanced bacterial activity in Arctic fast ice (Chukchi Sea). *Aquatic Microbial Ecology*, 52(2): 195-207. https://doi.org/10.3354/ame01214

Meiners, K. M., & Michel, C. (2017). *Dynamics of nutrients, dissolved organic matter and exopolymers in sea ice.* In: *Thomas, DN (ed.), Sea Ice.* Oxford, UK: Wiley-Blackwell, Wiley- Blackwell. https://doi.org/10.1002/9781118778371.ch17

Meiners, K. M., Vancoppenolle, M., Carnat, G., Castellani, G., Delille, B., Delille, D. et al. (2018). Chlorophyll-a in Antarctic Landfast Sea Ice: A First Synthesis of Historical Ice Core Data. *Journal of Geophysical Research: Oceans*, 123(11): 8444-8459. https://doi.org/10.1029/2018jc014245

Millero, F. J. (1998). Solubility of Fe (III) in seawater. *Earth and Planetary Science Letters*, 154(1-4): 323-329. https://doi.org/10.1016/S0012-821x(97)00179-9

Moore, J. K., Doney, S. C., Glover, D. M., & Fung, I. Y. (2001). Iron cycling and nutrient- limitation patterns in surface waters of the World Ocean. *Deep Sea Research Part II: Topical Studies in Oceanography*, 49(1-3): 463-507. https://doi.org/10.1016/s0967-0645(01)00109-6

Moore, J. K. and S. C. Doney (2007). Iron availability limits the ocean nitrogen inventory stabilizing feedbacks between marine denitrification and nitrogen fixation. *Global Biogeochemical Cycles,* 21(2): n/a-n/a. https://doi.org/10.1029/2006GB002762

Moore, J. K., S. C. Doney and K. Lindsay (2004). Upper ocean ecosystem dynamics and iron cycling in a global three-dimensional model. *Global Biogeochemical Cycles*, 18(4): n/a-n/a. https://doi.org/10.1029/2006GB002762

Morel, F. M. M., Kustka, A. B., & Shaked, Y. (2008). The role of unchelated Fe in the iron nutrition of phytoplankton. *Limnology and Oceanography*, 53(1): 400-404. https://doi.org/10.4319/lo.2008.53.1.0400

NASA Earth Observing System Data and Information System (EOSDIS) (2018). Terra / MODIS true color image from Davis Station. Retrieved from https://worldview.earthdata.nasa.gov

Nicol, S., Bowie, A., Jarman, S., Lannuzel, D., Meiners, K. M., & Van Der Merwe, P. (2010). Southern Ocean iron fertilization by baleen whales and Antarctic krill. *Fish and Fisheries*, 11(2): 203-209. https://doi.org/10.1111/j.1467-2979.2010.00356.x

Notz, D., & Worster , M. G. (2008). In situ measurements of the evolution of young sea ice. *Journal of Geophysical Research,* 113(C3). https://doi.org/10.1029/2007jc004333

Nunes Vaz, R. A., & Lennon, G. W. (1996). Physical oceanography of the Prydz Bay region of Antarctic waters. *Deep Sea Research Part I: Oceanographic Research Papers*, 43(5): 603-641. https://doi.org/10.1016/0967-0637(96)00028-3

Raiswell, R., Benning, L. G., Tranter, M., & Tulaczyk, S. (2008). Bioavailable iron in the Southern Ocean: the significance of the iceberg conveyor belt. *Geochemical Transactions*, 9(1). https://doi.org/10.1186/1467-4866-9-7

R Core Team (2013). R: A language and environment for statistical computing. R Foundation for Statistical Compluting, Viena, Austria. http://R-project.org/

Ratnarajah, L., Bowie, A. R., Lannuzel, D., Meiners, K. M., & Nicol, S. (2014). The biogeochemical role of baleen whales and krill in Southern Ocean nutrient cycling. *PLoS One*, 9(12): e114067. https://doi.org/10.1371/journal.pone.0114067

Redfield, A. C., Ketchum, B. H., & Richards, F.A. (1963). The influence of organisms on the composition of sea water. *In: M.N. Hill. The Sea.,* 2. Interscience Publishers, New York.

Rintala, J. M., Piiparinen, J., Blomster, J., Majaneva, M., Muller, S., Uusikivi, J. et al. (2014). Fast direct melting of brackish sea-ice samples results in biologically more accurate results than slow buffered melting. *Polar Biology*, 37(12): 1811-1822. https://doi.org/10.1007/s00300-014-10431563-1

Sachs, O., Sauter, E. J., Schlüter, M., Rutgers van der Loeff, M. M., Jerosch, K., & Holby, O. (2009). Benthic organic carbon flux and oxygen penetration reflect different plankton provinces in the Southern Ocean. *Deep Sea Research Part I: Oceanographic Research Papers*, 56(8): 1319-1335. https://doi.org/10.1016/j.dsr.2009.02.003

Sarthou, G., Timmermans, K. R., Blain, S., & Treguer, P. (2005). Growth physiology and fate of diatoms in the ocean: a review. *Journal of Sea Research*, 53(1-2): 25-42. https://doi.org/10.1016/j.seares.2004.01.007

Schmidt, K., Schlosser, C., Atkinson, A., Fielding, S., Venables, H. J., Waluda, C. M. et al. (2016). Zooplankton Gut Passage Mobilizes Lithogenic Iron for Ocean Productivity. *Current Biology*, 26(19): 2667-2673. https://doi.org/10.1029/PA005i001p00001

Schoemann, V., de Baar, H. J. W., de Jong, J. T. M., & Lancelot, C. (1998). Effects of phytoplankton blooms on the cycling of manganese and iron in coastal waters. *Limnology and Oceanography*, 43(7): 1427-1441. https://doi.org/10.4319/lo.1998.43.7.1427

Sedwick, P. N., & DiTullio, G. R. (1997). Regulation of algal blooms in Antarctic shelf waters by the release of iron from melting sea ice. *Geophysical Research Letters*, 24(20): 2515-2518. https://doi.org/10.1029/97gl02596

Sedwick, P. N., Edwards, P. R., Mackey, D. J., Griffiths, F. B., & Parslow, J. S. (1997). Iron and manganese in surface waters of the Australian subantarctic region. *Deep-Sea Research Part I: Oceanographic Research Papers*, 44(7): 1239-1253. https://doi.org/10.1016/S0967-0637(97)00021-6

Sheraton, J. W., Black, L. P., & McCulloch, M. T. (1984). Regional geochemical and isotopic characteristics of high-grade metamorphics of the Prydz bay area: The extent of proterozoic reworking of Qrchaean continental crust in East Antarctica. *Precambrian Research*, 26(2): 169-198. https://doi.org/10.1016/0301-9268(84)90043-3

Sheraton, W., & Collerson, K. D. (1984). Archaen and Proterozoic geological relationships in the estfold Hills - Prydz bay area, Antarctica. *Journal of Australian Geology & Geophysics*, 8: 19-128.

Smith, K. L., Jr., Robison, B. H., Helly, J. J., Kaufmann, R. S., Ruhl, H. A., Shaw, T. J. et al. 2007). Free-drifting icebergs: hot spots of chemical and biological enrichment in the Weddell Sea. *Science*, 317(5837): 478-482. https://doi.org/10.1126/science.1142834

Smith, N. R., Zhaoqian, D., Kerry, K. R., & Wright, S. (1984). Water masses and circulation in the region of Prydz Bay, Antarctica. *Deep Sea Research Part I: Oceanographic Research Papers*, 31(9): 1121-1147. https://doi.org/10.1016/0198-0149(84)90016-5

Sullivan, C. W., Arrigo, K. R., McClain, C. R., Comiso, J. C., & Firestone, J. (1993). Distributions of phytoplankton blooms in the Southern Ocean. *Science*, 262(5141): 1832-1837. https://doi.org/10.1126/science.262.5141.1832

Sulzberger, B., Suter, D., Siffert, C., Banwart, S., & Stumm, W. (1989). Dissolution of Fe(III)(Hydr)Oxides in Natural-Waters - Laboratory Assessment on the Kinetics Controlled by Surface Coordination. *Marine Chemistry*, 28(1-3): 127-144. https://doi.org/10.1016/0304-4203(89)90191-6

Taylor, S. R., & McLennan, S. M. (1985). The Continental Crust: Its Composition and Evolution. *Geological Magazine*, 122(06). https://doi.org/10.1017/s0016756800032167

van der Merwe, P., Lannuzel, D., Bowie, A. R., Nichols, C. A. M., & Meiners, K. M. (2011a). Iron fractionation in pack and fast ice in East Antarctica: Temporal decoupling between the release of dissolved and particulate iron during spring melt. *Deep Sea Research Part II: Topical Studies in Oceanography*, 58(9-10): 1222-1236. https://doi.org/10.1016/j.dsr2.2010.10.036

van der Merwe, P., Lannuzel, D., Bowie, A. R., & Meiners, K. M. (2011b). High temporal resolution observations of spring fast ice melt and seawater iron enrichment in East Antarctica. *Journal of Geophysical Research*, 116(G3). https://doi.org/10.1029/2010jg001628

van der Merwe, P., Lannuzel, D., Nichols, C. A. M., Meiners, K. M., Heil, P., Norman, L. et al. (2009). Biogeochemical observations during the winter–spring transition in East Antarctic sea ice:

Evidence of iron and exopolysaccharide controls. *Marine Chemistry*, 115(3-4): 163-175. https://doi.org/10.1016/j.marchem.2009.08.001

Vancoppenolle, M., Notz, D., Vivier, F., Tison, J., Delille, B., Carnat, G. et al. (2013). Technical Note: On the use of the mushy-layer Rayleigh number for the interpretation of sea-ice-core data. *The Cryosphere Discussions*, 7(4): 3209-3230. https://doi.org/10.5194/tcd-7-3209-2013

Weber, L., Völker, C., Schartau, M., & Wolf-Gladrow, D. A. (2005). Modeling the speciation and biogeochemistry of iron at the Bermuda Atlantic Time-series Study site. *Global Biogeochemical Cycles*, 19(1). https://doi.org/10.1029/2004gb002340

Wedepohl, K. H. (1995). The Composition of the Continental-Crust. *Geochimica et Cosmochimica Acta*, 59(7): 1217-1232. https://doi.org/10.1016/0016-7037(95)00038-2

Wells, M. L., & Goldberg, E. D. (1991). Occurrence of Small Colloids in Seawater. *Nature*, 353(6342): 342-344. https://doi.org/10.1038/353342a0

Wells, M. L., Price, N. M., & Bruland, K. W. (1995). Iron Chemistry in Seawater and Its Relationship to Phytoplankton - a Workshop Report. *Marine Chemistry*, 48(2): 157-182. https://doi.org/10.1016/0304-4203(94)00055-I

Wu, J., Boyle, E., Sunda, W., & Wen, L. S. (2001). Soluble and colloidal iron in the oligotrophic North Atlantic and North Pacific. *Science*, 293(5531): 847-849. https://doi.org/10.1126/science.1059251

Wu, J. F., & Luther, G. W. (1994). Size-Fractionated Iron Concentrations in the Water Column of the Western North-Atlantic Ocean. *Limnology and Oceanography*, 39(5): 1119-1129. https://doi.org/10.4319/lo.1994.39.5.1119

Wu, J. F., & Luther, G. W. (1996). Spatial and temporal distribution of iron in the surface water of the northwestern Atlantic Ocean. *Geochimica et Cosmochimica Acta*, 60(15): 2729-2741. https://doi.org/10.1016/0016-7037(96)00135-4

Wuttig, K., Townsend, A. T., van der Merwe, P., Gault-Ringold, M., Holmes, T., Schallenberg, C. et al. (2019). Critical evaluation of a seaFAST system for the analysis of trace metals in marine samples. *Talanta*, 197: 653-668. https://doi.org/10.1016/j.talanta.2019.01.047

Zhou, J., Delille, B., Eicken, H., Vancoppenolle, M., Brabant, F., Carnat, G. et al. (2013). Physical and biogeochemical properties in landfast sea ice (Barrow, Alaska): Insights on brine and gas dynamics across seasons. *Journal of Geophysical Research: Oceans*, 118(6): 3172-3189. https://doi.org/10.1002/jgrc.20232

Zhu, X. R., Prospero, J. M., & Millero, F. J. (1997). Diel variability of soluble Fe(II) and soluble total Fe in North African dust in the trade winds at Barbados. *Journal of Geophysical Research: Atmospheres*, 102(D17): 21297-21305. https://doi.org/10.1029/97jd01313

Journal of Geophysical Research: Oceans

Supporting Information for

Enhanced Iron flux to Antarctic Sea Ice via Dust Deposition from Ice-free Coastal Areas

L. Duprat[1], N. Kanna[2], J. Janssens[1,7], A. Roukaerts[3], F. Deman[3], A. T. Townsend[4], K.M. Meiners[5,6], P. van der Merwe[6] and D. Lannuzel[1, 5]

[1]Institute for Marine and Antarctic Studies, University of Tasmania, Hobart, Australia, [2] Arctic Research Center, Hokkaido University, Sapporo, Japan, [3]AMGC Department, Vrije Universiteit Brussel, Brussels, Belgium, [4]Central Science Laboratory, University of Tasmania, Hobart, Australia, [5]Australian Antarctic Division, Kingston, Tasmania, Australia, [6]Antarctic Climate and Ecosystems Cooperative Research Centre, Hobart, Tasmania, Australia.

Contents of this file

Figures S1

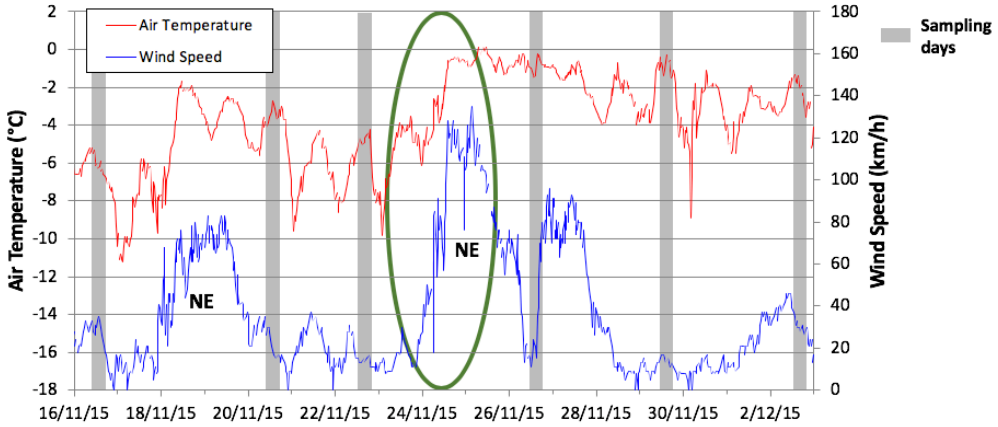

Figure S1. Air temperature and wind speed for the time series period (Davis station meteorological data, 2016). Note: Sampling days are indicated by the vertical bars in grey. Blizzard event between day 227 and 330 is shown by the green circle.

CHAPTER 3. NUTRIENT DISTRIBUTION IN EAST ANTARCTIC SUMMER SEA ICE: A POTENTIAL IRON CONTRIBUTION FROM GLACIAL BASAL MELT

L. Duprat[1], M. Corkill[1], C. Genovese[1], A.T. Townsend[2], S. Moreau[3], K.M. Meiners[4, 5] and D. Lannuzel[1]

[1]Institute for Marine and Antarctic Studies, University of Tasmania, Hobart, Australia, [2]Central Science Laboratory, University of Tasmania, Hobart, Australia, [3]Norwegian Polar Institute, Tromsø, Norway, [4]Australian Antarctic Division, Department of Agriculture, Water and the Environment, Kingston, Tasmania, Australia, Australian Antarctic Program Partnership, Institute for Marine and Antarctic Studies, University of Tasmania, Hobart, Tasmania, Australia.

Corresponding author: Luis Paulo Duprat (luis.duprat@utas.edu.au)

Key Points:

- Primary production in East Antarctic fast and pack sea ice is not Fe-limited during summer.
- Low nitrate and high exopolysaccharide concentrations suggest heterotrophic dominance in Antarctic summer sea ice.
- Fe-rich platelet sea ice near the Moscow University Ice Shelf indicates an influence of glacial meltwater in the coastal distribution of Fe.

Abstract

Antarctic sea ice can incorporate high levels of iron (Fe) during its formation and has been suggested as an important source of this essential micronutrient to Southern Ocean surface waters during the melt season. Over the last decade, a limited number of studies have quantified the Fe pool in Antarctic sea ice, with a focus on late winter and spring. Here we study the distribution of operationally defined dissolved and particulate Fe from nine sites sampled between Wilkes Land and King George V Land during austral summer 2016/17. Results point towards a net heterotrophic sea-ice community, consistent with the observed nitrate limitation (<1 μM). We postulate that the recycling of the high particulate Fe pool in summer sea ice supplies sufficient (~3 nM) levels of dissolved Fe to sustain ice algal growth. The remineralization of particulate Fe is likely favoured by high concentrations of exopolysaccharides (113 to 16,290 μg xeq L^{-1}) which can serve as a hotspot for bacterial activity. Finally, results indicate a potential relationship between glacial meltwater discharged from the Moscow University Ice Shelf and the occurrence of Fe-rich (~4.3 μM) platelet ice in its vicinity. As climate change is expected to result in enhanced Fe-rich glacial discharge and changes in summer sea-ice extent and quality, the processes influencing Fe distribution in sea ice that persists into summer need to be better constrained.

Plain summary

Iron (Fe) plays a crucial role in microalgal physiology and can control their growth in the Southern Ocean, where Fe concentrations are naturally low. Antarctic sea ice can incorporate high levels of Fe during its formation triggering phytoplankton blooms at the sea-ice edge during the melt season. No studies to date have assessed sea-ice Fe distributions in East Antarctica during mid-to late summer. Here we discuss Fe distribution in parallel with key sea-ice physical and biological parameters measured during an expedition to East Antarctica in summer 2016/17 to answer our central question: is Fe limiting sea-ice primary productivity during summer? Results suggest nitrate, rather than Fe is the key nutrient controlling sea-ice algal growth at this time of the year. We also found Fe-rich platelet ice incorporated underneath pack ice sampled near the Moscow University Ice Shelf which suggests the potential accretion of Fe-rich ice shelf waters under the sea ice. As climate change is expected to accelerate Antarctic ice shelf melting, a better understanding of how increased rates of glacial meltwater discharge will impact the distribution of Fe within the sea ice during summer is needed.

Keywords: Sea ice, iron, East Antarctica, platelet ice, summer.

3.1 Introduction

Phytoplankton growth can be limited by the availability of the essential nutrient iron (Fe) (de Baar et al., 1990, 1995). The Southern Ocean (SO) is a classic example where high concentrations of macronutrients (nitrate, phosphate, and silicic acid) do not support the expected level of primary production due to low Fe concentrations. The Southern Ocean has therefore been designated as a High Nutrient Low Chlorophyll (HNLC) area (Martin, 1990). In this context, sea ice plays a pivotal role as a natural and biogeochemically active Fe reservoir due to the high levels of Fe and organic matter concentrated from seawater during its formation (Gradinger & Ikävalko, 1998; Janssens et al., 2016; Lannuzel et al., 2007; Lannuzel et al., 2016b). As the sea ice begins to melt in spring, this Fe pool can sustain concentrated algal blooms at the retreating sea-ice edges and in opening polynyas, contributing to the spatial variability in Southern Ocean primary production (Arrigo 1998; Lancelot et al., 2009; Lannuzel et al., 2007, 2008; Massom & Stammerjohn, 2010; Sedwick et al., 1997). This process can alleviate Fe limitation at a critical time, when light availability and water stratification favour phytoplankton growth, making Antarctic sea ice an important natural Fe fertilizer in the SO (Tagliabue & Arrigo, 2006).

The availability of light can co-limit (with Fe) sea-ice primary productivity for the vast majority of the year (Thomas & Dieckmann, 2010). The distribution of solar radiation has major impacts on sea-ice physical and biological processes (Arrigo et al., 2012). Snow thickness is usually the most important factor regulating the availability of light for ice algae because of its high light attenuation properties (Arrigo et al., 1998). However, snow metamorphosis during summer can reduce this attenuation (Arndt et al., 2017; Haas et al., 2001; Hancke et al., 2018; Tison et al., 2008). Within non-flooded areas, the melting coarse-grained summer snowpack has a lower albedo than the cold fine-grained snow, allowing more light to pass through the snow (Brandt et al., 2005; Zhou et al., 2007). More important, enhanced areas of surface flooding in Antarctic summer sea ice can significantly reduce light attenuation (Arndt et al., 2017; Arrigo et al., 2012). On a larger scale, the common presence of features of higher light transmittance in summer sea ice, such as leads and cracks, should increase the lateral incidence of light (Katlein et al., 2015). Summer ice features associated with low salinity extremes, such as melt ponds, under-ice melt lenses and rotten ice, most likely select for microalgal species capable of tolerating these extremes as well (Torstensson et al., 2018). These observations

corroborate with a previous modelling study showing that nutrients rather than light or salinity, limit Antarctic sea-ice algae growth during summer (Saenz & Arrigo, 2014).

A high percentage of sea-ice dissolved Fe (DFe, filtered through a 0.2 µm pore size membrane), our best empirical measurement of potentially bioavailable Fe (Morel et al., 2008), is lost to the seawater in a rapid pulse over a few days during spring (Duprat et al., 2019; Lannuzel et al., 2008). This early release is likely rapidly consumed by phytoplankton with very low DFe concentrations reported for seawater after the spring bloom (Bertrand et al., 2011; Sedwick et al., 2000, 2011). Sea-ice melt may provide an additional later pulse of Fe to surface waters in the particulate form (PFe, > 0.2 µm), as the flushing of this pool from the sea ice is initially limited by brine channel transport (Lannuzel et al., 2013; van der Merwe et al., 2011a).

Studies conducted during the last two decades indicate that sea-ice DFe concentrations are relatively unaffected by the proximity to Fe sources (Lannuzel et al., 2016b and references therein). This apparent contradiction has been attributed to the fact that in the presence of saturated organic ligands, the dissolution equilibrium should impose a maximum threshold for DFe concentrations in sea ice. When all organic ligands are saturated, excess DFe precipitates into PFe. Much of East Antarctica's free-floating pack ice is formed in leads and polynyas (Allison, 1989), and due to an increased distance to coastal sources, it generally carries a lower concentration of lithogenic PFe than land-fast sea ice (sea ice fastened to coastal features; Lannuzel et al., 2016b). The accumulation of PFe in pack ice can still occur, either by uptake and conversion of DFe (e.g. from the continental shelf or icebergs) into PFe, or via direct incorporation of biogenic PFe from highly productive shelf waters where it originated (Lannuzel et al., 2016a).

In contrast to pack ice, fast ice can be affected by a greater input of Fe from lithogenic sources, such as coastal sediment (de Jong et al., 2012) and dust from ice-free continental areas (de Jong et al., 2013; Duprat et al., 2019). Less clear is the influence of subglacial meltwater on the fast-ice Fe pool via incorporation of ice platelets at the bottom of sea ice. The growth of ice platelets has been observed below sea ice under the influence of ice-shelf meltwater (Langhorne et al., 2015). There are several observations of platelet ice in the Ross and Weddell seas; otherwise, there are very few reports of platelet ice layers in East Antarctica (Langhorne et al., 2015). It is believed they are seeded by frazil crystals formed in supercooled ice shelf waters, although the processes behind the formation of these unique crystallographic structures are still poorly understood (Tison et al., 1998). The ice platelets can eventually be incorporated onto the base

of the ice shelf (marine ice) via buoyant accumulation (Oerter et al., 1992), or be carried out from the ice shelf cavity and deposited beneath neighbouring sea ice (sub-ice platelet layers) (Langhorne et al., 2015; Tison et al., 1998). Under sea ice, *in-situ* growth can continue, creating a porous and friable sub-ice platelet layer from which the highest concentrations of sea-ice algae (up to 374 mg C L^{-1} and 6.5 mg Chl*a* L^{-1}) have been reported (Arrigo et al., 2010; Bombosch, 2013; Smetacek et al., 1992; van der Linden et al., 2020). The origin of marine ice Fe is often associated with highly reactive glacial flour produced from subglacial physical and chemical weathering (Wadham et al., 2010). The presence of buoyant frazil and ice platelets could facilitate the incorporation of sediment and biogenic material from the ocean into the marine ice layer (Treverrow et al., 2010). While platelet ice incorporation under ice shelves has been associated with higher concentrations of Fe (Herraiz-Borreguero et al., 2016), no link has yet been made for platelet ice incorporation under sea ice due to the paucity of observations and measurements.

To date, most sea-ice surveys focused on investigating Fe distribution and biogeochemistry in late winter and spring (Lannuzel et al., 2016b). In this study, we report Fe concentrations obtained from between Wilkes Land and King George V Land coast (East Antarctica) and sampled during a marine science voyage carried out from December 2016 to January 2017. We aim to answer our central question: is sea-ice primary production Fe-limited in summer due to the advanced stage of brine and nutrient drainage? A further objective was to evaluate how the Fe biogeochemistry relates to macronutrients and other biological variables in summer sea ice, such as algae-produced exopolysaccharides (EPS). The final aim of this study was to investigate a potential link between glacial basal melt from ice shelves encountered during our expedition (e.g. Moscow University, Mertz and Ninnis) and the formation of Fe-rich platelet ice, as an important spatial determinant in sea-ice PFe distribution. Results from this study could guide studies on the potential impacts of future ice mass balance changes on local primary production, and carbon export of highly productive polynyas found downstream of the Dalton, Mertz and Ninnis ice shelves (Paolo et al., 2015; Rignot et al., 2019).

3.2 Methods

3.2.1 Sampling sites

Sea ice was sampled during an icebreaker RSV *Aurora Australis* voyage at nine different stations off the East Antarctic coast (Figure 3.1) during austral summer (December 2016 to January 2017). The mobility of the ice stations (e.g., fastened versus free-floating) was used as criteria to categorize the stations into fast and pack ice (see section 2.3.3.1). Casey1 and 2 were fast ice stations on first-year ice in O'Brien Bay near Casey Station (~5 km). Exposed rocky hills surrounded the site. Totten1 was sampled ~15 km from the Moscow University Ice Shelf and ~75 km from the Totten Ice Shelf. Pack ice stations were diverse: Casey3 and Totten2 consisted of thick rafted ice with a very uneven surface, while SR3-5, Mertz1, 2 and 3 were relatively level ice floes. Mertz1, 2 and 3 stations were approximately 95, 1 and 75 km from the Mertz Glacier Tongue, respectively. Snow depths were variable, and most snow was old and compacted. Sampling sites were selected away and upwind from the research vessel or any other operations likely to contaminate trace metal and organic matter samples.

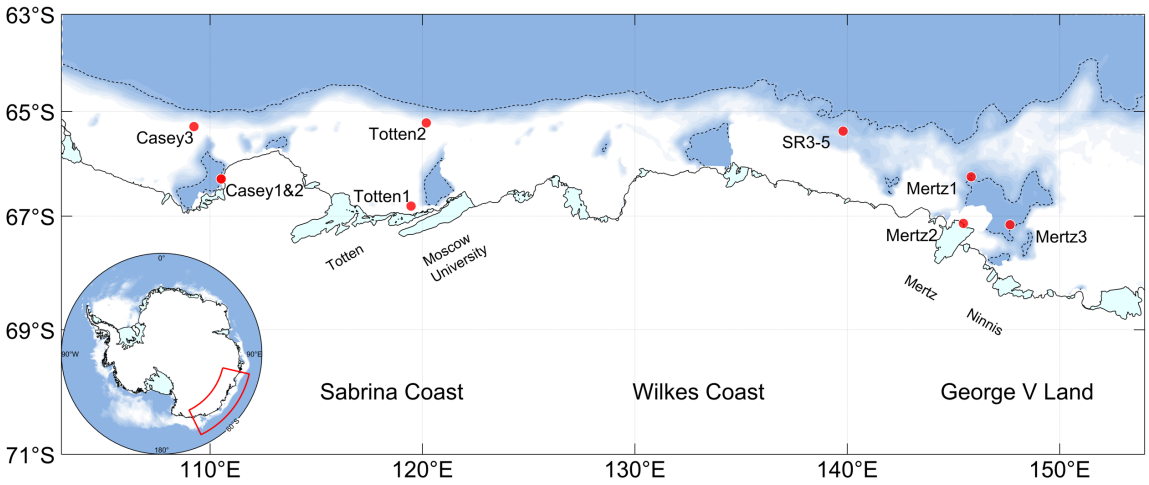

Figure 3.1 Map with the locations and names of sea-ice stations off East Antarctica visited between 19/12/2016 and 13/01/2017 during the RSV Aurora Australis Voyage 2. Sea-ice concentration averaged for the study period is shown by a gradient between blue (low) and white (high). Major ice shelves (Totten, Moscow University, Mertz and Ninnis) are also labelled.

3.2.2 Cleaning procedures

Plasticware used for sample collection (polypropylene (PP; Superlift®) melting containers) and storage (low-density polyethylene (LDPE; Nalgene®) sampling bottles) were kept in sealed

plastic bags after being acid-cleaned according to GEOTRACES recommendations (Cutter et al., 2017). Firstly, new LDPE bottles were soaked in 2% (v:v) Decon90 baths for one week. Bottles were then thoroughly rinsed with ultra-high purity water (UHP water, Barnstead), filled with 6 M hydrochloric acid (HCl, 50% v:v reagent grade, Merck) and immersed in 2 M HCl (~20% v:v reagent grade, Merck) for one month. Bottles were then rinsed with UHP water, filled with 1 M distilled HCl (~10% v:v instrument quality, Seastar) and kept for one week on a hot plate (60 °C). Finally, bottles were rinsed three times with UHP water in a class-100 laminar flow hood and stored triple bagged in plastic press seal bags until use. Between sampling days, plastic equipment (Teflon® filtration sets, plastic tubing and plastic scoops) used for collection and processing were rinsed with UHP water and soaked in an acid bath (10-20% v:v HCl, according to Nalgene® recommendations for each material) and thoroughly rinsed again with UHP water before use. Finally, glassware used for organic carbon and nitrogen filtrations were soaked in a 2% (v:v) HCl solution (reagent grade, Merck), rinsed with UHP water, wrapped in aluminium foil and combusted at 450 °C for 4 hours.

3.2.3 Sampling procedures

During field sampling, trace metal clean protocols were followed, as described by Lannuzel et al. (2006) and van der Merwe et al. (2009). The snow was collected using an acid-cleaned polyethylene (PE) hand shovel and stored in a 3.8 L wide-mouth Nalgene® HDPE bottle. Separate cores from the same vicinity were collected for temperature/salinity, particulate organic matter (POM), chlorophyll-*a* (Chl*a*), particulate exopolysaccharides (PEPS), macronutrient and Fe determinations. Ice cores were collected with an electric-powered, electro-polished stainless-steel corer of 0.14 m internal diameter (Lichtert Industrie, Belgium), previously shown appropriated for trace metal sampling (Lannuzel et al., 2006; van der Merwe et al., 2009). Ice cores were sectioned in the field using a medical-grade bone saw (Richards Analytical). Six or seven sections were obtained out of the entire core (from top, intermediate and bottom layers), 10-15 cm thick, in order to represent different depth horizons of the ice cores. Snow and sea-ice samples were melted at room temperature immediately after collection, filtered (for the dissolved fraction, see details in paragraph 2.4.2) and poured into 125 mL Superlift® PP bottles, double bagged and stored at –20 °C until analysis. Brine was collected from ~1 m deep sack holes, while underlying seawater was collected through full-ice-depth core holes, just below the ice (hereafter referred to as SW0m). Both brine and

seawater were collected using an acid-cleaned 0.5 L PFA bottle (Nalgene®) attached to an improvised 2 m long bamboo pole and transferred into acid-cleaned 1L LDPE bottles (Nalgene®).

3.2.4 Sample processing and analytical methods

3.2.4.1 Physical variables

Sea ice temperatures were measured with a Testotherm720 thermometer (accuracy ± 0.1 °C) immediately after ice core retrieval from small holes drilled in the core at 0.1 m intervals. Bulk salinities of brine, seawater, melted snow and sea-ice sections were measured using a Guildline Autosal salinometer (Ocean Scientific International Ltd, United Kingdom; ± 0.001 PSU). The texture of each ice core was analysed by photographing vertical thin sections between cross-polarizing filters, following the method of Langway (1958). The physical ice properties are discussed in more detail in a companion paper. Finally, a light sensor was deployed in the core hole to measure the luminous ice emittance (per square meter) at 0.1 m increments as an indication of the light intensity that passed through different depth horizons of the sea ice.

3.2.4.2. Fe physical fractionation

Dissolved and particulate Fe from snow, seawater, brine and melted sea-ice sections were obtained by filtration through 0.2 µm pore size 47 mm diameter polycarbonate (PC) membrane filters (Sterlitech) using Teflon® perfluoroalkoxy (PFA) filtration apparatus (Savillex, USA). A gentle vacuum (< 0.13 bar) was applied to avoid algal cell rupture during filtration. The dissolved fraction (< 0.2 µm, which includes the soluble (< 0.02 µm) and colloidal (0.02 – 0.2 µm) fractions) was collected in LDPE bottles, acidified to pH 1.8 by adding ~1% (v:v) of 12 M ultrapure HCl (Seastar Baseline, analytical grade), triple-bagged and stored at room temperature until analysis. Polycarbonate filters with the retained particulate fraction (> 0.2 µm) were placed into acid-clean polystyrene Petri dishes, triple-bagged, and stored at -20 °C in the dark until further processing and analysis at the University of Tasmania (Australia).

3.2.4.2.1 Dissolved Fe analysis

An automated off-line sample system (seaFAST-pico™, Elemental Scientific; Nobias Chelate-PA1 resin) was used to pre-concentrate trace metals and remove sea-ice and seawater filtrate matrices from our samples according to the method described by Wuttig et al. (2019). Comprehensive method testing using a variety of internationally recognized community reference samples and oceanographic standards (Wuttig et al., 2019) as well as NASS-6 verified method accuracy for Fe. A mean Fe value of 9.24 ± 0.24 nmol kg^{-1} (n=6) was measured for the NASS-6, in good agreement with the reported indicative value of 8.65 ± 0.81 nmol kg^{-1}. Collected samples were concentrated either 10× (bottom sections of sea ice and brines) or 40× (snow, remaining sections of sea ice and seawater) depending on the expected Fe concentrations. Dissolved Fe concentrations were then determined using a Sector Field Inductively Coupled Plasma Mass Spectrometer (SF-ICP-MS, Element 2; Central Science Laboratory – CSL, University of Tasmania). Cleaning procedures, calibrations and quality control of the SF-ICP-MS results for the samples analysed in this study followed those described in Duprat et al. (2019). The average detection limit for DFe was calculated as 7.8 × 10^{-4} ppb (0.014 nM; n = 15; 3× the standard deviation of the acidified internal blank). Concentrations reported here are all blank corrected. Finally, Fe* was calculated as a way to assess potential Fe deficiency relative to PO_4^{3-}. Fe* was estimated by subtracting the biological contribution based on the Fe:PO_4^{3-} assimilation ratio (0.47 mmol:mol), following Parekh et al. (2005).

3.2.4.2.2 Particulate Fe

Particulate Fe was quantified after complete filter digestion using a strong acid treatment (Bowie et al., 2010). First, a mixture of 250 µL 12 M HCl, 250 µL 16 M nitric acid (HNO_3, SeaStar Baseline), and 500 µL 29 M hydrofluoric acid (Seastar Baseline, Choice Analytical) was added to each sample and blank filter and placed into a Teflon® PFA (perfluoroalkoxy) vial (Savillex, USA). Vials were heated to 120 °C for 12 h over a Teflon® coated hotplate (SCP Science) housed within a class-100 fume hood. Vials were then left open until complete evaporation of the acids. Next, 9.9 mL of ultrapure 10% (v:v) HNO_3 was added to re-suspend the dried residues before the addition of 100 µL Indium solution (final concentration 87.1 nM) as an internal standard. Finally, an aliquot of 5 mL was transferred to PP tubes for Fe quantification using SF-ICP-MS following similar procedures as outlined in section 3.2.4.2.1. The detection limit for Fe was calculated as 3× the standard deviation of the digested acid filter

blank, determined as 8×10^{-4} ppb (0.14 nM). The theoretical biogenic fraction (PFe_{bio}) was calculated as the total PFe – lithogenic PFe (inferred by the Fe:Al ratio of 0.33; Taylor and McLennan, 1985). It is worth noting that Fe enrichment relatively to Al can occur via flocculation and increasing sorting of lithogenic material with distance from the coast (Markussen et al., 2016), therefore results should be interpreted with care. For the purpose of this work, we refer to biogenic Fe as any PFe form associated to biogenic pools (living, detrital, and authigenic) that are not refractory particles originated from terrestrial sources of rock, such as silicate minerals (lithogenic origin).

3.2.4.3 Particulate organic matter

Melted sea-ice and seawater samples for particulate organic matter determination were gently homogenized before filtration (0.14 to 0.6 L) on pre-combusted (450 °C, for 8 h) glass microfiber (GF/F) filters (0.7 µm nominal porosity, MGF Sartorius). Samples were dried overnight at 60 °C. Inorganic carbon contamination was removed from the filters with the addition of 10% (v:v) distilled HCl (80 µL) for 12 h inside a closed PCR well tray (Martin, 1993). Samples were then packed in silver cups (Elemental Microanalysis, UK) and stored in a desiccator until analysis for elemental composition at the CSL. Particulate organic carbon (POC) and particulate organic nitrogen (PON) concentrations were determined by flash combustion and oxygen pyrolysis using a Thermo Finnigan EA 1112 Series Flash Elemental Analyzer (estimated precision ~1%). POC and PON detection limits were calculated as 3× the standard deviation of the procedure blanks, determined as 2.5 and 1.8 µM, respectively (n = 6).

3.2.4.4 Particulate Exopolysaccharides

In aquatic systems, dissolved EPS are prone to coalesce into particulate form, also referred to particulate exopolysaccharides (PEPS). Sea-ice, brine and seawater PEPS concentrations were measured using the semi-quantitative colorimetric Alcian Blue (AB) assay (Passow & Alldredge, 1994) following van der Merwe et al. (2009). Calibration was achieved by measuring five different extracted solutions from filters previously treated with 0, 2.5, 5, 7.5 and 10 mL of a 0.75 µg L^{-1} Xanthan gum solution, following the same staining protocol used for the sample filters. A linear regression (R^2 = 0.92; n = 16) was calculated between

absorbance and the respective concentration of Xanthan gum. The detection limit (3× the standard deviation of the filter blank) was 28.6 µg Xanthan equivalent (xeq.) L^{-1} (n = 20).

3.2.4.5 Chlorophyll-*a* and macronutrients

Samples for Chl*a* analysis were melted at room temperature in the dark (Rintala et al., 2014). Chlorophyll *a* was concentrated by filtering samples (0.09 to 0.7 L) through GF/F filters under low vacuum (< 0.13 bar) followed by extraction with 90% acetone (HPLC grade) for 12 to 24 hours. Chlorophyll *a* concentrations were determined fluorometrically with a Turner Designs 10AU fluorometer (*in vitro* detection limit 0.02 µg L^{-1}). Fluorescence was measured at 750 nm before and after acidification with 0.1 M HCl, and phaeopigment-corrected Chl*a* was calculated according to Arar and Collins (1997). Macronutrient samples were collected via filtration over 0.2 µm pore size filters (Acrodiscs) placed inside a filter holder and stored frozen (-20 °C) in 60 mL HDPE bottles until analysis in the laboratory (CSIRO, Hobart, Australia). Concentrations of nitrate + nitrite (NO*x*), nitrite (NO_2^-), ammonium (NH_4^+), phosphate (PO_4^{3-}) and (ortho)silicic acid ($Si(OH)_4$) were determined using a segmented flow analyzer (SEAL Analytical Ltd AA3 HR Autoanalyzer) following standard colorimetric methods from Rees et al. (2018), and Kerouel and Aminot (1997) for NH_4^+. Salinity-normalized macronutrient concentrations (C*) were calculated to tease apart physical effects following the equation applied by Fripiat et al. (2017): $C^* = C \cdot (S_w/S)$, where C is the measured nutrient concentration in the bulk sea ice, S_w is the salinity of seawater and S the corresponding measured salinity of in the bulk ice sample.

3.2.5 Statistical Analysis

Distributions of variables were tested from all stations and within both the pack and fast ice groups. First, the normality and the homogeneity of variance of each variable was tested using the Shapiro-Wilk test and Levene's test, respectively. When the normality and homogeneity of variance could be verified, an ANOVA test was run. For non-normal distributed variables, the Kruskall-Wallis test was used. Multiple (paired) comparisons corrected by the Holm test were performed. Differences between fast and pack ice were also tested using either a Wilcoxon test or a t-test, depending on the distribution. Potential correlations between all physical and biogeochemical parameters were investigated using a Spearman correlation coefficient test due

to the non-normality observed in most variables. For this test, ice texture proportions were calculated for each section using rankings 0 for non-columnar (granular and platelet) and 1 for columnar. All analyses were performed using the R programming language (version 3.3.1; R Core Team, 2013).

3.3 Results

3.3.1 Ice Physics

All collected ice cores were relatively warm (> -2 °C). Porosities were almost always above the percolation threshold of 5% for columnar ice and often greater than 10%, which likely allowed brine movement through the more random brine inclusions of granular ice found in the ice cores. Brines were stratified, indicating exchange with the underlying seawater was limited to diffusive processes. The overall low brine salinities (0.9 – 32.2 PSU) were indicative of surface-melt input which was likely driving desalination. Of the textures sampled near ice shelves, columnar ice was often interspersed with layers of granular ice or platelet ice. Granular ice was found near the surface, especially as snow ice, while platelet ice was found at greater depths, beyond ~0.5 m (Totten and Mertz) and beyond ~1 m in one instance in front of the Mertz Glacier Tongue (Table 3.1). Measured illuminance reached optimum diatom growth values (1,000 lx; Azam and Singh, 2013) at the ice ~0.4 m depth. Average depth-adjusted illuminance varied from 2,730 lx at the ice surface to only 17 lx in basal ice.

Table 3.1 Sampling dates, location and general characteristic/texture of ice stations

Station	**Date of sampling (2016/17)**	**Location**		**General floe description / texture**
		Latitude (°N)	Longitude (°E)	
Casey 1	19/12/16	-66.3S	110.5E	Fast ice / superimposed ice, columnar ice
Casey 2	23/12/16	-66.3S	110.5E	Fast ice / no texture data
Casey 3	27/12/16	-65.3S	109.2E	Thick rafted pack ice with gap / no texture data
Totten 1	31/12/16	-66.8S	119.5E	Ex-fast ice / superimposed ice, snow ice, layers of columnar and granular ice, platelet ice
Totten 2	03/01/17	-63.2S	120.2E	Thick rafted pack ice / no texture data

SR3-5	07/01/17	-63.4S	139.8E	Rafted pack ice with gap / superimposed ice, snow ice, granular ice
Mertz 1	09/01/17	-66.3S	145.8E	Pack ice / superimposed ice, snow ice, layers of granular and columnar ice including a layer of platelet ice
Mertz 2	11/01/17	-67.1S	145.5E	Pack ice / superimposed ice, snow ice, granular ice, platelet ice
Mertz 3	13/01/17	-67.2S	147.7E	Surface flooded pack ice – no texture data

3.3.2 Distribution of Fe

Dissolved and particulate Fe concentrations measured in the snow, sea ice, brine and seawater are summarized in Table 3.2. A detailed description of values for each station and ice section is available via the link in section 3.6. The vertical DFe and PFe profiles for fast and pack ice show no clear pattern for most stations (Figure 3.2). Dissolved Fe was enriched in sea ice relative to concurrent seawater (SW0m) and to values found in winter seawater (Figure 3.3a; van der Merwe et al., 2009). Concentrations of PFe were up to an order of magnitude higher than the seawater below. The average concentrations of DFe and PFe for all pack and fast ice stations were 2.9 ± 1.9 nM and 323 ± 606 nM, respectively. The particulate fraction comprised 98% of the total Fe pool with average PFe:PAl ratios of 0.6 for fast ice and 1.0 for pack ice. Lithogenic PFe inferred from the ice PFe:PAl ratios represented approximately 70% in fast ice and 40% in pack ice. Fast ice showed significantly higher concentrations of DFe and PFe (4.7 ± 2.3 nM; 665 ± 980 nM) compared to pack ice (2.0 ± 0.7; 81.7 ± 48.2; $p < 0.01$). Totten1 showed significantly higher DFe and PFe ($p < 0.01$) than the other fast ice stations. Higher DFe and PFe were also found in fast ice (3.5 ± 3.4 nM; ± 99.6 ± 64.3 nM) compared to pack ice (2.0 ± 1.3 nM; 83.2 ± 124 nM) when Totten1 was treated as an outlier, albeit not statistically significant.

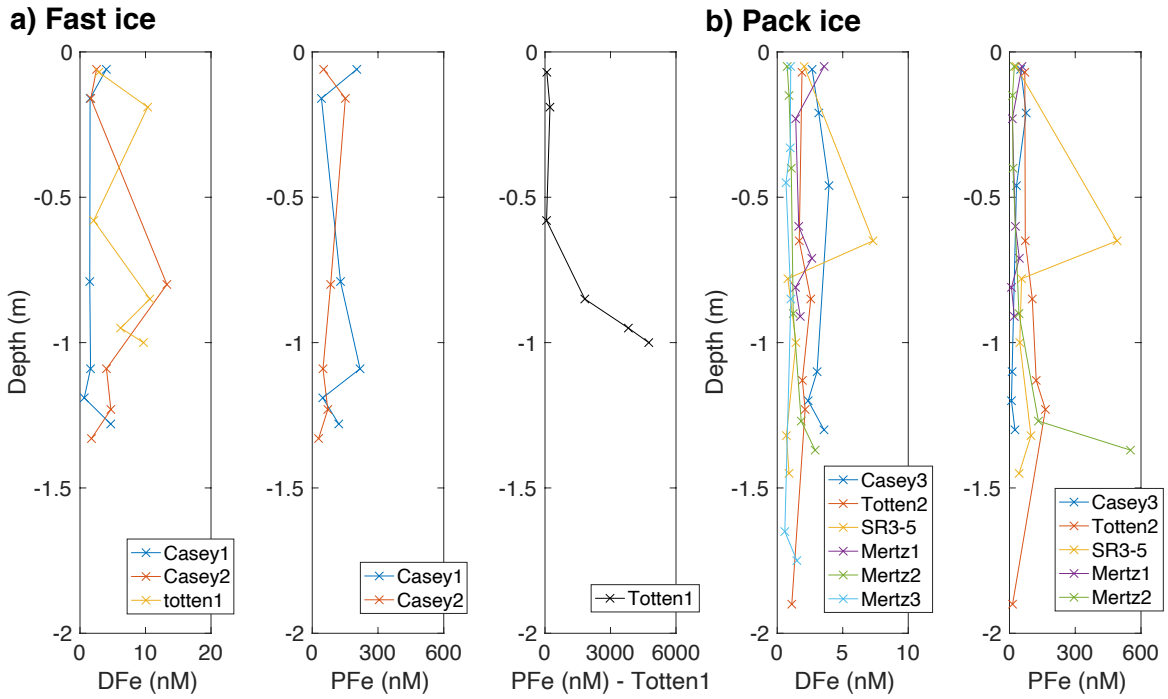

Figure 3.2 Vertical profiles of dissolved and particulate Fe for fast (a) and pack (b) ice stations. Different scales are used to reflect the variable concentrations.

Table 3.2 Summary statistics for all biogeochemical parameters.

	DFe (nM)	PFe (nM)	NO*x* (µM)	NH_4 (µM)	PO_4^{3-} (µM)	$Si(OH)_4$ (µM)	Chl*a* (µg L^{-1})	POC (µM)	PON (µM)	POC: PON (µM:µM)	PEPS (µg xeq L^{-1})
Fast ice											
snow	5.7 ± 7.1	112 ± 43.8									
Sea ice											
Min.	0.7	28.5	0.1	<dl	<dl	<dl	0.1	18.6	1.4	8.8	195
Max.	13.3	4,750	4.9	2.5	5.6	16.0	92.3	285	25.3	19.8	16,290
Mean ± S.D.	4.7 ± 2.3	665 ± 980	0.7 ± 0.5	0.4 ± 0.2	0.6 ± 0.5	0.6 ± 0.5	13.3 ± 29.6	79.3 ± 15.7	6.1 ± 0.2	13.9 ± 1.6	2,540 ± 1,290
SW0m	5.3 ± 3.4	30.1 ± 18.2	2.3 ± 2.1	0.3 ± 0.1	0.3 ± 0.2	16.9 ± 13.2	9.3 ± 12.9	36.6 ± 32.1	3.9 ± 2.2	8.8 ± 4.1	1,280 ± 861
Pack ice											
snow	0.8 ± 0.9	27.4 ± 22.1									
Sea ice											
Min.	0.6	8.7	<dl	0.1	<dl	<dl	0.1	4.1	0.7	4.1	113
Max.	7.3	552	9.5	1.1	2.0	15.1	67.7	270	31.2	26.6	10,440
Mean ± S.D.	2.0 ± 0.7	81.7 ± 48.2	1.3 ± 2.5	0.2 ± 0.1	0.4 ± 0.4	2.7 ± 2.3	13.4 ± 18.0	70.4 ± 33.0	5.8 ± 3.4	12.8 ± 4.5	1,750 ± 720
Deep brine	1.9 ± 0.4	37.9 ± 38.4	4.9 ± 6.1	0.2 ± 0.1	0.4 ± 0.4	21.7 ± 16.9	2.3 ± 2.6	29.0 ± 14.8	4.0 ± 2.6	7.8 ± 1.8	854 ± 442
SW0m	5.7 ± 8.0	33.2 ± 56.5	15.6 ± 8.5	0.3 ± 0.2	1.1 ± 0.5	39.5 ± 15.4	2.9 ± 3.9	19.7 ± 14.6	2.7 ± 2.0	8.4 ± 6.4	377 ± 199
All stations											
Snow	2.6 ± 4.6	63.5 ± 53.9									
Sea ice											

Min.	0.6	8.7	<dl	<dl	<dl	<dl	0.1	4.1	0.7	5.9	113
Max.	13.3	4,750	9.5	2.5	5.6	16.0	92.3	285	31.2	26.6	16,290
Mean ± S.D.	2.6 ± 4.6	2.6 ± 4.6	1.2 ± 2.4	0.3 ± 0.4	0.4 ± 0.9	2.7 ± 2.1	13.4 ± 22.1	73.3 ± 27.6	5.9 ± 2.7	13.2 ± 3.7	2,010 ± 947
SW0m	2.9 ± 1.9	2.9 ± 1.9	12.4 ± 8.6	0.4 ± 0.3	0.9 ± 0.5	31.0 ± 18.0	2.9 ± 2.8	20.6 ± 12.5	2.8 ± 1.7	7.9 ± 4.9	454 ± 223

3.3.3 Distribution of macronutrients

Average concentrations of NO*x* (NO_3^- + NO_2^-), PO_4^{3-}, $Si(OH)_4$ and NH_4^+ for fast and pack ice are shown in Table 3.2. Overall, lower concentrations of all macronutrients were found in our summer ice samples compared to other seasons (Fripiat et al., 2017). Nitrate was depleted relative to the Redfield N:P ratio (Figure 3.3b; Redfield, 1963). With exception of station SR3-5 and bottom ice data, $Si(OH)_4$ followed the Redfield-Brzezinski ratio for PO_4^{3-} relatively closely (Figure 3.3c; Brzezinski, 1985). Station SR3-5 presented significantly higher concentrations of PO_4^{3-}, NO_2^- and NO_3^- ($p < 0.01$). An average 6.4 ± 3.0 µM NO_3^- was found at this station, an order of magnitude higher than the other stations. SR3-5 station displayed a seawater-filled gap halfway through the ice cover, which could have supplied macronutrients to the ice.

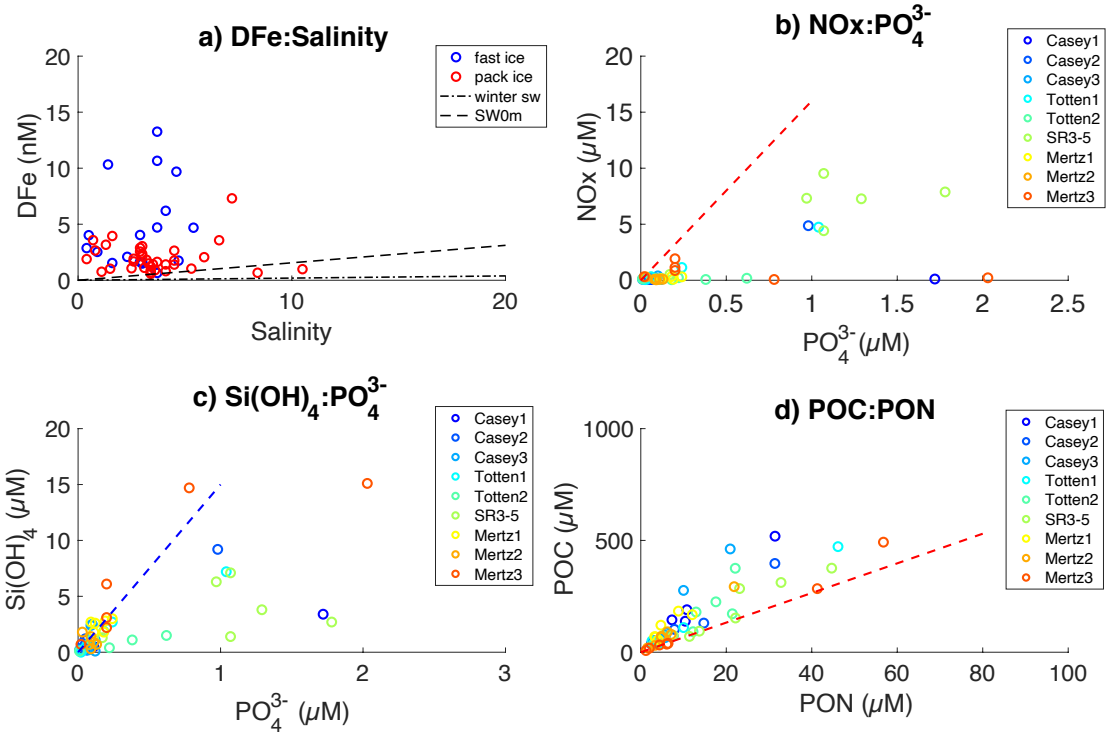

Figure 3.3 Relationship between biogeochemical parameters within sea ice: a) DFe (nM) vs salinity. Dashed black line represents the theoretical dilution line (TDL) obtained from SW0m Fe and salinity values. For comparison, dash-dotted black line represents the theoretical dilution line obtained from winter-spring transition (0-1m) seawater from East Antarctic (van der Merwe et al., 2009), b) NO_x (NO_3^- + NO_2^-) vs PO_4^{3-} (µM:µM), c) $Si(OH)_4$ vs PO_4^{3-} (µM:µM), d) POC vs PON (µM:µM). Dashed red (b and d) and blue line (c) represent the Redfield-Brzezinski nutrient ratio (Brzezinski, 1985).

3.3.4 Distribution of Chl*a* and POM

POC, PON and PEPS showed different vertical distributions between fast and pack ice stations. L-shaped profiles characterized fast ice stations, while no clear vertical pattern was observed for pack ice (Figure 3.4). Although average Chl*a*, POC, PON and PEPS did not statistically differ between pack and fast ice, higher bottom ice concentrations were found at the fast ice stations and higher surface-interior concentrations in pack ice stations ($p < 0.05$ for each parameter). Overall, PON and PEPS profiles matched the POC distribution for most stations. POC concentrations ranged from 4.1 µM in the ice surface layer of Mertz3 to 260 µM at the lowermost section of Totten1 (average 73.3 ± 27.6 µM for all stations). Exopolysaccharide concentrations in sea ice varied by three orders of magnitude, from 113 µg xeq. L^{-1} at the ice surface layer of Totten2 to 16,290 µg xeq L^{-1} at the bottom of Totten1. Average under-ice seawater POC and PEPS across all stations were 20.6 ± 12.5 µM and 454 ± 223 µg xeq L^{-1}, respectively (Table 3.2).

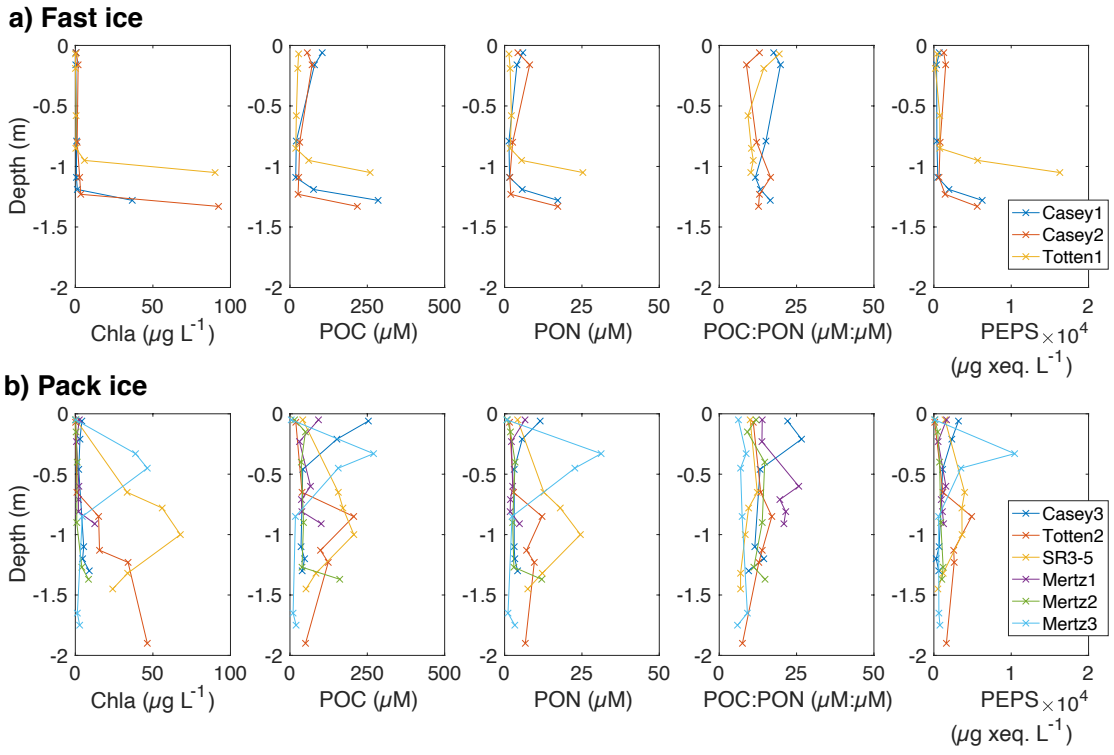

Figure 3.4 Vertical profiles of Chl*a*, POC, PON, POC:PON and PEPS for fast (a) and pack (b) ice stations.

3.3.5 Correlations between variables

Correlations between measured parameters were tested for fast and pack ice stations separately, and for all stations together (Figure 3.5). Results highlight a strong and significant correlation between PFe and PAl for both pack (0.8; $p < 0.01$) and fast ice (0.9; $p < 0.01$). PEPS was correlated with POC, PON and Chl*a* ($\rho > 0.7$; $p < 0.01$) in fast, pack and all sea-ice stations. There is also evidence of a moderate correlation of PEPS with salinity, ice porosity (0.5; 0.6; $p < 0.05$), macronutrients (0.5 to 0.8; $p < 0.05$) and NH_4^+ (0.5; $p < 0.01$) in fast ice, while PEPS was moderately correlated with PFe (0.5; $p < 0.01$) in pack ice. Chlorophyll *a*, POC and PON were all related to one or more types of macronutrient at different degrees (0.4 – 0.8; $p < 0.05$) in fast ice. When all stations were analysed together, salinity was moderately to strongly correlated (0.5 – 0.8; $p < 0.05$) with macronutrients but not with (dissolved and particulate) Fe. Finally, there is also a tendency of inverse correlation (not significant) of columnar ice with salinity, macronutrients and Fe for all ice stations.

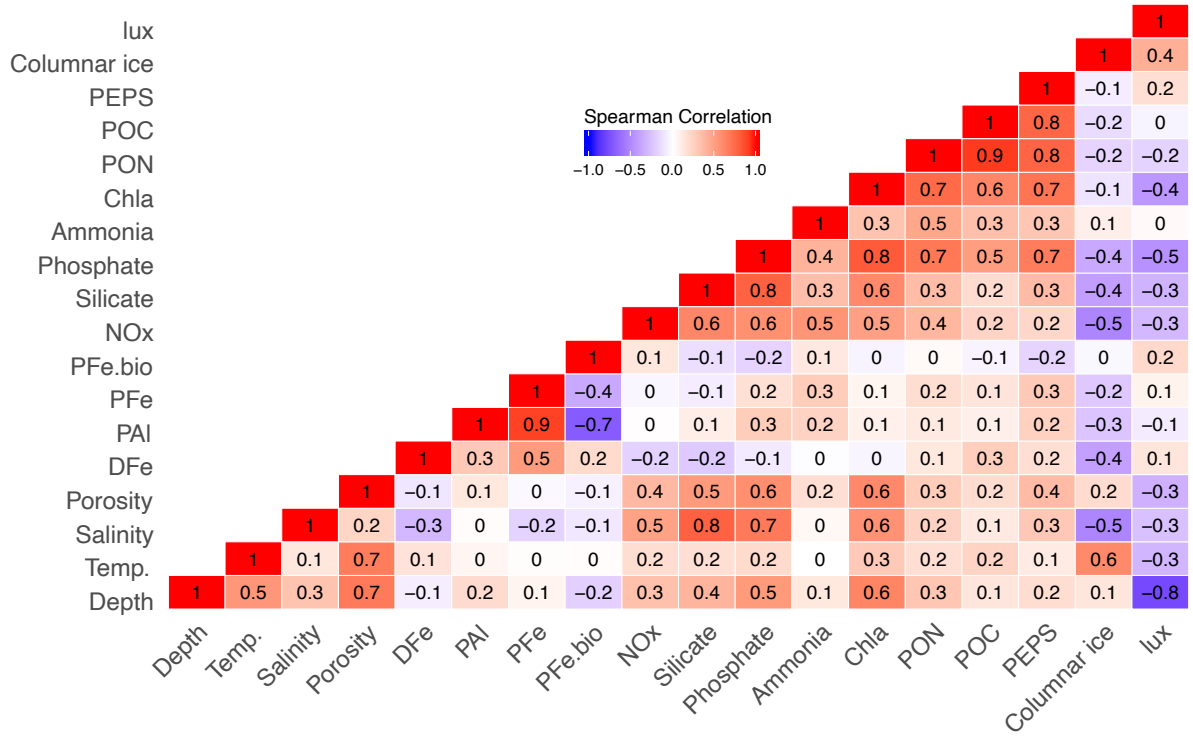

Figure 3.5 Spearman correlation matrix with all measured parameters for all (fast and pack ice) stations. Asterisks mark significant correlations at 95% confidence level ($p < 0.05$).

3.4 Discussion

3.4.1 Summer sea ice supports heterotrophic activity

Biomass and detritus are physically incorporated into newly forming sea ice and often show a uniform distribution over the ice thickness (Meiners et al., 2012; Thomas & Dieckmann, 2010). Throughout spring and summer though, other processes, e.g. *in-situ* production and grazing, start shaping the vertical distribution of biomass. The relatively higher POC concentrations (both in fast and pack stations) observed in the top and intermediate ice layers compared to other seasons (Becquevort et al., 2009; Duprat et al., 2019; Janssens et al., 2016; Meiners et al., 2011; van der Merwe et al., 2011b) suggest the upper ice cover becomes a more suitable habitat for sea-ice algae as the brine network connectivity increases during spring and summer. Heterotrophic processes are favoured by the abundant presence of algal cell detritus and, potentially, EPS build up within these layers (Meiners, 2004, 2008). In the lowermost sections of the ice, we found C:N ratios (~12) deviating from the Redfield ratio of 6.6 for phytoplankton (Redfield et al., 1963) and approaching those usually associated with the presence of anaerobic microorganisms in the rest of the ice (Rysgaard & Glud, 2004). A shift from an autotrophic bottom ice in spring toward a hetero-, and mixotrophic dominant environment could be driven by a potential decline in primary productivity associated with reduced nutrient availability and/or increased internal self-shading by ice algae. A higher C:N ratio could also indicate a relative increase of carbon associated with PEPS, which is known to be highly enriched in carbon relative to nitrogen (26 mol:mol; Engel & Passow, 2001).

Sea-ice concentrations of PEPS obtained here were consistently higher (average 946 µg xeq L^{-1}; 113 – 16,290 µg xeq L^{-1}) than those reported by van de Merwe et al. (2009) in East Antarctic spring sea ice (average 493 µg xeq L^{-1}; 2.84 – 2,690 µg xeq L^{-1}) indicating an ongoing microbial productivity from spring through summer. PEPS production could have also been intensified as a response to nutrient stress or changes in temperature and salinity conditions (Ewert & Deming, 2013). The relationship between PEPS and Chl*a* ($\rho = 0.7$; $p < 0.01$) suggests autotrophic protists are involved in PEPS production. To date, it is still unknown to what extent sea-ice bacteria hydrolyse and degrade PEPS as a source of nutrition. Nevertheless, observations of sea-ice EPS-particles colonized by bacteria indicate this substrate is available for bacterial degradation (Meiners et al., 2004, 2008; Underwood et al., 2010). Therefore, PEPS could be used as a carbon source for bacteria, also facilitating grazing by heterotrophic and mixotrophic protists. Tightly coupled bacteria-algae interactions have been reported in sea-ice systems (Stewart & Fritsen, 2004) and the microbial loop is considered an important

mechanism for recycling of organic matter in sea ice (Martin et al., 2012, Meiners & Michel, 2016).

3.4.2. Nitrate rather than Fe limits primary production in late summer sea ice

Results from previous modelling (Saenz & Arrigo, 2014) and field studies (Lim et al., 2019; McMinn et al., 2000; Petrou et al., 2010) suggest that nutrients rather than light limit Antarctic sea-ice algae growth for the vast majority of the sunlit season. Sea-ice algae are also adapted to survive in a broad range of salinities, with particular tolerance to the low summer-ice salinity levels (Arrigo et al., 1993; Bates & Cota, 1986; Kirst & Wiencke, 1995; Palmisano et al. 1987; Ralph et al., 2007, Ryan et al., 2004; Torstensson et al., 2018). Based on these findings, macro- or micronutrients rather than light or salinity controlled autotrophic activity during our summer study.

Iron is considered the most limiting nutrient for phytoplankton growth in HNLC waters (Sunda, 2012). Sea-ice DFe levels in our study (~3 nM) were above the limitation threshold (~0.2 nM) for SO phytoplankton growth (Timmermans et al., 2004). We use Fe* to evaluate the potential Fe deficiency relative to PO_4^{3-} at this time of year. Scavenging of Fe commonly results in the decoupling of these elements (lower Fe relative to PO_4^{3-}) in most of the ocean surface waters (Parekh et al., 2005), especially in the SO where input from aeolian deposition is low (Gao et al., 2001). In our study, Fe* was always positive, indicating DFe was present in sufficient concentrations for complete utilization of the available PO_4^{3-}. It is worth considering that Fe:PO_4^{3-} was estimated based on oceanic phytoplankton ratios and that it is plausible that sea-ice diatoms could have evolved to less efficiently use Fe compared to pelagic assemblages, due to the abundance of this nutrient in sea ice relative to seawater (Lim et al., 2019). However, a Fe:PO_4^{3-} uptake ratio an order of magnitude higher would be necessary to observe some degree of Fe depletion relative to PO_4^{3-} in summer sea ice. A positive Fe* is also observed for the majority of the sea-ice samples if Fe* is calculated based on Fe:DIN (total dissolved inorganic nitrogen) uptake ratios for oceanic diatoms under both Fe limited and replete conditions (0.1 – 3.2.1 mmol:mol; Price, 2005). Our positive Fe* values suggest organic ligands should be present in sea ice in excess relative to DFe concentrations, therefore preventing Fe precipitation. Fe does not seem to limit primary production in summer sea ice, although we cannot rule out a potential co-limitation imposed by other essential micronutrients such as

manganese and cobalt (Corami et al., 2005; Pausch et al., 2019; Koch & Trimborn, 2019; Schoffman et al., 2016),

A concomitant drawdown of PO_4^{3-} and $Si(OH)_4$ following the Redfield-Brzezinski nutrient ratio (Figure 3.3c; Brzezinski, 1985) was observed for most data points. This suggests a large contribution of diatoms to sea-ice primary production. Median (and interquartile) normalized PO_4^{3-} (2.0 µM (4.3 µM)) and $Si(OH)_4$ (16.1 µM (24.1 µM)) concentrations show that the studied sea ice was enriched and partially-depleted respectively compared to seawater (0.9 µM (0.6 µM) and 44.5 µM (34.3 µM)) at this time of the year. However, following the 'Liebig's Law' (von Liebig, 1840) which states that growth should be limited by the most deficient nutrient, the fact that PO_4^{3-} is above the Redfield N:P ratio (16; Figure 3.3b) indicates that DIN is the primary limiting nutrient in summer sea ice. Nitrate:PO_4^{3-} depletion was previously observed under Fe replete conditions during mesoscale Fe-enrichment experiments in HNLC waters (Boyd et al. 2000). In the present study, bulk nitrate and nitrite (NO_x) concentrations are close to exhaustion (< 0.2 µM) at Casey1, Totten 2, Mertz1, Mertz2 and Mertz3. Brine concentrations < 0.2 µM were also observed at Mertz2 and Mertz3. In the absence of other sources of nitrogen NH_4^+ would be readily consumed shortly after production. This could explain why our bulk NH_4^+ concentrations are amongst the lowest ever reported in Antarctic sea ice (Fripiat et al., 2017). The low concentrations of N-sources found in most ice floes could therefore impose severe limitations for sympagic algal growth. Enhanced ice melting during summer exacerbates stratification within the ice, preventing convection-driven brine exchanges and replenishment of nutrients from seawater. This scenario would render sea ice particularly dependent on recycling and/or seawater intrusion to alleviate macronutrient limitation at this time of the year.

3.4.3 Sea-ice PFe as a capacitor for summer blooms

Warmer air temperatures lead to increased connectivity of the brine network forming new pathways for brine, meltwater and associated nutrient drainage towards the seawater underneath. As a consequence, DFe concentrations in sea ice collected at this time of the year are expected to be low. However, the sea-ice DFe concentrations up to 13.3 nM (Figure 3.3a) were comparable to those reported from other seasons (Lannuzel et al., 2016b and references therein). Dissolved Fe is therefore likely continuously supplied to sea ice either as truly soluble Fe or in the colloidal form, despite brine drainage and ice decay. Many studies have shown the

importance of the PFe in replenishing the DFe pool via thermal, photochemical, biological and ligand-mediated dissolution (Borer et al., 2005; Ellwood et al., 2012; Kraemer, 2004; Sulzberger et al., 1989). These biogeochemical processes could have potentially maintained background levels of DFe (average 4.7 ± 3.8 nM and 2.0 ± 1.3 nM for fast and pack ice, respectively) at our sea ice stations. Particulate Fe is retained within sea ice longer than DFe because of the adsorption of particles to the walls of the brine channels, a process possibly facilitated by EPS (Becquevort et al., 2009; Lannuzel et al., 2016b; van der Merwe et al., 2011a). EPS are particularly abundant in waters characterized by high chlorophyll concentrations and in the sea ice (Gledhill & Buck, 2012). Although they are predominantly composed of neutral sugars, EPS contain a significant fraction of uronic acids which are known to complex Fe (Mancuso Nichols et al., 2004).

Relatively high concentrations of calculated PFe_{bio} (~50 nM) were observed for all pack ice stations over the entire ice thickness. Since Al is not appreciably accumulated into biogenic material, this result indicates the occurrence of biological assimilation and build-up of biogenic PFe at all ice depths. Based on the measurements of Fe concentration and sea-ice thickness from the sampled cores, if all of the sea ice represented by our samples melts by the end of austral summer (~60 days between the sampling period and the end of February), an average of 4.6 ± 7.1 μmol m^{-2} d^{-1} PFe would be released from sea ice into East-Antarctic surface waters. This input could be particularly important during this time of the year due to the stronger ocean stratification driven by sea-ice melt and ocean surface warming, which hamper the mixing with Fe-rich deep waters. Pack ice formed in coastal polynyas is exposed to coastal Fe inputs and could therefore play a crucial role in delivering biologically processed (and potentially bioavailable) PFe to open waters. In this context, the contribution of summer sea ice as a source of (both biogenic and lithogenic) PFe cannot be neglected. The direct link between PFe solubility and phytoplankton growth however needs to be established, as well as the possible forward trajectories of ice floes into Fe-limited waters, before we will be able to adequately assess the effect of sea ice on the carbon cycle.

3.4.4 Can sea ice enhance the fertilization potential from glacial Fe?

Iron distribution in East Antarctic sea ice did not show significant spatial variation in this study, except for Totten1, with DFe and PFe concentrations significantly higher than those found elsewhere (average 7.0 nM and 1,8 nM, respectively). The level of PFe measured in bottom

sea ice at Totten1 (~5 μM) was only comparable to concentrations found in bottom sea ice collected in the Ross Sea (Grotti et al., 2001; Noble et al., 2013) and at a study site of very shallow (~20 m depth) bathymetry near Casey station (van der Merwe et al. , 2011b). The average molar PFe:PAl (0.3 ± 0.1) obtained from Totten1 ice is very close to values previously reported for the continental crust (0.3; Taylor and McLennan, 1985), suggesting a predominantly lithogenic source. Interestingly, this elemental ratio differs significantly ($p < 0.01$) from the ones measured at Casey1 and Casey2 (0.5 ± 0.2), which were very close to the ratio reported for ocean floor sediments (0.48; Ravanelli, 1997). Therefore, while stations near Casey seem to be highly dependent on sediment resuspension as the main source of Fe, another source may prevail at Totten1. The low PFe content in the snow at Totten1 indicates atmospheric sources are unlikely. Iron must instead come from below, either by vertical or lateral transport. The most substantial geographical features in the proximity of Totten1 are the Totten Ice Shelf and the Moscow University Ice Shelf (MUIS). We therefore hypothesize the presence of basal meltwater from the adjacent MUIS and potentially meltwater runoff from the dominant Totten Ice Shelf could explain the high Fe content observed at this station.

Seawater Fe levels have been previously reported to be significantly influenced by glacial melting around Antarctica (Death et al., 2014; Herraiz-Borreguero et al., 2016; Kim et al., 2015; Person *at al*., 2019). This effect is attributed to the fact that glacial meltwater can supply intensively physically and chemically weathered Fe-rich labile sediments (Raiswell et al., 2018 and references therein; van der Merwe et al., 2019). Glaciogenic minerals are also enriched in labile Fe^{2+} nano particulates compared to other lithogenic sources which are mostly comprised of less bioavailable Fe^{3+} oxyhydroxide and other Fe^{3+} chemical-weathered oxide products (Hawkings et al., 2018; Shoenfelt et al., 2017). While some of this glacial material can be incorporated into marine ice along with upwelling transport, a fraction can also be carried within the ice shelf meltwater plume and reach surface waters (Herraiz-Borreguero et al., 2016). Layers of granular and platelet ice were evident at Totten1. Supercooled glacial meltwaters from the nearby MUIS could promote the formation of these ice structures. The abundant particles contained in these meltwaters could act as crystallization nuclei and therefore facilitate the formation of frazil ice. These crystals can then rise through the water column scavenging Fe-rich suspended sediments in shallow waters near the coast or at the grounding line of ice shelves to be incorporated into the sea ice, analogous to marine ice under an ice shelf (de Jong et al., 2013; Herraiz-Borreguero et al., 2016). The high proportion of

platelet ice within the non-columnar ice at Totten1 strengthens the link between Fe-rich glacial meltwater and the high concentration of PFe found at the bottom of Totten1.

Within the sea ice, Fe can be converted into more readily available forms via abiotic (photoreduction and chemical complexation) and biotic (biological and enzymatic reduction at the cell surface) processes (Genovese et al., 2018; Kaplan & Ward 2013; Tagliabue et al., 2009). Fe dissolution reactions could be augmented by freezing processes. Repetitive freeze/thaw cycles have been shown to continuously add DFe to the ice. Freezing concentrates water and solutes into microenvironments at grain boundaries (Jeong et al., 2012, 2020; Kim et al., 2010). However, Fe^{3+} addition to an enclosed system is limited by saturation, therefore Fe^{3+} is prone to incorporation into the colloidal phase or adsorption onto ice crystals (Raiswell et al., 2018). When sea ice melts, the undersaturated meltwater can stimulate further Fe dissolution to occur. Layers of superimposed ice found in our ice-core samples suggest that melting and refreezing is common in summer sea ice in this area. Therefore, the interaction between glacially derived reactive sediments and sea ice could enhance productivity by releasing elevated concentrations of highly recycled and potentially bioavailable Fe during the melting season, when this stock becomes exhausted in surface waters (Sedwick & DiTullio, 2000). Additional offshore transport of sea ice formed in coastal areas could further enhance the extent of Fe fertilization.

Findings from Totten1 raise the question why similar Fe enrichment in sea ice was not observed at the other stations near ice shelves that we sampled along the East Antarctic coast. Mertz2 station was relatively close (~1 km) to the Mertz glacier. Results from past oceanographic surveys could explain this difference. Waters on the continental shelf in East Antarctica are relatively cool, leading to low rates of basal melt from the ice shelves. The Totten and MUIS are exceptions to this general pattern as relatively warm modified Circumpolar Deep Water (mCDW) enters the cavity beneath the shelf through a deep trough, delivering sufficient heat to drive rapid basal melt (Rintoul et al., 2016). Silvano et al. (2017) showed that this mCDW is widespread over the continental shelf of the Sabrina Coast. Based on this oceanographic particularity, the Totten/MUIS glacial basin could offer the required hydrographic setting for the recurrent formation of Fe-rich platelet ice to potentially occur in large areas of the Sabrina Coast. While Fe supplied from these glaciers is not essential for the sea-ice communities, it might play an important role for phytoplankton communities when this sea ice melts along the Sabrina Coast.

Satellite Chl*a* imagery from 2002-16 supports the link between the presence of platelet ice and surface water fertilization in the surroundings of Totten 1 (Figure 3.6). The summer climatology suggests that large phytoplankton biomass accumulates when the sea ice in front of the Totten Glacier breaks out. This contrasts with the rather low productivity of the neighbouring Dalton Polynya that is in front of the MUIS (Moreau et al., 2019). The outflow of glacial meltwater from the Totten Ice Shelf is located on the western side of the calving front (Silvano et al., 2018). The outflow of glacial meltwater from the MUIS is widespread along the coast and south of the Dalton polynya, with productivity highest in the latter region (Moreau et al., 2019). To our knowledge, these observations could be the first evidence of a potential fertilization impact from the combined presence of platelet ice and Fe-rich glacial meltwaters. The Totten glacier mass loss has increased through time from 5.7 Gt y^{-1} in 1979–2003 to 7.3 Gt y^{-1} in 2003–2017; glaciers draining into MUIS show a slight net thinning in the last decades (Rignot et al., 2019). As climate change could drive the loss of up to 23% of the ice shelf volume in Antarctica by 2070 in a business-as-usual scenario (DeConto & Pollard, 2016; Rintoul et al., 2018), a better understanding of how marine and glacial sediment transport will be affected by increasing basal melting and grounding line retreat is needed.

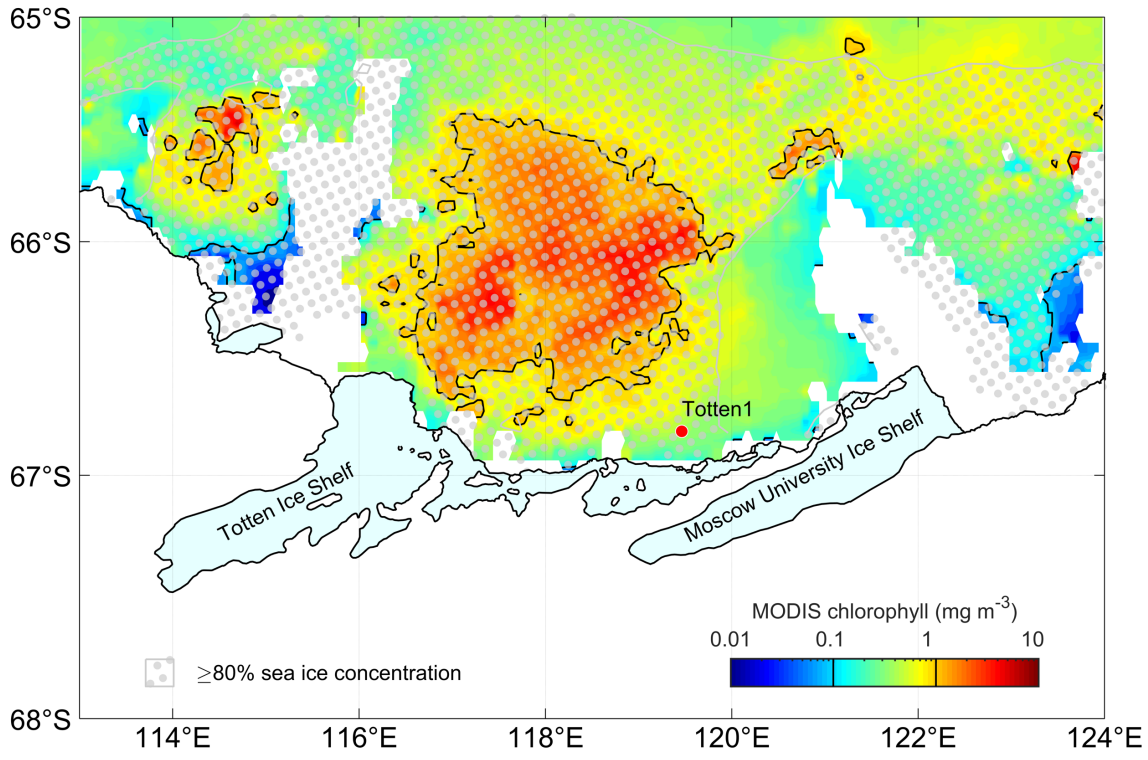

Figure 3.6 MODIS-Aqua summer chlorophyll-a concentrations (December – February climatology)

off the Sabrina Coast from 2002-16, also indicating the location of Totten1 station. White regions indicate areas where no data is available due to grounded iceberg and fast ice coverage.

3.5 Conclusion

The scarcity of inorganic nitrogen sources along with abundant particulate matter suggest the dominance of heterotrophic and potentially mixotrophic activity in sea ice during summer. At this time of the year, the sea ice can still retain a significant amount of Fe, both in the dissolved and, particularly, in the particulate fraction. Biotic and abiotic processes help sustain Fe supply during late summer. Projected changes in sea-ice thickness and snowfall could increase fluxes of macronutrients via surface flooding and brine percolation, alleviating nutrient depletion in summer, and potentially extending the period of habitability for sea-ice algae. Climate change might also impose indirect impacts on the sea-ice Fe distribution via reduction of glacial coverage in Antarctica. In East Antarctica, the Totten Ice Shelf is already experiencing rapid basal melt. A further increase in the supply of glacial meltwater to the East Antarctic shelf could potentially stimulate the formation of platelet ice layers in the surrounding sea ice. How phytoplankton will be affected by this reservoir of Fe will depend both on the timing of its release to surface waters and on the bioavailability of this source which is a function of the biological and physicochemical changes that Fe undergoes within the ice.

3.6 Acknowledgements and Data

This work was co-funded by the Australian Government Cooperative Research Centre Program through the Antarctic Climate and Ecosystems (ACE CRC), the Australian Antarctic Science (AAS) project no. 4291 and the Australian Research Council's Special Research Initiative for Antarctic Gateway Partnership (Project ID SR140300001). Access to ICP instrumentation was supported through ARC LIEF LE0989539 funding. Data supporting the analysis and conclusions here presented can be accessed through the Australian Antarctic Data Centre website (https://data.aad.gov.au/metadata/records/AAV2_seaice_BGC_2016)

3.7 References

Allison, I. (1998). The East Antarctic Sea Ice Zone: Ice characteristics and drift. *GeoJournal,* 18: 103-115.

Arar, E. J. & G. B. Collins (1997). Method 445.0 in vitro determination of chlorophyll-a and pheophytin-a in marine and freshwater algae by fluorescence. U.S Environmental Protection Agency. Washington, DC.

Arndt, S., K. M. Meiners, R. Ricker, T. Krumpen, C. Katlein & M. Nicolaus (2017). Influence of snow depth and surface flooding on light transmission through Antarctic pack ice. *Journal of Geophysical Research: Oceans,* 122(3): 2108-2119. https://doi.org/10.1002/2016jc012325

Arrigo, K. R., J. N. Kremer & C. W. Sullivan (1993). A simulated Antarctic fast ice ecosystem. *Journal of Geophysical Research: Oceans,* 98(C4): 6929-6946. https://doi.org/10.1029/93jc00141

Arrigo, K. R., M. M. Mills, L. R. Kropuenske, G. L. van Dijken, A. C. Alderkamp & D. H. Robinson (2010). Photophysiology in two major Southern-Ocean phytoplankton taxa: Photosynthesis and growth of *Phaeocystis antarctica* and *Fragilariopsis cylindrus* under different irradiance levels. *Integrative and Comparative Biology,* 50(6): 950-966. https://doi.org/10.1093/icb/icq021

Arrigo, K. R., D. K. Perovich, R. S. Pickart, Z. W. Brown, G. L. van Dijken, K. E. Lowry et al. (2012). Massive phytoplankton blooms under Arctic sea ice. *Science,* 336(6087): 1408. https://doi.org/10.1126/science.1215065

Arrigo, K. R., A. M. Weiss & W. O. Smith (1998). Physical forcing of phytoplankton dynamics in the southwestern Ross Sea. *Journal of Geophysical Research: Oceans,* 103(C1): 1007-1021. https://doi.org/10.1029/97jc02326

Azam K, S. N. K. (2013). Evaluation of relationship between light intensity (lux) and growth of *Chaetoceros muelleri*. *Oceanography: Open Access,* 01(03). https://doi.org/10.4172/2332-2632.1000111

Baar, H. J. W. d., A. G. Burna, R. F. Nolting, G. c. Cadee, G. Jacques & P. Treguer (1990). On iron limitation of the Southern Ocean: Experimental observations in the Weddell and Scotia Seas. *Marine Ecology Progress Series,* 65: 105-122. https://doi.org/10.3354/meps065105

Baar, H. J. W. d., J. T. M. Dejong, D. C. E. Bakker, B. M. Loscher, C. Veth, U. Bathmann & V. Smetacek (1995). Importance of iron for plankton blooms and carbon-dioxide drawdown in the Southern Ocean. *Nature,* 373(6513): 412-415. https://doi.org/10.1038/373412a0

Bates, S. S. & G. F. Cota (1986). Fluorescence induction and photosynthetic responses of Arctic ice algae to sample treatment and salinity. *Journal of Phycology,* 22(4): 421-429. https://doi.org/10.1111/j.1529-8817.1986.tb02484.x

Becquevort, S., I. Dumont, J. L. Tison, D. Lannuzel, M. L. Sauvée, L. Chou & V. Schoemann (2009). Biogeochemistry and microbial community composition in sea ice and underlying seawater off East Antarctica during early spring. *Polar Biology,* 32(6): 879-895. https://doi.org/10.1007/s00300-009-0589-2

Bertrand, E. M., M. A. Saito, P. A. Lee, R. B. Dunbar, P. N. Sedwick & G. R. Ditullio (2011). Iron limitation of a springtime bacterial and phytoplankton community in the Ross Sea: Implications for vitamin B(12) nutrition. *Frontiers in Microbiology,* 2: 160. https://doi.org/10.3389/fmicb.2011.00160

Bombosch, A. (2013). Interactions Between Floating Ice Platelets and Ocean Water in the Southern Weddell Sea. *Ocean, Ice, and Atmosphere: Interactions at the Antarctic Continental Margin*. S. S. Jacobs and R. F. Weiss. Washington, D.C., American Geophysical Union. 75: 257-266. https://doi.org/10.1029/AR075p0257

Borer, P. M., B. Sulzberger, P. Reichard & S. M. Kraemer (2005). Effect of siderophores on the light-induced dissolution of colloidal iron(III) (hydr)oxides. *Marine Chemistry,* 93(2-4): 179-193. https://doi.org/10.1016/j.marchem.2004.08.006

Bowie, A. R., A. T. Townsend, D. Lannuzel, T. A. Remenyi & P. van der Merwe (2010). Modern sampling and analytical methods for the determination of trace elements in marine particulate material using magnetic sector inductively coupled plasma-mass spectrometry. *Analytica Chimica Acta,* 676(1-2): 15-27. https://doi.org/10.1016/j.aca.2010.07.037

Boyd, P. W., A. J. Watson, C. S. Law, E. R. Abraham, T. Trull, R. Murdoch et al. (2000). A mesoscale phytoplankton bloom in the polar Southern Ocean stimulated by iron fertilization. *Nature,* 407(6805): 695-702. https://doi.org/10.1038/35037500

Brandt, R. E., S. G. Warren, A. P. Worby & T. C. Grenfell (2005). Surface albedo of the Antarctic Sea Ice Zone. *Journal of Climate,* 18(17): 3606-3622. https://doi.org/10.1175/jcli3489.1

Brzezinski, M. A. (1985). The Si:C:N ratio of marine diatoms: Interspecific variability and the effect of some environmental variables. *Journal of Phycology,* 21(3): 347-357. https://doi.org/10.1111/j.0022-3646.1985.00347.x.

Corami, F., G. Capodaglio, C. Turetta, F. Soggia, E. Magi & M. Grotti (2005). Summer distribution of trace metals in the western sector of the Ross Sea, Antarctica. *Journal of Environmental Monitoring,* 7(12): 1256-1264. https://doi.org/10.1039/b507323p

Cutter, G., Casciotti, K., Cullen, P., Geibert, W., Heimbürger, L.-E., Lohan, M. C. et al. (2017). *Sampling and Sample-handling Protocols for GEOTRACES Cruises*. Retrieved from https://geotracesold.sedoo.fr/images/Cookbook.pdf

de Jong, A., V. Schoemann, N. Maricq, N. Mattielli, L. Patricia, H. T. & J. L. Tison (2013). Iron in land-fast sea ice of McMurdo Sound derived from sediment resuspension and wind-blown dust attributes to primary productivity in the Ross Sea, Antarctica. *Marine Chemistry,* 157: 24–40. https://doi.org/10.1016/j.marchem.2013.07.001

de Jong, J., V. Schoemann, D. Lannuzel, P. Croot, H. de Baar & J.-L. Tison (2012). Natural iron fertilization of the Atlantic sector of the Southern Ocean by continental shelf sources of the Antarctic Peninsula. *Journal of Geophysical Research: Biogeosciences,* 117(G1). https://doi.org/10.1029/2011jg001679

Death, R., J. L. Wadham, F. Monteiro, A. M. Le Brocq, M. Tranter, A. Ridgwell, S. Dutkiewicz & R. Raiswell (2014). Antarctic ice sheet fertilises the Southern Ocean. *Biogeosciences,* 11(10): 2635-2643. https://doi.org/10.5194/bg-11-2635-2014

DeConto, R. M. & D. Pollard (2016). Contribution of Antarctica to past and future sea-level rise. *Nature,* 531(7596): 591-597. https://doi.org/10.1038/nature17145

Duprat, L., N. Kanna, J. Janssens, A. Roukaerts, F. Deman, A. T. Townsend et al. (2019). Enhanced iron flux to Antarctic sea ice via dust deposition from ice-free coastal areas. *Journal of Geophysical Research: Oceans*, 124(12): 8538-8557. https://doi.org/10.1029/2019jc015221

Ellwood, M. J., Hutchins, D. A., Lohan, M. C., Milne, A., Nasemann, P., Nodder, S. D. et al. (2015). Iron stable isotopes track pelagic iron cycling during a subtropical phytoplankton bloom. *Proceedings of the Natinal Academic of Science U S A,* 112**,** E15-20. https://doi.org/10.1073/pnas.1421576112

Engel, A. & U. Passow (2001). Carbon and nitrogen content of Transparent Exopolymer Particles (TEP) in relation to their Alcian Blue adsorption. *Marine Ecology Progress Series,* 219: 1-10. https://doi.org/10.3354/meps219001

Ewert, M. & Deming, J. W. (2013). Sea ice microorganisms: environmental constraints and extracellular responses. *Biology (Basel),* 2**,** 603-28. https://doi.org/10.3390/biology2020603

Fripiat, F., K. M. Meiners, M. Vancoppenolle, S. Papadimitriou, D. N. Thomas, S. F. Ackley et al. (2017). Macro-nutrient concentrations in Antarctic pack ice: Overall patterns and overlooked processes. *Elementa-Science of the Anthropocene,* 5(13):2-24. https://doi.org/10.1525/elementa.217

Gao, Y., Y. J. Kaufman, D. Tanre, D. Kolber & P. G. Falkowski (2001). Seasonal distributions of aeolian iron fluxes to the global ocean. *Geophysical Research Letters,* 28(1): 29-32. https://doi.org/10.1029/2000gl011926

Genovese, C., M. Grotti, J. Pittaluga, F. Ardini, J. Janssens, K. Wuttig et al. (2018). Influence of organic complexation on dissolved iron distribution in East Antarctic pack ice. *Marine Chemistry,* 203: 28-37. https://doi.org/10.1016/j.marchem.2018.04.005

Gledhill, M. & Buck, K. N. (2012). The organic complexation of iron in the marine environment: a review. *Frontiers in Microbiology,* 3**,** 69 https://doi.org/10.3389/fmicb.2012.00069

Gradinger, R. & J. Ikavalko (1998). Organism incorporation into newly forming Arctic sea ice in the Greenland Sea. *Journal of Plankton Research,* 20(5): 871-886. https://doi.org/10.1093/plankt/20.5.871

Grotti, M., F. Soggia, M. L. Abelmoschi, P. Rivaro, E. Magi & R. Frache (2001). Temporal distribution of trace metals in Antarctic coastal waters. *Marine Chemistry,* 76(3): 189-209. https://doi.org/10.1016/S0304-4203(01)00063-9

Haas, C., D. N. Thomas & J. Bareiss (2017). Surface properties and processes of perennial Antarctic sea ice in summer. *Journal of Glaciology,* 47(159): 613-625. https://doi.org/10.3189/172756501781831864

Hancke, K., L. C. Lund-Hansen, M. L. Lamare, S. Højlund Pedersen, M. D. King, P. Andersen & B. K. Sorrell (2018). Extreme low light requirement for algae growth underneath sea ice: A case study from station Nord, NE Greenland. *Journal of Geophysical Research: Oceans,* 123(2): 985-1000. https://doi.org/10.1002/2017jc013263

Hawkings, J. R., L. G. Benning, R. Raiswell, B. Kaulich, T. Araki, M. Abyaneh et al. (2018). Biolabile ferrous iron bearing nanoparticles in glacial sediments. *Earth and Planetary Science Letters,* 493: 92-101. https://doi.org/10.1016/j.epsl.2018.04.022

Herraiz-Borreguero, L., D. Lannuzel, P. van der Merwe, A. Treverrow & J. B. Pedro (2016). Large flux of iron from the Amery Ice Shelf marine ice to Prydz Bay, East Antarctica. *Journal of Geophysical Research-Oceans,* 121(8): 6009-6020. https://doi.org/10.1002/2016jc011687

Janssens, J., K. M. Meiners, J. L. Tison, G. Dieckmann, B. Delille & D. Lannuzel (2016). Incorporation of iron and organic matter into young Antarctic sea ice during its initial growth stages. *Elementa-Science of the Anthropocene,* 4: 000123. https://doi.org/10.12952/journal.elementa.000123

Jeong, D., Kim, K. & Choi, W. (2012). Accelerated dissolution of iron oxides in ice. *Atmospheric Chemistry and Physics,* 12**,** 11125-11133.https://doi.org/10.5194/acp-12-11125-2012

Jeong, D., Kim, K., Min, D. W. & Choi, W. (2020). Freezing-Enhanced Dissolution of Iron Oxides: Effects of Inorganic Acid Anions. *Environmental Science Technology,* 49**,** 12816-22. https://doi.org/10.1021/acs.est.5b04211

Kaplan, J. & D. M. Ward (2013). The essential nature of iron usage and regulation. *Current Biology,* 23(15): R642-646. https://doi.org/10.1016/j.cub.2013.05.033

Katlein, C., S. Arndt, M. Nicolaus, D. K. Perovich, M. V. Jakuba, S. Suman et al. (2015). Influence of ice thickness and surface properties on light transmission through Arctic sea ice. *Journal of Geophysical Research-Oceans,* 120(9): 5932-5944. https://doi.org/10.1002/2015JC010914

Kérouel, R. & A. Aminot (1997). Fluorometric determination of ammonia in sea and estuarine waters by direct segmented flow analysis. *Marine Chemistry,* 57(3-4): 265-275. https://doi.org/10.1016/s0304-4203(97)00040-6

Kim, I., G. Kim & E. J. Choy (2015). The significant inputs of trace elements and rare earth elements from melting glaciers in Antarctic coastal waters. *Polar Research,* 34(1). https://doi.org/10.3402/polar.v34.24289

Kim, K., W. Choi, M. R. Hoffmann, H. I. Yoon & B. K. Park (2010). Photoreductive dissolution of iron oxides trapped in ice and its environmental implications. *Environmental Science & Technolology,* 44(11): 4142-4148. https://doi.org/10.1021/es9037808

Kirst, G. O. & C. Wiencke (1995). Ecophysiology of polar algae. *Journal of Phycology,* 31(2): 181-199. https://doi.org/10.1111/j.0022-3646.1995.00181.x

Koch, F. & Trimborn, S. (2019). Limitation by Fe, Zn, Co, and B12 Results in Similar Physiological Responses in Two Antarctic Phytoplankton Species. *Frontiers in Marine Science,* 6. https://doi.org/10.3389/fmars.2019.00514

Kraemer, S. M. (2004). Iron oxide dissolution and solubility in the presence of siderophores. *Aquatic Sciences - Research Across Boundaries,* 66(1): 3-18. https://doi.org/10.1007/s00027-003-0690-5

Lancelot, C., A. de Montety, H. Goosse, S. Becquevort, V. Schoemann, B. Pasquer & M. Vancoppenolle (2009). Spatial distribution of the iron supply to phytoplankton in the Southern Ocean: A model study. *Biogeosciences,* 6(12): 2861-2878. https://doi.org/10.5194/bg-6-2861-2009

Langhorne, P. J., K. G. Hughes, A. J. Gough, I. J. Smith, M. J. M. Williams, N. J. Robinson et al. (2015). Observed platelet ice distributions in Antarctic sea ice: An index for ocean-ice shelf heat flux. *Geophysical Research Letters,* 42(13): 5442-5451. https://doi.org/10.1002/2015gl064508

Langway, C. C., Jr. (1958). Ice fabrics and the universal stage. *Snow, Ice and Permafrost Research Establishment, Technical*. U.S. 62.

Lannuzel, D., F. Chever, P. C. van der Merwe, J. Janssens, A. Roukaerts, A. J. Cavagna et al. (2016a). Iron biogeochemistry in Antarctic pack ice during SIPEX-2. *Deep-Sea Research Part II-Topical Studies in Oceanography,* 131: 111-122. https://doi.org/10.1016/j.dsr2.2014.12.003

Lannuzel, D., J. de Jong, V. Schoemann, A. Trevena, J. L. Tison & L. Chou (2006). Development of a sampling and flow injection analysis technique for iron determination in the sea ice

environment. *Analytica Chimica Acta,* 556(2): 476-483. https://doi.org/10.1016/j.aca.2005.09.059

Lannuzel, D., V. Schoemann, J. de Jong, L. Chou, B. Delille, S. Becquevort & J. L. Tison (2008). Iron study during a time series in the western Weddell pack ice. *Marine Chemistry,* 108(1-2): 85-95. https://doi.org/10.1016/j.marchem.2007.10.006

Lannuzel, D., V. Schoemann, J. de Jong, J. L. Tison & L. Chou (2007). Distribution and biogeochemical behaviour of iron in the East Antarctic sea ice. *Marine Chemistry,* 106(1-2): 18-32. https://doi.org/10.1016/j.marchem.2006.06.010

Lannuzel, D., V. Schoemann, I. Dumont, M. Content, J. de Jong, J. L. Tison et al. (2013). Effect of melting Antarctic sea ice on the fate of microbial communities studied in microcosms. *Polar Biology,* 36(10): 1483-1497. https://doi.org/10.1007/s00300-013-1368-7

Lannuzel, D., M. Vancoppenolle, P. van der Merwe, J. de Jong, K. M. Meiners, M. Grotti et al. (2016b). Iron in sea ice: Review and new insights. *Elementa: Science of the Anthropocene,* 4: 000130. https://doi.org/10.12952/journal.elementa.000130

Liebig, J. Y. (1940). *Organic chemistry in its applications to agriculture and physiology.* L. Playfair. 1st Edition. Cambridge, UK. https://doi.org/10.5962/bhl.title.40751

Lim, S. M., S. Moreau, M. Vancoppenolle, F. Deman, A. Roukaerts, K. M. Meiners et al (2019). Field observations and physical-biogeochemical modeling suggest low silicon affinity for Antarctic fast-ice diatoms. *Journal of Geophysical Research: Oceans*, 124(11):7837-7853 https://doi.org/10.1029/2018jc014458

Mancuso Nichols, C. A., Garon, S., Bowman, J. P., Raguenes, G. & Guezennec, J. (2004). Production of exopolysaccharides by Antarctic marine bacterial isolates. *Journal of Applied Microbiol,* 96**,** 1057-66. https://doi.org/10.1111/j.1365-2672.2004.02216.x

Markussen, T. N., Elberling, B., Winter, C. & Andersen, T. J. (2016). Flocculated meltwater particles control Arctic land-sea fluxes of labile iron. *Scientific Reports,* 6**,** 24033 https://doi.org/10.1038/srep24033

Martin, A., A. McMinn, S. K. Davy, M. J. Anderson, H. C. Miller, J. A. Hall & K. G. Ryan (2012). Preliminary evidence for the microbial loop in Antarctic sea ice using microcosm simulations. *Antarctic Science,* 24(6): 547-553. https://doi.org/10.1017/S0954102012000491

Martin, J. H. (1990). Glacial-interglacial CO_2 change: The iron hypothesis. *Paleoceanography,* 5(1): 1-13. https://doi.org/10.1029/PA005i001p00001

Martin, J. H. (1993). Determination of Particulate Organic Carbon (POC) and Nitrogen (PON) in Seawate. *In:* Kadar, S., Leinen, M. and Murray, J. W. (Eds.) *U. S. Jgofs Equatorial Pacific Process Study Sampling And - Analytical Protocol*

Massom, R. A. & S. E. Stammerjohn (2010). Antarctic sea ice change and variability - Physical and ecological implications. *Polar Science,* 4(2): 149-186. https://doi.org/10.1016/j.polar.2010.05.001

McMinn, A., C. Ashworth & K. G. Ryan (2000). In situ net primary productivity of an Antarctic fast ice bottom algal community. *Aquatic Microbial Ecology,* 21(2): 177-185. https://doi.org/10.3354/ame021177

Meiners, K.M., R. Brinkmeyer, M. A. Granskog & A. Lindfors (2004). Abundance, size distribution and bacterial colonization of exopolymer particles in Antarctic sea ice (Bellingshausen Sea). *Aquatic Microbial Ecology,* 35(3): 283-296. https://doi.org/10.3354/ame035283

Meiners, K.M., C. Krembs & R. Gradinger (2008). Exopolymer particles: Microbial hotspots of enhanced bacterial activity in Arctic fast ice (Chukchi Sea). *Aquatic Microbial Ecology,* 52(2): 195-207. https://doi.org/10.3354/ame01214

Meiners, K.M., Norman, L., Granskog, M.A., Krell, A., Heil, P. & Thomas, D.N. (2011). Physico-ecobiogeochemistry of East Antarctic pack ice during the winter-spring transition. *Deep Sea Research Part II: Topical Studies in Oceanography*, 58(9-10), pp.1172-1181. https://doi.org/10.1016/j.dsr2.2010.10.033

Meiners, K. M. & Michel, C. (2016). Dynamics of nutrients dissolved organic matter and exopolymers in sea ice. In D. N. Thomas (Ed.), *Sea Ice* (pp. 415-432). Wiley-Blackwell: Oxford. https://doi.org/10.1002/9781118778371.ch17

Meiners, K.M., M. Vancoppenolle, S. Thanassekos, G. S. Dieckmann, D. N. Thomas, J. L. Tison et al. (2012). Chlorophylla in Antarctic sea ice from historical ice core data. *Geophysical Research Letters,* 39(21): n/a-n/a. https://doi.org/10.1029/2012gl053478

Moreau, S., D. Lannuzel, J. Janssens, M. C. Arroyo, M. Corkill, E. Cougnon et al. (2019). Sea ice meltwater and Circumpolar Deep-Water drive contrasting productivity in three Antarctic polynyas. *Journal of Geophysical Research-Oceans,* 124(5): 2943-2968. https://doi.org/10.1029/2019jc015071

Morel, F. M. M., A. B. Kustka & Y. Shaked (2008). The role of unchelated Fe in the iron nutrition of phytoplankton. *Limnology and Oceanography,* 53(1): 400-404. https://doi.org/10.4319/lo.2008.53.1.0400

Noble, A. E., D. M. Moran, A. E. Allen & M. A. Saito (2013). Dissolved and particulate trace metal micronutrients under the McMurdo Sound seasonal sea ice: Basal sea ice communities as a capacitor for iron. *Frontiers in Chemistry,* 1(25): 25. https://doi.org/10.3389/fchem.2013.00025

Oerter, H., J. Kipfstuhl, J. Determann, H. Miller, D. Wagenbach, A. Minikin & W. Graf (1992). Evidence for basal marine ice in the Filchner-Ronne Ice Shelf. *Nature,* 358(6385): 399-401. https://doi.org/10.1038/358399a0

Palmisano, A. C., J. Beeler SooHoo & C. W. Sullivan (1987). Effects of four environmental variables on photosynthesis-irradiance relationships in Antarctic sea-ice microalgae. *Marine Biology,* 94(2): 299-306. https://doi.org/10.1007/bf00392944

Paolo, F. S., H. A. Fricker & L. Padman (2015). Ice sheets. Volume loss from Antarctic ice shelves is accelerating. *Science,* 348(6232): 327-331. https://doi.org/10.1126/science.aaa0940

Parekh, P., M. J. Follows & E. A. Boyle (2005). Decoupling of iron and phosphate in the global ocean. *Global Biogeochemical Cycles,* 19(2): n/a-n/a. https://doi.org/10.1029/2004gb002280

Passow, U. & A. L. Alldredge (1994). Distribution, size and bacterial colonization of Transparent Exopolymer Particles (TEP) in the Ocean. *Marine Ecology Progress Series,* 113(1-2): 185-198. https://doi.org/10.3354/meps113185

Pausch, F., K. Bischof & S. Trimborn (2019). Iron and manganese co-limit growth of the Southern Ocean diatom Chaetoceros debilis. *PLoS One,* 14(9): e0221959. https://doi.org/10.3354/meps113185

Person, R., O. Aumont, G. Madec, M. Vancoppenolle, L. Bopp and N. Merino (2019). Sensitivity of ocean biogeochemistry to the iron supply from the Antarctic Ice Sheet explored with a biogeochemical model. *Biogeosciences,* 16(18): 3583-3603. https://doi.org/10.5194/bg-16-3583-2019

Petrou, K., R. Hill, C. M. Brown, D. A. Campbell, M. A. Doblin & P. J. Ralph (2010). Rapid photoprotection in sea-ice diatoms from the East Antarctic pack ice. *Limnology and Oceanography,* 55(3): 1400-1407. https://doi.org/10.4319/lo.2010.55.3.1400

Price, N. M. (2005). The elemental stoichiometry and composition of an iron-limited diatom. *Limnology and Oceanography,* 50(4): 1159-1171. https://doi.org/10.4319/lo.2005.50.4.1159

R Core (2013). *R: A language and environment for statistical computing*. R. C. Team. Viena, Austria.

Raiswell, R., J. Hawkings, A. Eisenousy, R. Death, M. Tranter & J. Wadham (2018). Iron in glacial systems: Speciation, reactivity, freezing behavior, and alteration during transport. *Frontiers in Earth Science,* 6. https://doi.org/10.3389/feart.2018.00222

Ralph, P. J., K. G. Ryan, A. Martin & G. Fenton (2007). Melting out of sea ice causes greater photosynthetic stress in algae than freezing in. *Journal of Phycology,* 43(5): 948-956. https://doi.org/10.1111/j.1529-8817.2007.00382.x

Ravanelli, M., O. Tubertini, S. Valcher & W. Martinotti (1997). Heavy metal distribution in sediment cores from Western Ross Sea (Antarctica). *Water Air and Soil Pollution,* 99(1-4): 697-704. https://doi.org/10.1007/Bf02406909

Redfield, A. C., B. H. Ketchum & B. F.A. (1963). The influence of organisms on the composition of sea water. In: M.N. Hill. The Sea, Interscience. M. N. Hill. New York Interscience Publishers. 2, 26-77.

Rees, C., L. Pender, K. Sherrin, C. Schwanger, P. Hughes, S. Tibben et al. (2018). Methods for reproducible shipboard SFA nutrient measurement using RMNS and automated data processing. *Limnolology and Oceanography: Methods,* 17(1): 25-41. https://doi.org/10.1002/Iom3.10294

Rignot, E., J. Mouginot, B. Scheuchl, M. van den Broeke, M. J. van Wessem & M. Morlighem (2019). Four decades of Antarctic Ice Sheet mass balance from 1979–2017. *Proceedings of the National Academy of Sciences,* 116(4): 1095-1103. https://doi.org/10.1073/pnas.1812883116

Rintala, J. M., J. Piiparinen, J. Blomster, M. Majaneva, S. Muller, J. Uusikivi & R. Autio (2014). Fast direct melting of brackish sea-ice samples results in biologically more accurate results than slow buffered melting. *Polar Biology,* 37(12): 1811-1822. https://doi.org/10.1007/s00300-014-1563-1v

Rintoul, S. R., S. L. Chown, R. M. DeConto, M. H. England, H. A. Fricker, V. Masson-Delmotte et al. (2018). Choosing the future of Antarctica. *Nature,* 558(7709): 233-241. https://doi.org/10.1038/s41586-018-0173-4

Rintoul, S. R., A. Silvano, B. Pena-Molino, E. van Wijk, M. Rosenberg, J. S. Greenbaum & D. D. Blankenship (2016). Ocean heat drives rapid basal melt of the Totten Ice Shelf. *Science Advances,* 2(12): e1601610. https://doi.org/10.1126/sciadv.1601610

Ryan, K. G., P. Ralph & A. McMinn (2004). Acclimation of Antarctic bottom-ice algal communities to lowered salinities during melting. *Polar Biology,* 27(11): 679-686. https://doi.org/10.1007/s00300-004-0636-y

Rysgaard, S. & R. N. Glud (2004). Anaerobic N_2 production in Arctic sea ice. *Limnology and Oceanography,* 49(1): 86-94. https://doi.org/10.4319/lo.2004.49.1.0086

Saenz, B. T. & K. R. Arrigo (2014). Annual primary production in Antarctic sea ice during 2005-2006 from a sea ice state estimate. *Journal of Geophysical Research-Oceans,* 119(6): 3645-3678. https://doi.org/10.1002/2013jc009677

Schoffman, H., H. Lis, Y. Shaked & N. Keren (2016). Iron-nutrient interactions within phytoplankton. *Frontiers in Plant Science,* 7: 1223. https://doi.org/10.3389/fpls.2016.01223

Sedwick, P. N., G. R. DiTullio & D. J. Mackey (2000). Iron and manganese in the Ross Sea, Antarctica: Seasonal iron limitation in Antarctic shelf waters. *Journal of Geophysical Research-Oceans,* 105(C5): 11321-11336. https://doi.org/10.1029/2000jc000256

Sedwick, P. N., P. R. Edwards, D. J. Mackey, F. B. Griffiths & J. S. Parslow (1997). Iron and manganese in surface waters of the Australian subantarctic region. *Deep-Sea Research Part I: Oceanographic Research Papers,* 44(7): 1239-1253. https://doi.org/10.1016/S0967-0637(97)00021-6

Sedwick, P. N., C. M. Marsay, B. M. Sohst, A. M. Aguilar-Islas, M. C. Lohan, M. C. Long et al. (2011). Early season depletion of dissolved iron in the Ross Sea polynya: Implications for iron dynamics on the Antarctic continental shelf. *Journal of Geophysical Research-Oceans,* 116(C12). https://doi.org/10.1029/2010jc006553

Shoenfelt, E. M., J. Sun, G. Winckler, M. R. Kaplan, A. L. Borunda, K. R. Farrell et al. (2017). High particulate iron(II) content in glacially sourced dusts enhances productivity of a model diatom. *Science Advances,* 3(6): e1700314. https://doi.org/10.1126/sciadv.1700314

Silvano, A., S. R. Rintoul, B. Pena-Molino, W. R. Hobbs, E. van Wijk, S. Aoki et al. (2018). Freshening by glacial meltwater enhances melting of ice shelves and reduces formation of Antarctic Bottom Water. *Science Advances,* 4(4): eaap9467. https://doi.org/10.1126/sciadv.aap9467

Silvano, A., S. R. Rintoul, B. Pena-Molino & G. D. Williams (2017). Distribution of water masses and meltwater on the continental shelf near the Totten and Moscow University ice shelves. *Journal of Geophysical Research-Oceans,* 122(3): 2050-2068. https://doi.org/10.1002/2016jc012115

Smetacek, V., R. Scharek, L. I. Gordon, H. Eicken, E. Fahrbach, G. Rohardt & S. Moore (1992). Early spring phytoplankton blooms in ice platelet layers of the Southern Weddell Sea, Antarctica. *Deep-Sea Research Part A-Oceanographic Research Papers,* 39(2a): 153-168. https://doi.org/10.1016/0198-0149(92)90102-Y

Stewart, F. J. & C. H. Fritsen (2004). Bacteria-algae relationships in Antarctic sea ice. *Antarctic Science,* 16(2): 143-156. https://doi.org/10.1017/S0954102004001889

Sulzberger, B., D. Suter, C. Siffert, S. Banwart & W. Stumm (1989). Dissolution of Fe(III)(hydr)oxides in natural-waters - Laboratory assessment on the kinetics controlled by surface coordination. *Marine Chemistry,* 28(1-3): 127-144. https://doi.org/10.1016/0304-4203(89)90191-6

Sunda, W. G. (2012). Feedback Interactions between Trace Metal Nutrients and Phytoplankton in the Ocean. Frontiers of Microbiology, 3, 204. https://doi.org/10.3389/fmicb.2012.00204

Tagliabue, A., L. Bopp, O. Aumont & K. R. Arrigo (2009). Influence of light and temperature on the marine iron cycle: From theoretical to global modeling. *Global Biogeochemical Cycles,* 23(2): n/a-n/a. https://doi.org/10.1029/2008gb003214

Tagliabue, A. L. & K.R. Arrigo (2006). Processes governing the supply of iron to phytoplankton in stratified seas. *Journal of geophysical Research,* 111(C6). https://doi.org/10.1029/2005jc003363

Taylor, S. R. M., S. M. (1985). The continental crust: Its composition and evolution. *Geological Magazine*. Oxford, London, Edinburgh, Boston, Palo Alto, Melbourne, Blackwell Scientific. 122: 673-674.

Thomas, D. & G. Dieckmann (2010). *Sea Ice*. 2nd Edition, Oxford: Wiley-Blackwell. https://doi.org/10.1002/9781444317145

Timmermans, K. R., B. van der Wagt & H. J. W. de Baar (2004). Growth rates, half-saturation constants, and silicate, nitrate, and phosphate depletion in relation to iron availability of four large, open-ocean diatoms from the Southern Ocean. *Limnology and Oceanography,* 49(6): 2141-2151. https://doi.org/10.4319/lo.2004.49.6.2141

Tison, J. L., R. D. Lorrain, A. Bouzette, M. Dini, A. Bondesan & M. Stiévenard (1998). Linking landfast sea ice variability to marine ice accretion at Hell Gate Ice Shelf, Ross Sea. *Antarctic Research Series,* 74: 375-407.

Tison, J. L., A. Worby, B. Delille, F. Brabant, S. Papadimitriou, D. Thomas et al. (2008). Temporal evolution of decaying summer first-year sea ice in the Western Weddell Sea, Antarctica. *Deep-Sea Research Part II-Topical Studies in Oceanography,* 55(8-9): 975-987. https://doi.org/10.1016/j.dsr2.2007.12.021

Torstensson, A., A. Fransson, K. Currie, A. Wulff & M. Chierici (2018). Microalgal photophysiology and macronutrient distribution in summer sea ice in the Amundsen and Ross Seas, Antarctica. *PLoS, One* 13(4): e0195587. https://doi.org/10.1371/journal.pone.0195587

Treverrow, A., R. C. Warner, W. F. Budd & M. Craven (2010). Meteoric and marine ice crystal orientation fabrics from the Amery Ice Shelf, East Antarctica. *Journal of Glaciology,* 56(199): 877-890. https://doi.org/10.3189/002214310794457353

Underwood, G. J. C., S. Fietz, S. Papadimitriou, D. N. Thomas & G. S. Dieckmann (2010). Distribution and composition of dissolved extracellular polymeric substances (EPS) in Antarctic sea ice. *Marine Ecology Progress Series,* 404: 1-19. https://doi.org/10.3354/meps08557

van der Linden, F. C., Tison, J. L., Champenois, W., Moreau, S., Carnat, G., Kotovitch, M., et al. (2020). Sea Ice CO2 Dynamics Across Seasons: Impact of Processes at the Interfaces. Journal of *Geophysical Research: Oceans*, 125(6). https://doi.org/10.1029/2019jc015807

van der Merwe, P., D. Lannuzel, A. R. Bowie, C. A. Mancuso Nichols & K. M. Meiners (2011a). Iron fractionation in pack and fast ice in East Antarctica: Temporal decoupling between the release of dissolved and particulate iron during spring melt. *Deep Sea Research Part II: Topical Studies in Oceanography,* 58(9-10): 1222-1236. https://doi.org/10.1016/j.dsr2.2010.10.036

van der Merwe, P., D. Lannuzel, A. R. Bowie & K. M. Meiners (2011b). High temporal resolution observations of spring fast ice melt and seawater iron enrichment in East Antarctica. *Journal of Geophysical Research,* 116(G3). https://doi.org/10.1029/2010jg001628

van der Merwe, P., D. Lannuzel, C. A. M. Nichols, K. Meiners, P. Heil, L. Norman et al. (2009). Biogeochemical observations during the winter–spring transition in East Antarctic sea ice: Evidence of iron and exopolysaccharide controls. *Marine Chemistry,* 115(3-4): 163-175. https://doi.org/10.1016/j.marchem.2009.08.001

van der Merwe, P., K. Wuttig, T. Holmes, T. W. Trull, Z. Chase, A. T. Townsend et al. (2019). High lability Fe particles sourced from glacial erosion can meet previously unaccounted biological demand: Heard Island, Southern Ocean. *Frontiers in Marine Science,* 6. https://doi.org/10.3389/fmars.2019.00332

Wadham, J. L., M. Tranter, M. Skidmore, A. J. Hodson, J. Priscu, W. B. Lyons et al. (2010). Biogeochemical weathering under ice: Size matters. *Global Biogeochemical Cycles,* 24(3): n/a-n/a. https://doi.org/10.1029/2009gb003688

Wuttig, K., A. T. Townsend, P. van der Merwe, M. Gault-Ringold, T. Holmes, C. Schallenberg et al. (2019). Critical evaluation of a seaFAST system for the analysis of trace metals in marine samples. *Talanta,* 197: 653-668. https://doi.org/10.1016/j.talanta.2019.01.047

Zhou, X., S. Li, K. Morris & M. O. Jeffries (2007). Albedo of summer snow on sea ice, Ross Sea, Antarctica. *Journal of Geophysical Research,* 112(D16). https://doi.org/10.1029/2006jd007907

CHAPTER 4. DISTRIBUTION OF TRACE METALS IN ANTARCTIC SEA ICE FROM THREE DIFFERENT LOCATIONS AND SEASONS: FERTILIZATION, LIMITATION AND TOXICITY

Abstract

Iron (Fe) has been shown to limit growth of marine phytoplankton in the Southern Ocean, regulating productivity and species composition. While Fe does not seem to limit productivity in Antarctic sea ice, little is known about the potential impact of other trace metals (TM) in controlling sea-ice algal growth. Here we report on the distribution of dissolved and particulate cadmium (Cd), manganese (Mn), cobalt (Co), nickel (Ni), copper (Cu) and zinc (Zn) concentrations in sea-ice cores collected during three Antarctic expeditions off East Antarctica spanning across the winter, spring and summer seasons. Results show bulk sea ice is generally enriched in particulate TM but shows similar dissolved TM concentrations relative to the underlying seawater. Our results point toward an environment controlled by a subtle balance between thermodynamics and biological processes, where TM do not appear to limit sea-ice algal growth. Contrary, high concentrations of dissolved Cu and Zn found in our sea ice samples raise concern on potential toxicity played by both elements if they are not appreciably chelated by natural ligands. Finally, Cu, Mn, Ni and Zn quotas of sea-ice assemblages (inferred by bulk particulate Me:P) were higher than values previously reported for pelagic diatoms. However, they were all consistently lower than the sea-ice Fe quotas calculated from the available literature, indicating a large accumulation of Fe relative to other TM in sea ice. We suggest a sea-ice algae generalized metal abundance ranking of Fe >>Zn ≈ Ni ≈ Cu ≈ Mn > Co ≈ Cd.

Key Points:

- Concentrations of dissolved trace metals in sea ice are unlikely to impose a direct limitation to sea-ice algae growth year around.
- High concentrations of dissolved Cu and Zn found in sea ice could be potentially toxic if not appreciably chelated by natural ligands.
- A larger accumulation of Fe relative to other trace metals suggests Fe remains an obligate cofactor of many essential metalloproteins in sea-ice algae.

4.1 Introduction

In the Southern Ocean (SO), the isolation from land masses and associated dust supply leads to low iron (Fe) in surface waters. As a consequence, marine phytoplankton are unable to fully utilize the available macronutrients (Boyd et al., 2007). This is because Fe is required in many metabolic pathways in phytoplankton cells, such as carbon fixation and respiration (Schulz et al., 2007). The widespread Fe limitation leads to low chlorophyll concentrations, making the SO the largest high nutrient low chlorophyll (HNLC) area in the world (de Baar et al., 2005; Martin, 1990). In this context, seasonal sea ice can store 1-2 orders of magnitude greater concentrations of Fe and chlorophyll *a* (Chl*a*) relative to seawater (see review Lannuzel et al., 2016b and references therein). In this highly biologically productive environment Fe does not seem to limit algal growth. However, little is known about the role of other trace metals (TMs) in controlling sea-ice algal productivity (Lannuzel et al., 2011). Trace metals such as zinc (Zn), cobalt (Co), copper (Cu) and manganese (Mn) can regulate productivity and species composition in pelagic systems because of large differences in metal requirements among species (Sunda, 2012).

Zinc is widely used in eukaryotic cells and plays an important role in carbon assimilation during photosynthesis (Lane & Morel, 2000). It is further involved in cell pH regulation, silicification, dephosphorylation of organic compounds as well as DNA and RNA replication (Koch & Trimborn, 2019). Despite its crucial biochemical role, a physiological Zn requirement has been shown to be replaced by either Co or Cd in several species of centric marine diatoms and *Phaeocystis antarctica* (Price & Morel, 1990; Saito & Goepfert, 2008; Sunda & Huntsman, 1995a). Cobalt is also an essential element for vitamin B12 production by bacteria and archaea, which phytoplankton depend on (Banerjee & Ragsdale, 2003). Vitamin B12 and Fe availability can simultaneously limit phytoplankton growth in coastal sea-ice edge communities during late austral summer (Bertrand et al., 2015). Manganese may be equally limiting in HNLC waters (Middag et al., 2013; Pausch et al., 2019). Manganese is required in the photosystem II and to neutralize reactive oxygen species (ROS) as part of the antioxidant enzyme superoxide-dismutase (SOD; Twining et al., 2004; Wolfe-Simon et al., 2005). Enhanced production of ROS by diatoms has been observed in Fe-limited environments, leading to increased oxidative stress and higher Mn to Fe ratios in particulate matter compared to Fe-replete waters (Peers & Price, 2004). Copper is used in both photosynthetic and respiratory electron transport chains (Twining & Baines, 2013). It is also present as SOD and plays a part in cellular Fe uptake (Maldonado et al., 2006). Whilst beneficial when found in trace concentrations, high

concentrations of free Cu and Zn ions can become toxic for some algae (Bruland, 1980; Sunda, 2012; Yang et al., 2019).

To date, the only established role of nickel (Ni) in eukaryotes is as a constituent of metalloenzyme urease, which is responsible for the breakdown of urea (Twining & Baines, 2013). However, a Ni-containing form of superoxide dismutase (Ni-SOD), similar to those found in prokaryotes, has been observed in some oceanic diatoms (Cuvelier et al., 2010). Nickel was also found to be associated to diatoms frustules, although the biological explanation for this association remains unknown (Twining et al., 2012). Trace metals are constituents of many other metalloproteins and therefore likely to be involved in other biological functions yet to be discovered. Regardless of their specific roles, microalgae cellular uptake and TM quota are determined by complex and sometimes competing mechanisms (Sunda, 2012). Physiological limitation by one metal can reduce the quotas of others, which can also be controlled by the substitution of one metal by another in some phytoplankton species, as observed for Zn, Co and Cd (Koch & Trimborn, 2019). These intricate relationships are further complicated by the different affinity TMs have with organic ligands. Ligands can control the concentration of TM hydrate ions (TM′), hence their bioavailability (Sunda, 2012).

During the last decades, advances in clean sampling and analytical techniques have increased the wealth of data used to investigate the biogeochemical cycling of TMs in seawater. However, TM data from Antarctic sea-ice environments remain scarce, in particular relative to the vast area that sea ice seasonally covers and the recognition of sea ice as an ocean fertilizer. Only a few studies have reported TMs, other than Fe, in Antarctic pack ice (Lannuzel et al., 2011) and fast ice (Grotti et al., 2001, 2005; Lannuzel et al., 2011; Noble et al., 2013), and are limited to spring-time observations. Lannuzel et al. (2011) showed sea ice was not enriched in dissolved TMs compared to Antarctic seawater in late winter/early spring. However, particulate TMs were one to two orders of magnitude higher relative to seawater collected below the ice (0 – 10 m; Lannuzel et al., 2011). In the Ross Sea, particulate Mn (PMn), Co (PCo) and Cu (PCu) concentrations and speciation patterns indicating TM incorporation into sea ice was driven by resuspension of sediments, followed by release during melting as the main process affecting their distribution in coastal waters (Frache et al., 2001; Grotti et al., 2001; 2005). On the other hand, Noble et al. (2013) found elevated particulate TM:Aluminium ratios in basal ice in comparison to the underlying sediments, suggesting that bioaccumulation is also an important source of PMn and PCo. In this work, we investigate and report the

distribution of dissolved and particulate Cd, Mn, Co, Ni, Cu and Zn obtained from three Antarctic sea-ice sampling campaigns conducted off East Antarctica between 2012 and 2017. Particulate Al (PAl) was also measured as a tracer of lithogenic input (Taylor & McLennan, 1985). Data were used to identify key drivers of the spatial and temporal distribution of TMs in sea ice and to answer our main question: can TMs other than Fe control algal productivity in sea ice?

4.2 Methods

4.2.1 Sampling sites

Sea-ice cores were collected off the East Antarctic coast during three field campaigns (Figure 4.1): the Sea Ice Physics and Ecosystem eXperiment-2 (SIPEX-2; conducted during the austral winter/spring 2012 transition; Meiners et al., 2016), the Davis time series (conducted in late spring 2015; Duprat et al., 2019), and AAV2 (carried-out in summer 2016/2017; Duprat et al., 2020). Ice cores for SIPEX-2 were collected at six different locations within first-year pack ice (64–65.1° S/116–121.1° E) between Sept 26th and Nov 10th, 2012. Ice cores for Davis were collected on six different dates (between Nov 16th and Dec 2nd, 2015) at a single site located approximately 2 km north of Davis Station (68.5° S /77.9° E) in an area of undeformed fast ice (maximum water depth of 20 m). Ice cores from AAV2 were collected at nine different sites (3 fast ice and 6 pack ice stations) between Wilkes Land and King George V Land, during the austral summer 2016/17 (63.2 – 67.2° S /110.5 – 147.7° E). Brine and seawater samples were also collected during the Davis and AAV2 sea-ice campaigns. Sampling sites were selected away and upwind from the study vessel (SIPEX-2 and AAV2) and research station (Davis). The sampling sites were off-limits to unauthorized personnel and any operations likely to contaminate TM and organic matter samples. Additional information about the sampling sites can be found in Duprat et al. (2019), Duprat et al. (2020) and Lannuzel et al. (2016a).

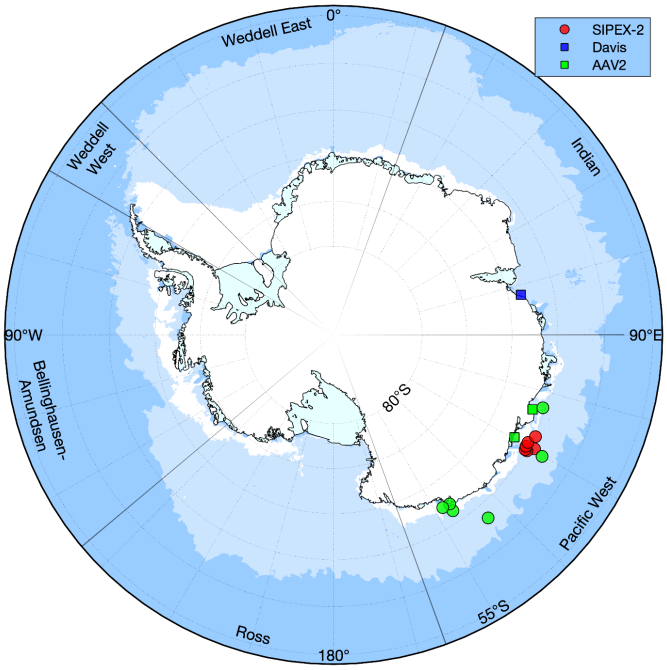

Figure 4.1 Map showing the locations of sea-ice cores sampled off the East Antarctic coast. Squares and circles represent fast ice and pack ice stations, respectively. Sea ice mean minimum (1st March) and maximum extent (30th September, ≥ 15% ice cover; Spreen et al., 2008) are represented by the white and light blue shades, respectively.

4.2.2 Cleaning and sampling procedures

Cleaning and sampling procedures were carried out following the protocols described in detail in Duprat et al. (2019), Duprat et al. (2020) and Lannuzel et al. (2016a). Plasticware was acid-cleaned according to GEOTRACES recommendations (Cutter et al., 2017). New Low-Density Polyethylene (LDPE) sampling bottles were immersed in 2% (v:v) Decon90 baths for one week. Bottles were then thoroughly rinsed with ultra-high purity water (UHP water, Barnstead), filled with 6 M hydrochloric acid (HCl, 50% v:v reagent grade, Merck) and left to soak in a 2 M (20% v:v reagent grade, Merck) HCl bath for a month. Next, bottles were rinsed with UHP water again and filled with 1 M distilled HCl (10% v:v instrument quality, Seastar) for a week on a hot plate (60 °C). Lastly, bottles were thoroughly rinsed (3-5 times) with UHP water in a class-100 laminar flow hood and stored triple bagged in plastic press seal bags until use.

In the field, researchers wore cleanroom garments (Tyvek overalls, overshoes and polyethylene gloves) over their warm clothing. Sampling and processing for TM analysis followed protocols described by Lannuzel et al. (2006) and van der Merwe et al. (2009). Snow was collected using

an acid-cleaned polyethylene (PE) hand shovel and stored in wide-mouth Nalgene® PE bottles. Ice cores were collected with an electric-powered, electropolished stainless steel corer (0.14 m internal diameter; Lichtert Industrie, Belgium). Previous work has demonstrated that the coring strategy is fit for trace metal work (Lannuzel et al., 2006; Lannuzel et al., 2011; van der Merwe et al., 2009). After coring, ice cores were immediately sectioned using a medical-grade bone saw (Richards Analytical) into six to seven discrete sections over the length of the core (10-15 cm from top, intermediate and bottom layers), and placed into individual acid cleaned polyethylene (PE) containers. After melting, snow and sea-ice samples were filtered for analysis of dissolved and particulate fractions (see paragraph 4.2.4.2). All plastic equipment (Teflon® filtration sets, plastic tubing, plastic scoops) used for sample collection and processing was rinsed with UHP water and immersed in an 10-20% (v:v;) HCl acid bath between samples (following recommendations for each material), and thoroughly rinsed again with UHP water before use. The saw, ice corer and shovel were thoroughly rinsed with UHP water after every sampling day, dried under a laminar flow bench and stored in triple plastic bags until next use. Brine and seawater were collected during the Davis and AAV2 studies only. Brine was collected by allowing it to drain and fill a sack hole (Miller et al., 2015), while seawater was collected just below the ice (SW0m), both using acid-clean C-flex tubing connected to a peristaltic pump. Samples were stored in acid-cleaned LDPE Nalgene® bottles, avoiding light exposure as much as possible until further processing.

4.2.3 Sample processing and analytical methods

4.2.3.1. Physical fractionation

Snow, seawater, brine and melted sea-ice sections were filtered under gentle vacuum (<0.13 bar) through 0.2 µm pore size polycarbonate (PC) membrane filters (Sterlitech, 47 mm diameter) using a Teflon® perfluoroalkoxy (PFA) filtration apparatus (Savillex, USA) to obtain the particulate (> 0.2 µm) and dissolved (< 0.2 µm) metal fractions. The dissolved fraction was collected in 125 ml LDPE bottles and acidified to pH 1.8 (~1% v:v of 12 M ultrapure HCl, Seastar Baseline, analytical grade) before triple-bagging and storage at room temperature until analysis. Polycarbonate filters retaining the particulate material were placed into acid-clean polystyrene Petri dishes, triple-bagged, and stored frozen (–20 °C) in the dark until further processing and analysis.

4.2.3.1.1 Dissolved TM analysis

Collected samples for Davis and AAV2 were concentrated 10×, 20× or 40× (depending on the expected analyte concentrations) using an automated off-line sample pre-concentration system (seaFAST-pico™, Elemental Scientific; Nobias Chelate-PA1 resin) according to the method described by Wuttig et al. (2019). The system was proven effective and reliable for the determination of the range of trace elements and salinities encountered in the samples reported here. The method's short- and long-term accuracy was verified through comprehensive testing using a variety of standard oceanographic reference samples over four years (2015 - 2018), as discussed in Wuttig et al. (2019). Dissolved TM concentrations were then determined using a Sector Field Inductively Coupled Plasma Mass Spectrometer (SF-ICP-MS, Element 2). SIPEX-2 samples were analysed direct using SF-ICP-MS without any offline preconcentration steps due to the higher concentration of dissolved metals expected in these early-season samples (Lannuzel et al., 2016a). Considering the SF-ICP-MS system, isotopes of interest were measured in both "low" and "medium" spectral resolution modes, as applicable. Cleaning procedures, calibrations and quality control of the SF-ICP-MS results followed those described in Duprat et al. (2019) and Wuttig et al. (2019). Daily instrument drift and performance were monitored using standard quality control samples. The average blank concentrations and calculated detection limits (3× the standard deviation of the acidified internal blank) for Cd, Co, Cu, Mn, Ni, and Zn are shown in Table 4.1. Final concentrations reported here are all blank corrected.

Table 4.1 SF-ICP-MS results for ultrapure 10% (v:v) HNO_3 rinse solution (SIPEX-2) and for Seafast MQ blank solutions (Davis and AAV2). The detection limit (DL) is three times the standard deviation (SD) of averaged rinses / blanks. Seafast pre-concentration factors (x) are also indicated.

		Cd (nM)	**Co (nM)**	**Cu (nM)**	**Mn (nM)**	**Ni (nM)**	**Zn (nM)**
10% HNO_3 rinse solution (SIPEX-2)							
Average	(n = 10)	0.020	0.143	0.189	0.073	0.204	0.425
SD		0.011	0.357	0.189	0.182	0.222	0.228
DL		0.033	0.534	0.579	0.563	0.648	0.666
Seafast MQ blank 10x (Davis)							
Average	(n = 9)	0.002	0.004	0.040	0.006	0.079	0.088
SD		0.001	0.002	0.012	0.006	0.045	0.054
DL		0.004	0.006	0.037	0.018	0.135	0.162

Seafast MQ blank 40x (Davis)							
Average	(n = 6)	<dl	<dl	0.008	0.001	0.017	0.017
SD		<dl	0.001	0.002	0.001	0.008	0.006
DL		0.001	0.002	0.006	0.003	0.023	0.018
Seafast MQ blank 20x (AAV2)							
Average	(n = 3)	<dl	0.003	0.009	0.001	0.163	0.047
SD		<dl	0.001	0.005	0.001	0.031	0.032
DL		<dl	0.004	0.014	0.002	0.093	0.097
Seafast MQ blank 40x (AAV2)							
Average	(n = 5)	0.001	0.082	0.127	0.001	0.010	0.001
SD		<dl	0.013	0.037	<dl	0.007	<dl
DL		0.001	0.039	0.111	0.001	0.020	0.001

As described in section 4.2.3.1, the method used to solubilize metal-associated colloidal matter and metal-organic complexes to the free inorganic form (before the determination of total dissolved metal using the cation exchange resin) was done through sample acidification. Nonetheless, it should be noted that systematic assessments (Milne et al., 2010; Saito & Moffett, 2002; Shelley et al., 2010; Vega & van den Berg, 1997; Wuttig et al., 2019) suggest that a partial amount of Co (and to a lesser extent Cu) remains very strongly bound to either dissolved or colloidal organic matter and can resist the acid-induced solubilization. Therefore, concentrations reported here for “dissolved Cu” and particularly “dissolved Co” should better reflect the “labile fraction”, rather than the “total dissolved fraction”. The absence of any further sample processing to ensure a complete metal-organic complexes dissociation (such as the use of an additional pre-treatment UV irradiation step) could therefore underestimate the total dissolved fraction concentration (15 - 50% for Co; Milne et al., 2010; Rapp et al., 2017; Wuttig et al., 2019). However, this effect is also expected to be minimized in our samples due to the commonly lower concentrations of this element in surface waters compared to deep waters (Milne et al., 2010).

Finally, following Gradinger & Ikävalko (1998) TM data were normalized to sea-ice bulk salinity and compared to sea water concentrations using an enrichment index (EI) approach, calculated as:

$$EI = ([TM]_{ice} / [Sal]_{ice}) \times ([Sal]_{sw} / [TM]_{sw}) \quad \text{Eqn 1}$$

where $[Sal]_{sw}$ and $[Sal]_{ice}$ are the salinity of the underlying seawater and the bulk salinity of the ice respectively, whilst $[TM]_{ice}$ is the concentration of the dissolved metal in the ice and $[TM]_{sw}$ is the concentration of the dissolved metal in the underlying seawater. Values of 1, < 1 or > 1 will correspond to conservative, depleted or enriched as compared to bulk salinity, respectively.

4.2.3.1.2 Particulate TM

A strong acid treatment was applied to the filters to ensure the complete digestion of most refractory particles (Bowie et al., 2010). First, a mixture of acids (750 µL of 12 M HCl, 250 µL of 16 M HNO_3, and 250 µL of 29 M HF, all ultrapure Seastar Baseline®, Choice Analytical) was added to each sample and blank filter and placed into a Teflon® PFA (perfluoroalkoxy) vial (Savillex, USA). Vials were capped and heated at 120 °C for 12 h over a Teflon® coated hotplate (SCP Science) under a class-100 fume hood, followed by dry evaporation of the acids in opened vials at 120 °C overnight. The dry residues were then re-suspended in 9.9 mL ultrapure 10% (v:v) HNO_3 (Seastar Baseline®) and spiked with 100 µL Indium commercial solution (final concentration 87.1 nM) as an internal standard. Finally, an aliquot of 5 mL was transferred to acid-cleaned polypropylene tubes for metal quantification using SF-ICP-MS following procedures outlined in section 4.2.4.2.1. The detection limit (DL) for each metal was calculated as 3× the standard deviation of the digested acid filter blank (Table 4.2). Particulate inventories (µmol.m^{-2}) for each TM were determined by multiplying the concentration of each ice core section (assuming seawater density ≅ 1 g/cm^3) with the section thickness and summing them. For this purpose, linear interpolations were applied to core sections where concentrations were not measured.

Table 4.2 SF-ICP-MS results (in nM) for acid digested filter blanks (0.25 ml HNO_3 + 0.25 ml HF + 0.75 ml HCl). The detection limit (DL) is 3 times the standard deviation of the procedural blank.

	Al (nM)	**Cd (nM)**	**Co (nM)**	**Cu (nM)**	**Mn (nM)**	**Ni (nM)**	**Zn (nM)**
Digested filter blanks (SIPEX-2)							
Average	1.382	0.001	0.003	0.03	0.013	0.058	1.097

SD	0.606	0.001	0.001	0.01	0.002	0.020	0.476
DL	1.818	0.002	0.003	0.03	0.006	0.059	1.427
*Digested filter blanks (Davis and AAV2)**							
Average	0.963	<dl	0.001	0.011	0.004	0.016	0.700
SD	0.238	<dl	<dl	0.005	0.001	0.003	0.457
DL	0.713	<dl	0.001	0.014	0.003	0.008	1.370

*Samples for Davis and AAV2 were processed and analysed together.

4.2.3.2 Physico-chemical and biological parameters

Standard physico-chemical and biological parameters such as sea-ice and snow thicknesses, *in situ* ice temperatures, salinities, chlorophyll-*a* (Chla), macronutrient (nitrate (NO_3^-), nitrite (NO_2^-), phosphate (PO_4^{3-}), silicic acid ($Si(OH)_4$) and ammonium (NH_4^+)) and particulate organic carbon and nitrogen (POC and PON) concentrations were also determined in each sample, following the methods described in Duprat et al. (2020).

4.2.4 Statistical Analysis

Non-parametric Kruskall-Wallis and Mann-Whitney tests were performed in three groups (SIPEX-2, Davis and AAV2) to test for temporal variability. For this purpose, ice section values within each group were treated as independent. The Mann-Whitney test was also used to verify differences between particulate TM:Al ratios from pack and fast ice and TM quotas from late winter/spring and summer ice. Finally, a one sample t-test (assuming unequal variance) was used to check if our quotas differ from the literature mean. A generalized mixed model (gamma distribution) was used to test the spatial (two groups: fast ice and pack ice) variation considering the dependence between measurements at different depths in the same core. This choice was based on the different vertical distributions of TMs observed in pack ice and fast ice. The Spearman correlation coefficient test was used to investigate potential correlations between all physical and biogeochemical parameters due to the non-normality observed in most variables. All analyses were performed using the R programming language (version 3.3.1; R Core Team, 2013).

4.3 Results

4.3.1 Dissolved metal distribution

Summary statistics for salinity, macronutrients and Chl*a* are shown in Figure 4.2. Median and range concentrations in snow (n = 14), pack ice (n = 74), fast ice (n = 38), brine (n = 10) and seawater (n = 14) are summarized in Table 4.3. The dissolved fraction contributed 92% (Cd), 24% (Co), 75% (Cu), 77% (Mn), 85% (Ni) and 82% (Zn) to the total (dissolved + particulate) TM pools, respectively. The notable lover dissolved-to-total ratio observed for Co could have resulted from a potential underestimation of the total dissolved Co, as considered in the method section 4.2.3.1.1. Dissolved TM concentrations were enriched relative to sea water below (Tables 4.4). Dissolved TM concentrations in snow were low compared to sea ice and seawater (Table 4.3). Higher DMn and DCo ($p < 0.01$) and lower DNi and DZn ($p < 0.05$) were found in fast ice compared to pack ice, albeit concentrations for both types of ice were within the same order of magnitude. Vertical profiles of dissolved TM resemble an L-shaped vertical distribution for fast ice, with no clear pattern for pack ice (Figure 4.3).

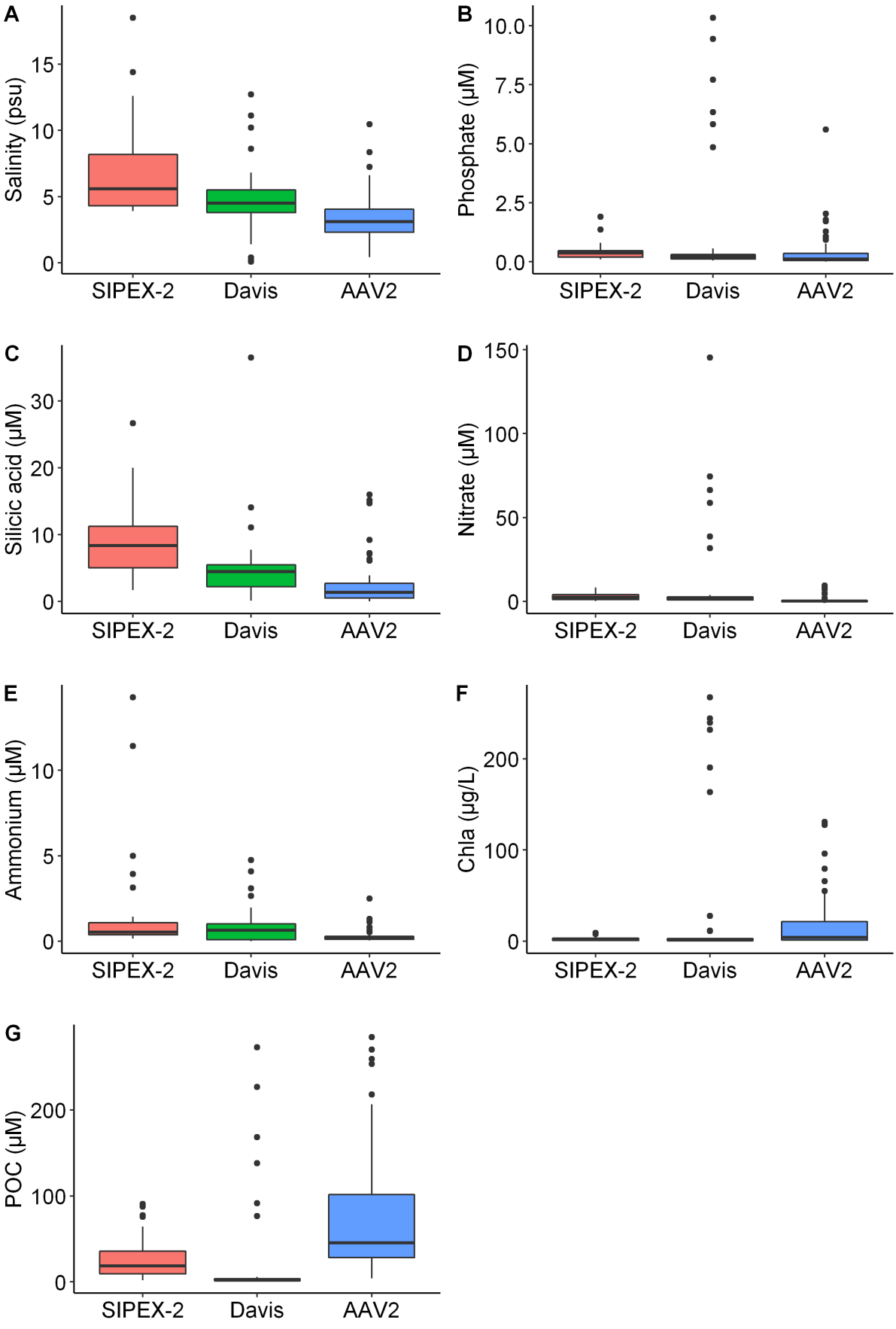
A
Salinity (psu)
0
5
10
15
SIPEX-2
Davis
AAV2
B
Phosphate (µM)
0.0
2.5
5.0
7.5
10.0
SIPEX-2
Davis
AAV2
C
Silicic acid (µM)
0
10
20
30
SIPEX-2
Davis
AAV2
D
Nitrate (µM)
0
50
100
150
SIPEX-2
Davis
AAV2
E
Ammonium (µM)
0
5
10
SIPEX-2
Davis
AAV2
F
Chla (µg/L)
0
100
200
SIPEX-2
Davis
AAV2
G
POC (µM)
0
100
200
SIPEX-2
Davis
AAV2

Figure 4.2 Summary statistics for salinity (A), phosphate (B), silicic acid (C), nitrate (D), ammonium (E), chlorophyll *a* (F) and POC (G) for the three sampling campaigns obtained from bulk sea ice. SIPEX-2 samples were collected in winter/early spring, Davis in late spring and AAV2 in summer. The box represents the inter-quartile range where 50% of the values lies. The median is shown by the line that divides the box into two parts. The upper and lower whiskers show values outside the middle 50% with limits representing the maximum and minimum values without outliers

Table 4.3 Median and range of dissolved (<0.2 μm) TMs for snow, pack ice, fast ice, brine and seawater collected below ice (nM) in East Antarctica. Median values for each expedition (season) are also reported.

Dissolved (<0.2 μm)	**Cd (nM)**	**Co (nM)**	**Cu (nM)**	**Mn (nM)**	**Ni (nM)**	**Zn (nM)**
snow						
Median	0.01	0.04	0.37	0.35	0.15	4.13
range	<0.01 – 0.05	0.01 – 0.53	0.07 – 2.77	0.08 – 31.0	0.04 – 1.65	1.66 – 15.2
winter/spring sea ice (SIPEX-2)						
Median	0.47	<dl	5.55	1.46	12.4	63.7
range	0.18 – 1.57		0.32 – 26.5	0.47 – 8.70	2.31 – 533	14.1 – 543
late spring sea ice (Davis)						
Median	0.23	0.06	1.65	1.70	1.70	40.2
range	0.07 – 3.72	0.02 – 0.29	0.68 –19.5	0.58 – 23.1	0.43 – 17.3	13.6 – 97.6
summer sea ice (AAV2)						
Median	0.16	0.03	3.05	1.23	4.29	18.0
range	0.01 – 2.61	0.01 – 0.42	0.72 –18.7	0.31 – 13.4	1.33 – 119	2.34 – 79.0
pack ice						
Median	0.37	0.03	3.49	1.40	6.24	34.4
range	0.04 – 2.61	0.01 – 0.16	0.32 –19.7	0.47 – 13.4	0.46 – (533)	2.34 – 543
fast ice						
Median	0.21	0.05	1.94	1.58	1.96	33.5
range	0.04 – 3.72	0.01 – 0.42	0.66 – 19.5	0.31 – 30.0	0.43 – 119	2.94 – 98.6
brine						
Median	0.73	0.11	3.26	1.42	14.9	7.92
range	0.05 – 1.91	0.01 – 2.89	1.07 – 18.8	0.64 – 4.49	11.1 – 17.9	1.56 – 65.7
seawater (SW0m)						
Median	0.28	0.06	2.01	2.22	6.25	12.0
range	0.23 – 2.06	0.02 – 0.20	1.34 – 4.95	0.74 – 13.0	3.13 – 7.12	3.78 – 40.0

Antarctic seawater (south of the Polar Front)						
Weddell/Scotia confluence (0–100 m) [a]	0.29 – 0.76		1.64 – 10.2			
Weddell Sea (0–100 m) [b]	0.46 – 0.71	0.01 – 0.05	1.65 – 3.35	0.15 – 1.24	4.75 – 7.24	1.82 – 9.62
Atlantic sector (40–100 m) [c]	0.15 – 0.90					
Atlantic sector (40–100 m) [d]			0.95 – 6.66		3.70 – 6.90	1.70 – 10.8
Atlantic sector (0–300m) e	0.17 – 0.95		1.53 – 6.44		3.07 – 10.4	1.38 – 14.0
Atlantic sector (0–100 m) [f]		<0.01 – 0.12				
Atlantic sector (0–100m) [g]	~0.60 – 0.80		~1.00 – 1.60	~0.30 – 0.60		
Ross Sea (0–375 m) [h]	0.04 – 0.73	<0.01 – 0.04	1.23 – 2.16		4.78 – 6.88	0.24 – 5.17
Ross Sea (0–380 m) [i]	0.08 – 0.99		0.90 – 3.75			
Ross Sea (0–380 m) [j]			0.50 – 11.6	0.01 – 6.60		
Ross Sea (0–100 m) [k]	0.34 – 0.86		0.43 – 3.30	0.33 – 1.20		2.20 – 8.20
Ross Sea (0–100 m) [l]						0.28 – 5.58
Australian sector (0–100 m) [m]				~ 0.1		
Australian sector (0–100 m) [n]			1.04 – 2.96		2.20 – 7.90	
Australian sector (40 m), SOIREE [o] **	0.25 – 0.27		1.20 – 1.40		6.20 – 6.30	2.30 – 2.4

Pacific sector (0–100 m) [p]	~0.20 – 0.40	~ 0.02 – 0.04	~ 0.80– 1.00	~ 4.00 – 5.00	~ 0.30 – 0.70
Pacific and Indian sector (0-100 m) [q]	~0.20 – 0.70		~1.00 – 2.00	~5.50 – 6.50	~1.00 – 4.00

* Concentration of dissolved Co below detection limit for SIPEX-2.
**Concentrations measured outside the SOIREE patch.
a) Nolting et al., 1991
b) Westerlund & Ohman, 1991a, 1991b
c) Loscher et al., 1998
d) Löscher, 1999
e) Nolting & de Baar, 1994
f) Ellwood et al., 2005
g) Boye et al., 2012
h) Fitzwater et al., 2000
i) Frache et al., 2001
j) Grotti et al., 2001
k) Corami et al., 2005
l) Coale et al., 2005
m) Sedwick et al., 1997
n) Lai et al., 2008
o) Frew et al., 2001
p) Elwood, 2008
q) Janssen et al. 2020

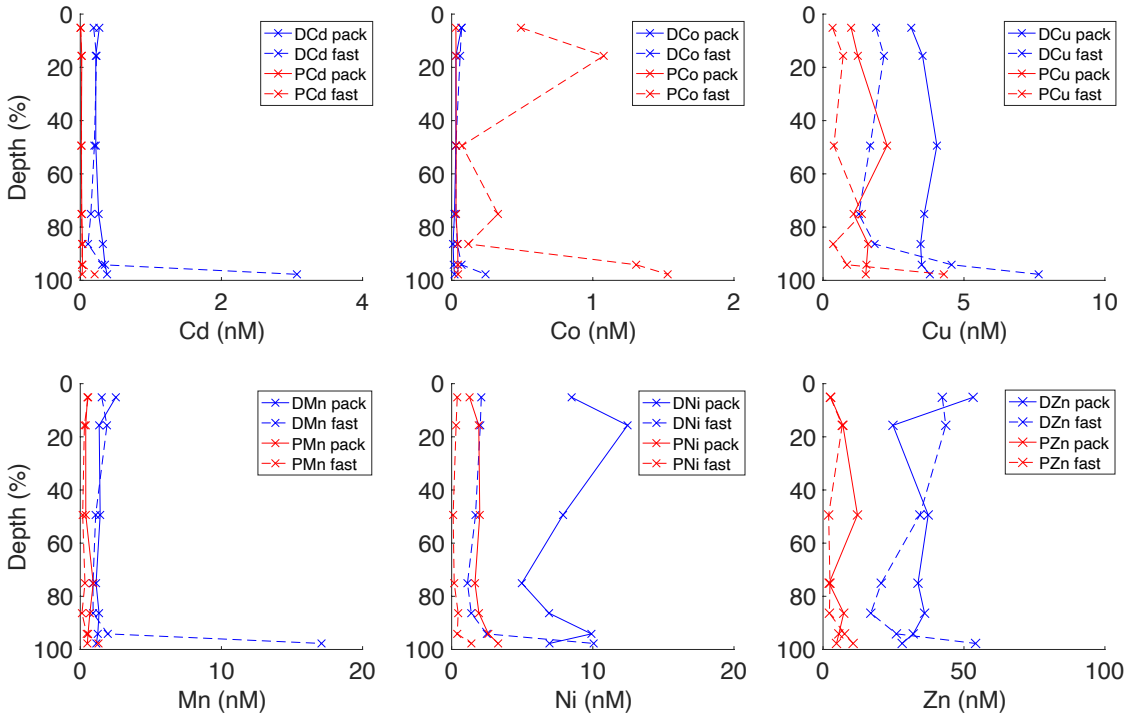

Figure 4.3 Vertical profile of dissolved and particulate TMs composed from the median concentration throughout sections of all pack and fast ice stations sampled in SIPEX-2, Davis and AAV2.

A significant decrease ($p < 0.01$) in the dissolved concentrations of Cd, Ni, Cu and Zn in summer (AAV2) compared to winter/spring (SIPEX-2; Figure 4.4; Table 4.3) sea ice was observed. No clear temporal trends were observed in the overall dissolved fractions (dissolved / total; Figure 4.5). Finally, the absence of correlations between dissolved TM concentrations and salinity supports their non-conservative distribution relative to salts (Figure 4.6). No correlations were observed between dissolved TMs and Chl*a* or POC. Moderate correlations were observed between DMn and DCo (0.69; $p < 0.01$) and between DCo and DNi (0.76; $p < 0.01$). DCd was the only element which correlated with macronutrient concentrations: PO_4^{3-} (0.88; $p < 0.01$), NO_3^- (0.62 $p < 0.01$) and $Si(OH)_4$ (0.67; $p < 0.01$).

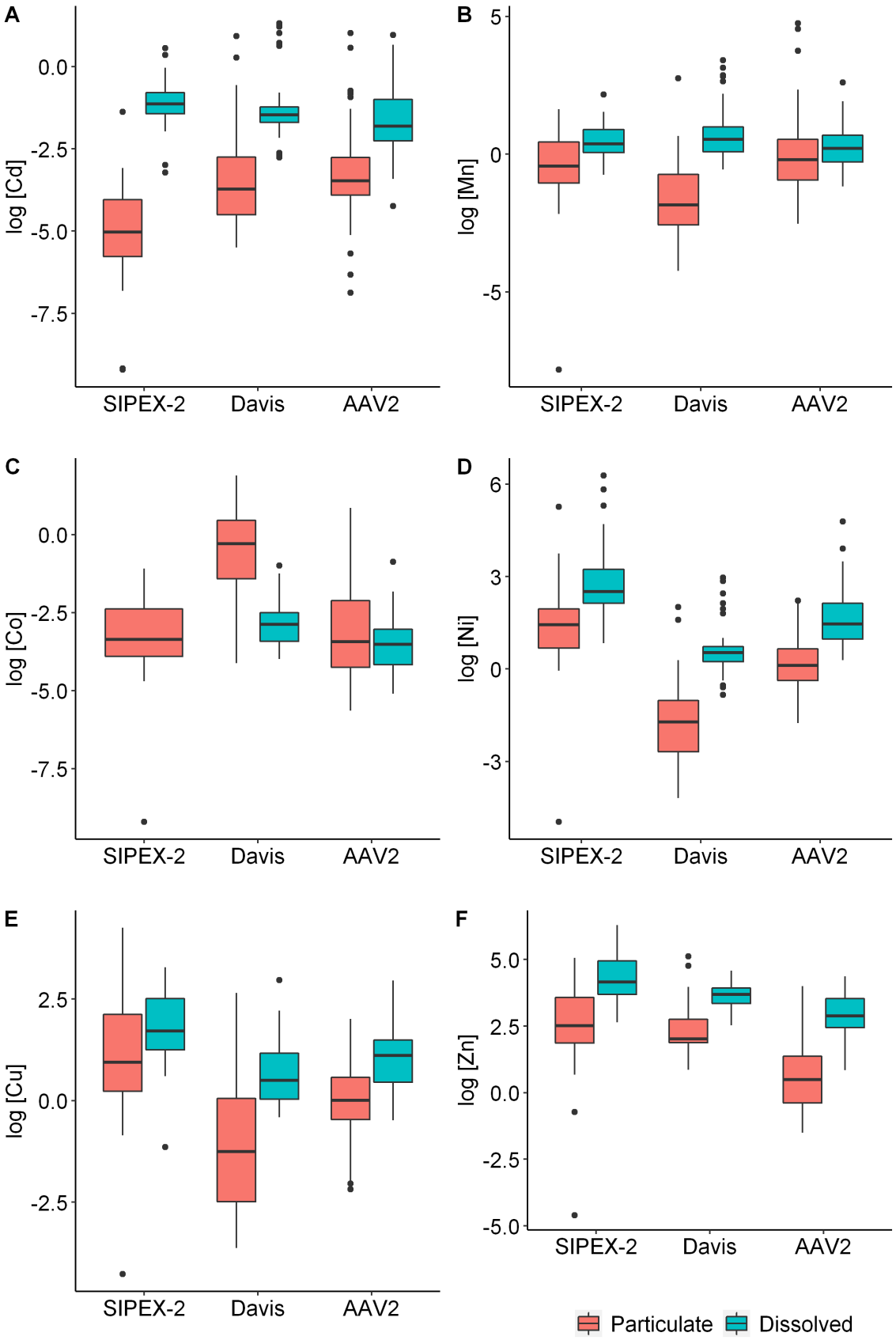
A
log [Cd]
0.0
-2.5
-5.0
-7.5
SIPEX-2
Davis
AAV2
B
log [Mn]
5
0
-5
SIPEX-2
Davis
AAV2
C
log [Co]
0.0
-2.5
-5.0
-7.5
SIPEX-2
Davis
AAV2
D
log [Ni]
6
3
0
-3
SIPEX-2
Davis
AAV2
E
log [Cu]
2.5
0.0
-2.5
SIPEX-2
Davis
AAV2
F
log [Zn]
5.0
2.5
0.0
-2.5
-5.0
SIPEX-2
Davis
AAV2
Particulate
Dissolved

Figure 4.4 Summary statistics of dissolved and particulate bioactive metals for the three sampling campaigns obtained from bulk sea ice. SIPEX-2 samples were collected in winter/early spring, Davis in late spring and AAV2 in summer. The box represents the inter-quartile range where 50% of the (log transformed) values lies. The median is shown by the line that divides the box into two parts. The upper and lower whiskers show values outside the middle 50% with limits representing the maximum and minimum values without outliers. Concentration of dissolved Co was below detection limit for SIPEX-2 and is not shown.

Table 4.4 Median Enrichment Index (EI) for pack and fast ice. EI values indicate the degree to which the concentration of the dissolved TM has increased in sea ice compared to underlying seawater relative to the salinity of each fraction (Eqn. 1).

EI	**Cd (nM)**	**Co (nM)**	**Cu (nM)**	**Mn (nM)**	**Ni (nM)**	**Zn (nM)**
all sea ice	3.3	4.8	12	3.4	7.0	17
pack ice	3.5	3.7	13	3.4	9.1	18
winter pack ice*	3.1	-	15	3.2	13	23
summer pack ice	3.9	3.7	12	4.1	6.8	11
fast ice	6.1	4.8	9.2	16	3.2	30

* Concentration of dissolved Co below detection limit for SIPEX-2.

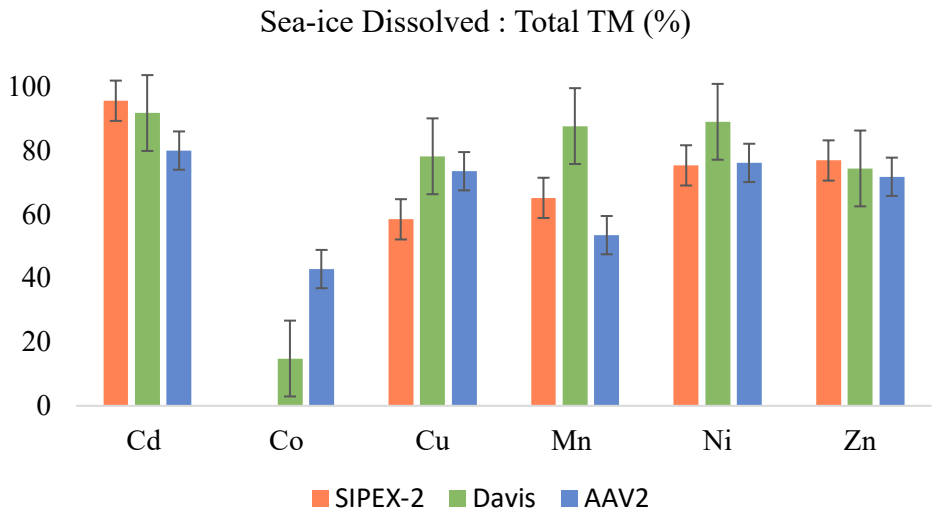

Figure 4.5 Percentage contribution (with standard error) of dissolved to total (dissolved + particulate) TMs in sea ice during SIPEX-2 (winter/spring transition), Davis (late spring) and AAV2 (summer) campaigns. Concentration of dissolved Co was below detection limit for SIPEX-2 and is not shown.

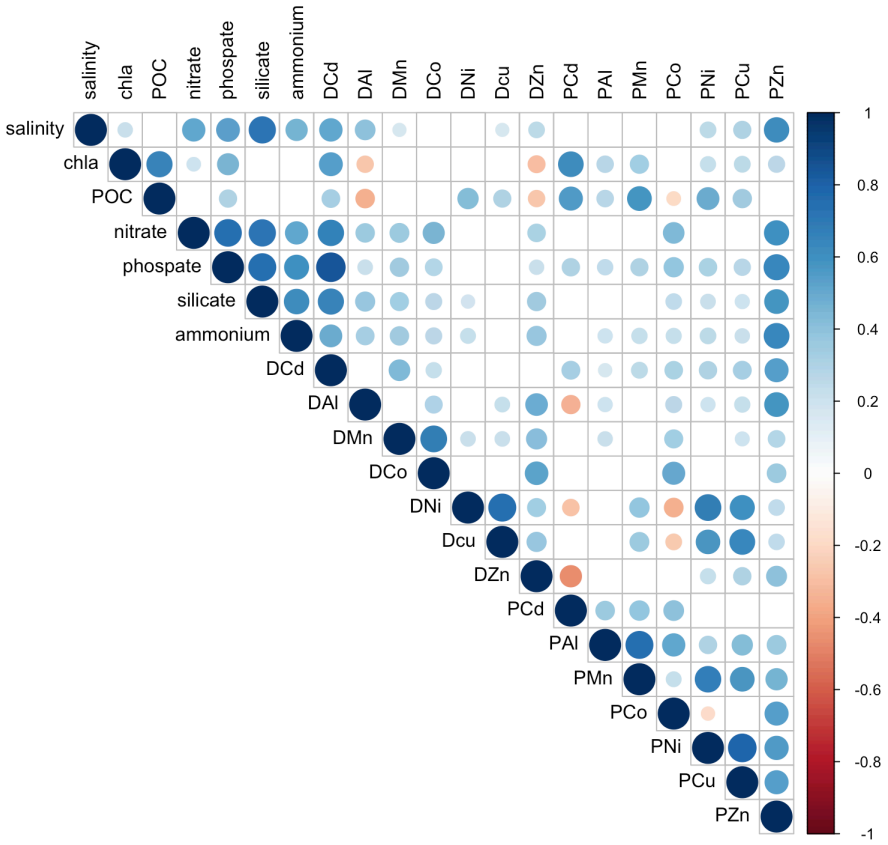

Figure 4.6 Spearman's Rank correlations between sea-ice salinity, dissolved and particulate TM, macronutrients, Chla and POC concentrations.

4.3.2 Particulate metals distribution

Median and range concentrations in snow (n = 14), pack ice (n = 68), fast ice (n = 38), brine (n = 10) and seawater (n = 14) are summarized in Table 4.5. With the exception of Cd, concentrations of particulate TMs were all higher in sea ice compared to seawater (Table 4.5). Sack-hole brine concentrations of particulate TMs were in general lower than bulk sea ice whereas snow concentrations were comparable to seawater (Table 4.5). In fast ice, particulate TMs displayed an L-shaped distribution with basal ice concentrations generally greater than pack ice (Figure 4.3). Significantly higher concentrations of PAl, PMn and PCo were found in fast ice ($p < 0.01$) compared to pack ice, while PCu and PNi concentrations were higher in pack ice than fast ice ($p < 0.01$). The particulate TM:Al ratio was used to fingerprint the lithogenic contribution to the total particulate pool, with Al used here as the normalising lithogenic element (Taylor & McLennan, 1985). Ratios of PCd, PMn, PNi and PCu relative to PAl in fast ice were an order of magnitude higher than in pack ice ($p < 0.01$; Table 4.5). Finally, there is evidence of a decrease of PCu, PNi and PZn in summer sea ice (AAV2) compared to

winter/spring sea ice (SIPEX-2; $p < 0.01$; Figure 4.4). Positive correlations between PMn and PAl (0.75; $p < 0.75$) and between PCu and PNi (0.79; $p < 0.01$; Figure 4.6) were found. Only PCu and PNi showed a moderate correlation (0.64 and 0.68 respectively; $p < 0.01$) with their corresponding dissolved form. Chl*a* was only correlated to PCd (0.63; $p < 0.01$).

Table 4.5 Median and range of particulate (>0.2 μm) TM for snow, pack ice, fast ice, brine and under ice seawater (nM) in East Antarctica. Median particulate TM:Al ratio (nM:nM) for pack and fast ice and median values for each expedition (season) are also reported.

Particulate (>0.2 μm)	Cd (nM)	Co (nM)	Cu (nM)	Mn (nM)	Ni (nM)	Zn (nM)
snow						
Median	<0.01	0.02	0.09	0.73	0.07	1.40
range	<0.01 – 0.01	<0.01 – 1.27	0.03 – 11.5	0.09 – 66.6	0.01 – 11.2	0.17 – 16.0
winter/spring sea ice (SIPEX-2)						
Median	0.01	0.04	2.60	0.65	4.22	12.4
range	<0.01 – 0.25	<dl – 0.23	0.01 – 70.4	<0.01 – 5.11	0.01 –195	0.01 –158
late spring sea ice (Davis)						
Median	0.02	0.75	0.29	0.16	0.18	7.54
range	<0.01 – 2.53	0.02 – 6.62	0.03 – 14.2	0.01 – 15.6	0.02 – 7.46	2.37 – 168
summer sea ice (AAV2)						
Median	0.03	0.03	1.01	0.82	1.12	1.85
range	<0.01 – 2.77	<0.01 – 2.36	0.11 – 4.48	0.08 – 113	0.17 – 8.48	1.28 – 73.4
pack ice						
Median	0.02	0.03	1.34	0.60	1.90	8.69
range	<0.01 – 1.78	<0.01 – 2.35	0.01 – 70.4	<0.01 – 10.4	<0.01 – 195	0.01 – 158
TM:Al	0.0012	0.001	0.071	0.014	0.064	0.409
fast ice						
Median	0.02	0.46	0.83	0.39	0.33	7.21
range	<0.01 – 2.77	0.01 – 6.62	0.03 – 14.1	0.01 – 115	0.02 – 9.25	0.29 – 168
TM:Al	0.0003	0.009	0.007	0.004	0.006	0.026
brine						
Median	0.02	0.01	0.47	0.21	0.22	2.69
range	0.02 – 0.20	<0.01 – 0.01	0.07 – 1.50	0.05 – 4.49	0.04 – 5.17	0.50 – 7.72
seawater						
Median	0.05	0.01	0.09	0.25	0.22	0.79

range	0.01 – 0.18	<0.01 – 6.91	0.03 – 1.63	0.06 – 2.07	0.03 – 1.88	0.47 – 33.6

4.3.3 TMetal:P ratios in Antarctic pack ice

Trace metal cellular quotas were inferred from analyses of bulk particles in sea ice. For this purpose, fast ice stations were excluded due to the expected overwhelming lithogenic contribution originating from nearby continental sources, as suggested from biogenic versus lithogenic contributions found in Fe particles (Lannuzel et al., 2014; Duprat et al., 2020). Particulate TM:P (Phosphorus-normalized following the Redfield C:P ratio 106:1; Redfield, 1963) were higher in winter/spring (SIPEX-2) compared to summer (AAV2) and to values previously reported for natural assemblages of marine diatoms in Fe-rich conditions for Cu, Mn, Ni and Zn ($p < 0.01$; Table 4.6). We also show the particulate Fe:P ratios obtained from published Fe data of the respective voyages studied here (Duprat et al., 2019, 2020; Lannuzel et al., 2016a) in an attempt to understand how the uptake of Fe compares to other TMs. Sea-ice particulate Fe:P ratios are two orders of magnitude higher than the maximum Fe:P of 1.9 mmol:mol obtained for marine phytoplankton using synchrotron-based X-ray fluorescence SXRF in a SO Fe-enrichment experiment (Twining et al., 2004). Assuming that the vast majority of our pack ice particulate pool is of biogenic nature (Duprat et al, 2020; Lannuzel et al., 2014), these results point towards a sea-ice generalized metal abundance ranking of Fe >>Zn ≈ Ni ≈ Cu ≈ Mn > Co ≈ Cd.

Table 4.6 Median particulate TM:P for pack ice stations. Fe:P was calculated from published Fe results obtained during the respective voyages (Duprat et al., 2019, 2020, Lannuzel et al., 2016a). For comparison, bulk particulate TM:P in Fe-limited (Cullen et al., 2003) and replete conditions (Cullen et al., 2003; Collier & Edmond 1984) are also reported.

TM:P (mmol:mol)	**Cd**	**Co**	**Cu**	**Fe**	**Mn**	**Ni**	**Zn**
all pack ice	0.06	0.19	3.6	140	2.2	6.1	61
winter/early spring pack ice (SIPEX-2)	0.05	0.26	17	540	4.6	17	91
summer pack ice (AAV2)	0.07	0.10	1.2	73	1.5	1.7	28
Southern Ocean diatoms							

*Fe limited (<0.1 nM)**	1.29	0.15	1.44	-	1.7	-	11.1
*Fe replete (>0.5 nM)**	0.36 – 0.41	0.02 – 0.10	0.45 – 0.60	-	0.53 – 0.70	-	2.14 – 2.91
*Antarctic upwelling waters***	0.07	-	2.0	-	-	0.68	13.3

* bulk particulate values from shipboard Fe-enrichment incubation experiment in the Antarctic Zone of the Pacific sector of the Southern Ocea (Cullen et al., 2003)
** bulk particulate values from Antarctic upwelling waters (station M) with high dissolved TM concentrations (Collier & Edmond,1984)

4.4 Discussion

4.4.1 Drivers of dissolved metal distribution

In this study, median dissolved metal concentrations in bulk sea-ice samples were of the same order of magnitude as the seawater below (SW0m). Values were generally in the upper range of concentrations measured in ice-free Antarctic surface (0-100m) waters using rosette sampling methods (Table 4.3). The only exception is DZn, for which concentrations in our study were three times greater than the highest concentration reported for SO surface waters (~12 nM; Nolting & de Baar, 1994). Based on these results and in agreement with previous findings (Lannuzel et al., 2011), sea-ice melt should not represent a major source of the elements analysed here to surface waters when it melts, except maybe for a DZn signal (Neff, 2002). Other mechanisms such as advection of seawater masses which have interacted with the shelf are likely to have a greater impact than sea ice on their distribution in surface waters.

The three campaigns showed comparable concentration ranges of dissolved TM (Table 4.3). This observation suggests low spatio-temporal variability in dissolved TM concentrations in sea ice. However, subtle differences emerge when fast ice and pack ice are compared. For example, DMn and DCo concentrations were significantly higher in fast ice than pack ice ($p < 0.01$). Considering the shallow bathymetry on the Antarctic coast, sediments can represent a major source of metals to fast ice compared to pack ice. Benthic inputs of dissolved Fe, Co, and Mn have been observed in highly productive coastal waters (Tappin et al., 1995) and water column profiles of Mn were also found closely correlated with those of Co in pore waters

(Zhang et al, 2002). Results also show lower concentrations of DCd, DCu, DNi and DZn in summer (AAV2) compared to winter/spring sea ice (SIPEX-2; Figure 4.4), which could suggest an overall faster removal than replenishment over time. However, the absence of any substantial changes in the dissolved-to-total ratio between SIPEX-2 and AAV2 data (Figure 4.5) points toward a net concentration of dissolved bioactive trace elements determined by a subtle balance between rates of autotrophic and heterotrophic/mixotrophic activities.

Finally, all TMs analysed here were enriched in sea ice relative to seawater when thermodynamic processes are filtered by normalizing sea-ice TM concentrations to salinity (Table 4.4). We suggest that organic ligands, most likely exopolymeric substances (EPS), are responsible for this enrichment in sea ice as they can bind a wide range of metal cations due to their negatively charged surfaces (Janssens et al., 2018; van der Merwe et al., 2009). Their high uronic acid content (Decho & Gutierrez, 2017) provides EPS with the ability to chemically complex and adsorb metal species. The gel-like three-dimensional nature of EPS is especially prone to physically scavenge particles from the water column during frazil ice ascent (Decho & Gutierrez, 2017), and therefore suggested here as a prime pathway for organic matter and TM incorporation into newly formed sea ice. Several studies have assessed the binding potential of EPS on a range of metals at seawater ionic strength (Gutierrez et al., 2008, 2012; Hassler et al., 2011, 2017). These studies shared similar levels of uronic acids (~25%) in the EPS and predominantly, DZn, DFe and DCu as major associated metals (Hassler et al., 2011; Gutierrez et al., 2008, 2012; Nichols et al., 2005). In the present study, DZn and DCu showed the highest EI (23 and 15 respectively, in winter sea ice; Table 4.4), close to the EI of 24 observed for Fe in newly formed Antarctic sea ice (Janssen et al., 2016). On the other hand, DCo and DCd showed the lowest EI (4.8 and 3.3, respectively). Based on our EI results, TM enrichment in sea ice may not only be a function of their concentration in seawater, but also their affinity to bind with organic ligands present in seawater or produced *in situ* in sea ice (Aslam et al., 2012; Genovese et al., 2018).

4.4.2 Drivers of particulate metals distribution

Positive correlations for all particulate TMs with PAl (significant for Mn; Figure 4.6) suggest the influence of continental inputs such as ice-free land masses, sediments and icebergs (Hawking et al., 2018; Grotti et al., 2001; Noble et al., 2013; Smith et al., 2007) as important sources of lithogenic particles to sea ice. The lithogenic signature is indeed most pronounced

near the coast, as evidenced by the lower particulate TM:Al ratio in fast ice compared to the predominantly biogenic nature of particles present in pack ice (Table 4.5). The proximity to coastal sources is suggested as the likely driver of the significantly higher concentrations of PMn and PCo in fast ice compared to pack ice, as previously observed for Fe (Duprat at al., 2019; 2020; Lannuzel et al., 2016a). This coastal signature is however less clear for other metals. For example, concentrations of PCd and PZn were similar between fast ice and pack ice, and significantly lower PCu, PNi were observed in fast ice compared to pack ice stations. Lower PCu in fast ice than pack ice was also observed by Lannuzel et al. (2011), suggesting that the influence of biological processes on the Cu cycle is greater than the physically mediated coastal inputs. This behaviour could potentially apply to other elements which show a nutrient-type nature in oceanic waters (Cd, Ni, Zn), where their distribution is highly influenced by biological uptake at the surface and remineralization at depth (Bruland & Lohan, 2003). The correlations between PCu and PNi and between Cd and Chl*a* support this hypothesis.

Our data also reveal an interesting contrast between our fast ice particulate samples and those previously reported in the Ross Sea, where a sedimentary supply seems to dominate the sea-ice pool (de Jong et al., 2013). PMn concentrations in fast ice in the Ross Sea (Grotti et al., 2005; Noble et al., 2013) are substantially higher than those obtained from our East Antarctic fast ice. In modern marine sediments, Mn is present above its crustal abundance (Calvert & Pedersen, 1996) and its incorporation into sea ice over shallow bathymetry would contribute to the supply of authigenic Mn to sea-ice communities in the Ross Sea (see Section 4.4.4). On the other hand, particulate TM:Al values close to crustal ratios, and observed correlations with Al, indicate a highly lithogenic content in our fast ice samples. This observation could be explained by the high influence of dust (Davis; Duprat et al., 2019) and terrigenous input from glacial melt (AAV2; Duprat et al., 2020) in our fast ice samples. This difference clearly affects the availability of PMn in fast ice from these two areas, with a potential impact on their biological productivity and microbial composition (Grotti et al., 2005; Noble et al., 2013; Pausch et al. 2019).

The concentration of particulate metals in sea ice results from a balance between physical and biological processes. Initial load (frazil ice scavenging of suspended particles during sea-ice formation), replenishment (seawater percolation and/or meteoric deposition), and biological uptake can all contribute to the particulate pool. Temperature-driven brine drainage, ice ablation and sloughing-off processes of ice algae and EPS drive the loss (Meiners & Michel

2017). Brine-sample concentrations of particulate TMs were in general lower than bulk sea ice, potentially due to a preferential retention of this fraction in the brine channel network during sampling. However, the fact that significantly lower bulk particulate concentrations of PCu, PNi and PZn were found in summer (AAV2) compared to winter/spring (SIPEX-2; $p < 0.01$) sea ice suggests that losses generally overtake accumulation for the TMs analysed here (Figure 4.4). The lack of seasonal increase contrasts findings for Fe, where PFe continuously accumulates in sea ice between winter and summer, despite brine drainage and ice decay, to reach the highest concentrations in summer (average 294 nM; Duprat et al., 2020). This difference highlights the decoupling between the processes driving Fe and other TMs distributions.

Finally, one common trend among particulate Mn, Co, Ni, Cu and Zn is that they were up to an order of magnitude higher in bulk sea ice compared to the seawater below. An estimated 1.4 $\mu mol.m^{-2}$ PMn, 0.07 $\mu mol.m^{-2}$ PCo, 3.1 $\mu mol.m^{-2}$ PNi, 1.8 $\mu mol.m^{-2}$ PCu and 12.4 $\mu mol.m^{-2}$ PZn (median depth integrated for both winter/spring and summer pack sea ice) could be released from sea ice if all of the sea ice represented by our samples melts by the end of austral summer. Like Fe, Mn and Co concentrations in Southern Ocean can be extremely low due to limited atmospheric input (Middag et al., 2011). If bioavailable within surface waters, this addition could alleviate phytoplankton limitation, representing a coupled Fe-Mn-Co fertilization mechanism supplied by sea ice melt.

4.4.3 Sea-ice algae stoichiometry in a trace metal rich environment

Pelagic phytoplankton generally require metals as follows Fe ≈ Zn > Mn ≈ Ni ≈ Cu > Co ≈ Cd, from most to least needed (Twining & Beines, 2013). Sea ice imposes a unique regime, with steep gradients in light, salinity, temperature and nutrients compared to seawater. One could therefore expect different nutritional requirements between sea-ice and pelagic algae, as suggested in the case of $SiOH_4$ for diatoms (Lim et al., 2019). Based on calculated P-normalized particulate TM and considering autotrophic cells make up the vast majority of sea-ice biomass during the sunlit seasons (Archer et. al., 1996), we present a generalized TM cellular quota stoichiometry for sea-ice algae: Fe >> Zn > Ni ≈ Cu ≈ Mn > Co ≈ Cd. Except for Cd, our results from pack ice suggest an overall higher sea-ice TM stoichiometry compared to seawater (Table 4.6). However, this trend was only significant ($p< 0.01$; one sample t-test)

for the winter/spring dataset. Non-metabolic incorporation of TM following adsorption isotherm relative to their ambient free ion concentration and in excess of nutritional requirement has been reported before (Miao et al., 2005). It is plausible that sea-ice algae could accumulate metals during early spring in advance of favourable conditions later in the season or in response to stimulation of the cell metabolism as conditions improve (Baines et al., 2011; Marchetti et al., 2012; Twining et al., 2004).

The relative TM abundance in sea-ice particles (Fe >> Zn > Ni ≈ Cu ≈ Mn > Co ≈ Cd) reflects, to a certain degree, the sequence in the dissolved fraction (Zn > Fe > Ni ≈ Cu ≈ Mn > Cd > Co). Thus, dissolved TM concentrations present in the sea ice could be seen as the primary factor controlling sea-ice algal cellular TM content. Regardless of this similarity in the sequence, a disproportionate enrichment of Fe relative to other elements is observed. Bioaccumulation of PFe (~110 nM; Duprat et al., 2020) is five-fold higher than PZn (~23 nM; this study). The sea-ice median particulate Fe:P of 140 mmol:mol is almost two orders of magnitude higher than values reported for temperate marine diatoms (Twining & Beines, 2013). Our results point towards either a storage mechanism or passive allocation of Fe into a range of sea-ice algal cellular functions. This behaviour of luxury uptake and storage amidst excessive availability of Fe has been previously seen in diatoms (Marchetti et al., 2006, 2009; Sunda & Huntsman, 1995b) and contrasts with the uniquely low Fe quota observed for marine phytoplankton isolated from the SO (Kustka et al., 2007; Strzepek et al., 2011). It is possible that sea-ice algae evolved to favour the use of Fe among the many metabolic functions where Fe can replace other metals (LaRoche et al., 1996; McKay et al., 1999). In doing so, the allocation of other essential TMs that are not as abundant as Fe in sea ice (such as Mn), but still essential to cellular growth, could be optimized.

Another interesting deviation from phytoplankton stoichiometry was the elevated Ni and Cu relative to Mn in winter/spring sea ice. In eukaryotes, urease is the only characterized Ni-dependent function (Mulrooney & Hausinger, 2003; Price & Morel, 1991). The overall six-fold higher Ni quotas found in sea ice compared to oceanic assemblages could reflect the extremely high fraction of (pennate) diatoms found in sea ice (van Leeuwe et al., 2018). Recent SXRF analyses showed Ni association with diatom opal frustules, bringing new evidences of its contribution to cellular quota (Twining et al., 2012). Sea-ice algae could also have developed alternative metabolic pathways allocating Cu, such as in the antioxidant enzyme superoxide dismutase enzyme, as well as other strategies to cope with the potentially toxic

levels of Cu′ (Peers & Price, 2006; Wolfe-Simon et al., 2005). A physiological adaptation amid high concentration of Cu′ would be particularly important because the high particulate Cu:P observed here suggest that a significant percentage of DCu in sea ice is not complexed to ligands. This assumption is made based on the fact that uptake of Cu is believed to be related to the concentration of its dissolved inorganic species (Cu′), whereas chelated Cu species are generally not directly available for uptake (Guo et al., 2010; Hudson, 1998; Sunda & Huntsman, 1998b).

The particulate Cd:P obtained for both the winter/spring and summer datasets were relatively low and comparable to marine plankton. This could be due to the high concentration of DZn observed in sea ice, which could potentially inhibit DCd uptake (Sunda & Huntsman, 2000). Past studies showed that DZn at concentrations found in coastal waters strongly suppress DCd uptake by diatoms (Sunda & Huntsman, 1998a) and that addition of Zn to incubations above background concentrations can suppress Cd uptake in productive waters, also decreasing phytoplankton Cd:P ratios compared to controls (Cullen & Sharrell, 2005). Therefore, our low particulate Cd:P ratio could result from the strong control exerted by DZn in the uptake of DCd by sea-ice algae.

4.4.4 Can metals regulate sea-ice productivity?

Trace metal availability has been shown to limit growth of marine phytoplankton, shaping the abundance and diversity of algal communities in a way that can influence both the carbon and nitrogen cycles (Sunda, 2012). Since Co, Cu, Mn, Zn, and circumstantially Cd, are co-factors of metalloenzymes that are essential for phytoplankton metabolism, it has been speculated that these elements could, along with Fe, control phytoplankton productivity in the Southern Ocean (Hassler et al., 2012). In the sea-ice realm, however, when bulk ice concentrations of TMs are normalized to the brine volume fraction (~12%; inferred from the bulk ice salinity and temperature; Cox and Weeks, 1983), approximately an order of magnitude higher levels of TMs relative to bulk ice concentrations reported here (Table 4.3) are found. This suggests concentrations experienced by micro-organisms within the brine channels are unlike to impose direct limitation to sea algae growth.

4.4.4.1 Zinc

In surface waters, Zn can exist as a soluble divalent cation, mostly complexed to organic ligands (Sunda, 2012). Addition of Zn was shown to stimulate algal growth when DFe is replete, particularly in the case of small diatoms and flagellates (Crawford et al., 2003; Coale, 1991; Franck et al., 2003; Oslo et al., 2000). Zinc is also known to be involved in the silicification of diatoms (De La Rocha et al. 2000; Jaccard et al., 2009; Ingall et al., 2013; Rueter & Morel 1981a, b). In marine phytoplankton, quantitative requirements for Zn are similar to those for Mn (Sunda, 2012). An enrichment of PZn relative to PMn (ratio 6.5) was previously observed for SO diatoms (Cullen et al., 2003) and is in alignment with our results in sea ice (PZn:PMn ratio = 4.7) where diatoms are expected to be the dominant taxonomic group (van Leeuwe et al., 2018). A continued production of biogenic silica during spring (Fipriat at al., 2017) could help explain the temporal reduction observed for sea-ice DZn via a coupled physiological mechanism connecting $SiOH_4$ and DZn uptake (Ellwood et al., 2008). However, concentrations of DZn in sea ice remained consistently high (~35 nM), well above the concentrations found to limit cultured diatom growth (0.44 – 1.51 nM; Koch, 2019). The abundance of DZn in sea ice potentially reflects the high levels of this element in the SO (>1 nM; Baars & Croot, 2011; Croot et al., 2011) as well as its high affinity to EPS (Gutierrez et al., 2012). Therefore, Zn is unlikely to limit sea-ice algae growth. Instead, sea-ice Zn concentrations raise the question on toxicity if it is not appreciably chelated (Miao et al., 2005). Zn toxicity can manifest in several ways, by affecting the assimilation of other bio-metals such as Cd, Co and Mn (Sunda & Huntsman, 1996).

4.4.4.2 Cobalt and Cadmium

Cadmium and Co uptake systems are downregulated at high Zn′ levels, and intracellular transport of both elements is repressed (Sunda, 2012). The high DZn concentrations found in sea ice could therefore explain the low particulate Cd:P and Co:P ratios observed in our study (Lane et al., 2008; Sunda & Huntsman, 2000). Still, mounting evidence suggests that Co and Zn can metabolically replace one another in the enzyme carbonic anhydrase in eukaryotic species (Lane & Morel, 2000; Price & Morel, 1990; Saito et al., 2008; Sunda & Huntsman, 1995a), potentially minimizing the effect of Co limitation. Nevertheless, Co could still indirectly influence growth and species composition in the ice by limiting bacterial vitamin B12 production (Panzeca et al., 2008). The Co-containing vitamin B12 together with Fe showed an enhancement in phytoplankton growth and changed community composition

relative to Fe additions alone (Bertrand et al., 2007, 2015). Hence, Co control on B12-auxotrophic algae growth in sea ice cannot be ruled out. This could be particularly important in polar areas where the distribution of vitamin B12 producing cyanobacteria is drastically reduced (Saito, 2002).

4.4.4.3 Manganese and Copper

Manganese is the second most abundant TM in the photosynthetic system after Fe. It is essential for phytoplankton growth as four Mn ions are required for the oxidation of each water molecule. It is also needed for the antioxidant enzyme superoxide dismutase (SOD), which detoxifies reactive oxygen species and prevents cell damage. A recent study showed that Mn and Fe co-limit the growth of the Antarctic diatom *C. debilis* (Pausch et al., 2019). Using natural Antarctic seawater, Mn limitation was observed at concentrations of ~ 0.6 nM despite the addition of Fe (Pausch et al., 2019). Based on this observation, Mn does not seem to impose limitations on diatom physiology within the sea-ice environment, where concentrations of both median bulk ice and brine were generally above this threshold, even during summer. However, it is likely that sea-ice algae have different Mn requirement than phytoplankton.

Copper is involved in eukaryotic cell respiration and therefore essential for phytoplankton growth. Nevertheless, in the absence of organic complexation, Cu can be toxic and preclude growth of some diatom species due to competition between Cu and Mn for a critical cellular site involved in Mn transport (Sunda et al., 1981, 1983). Copper can therefore antagonize Mn nutrition. Most DMn in oceanic surface waters is found in its photochemical reduced state of Mn (II), since Mn (III) and Mn (IV) are predominantly insoluble oxides (Sunda, 2012). Mn (II) is, however, not appreciably bound to organic ligands (Sunda and Huntsman, 1994), a fact that could facilitate algae uptake and assimilation. On the other hand, Cu has a high affinity for organic ligands (Buck & Bruland, 2005; Buck et al., 2007; Leal and Van den Berg, 1998; Sunda & Ferguson, 1983; Piotrowicz et al., 1984). The abundance of natural ligands in sea ice, as observed in the case of Fe (Genovese et al., 2018), could therefore potentially reduce Cu′ availability and toxicity while not affecting Mn uptake (Sunda & Ferguson, 1983; Piotrowicz et al., 1983). Ultimately, a more conclusive answer on Mn limitation will largely depend on future work assessing concentrations of Cu′ and Zn′ and their potential toxicity to sea-ice algae.

4.4.5 Conceptual model of co-limitation of macro and micronutrients.

Although light, Fe and Si are often considered to be the primary drivers of Southern Ocean productivity (Hoffmann et al., 2007), other elements play an important part in the sea-ice ecosystem. Within the sea-ice environment, Fe availability can stimulate phytoplankton growth. Enhanced algal biomass could further stimulate bacterial growth, increasing vitamin B12 production, which can also boost algal growth (Bertrand et al., 2015). At the same time, Fe availability can increase the consumption of nitrogen and the maximum specific uptake rate of $SiOH_4$ via increase in the number of active Si transporters in the diatoms' cell membrane (Brzezinski et al., 2005; De La Rocha et al., 2000; Franck et al., 2003; Lim et al., 2019). Higher growth also demands higher capability to photosynthesize and to detoxify reactive oxygen species, thereby increasing the intracellular demand for Mn. Ultimately, at some point of this enhancive cycle played by sea-ice algae and bacteria, the supply of inorganic sources such as $SiOH_4$ (Lim et al., 2019), NO_3^- (Duprat et al., 2020) and Co (Bertrand, 2015) could become limiting. While this hypothesis still needs to be tested, if Mn uptake is antagonized by Cu′ or Zn′ activity, Mn limitation could occur before other nutrients.

4.5 Conclusion

The role, availability and potential toxicity of TM, other than Fe, within sea ice is still largely unexplored. Our results point toward a TM enriched sea-ice environment, however, DCu and DZn concentrations may become toxic if present in the free ion forms. Ligands may alleviate this toxicity by complexation, but Cu- and Zn- binding ligands have not yet been quantified in sea ice. Results found for Fe suggest EPS largely contributes to the organic ligand pool. Further quantitative and qualitative assessments of kinetic processes between different TM and EPS in sea ice would improve our understanding of their nutritional and potential toxicological effect on sea-ice algae.

4.6 Acknowledgments

This work was co-funded by the Australian Government Cooperative Research Centre Program through the Antarctic Climate and Ecosystems Cooperative Research Centre (ACE CRC), the Australian Antarctic Science (AAS) project no. 4291 and the Australian Research Council's Special Research Initiative for Antarctic Gateway Partnership (Project ID SR140300001).

Access to ICP instrumentation was supported through ARC LIEF LE0989539 funding. We thank all personnel involved in the laboratory and fieldwork which data were here analysed.

4.7 References

Archer, S. D., Leakey, R. J. G., Burkill, P. H., Sleigh, M. A., & Appleby, C. J. (1996). Microbial ecology of sea ice at a coastal Antarctic site: Community composition, biomass and temporal change. *Marine Ecology Progress Series, 135*(1-3), 179-195. doi:10.3354/meps135179

Aslam, S. N., Cresswell-Maynard, T., Thomas, D. N., & Underwood, G. J. (2012). Production and Characterization of the Intra- and Extracellular Carbohydrates and Polymeric Substances (EPS) of Three Sea-Ice Diatom Species, and Evidence for a Cryoprotective Role for EPS. *Journal of Phycology, 48*(6), 1494-1509. doi:10.1111/jpy.12004

Baars, O., & Croot, P. L. (2011). The speciation of dissolved zinc in the Atlantic sector of the Southern Ocean. *Deep Sea Research Part II: Topical Studies in Oceanography, 58*(25-26), 2720-2732. doi:10.1016/j.dsr2.2011.02.003

Baines, S. B., Twining, B. S., Vogt, S., Balch, W. M., Fisher, N. S., & Nelson, D. M. (2011). Elemental composition of equatorial Pacific diatoms exposed to additions of silicic acid and iron. *Deep Sea Research Part II: Topical Studies in Oceanography, 58*(3-4), 512-523. doi:10.1016/j.dsr2.2010.08.003

Banerjee, R., & Ragsdale, S. W. (2003). The many faces of vitamin B12: catalysis by cobalamin-dependent enzymes. *Annual Reviews of Biochemistry, 72*, 209-247. doi:10.1146/annurev.biochem.72.121801.161828

Bertrand, E. M., McCrow, J. P., Moustafa, A., Zheng, H., McQuaid, J. B., Delmont, T. O. et al. (2015). Phytoplankton-bacterial interactions mediate micronutrient colimitation at the coastal Antarctic sea ice edge. *Proccedings of the National Academy of Sciences U S A, 112*(32), 9938-9943. doi:10.1073/pnas.1501615112

Bertrand, E. M., Saito, M. A., Rose, J. M., Riesselman, C. R., Lohan, M. C., Noble, A. E. et al. (2007). Vitamin B12and iron colimitation of phytoplankton growth in the Ross Sea. *Limnology and Oceanography, 52*(3), 1079-1093. doi:10.4319/lo.2007.52.3.1079

Bowie, A. R., Townsend, A. T., Lannuzel, D., Remenyi, T. A., & van der Merwe, P. (2010). Modern sampling and analytical methods for the determination of trace elements in marine particulate material using magnetic sector inductively coupled plasma-mass spectrometry. *Analytica Chimica Acta, 676*(1-2), 15-27. doi:10.1016/j.aca.2010.07.037

Boyd, P. W., Jickells, T., Law, C. S., Blain, S., Boyle, E. A., Buesseler, K. O., et al. (2007). Mesoscale iron enrichment experiments 1993-2005: synthesis and future directions. *Science, 315*(5812), 612-617. doi:10.1126/science.1131669

Boye, M., Wake, B. D., Lopez Garcia, P., Bown, J., Baker, A. R., & Achterberg, E. P. (2012). Distributions of dissolved trace metals (Cd, Cu, Mn, Pb, Ag) in the southeastern Atlantic and the Southern Ocean. *Biogeosciences, 9*(8), 3231-3246. doi:10.5194/bg-9-3231-2012

Bruland, K. W. (1980). Oceanographic distributions of cadmium, zinc, nickel, and copper in the North Pacific. *Earth and Planetary Science Letters, 47*(2), 176-198. doi:10.1016/0012-821x(80)90035-7

Bruland, K. W., & Lohan, M. C. (2003). Controls of Trace Metals in Seawater. In M. J. Mottl & H. Elderfield (Eds.), *Treatise on Geochemistry* (Second Edition ed., pp. 23-47). Philadelphia, USA. : Saunders, Elsevier Inc.

Brzezinski, M. A., Jones, J. L., & Demarest, M. S. (2005). Control of silica production by iron and silicic acid during the Southern Ocean Iron Experiment (SOFeX). *Limnology and Oceanography, 50*(3), 810-824. doi:DOI 10.4319/lo.2005.50.3.0810

Buck, K. N., & Bruland, K. W. (2005). Copper speciation in San Francisco Bay: A novel approach using multiple analytical windows. *Marine Chemistry, 96*(1-2), 185-198. doi:10.1016/j.marchem.2005.01.001

Buck, K. N., Ross, J. R., Russell Flegal, A., & Bruland, K. W. (2007). A review of total dissolved copper and its chemical speciation in San Francisco Bay, California. *Environmental Research 105*(1), 5-19. doi:10.1016/j.envres.2006.07.006

Calvert, S. E., & Pedersen, T. F. (1996). Sedimentary geochemistry of manganese; implications for the environment of formation of manganiferous black shales. *Economic Geology, 91*(1), 36-47. doi:10.2113/gsecongeo.91.1.36

Coale, K. (1991). Effects of iron, manganese, copper, and zinc enrichments on productivity and biomass in the subarctic Pacific. *Limnology and Oceanography, 36*, 1851–1864. doi:10.4319/lo.1991.36.8.1851

Coale, K. H., Michael Gordon, R., & Wang, X. (2005). The distribution and behavior of dissolved and particulate iron and zinc in the Ross Sea and Antarctic circumpolar current along 170°W. *Deep Sea Research Part I: Oceanographic Research Papers, 52*(2), 295-318. doi:10.1016/j.dsr.2004.09.008

Collier, R., & Edmond, J. (1984). The trace element geochemistry of marine biogenic particulate matter. *Progress in Oceanography, 13*(2), 113-199. doi:10.1016/0079-6611(84)90008-9

Corami, F., Capodaglio, G., Turetta, C., Soggia, F., Magi, E., & Grotti, M. (2005). Summer distribution of trace metals in the western sector of the Ross Sea, Antarctica. *Journal of Environmental Monitoring, 7*(12), 1256-1264. doi:10.1039/b507323p

Cox, G. F. N., & Weeks, W. F. (2017). Equations for Determining the Gas and Brine Volumes in Sea-Ice Samples. *Journal of Glaciology, 29*(102), 306-316. doi:10.1017/s0022143000008364

Crawford, D. W., Lipsen, M. S., Purdie, D. A., Lohan, M. C., Statham, P. J., Whitney, F. A. et al. (2003). Influence of zinc and iron enrichments on phytoplankton growth in the northeastern subarctic Pacific. *Limnology and Oceanography, 48*(4), 1583-1600. doi:10.4319/lo.2003.48.4.1583

Croot, P. L., Baars, O., & Streu, P. (2011). The distribution of dissolved zinc in the Atlantic sector of the Southern Ocean. *Deep Sea Research Part II: Topical Studies in Oceanography, 58*(25-26), 2707-2719. doi:10.1016/j.dsr2.2010.10.041

Cullen, J. T., Chase, Z., Coale, K. H., Fitzwater, S. E., & Sherrell, R. M. (2003). Effect of iron limitation on the cadmium to phosphorus ratio of natural phytoplankton assemblages from the Southern Ocean. *Limnology and Oceanography, 48*(3), 1079-1087. doi:10.4319/lo.2003.48.3.1079

Cullen, J. T., & Sherrell, R. M. (2005). Effects of dissolved carbon dioxide, zinc, and manganese on the cadmium to phosphorus ratio in natural phytoplankton assemblages. *Limnology and Oceanography, 50*(4), 1193-1204. doi:10.4319/lo.2005.50.4.1193

Cutter, G., Casciotti, K., Cullen, P., Geibert, W., Heimbürger, L.-E., Lohan, M. C. et al. (2017). *Sampling and Sample-handling Protocols for GEOTRACES Cruises*. Retrieved from https://geotracesold.sedoo.fr/images/Cookbook.pdf

Cuvelier, M. L., Allen, A. E., Monier, A., McCrow, J. P., Messie, M., Tringe, S. G. et al. (2010). Targeted metagenomics and ecology of globally important uncultured eukaryotic phytoplankton. *Proccedings of the National Academy of Sciences U S A, 107*(33), 14679-14684. doi:10.1073/pnas.1001665107

de Baar, H. J. W. (2005). Synthesis of iron fertilization experiments: From the Iron Age in the Age of Enlightenment. *Journal of Geophysical Research, 110*(C9). doi:10.1029/2004jc002601

de Jong, J., Schoemann, V., Maricq, N., Mattielli, N., Langhorne, P., Haskell, T., & Tison, J.-L. (2013). Iron in land-fast sea ice of McMurdo Sound derived from sediment resuspension and wind-blown dust attributes to primary productivity in the Ross Sea, Antarctica. *Marine Chemistry, 157*, 24-40. doi:10.1016/j.marchem.2013.07.001

De La Rocha, C. L., Hutchins, D. A., Brzezinski, M. A., & Zhang, Y. (2000). Effects of iron and zinc deficiency on elemental composition and silica production by diatoms. *Marine Ecology Progress Series, 195*, 71-79. doi:10.3354/meps195071

Decho, A. W., & Gutierrez, T. (2017). Microbial Extracellular Polymeric Substances (EPSs) in Ocean Systems. *Frontiers in Microbiology, 8*, 922. doi:10.3389/fmicb.2017.00922

Duprat, L., Corkill, M., Genovese, C., Moreau, S., Townsen, A., Meiners, K., & Lannuzel, D. (2020). Nutrient distribution in East Antarctic summer sea ice: a potential Iron contribution from glacial basal melt. *Journal of Geophys Research-Oceans*.

Duprat, L., Kanna, N., Janssens, J., Roukaerts, A., Deman, F., Townsend, A. T. et al. (2019). Enhanced Iron Flux to Antarctic Sea Ice via Dust Deposition From Ice-Free Coastal Areas. *Journal of Geophysical Research: Oceans, 124*(12), 8538-8557. doi:10.1029/2019jc015221

Ellwood, M. J. (2008). Wintertime trace metal (Zn, Cu, Ni, Cd, Pb and Co) and nutrient distributions in the Subantarctic Zone between 40–52°S; 155–160°E. *Marine Chemistry, 112*(1-2), 107-117. doi:10.1016/j.marchem.2008.07.008

Ellwood, M. J., van den Berg, C. M. G., Boye, M., Veldhuis, M., de Jong, J. T. M., de Baar, H. J. W. et al. (2005). Organic complexation of cobalt across the Antarctic Polar Front in the Southern Ocean. *Marine and Freshwater Research, 56*(8). doi:10.1071/mf05097

Fitzwater, S. E., Johnson, K. S., Gordon, R. M., Coale, K. H., & Smith, W. O. (2000). Trace metal concentrations in the Ross Sea and their relationship with nutrients and phytoplankton growth. *Deep-Sea Research Part Ii-Topical Studies in Oceanography, 47*(15-16), 3159-3179. doi:10.1016/S0967-0645(00)00063-1

Frache, R., Abelmoschi, M. L., Grotti, M., Ianni, C., Magi, E., Soggia, F. et al. (2001). Effects of Ice Melting on Cu, Cd and Pb Profiles in Ross Sea Waters (Antarctica). *International Journal of Environmental Analytical Chemistry, 79*(4), 301-313. doi:10.1080/03067310108044391

Franck, V. M., Bruland, K. W., Hutchins, D. A., & Brzezinski, M. A. (2003). Iron and zinc effects on silicic acid and nitrate uptake kinetics in three high-nutrient, low-chlorophyll (HNLC) regions. *Marine Ecology Progress Series, 252*, 15-33. doi:10.3354/meps252015

Frew, R., Bowie, A., Croot, P., & Pickmere, S. (2001). Macronutrient and trace-metal geochemistry of an in situ iron-induced Southern Ocean bloom. *Deep Sea Research Part II: Topical Studies in Oceanography, 48*(11-12), 2467-2481. doi:10.1016/s0967-0645(01)00004-2

Fripiat, F., Meiners, K. M., Vancoppenolle, M., Papadimitriou, S., Thomas, D. N., Ackley, S. F. et al. (2017). Macro-nutrient concentrations in Antarctic pack ice: Overall patterns and overlooked processes. *Elementa-Science of the Anthropocene, 5*. doi:10.1525/elementa.217

Genovese, C., Grotti, M., Pittaluga, J., Ardini, F., Janssens, J., Wuttig, K. et al. (2018). Influence of organic complexation on dissolved iron distribution in East Antarctic pack ice. *Marine Chemistry, 203*, 28-37. doi:10.1016/j.marchem.2018.04.005

Gradinger, R., & Ikavalko, J. (1998). Organism incorporation into newly forming Arctic sea ice in the Greenland Sea. *20*(5), 871-876.

Grotti, M., Soggia, F., Abelmoschi, M. L., Rivaro, P., Magi, E., & Frache, R. (2001). Temporal distribution of trace metals in Antarctic coastal waters. *Marine Chemistry, 76*(3), 189-209. doi:10.1016/s0304-4203(01)00063-9

Grotti, M., Soggia, F., Ianni, C., & Frache, R. (2005). Trace metals distributions in coastal sea ice of Terra Nova Bay, Ross Sea, Antarctica. *Antarctic Science, 17*(2), 289-300. doi:10.1017/s0954102005002695

Guo J., Annett A. L., Taylor R. L., Lapi S., Ruth T. J., & T., M. M. (2010). Copper-uptake kinetics of coastal and oceanic diatoms. *Journal of Phycology, 46*, 1218–1228. doi:10.1111/j.1529-8817.2010.00911.x

Gutierrez, T., Biller, D. V., Shimmield, T., & Green, D. H. (2012). Metal binding properties of the EPS produced by Halomonas sp. TG39 and its potential in enhancing trace element bioavailability to eukaryotic phytoplankton. *Biometals, 25*(6), 1185-1194. doi:10.1007/s10534-012-9581-3

Gutierrez, T., Shimmield, T., Haidon, C., Black, K., & Green, D. H. (2008). Emulsifying and metal ion binding activity of a glycoprotein exopolymer produced by Pseudoalteromonas sp. strain TG12. *Applied and Environmental Microbiology, 74*(15), 4867-4876. doi:10.1128/AEM.00316-08

Hassler, C. S., Schoemann, V., Nichols, C. M., Butler, E. C., & Boyd, P. W. (2011). Saccharides enhance iron bioavailability to Southern Ocean phytoplankton. *Proccedings of the National Academy of Science U S A, 108*(3), 1076-1081. doi:10.1073/pnas.1010963108

Hassler, C. S., Sinoir, M., Clementson, L. A., & Butler, E. C. (2012). Exploring the Link between Micronutrients and Phytoplankton in the Southern Ocean during the 2007 Austral Summer. *Frontiers in Microbiology, 3*, 202. doi:10.3389/fmicb.2012.00202

Hassler, C. S., van den Berg, C. M. G., & Boyd, P. W. (2017). Toward a Regional Classification to Provide a More Inclusive Examination of the Ocean Biogeochemistry of Iron-Binding Ligands. *Frontiers in Marine Science, 4*. doi:10.3389/fmars.2017.00019

Hawkings, J. R., Benning, L. G., Raiswell, R., Kaulich, B., Araki, T., Abyaneh, M. et al. (2018). Biolabile ferrous iron bearing nanoparticles in glacial sediments. *Earth and Planetary Science Letters, 493*, 92-101. doi:10.1016/j.epsl.2018.04.022

Hoffmann, L. J., Peeken, I., & Lochte, K. (2007). Co-limitation by iron, silicate, and light of three Southern Ocean diatom species. *Biogeosciences Discussions, 4*(1), 209-247. doi:10.5194/bgd-4-209-2007

Hudson, R. J. M. (1998). Which aqueous species control the rates of trace metal uptake by aquatic biota? Observations and predictions of non-equilibrium effects. *Science of The Total Environment, 219*(2-3), 95-115. doi:10.1016/s0048-9697(98)00230-7

Ingall, E. D., Diaz, J. M., Longo, A. F., Oakes, M., Finney, L., Vogt, S. et al. (2013). Role of biogenic silica in the removal of iron from the Antarctic seas. *Nature Communications, 4*, 1981. doi:10.1038/ncomms2981

Jaccard, T., Ariztegui, D., & Wilkinson, K. J. (2009). Incorporation of zinc into the frustule of the freshwater diatom Stephanodiscus hantzschii. *Chemical Geology, 265*(3-4), 381-386. doi:10.1016/j.chemgeo.2009.04.016

Janssen, D. J., Sieber, M., Ellwood, M. J., Conway, T. M., Barrett, P. M., Chen, X. et al. (2020). Trace metal and nutrient dynamics across broad biogeochemical gradients in the Indian and Pacific sectors of the Southern Ocean. *Marine Chemistry, 221*. doi:10.1016/j.marchem.2020.103773

Janssens, J., Meiners, K. M., Tison, J. L., Dieckmann, G., Delille, B., & Lannuzel, D. (2016). Incorporation of iron and organic matter into young Antarctic sea ice during its initial growth stages. *Elementa-Science of the Anthropocene, 4*, 000123. doi:10.12952/journal.elementa.000123

Janssens, J., Meiners, K. M., Townsend, A. T., & Lannuzel, D. (2018). Organic Matter Controls of Iron Incorporation in Growing Sea Ice. *Frontiers in Earth Science, 6*. doi:10.3389/feart.2018.00022

Koch, F., Beszteri, S., Harms, L., & Trimborn, S. (2019). The impacts of iron limitation and ocean acidification on the cellular stoichiometry, photophysiology, and transcriptome of Phaeocystis antarctica. *Limnology and Oceanography, 64*(1), 357-375. doi:10.1002/lno.11045

Koch, F., & Trimborn, S. (2019). Limitation by Fe, Zn, Co, and B12 Results in Similar Physiological Responses in Two Antarctic Phytoplankton Species. *Frontiers in Marine Science, 6*. doi:10.3389/fmars.2019.00514

Kustka, A. B., Allen, A. E., & Morel, F. M. M. (2007). Sequence Analysis and Transcriptional Regulation of Iron Acquisition Genes in Two Marine Diatoms1. *Journal of Phycology, 43*(4), 715-729. doi:10.1111/j.1529-8817.2007.00359.x

Lai, X., Norisuye, K., Mikata, M., Minami, T., Bowie, A. R., & Sohrin, Y. (2008). Spatial and temporal distribution of Fe, Ni, Cu and Pb along 140°E in the Southern Ocean during austral summer 2001/02. *Marine Chemistry, 111*(3-4), 171-183. doi:10.1016/j.marchem.2008.05.001

Lane, E. S., Jang, K., Cullen, J. T., & Maldonado, M. T. (2008). The interaction between inorganic iron and cadmium uptake in the marine diatom Thalassiosira oceanica. *Limnology and Oceanography, 53*(5), 1784-1789. doi:10.4319/lo.2008.53.5.1784

Lane, T. W., & Morel, F. M. (2000). A biological function for cadmium in marine diatoms. *Proc Natl Acad Sci U S A, 97*(9), 4627-4631. doi:10.1073/pnas.090091397

Lannuzel, D., Bowie, A. R., van der Merwe, P. C., Townsend, A. T., & Schoemann, V. (2011). Distribution of dissolved and particulate metals in Antarctic sea ice. *Marine Chemistry, 124*(1-4), 134-146. doi:10.1016/j.marchem.2011.01.004

Lannuzel, D., Chever, F., van der Merwe, P. C., Janssens, J., Roukaerts, A., Cavagna, A. J. et al. (2016a). Iron biogeochemistry in Antarctic pack ice during SIPEX-2. *Deep-Sea Research Part Ii-Topical Studies in Oceanography, 131*, 111-122. doi:10.1016/j.dsr2.2014.12.003

Lannuzel, D., de Jong, J., Schoemann, V., Trevena, A., Tison, J. L., & Chou, L. (2006). Development of a sampling and flow injection analysis technique for iron determination in the sea ice environment. *Analytica Chimica Acta, 556*(2), 476-483. doi:10.1016/j.aca.2005.09.059

Lannuzel, D., van der Merwe, P. C., Townsend, A. T., & Bowie, A. R. (2014). Size fractionation of iron, manganese and aluminium in Antarctic fast ice reveals a lithogenic origin and low iron solubility. *Marine Chemistry, 161*, 47-56. doi:10.1016/j.marchem2014.02.006

Lannuzel, D., Vancoppenolle, M., van der Merwe, P., de Jong, J., Meiners, K. M., Grotti, M. et al. (2016b). Iron in sea ice: Review and new insights. *Elementa: Science of the Anthropocene, 4*, 000130. doi:10.12952/journal.elementa.000130

Leal, M. F. C., & Van Den Berg, C. M. G. (1998). Evidence for Strong Copper(I) Complexation by Organic Ligands in Seawater. *Aquatic Geochemistry, 4*(1), 49-75. doi:10.1023/a:1009653002399

Lim, S. M., Moreau, S., Vancoppenolle, M., Deman, F., Roukaerts, A., Meiners, K. M. et al. (2019). Field Observations and Physical-Biogeochemical Modeling Suggest Low Silicon Affinity for Antarctic Fast Ice Diatoms. *Journal of Geophysical Research: Oceans, 124*(11), 7837-7853. doi:10.1029/2018jc014458

Löscher, B. M. (1999). Relationships among Ni, Cu, Zn, and major nutrients in the Southern Ocean. *Marine Chemistry, 67*(1-2), 67-102. doi:10.1016/s0304-4203(99)00050-x

Löscher, B. M., de Jong, J. T. M., & de Baar, H. J. W. (1998). The distribution and preferential biological uptake of cadmium at 6°W in the Southern Ocean. *Marine Chemistry, 62*(3-4), 259-286. doi:10.1016/s0304-4203(98)00045-0

Maldonado, M. T., Allen, A. E., Chong, J. S., Lin, K., Leus, D., Karpenko, N., & Harris, S. L. (2006). Copper-dependent iron transport in coastal and oceanic diatoms. *Limnology and Oceanography, 51*(4), 1729-1743. doi:10.4319/lo.2006.51.4.1729

Marchetti, A., Maldonado, M. T., Lane, E. S., & Harrison, P. J. (2006). Iron requirements of the pennate diatomPseudo-nitzschia: Comparison of oceanic (high-nitrate, low-chlorophyll waters) and coastal species. *Limnology and Oceanography, 51*(5), 2092-2101. doi:10.4319/lo.2006.51.5.2092

Marchetti, A., Parker, M. S., Moccia, L. P., Lin, E. O., Arrieta, A. L., Ribalet, F. et al. (2009). Ferritin is used for iron storage in bloom-forming marine pennate diatoms. *Nature, 457*(7228), 467-470. doi:10.1038/nature07539

Marchetti, A., Schruth, D. M., Durkin, C. A., Parker, M. S., Kodner, R. B., Berthiaume, C. T. et al. (2012). Comparative metatranscriptomics identifies molecular bases for the physiological responses of phytoplankton to varying iron availability. *Proccedings of the National Academy of Sciences U S A, 109*(6), E317-325. doi:10.1073/pnas.1118408109

Martin, J. H. (1990). Glacial-interglacial CO_2 change: The Iron Hypothesis. *Paleoceanography, 5*(1), 1-13. doi:10.1029/PA005i001p00001

McKay, R. M. L., La Roche, J., Yakunin, A. F., Durnford, D. G., & Geider, R. J. (1999). Accumulation of Ferredoxin and Flavodoxin in a Marine Diatom in Response to Fe. *Journal of Phycology, 35*(3), 510-519. doi:10.1046/j.1529-8817.1999.3530510.x

Meiners, K. M., Golden, K. M., Heil, P., Lieser, J. L., Massom, R., Meyer, B., & Williams, G. D. (2016). Introduction: SIPEX-2: A study of sea-ice physical, biogeochemical and ecosystem processes off East Antarctica during spring 2012. *Deep Sea Research Part II: Topical Studies in Oceanography, 131*, 1-6. doi:10.1016/j.dsr2.2016.06.010

Meiners, K. M., & Michel, C. (2017). *Dynamics of nutrients, dissolved organic matter and exopolymers in sea ice. In: Thomas, DN (ed.), Sea Ice*. Oxford, UK: Wiley-Blackwell: Wiley-Blackwell.

Miao, A. J., Wang, W. X., & Juneau, P. (2005). Comparison of Cd, Cu, and Zn toxic effects on four marine phytoplankton by pulse-amplitude-modulated fluorometry. *Environmental Toxicology and Chemistry, 24*(10), 2603-2611. doi:10.1897/05-009r.1

Middag, R., de Baar, H. J. W., Laan, P., Cai, P. H., & van Ooijen, J. C. (2011). Dissolved manganese in the Atlantic sector of the Southern Ocean. *Deep Sea Research Part II: Topical Studies in Oceanography, 58*(25-26), 2661-2677. doi:10.1016/j.dsr2.2010.10.043

Middag, R., de Baar, H. J. W., Klunder, M. B., & Laan, P. (2013). Fluxes of dissolved aluminum and manganese to the Weddell Sea and indications for manganese co-limitation. *Limnology and Oceanography, 58*(1), 287-300. doi:10.4319/lo.2013.58.1.0287

Miller, L. A., Fripiat, F., Else, B. G. T., Bowman, J. S., Brown, K. A., Collins, R. E. et al. (2015). Methods for biogeochemical studies of sea ice: The state of the art, caveats, and recommendations. *Elementa: Science of the Anthropocene, 3*. doi:10.12952/journal.elementa.000038

Milne, A., Landing, W., Bizimis, M. & Morton, P. (2010). Determination of Mn, Fe, Co, Ni, Cu, Zn, Cd and Pb in seawater using high resolution magnetic sector inductively coupled mass spectrometry (HR-ICP-MS). *Analytica Chimica Acta*, 665, 200-7. doi: 10.1016/j.aca.2010.03.027

Mulrooney, S. B., & Hausinger, R. P. (2003). Nickel uptake and utilization by microorganisms. *FEMS Microbiology Reviews, 27*(2-3), 239-261. doi:10.1016/s0168-6445(03)00042-1

Neff, J. M. (2002). Zinc in the Ocean. In *Bioaccumulation in Marine Organisms* (pp. 175-189).

Nichols, C. M., Lardiere, S. G., Bowman, J. P., Nichols, P. D., J, A. E. G., & Guezennec, J. (2005). Chemical characterization of exopolysaccharides from Antarctic marine bacteria. *Microbial Ecology, 49*(4), 578-589. doi:10.1007/s00248-004-0093-8

Noble, A. E., Moran, D. M., Allen, A. E., & Saito, M. A. (2013). Dissolved and particulate trace metal micronutrients under the McMurdo Sound seasonal sea ice: basal sea ice communities as a capacitor for iron. *Frontiers in Chemistry, 1*(25), 25. doi:10.3389/fchem.2013.00025

Nolting, R. F., & de Baar, H. J. W. (1994). Behaviour of nickel, copper, zinc and cadmium in the upper 300 m of a transect in the Southern Ocean (57°–62°S, 49°W). *Marine Chemistry, 45*(3), 225-242. doi:10.1016/0304-4203(94)90006-x

Nolting, R. F., De Baar, H. J. W., Van Bennekom, A. J., & Masson, A. (1991). Cadmium, copper and iron in the Scotia Sea, Weddell Sea and Weddell/Scotia Confluence (Antarctica). *Marine Chemistry, 35*(1-4), 219-243. doi:10.1016/s0304-4203(09)90019-6

Olson, R. J., Sosik, H. M., Chekalyuk, A. M., & Shalapyonok, A. (2000). Effects of iron enrichment on phytoplankton in the Southern Ocean during late summer: active fluorescence and flow cytometric analyses. *Deep-Sea Research Part Ii-Topical Studies in Oceanography, 47*(15-16), 3181-3200. doi:Doi 10.1016/S0967-0645(00)00064-3

Panzeca, C., Beck, A. J., Leblanc, K., Taylor, G. T., Hutchins, D. A., & Sañudo-Wilhelmy, S. A. (2008). Potential cobalt limitation of vitamin B12synthesis in the North Atlantic Ocean. *Global Biogeochemical Cycles, 22*(2), n/a-n/a. doi:10.1029/2007gb003124

Pausch, F., Bischof, K., & Trimborn, S. (2019). Iron and manganese co-limit growth of the Southern Ocean diatom Chaetoceros debilis. *PLoS One, 14*(9), e0221959. doi:10.1371/journal.pone.0221959

Peers, G., & Price, N. M. (2004). A role for manganese in superoxide dismutases and growth of iron-deficient diatoms. *Limnology and Oceanography, 49*(5), 1774-1783. doi:10.4319/lo.2004.49.5.1774

Peers, G., & Price, N. M. (2006). Copper-containing plastocyanin used for electron transport by an oceanic diatom. *Nature, 441*(7091), 341-344. doi:10.1038/nature04630

Piotrowicz, S. R., Harvey, G. R., Boran, D. A., Weisel, C. P., & Springer-Young, M. (1984). Cadmium, copper, and zinc interactions with marine humus as a function of ligand structure. *Marine Chemistry, 14*(4), 333-346. doi:10.1016/0304-4203(84)90029-x

Rapp, I., Schlosser, C., Rusiecka, D., Gledhill, M. & Achterberg, E. P. (2017). Automated preconcentration of Fe, Zn, Cu, Ni, Cd, Pb, Co, and Mn in seawater with analysis using high-resolution sector field inductively-coupled plasma mass spectrometry. *Analytica Chimica Acta*, 976, 1-13. doi:10.1016/j.aca.2017.05.008

Price, N. M., & Morel, F. M. M. (1990). Cadmium and cobalt substitution for zinc in a marine diatom. *Nature, 344*(6267), 658-660. doi:10.1038/344658a0

Price, N. M., & Morel, F. M. M. (1991). Colimitation of phytoplankton growth by nickel and nitrogen. *Limnology and Oceanography, 36*(6), 1071-1077. doi:10.4319/lo.1991.36.6.1071

Redfield, A. C., Ketchum, B. H., & F.A., B. (1963). The influence of organisms on the composition of sea water. In: M.N. Hill. The Sea, Interscience. In M. N. Hill (Ed.), *The Sea* (Vol. 2). New York Interscience Publishers.

Roche, J. L., Boyd, P. W., McKay, R. M. L., & Geider, R. J. (1996). Flavodoxin as an in situ marker for iron stress in phytoplankton. *Nature, 382*(6594), 802-805. doi:10.1038/382802a0

Rueter, J. G., Chisholm, S. W., & Morel, F. M. M. (1981). Effects of Copper Toxicity on Silicic Acid Uptake and Growth in Thalassiosira Pseudonana1. *Journal of Phycology, 17*(3), 270-278. doi:10.1111/j.1529-8817.1981.tb00850.x

Rueter, J. G., & Morel, F. M. M. (1981). The interaction between zinc deficiency and copper toxicity as it affects the silicic acid uptake mechanisms in Thalassiosira pseudonana1. *Limnology and Oceanography, 26*(1), 67-73. doi:10.4319/lo.1981.26.1.0067

Saito, M. A., & Goepfert, T. J. (2008). Zinc-cobalt colimitation ofPhaeocystis antarctica. *Limnology and Oceanography, 53*(1), 266-275. doi:10.4319/lo.2008.53.1.0266

Saito, M. A., & Moffett, J. W. (2002). Temporal and spatial variability of cobalt in the Atlantic Ocean. *Geochimica et Cosmochimica Acta, 66*(11), 1943-1953. doi:10.1016/s0016-7037(02)00829-3

Schulz, K. G., Rost, B., Burkhardt, S., Riebesell, U., Thoms, S., & Wolf-Gladrow, D. A. (2007). The effect of iron availability on the regulation of inorganic carbon acquisition in the coccolithophore Emiliania huxleyi and the significance of cellular compartmentation for stable carbon isotope fractionation. *Geochimica et Cosmochimica Acta, 71*(22), 5301-5312. doi:10.1016/j.gca.2007.09.012

Sedwick, P. N., Edwards, P. R., Mackey, D. J., Griffiths, F. B., & Parslow, J. S. (1997). Iron and manganese in surface waters of the Australian subantarctic region. *Deep Sea Research Part I: Oceanographic Research Papers, 44*(7), 1239-1253. doi:10.1016/s0967-0637(97)00021-6

Shelley, R. U., Zachhuber, B., Sedwick, P. N., Worsfold, P. J. & Lohan, M. C. (2010). Determination of total dissolved cobalt in UV-irradiated seawater using flow injection with chemiluminescence detection. *Limnology and Oceanography*: Methods, 8, 352-362. doi: 10.4319/lom.2010.8.352

Smith, K. L., Jr., Robison, B. H., Helly, J. J., Kaufmann, R. S., Ruhl, H. A., Shaw, T. J. et al. (2007). Free-drifting icebergs: hot spots of chemical and biological enrichment in the Weddell Sea. *Science, 317*(5837), 478-482. doi:10.1126/science.1142834

Spreen, G., L. Kaleschke, & G.Heygster (2008), Sea ice remote sensing using AMSR-E 89 GHz channels *Journal of Geophysical Research*, 113, C02S03, doi:10.1029/2005JC003384.

Strzepek, R. F., Maldonado, M. T., Hunter, K. A., Frew, R. D., & Boyd, P. W. (2011). Adaptive strategies by Southern Ocean phytoplankton to lessen iron limitation: Uptake of organically complexed iron and reduced cellular iron requirements. *Limnology and Oceanography, 56*(6), 1983-2002. doi:10.4319/lo.2011.56.6.1983

Sunda, W. G. (1998). Trace Metal Interactions with Marine Phytoplankton. doi:10.1080/01965581.1988.10749543

Sunda, W. G. (2012). Feedback Interactions between Trace Metal Nutrients and Phytoplankton in the Ocean. *Frontiers in Microbiology, 3*, 204. doi:10.3389/fmicb.2012.00204

Sunda, W. G., Barber, R. T., & Huntsman, S. A. (1981). Phytoplankton growth in nutrient rich seawater: importance of copper-manganese cellular interactions. *Journal of Marine Research, 39*, 567-586.

Sunda, W. G., & Ferguson, R. L. (1983). Sensitivity of Natural Bacterial Communities to Additions of Copper and to Cupric Ion Activity: A Bioassy of Copper Complexation in Seawater. In W. C.S., B. E., B. K.W., B. J.D., & G. E.D. (Eds.), *Trace Metals in Sea Water* (Vol. vol 9, pp. 871-891). Boston, MA.: Springer.

Sunda, W. G., & Huntsman, S. A. (1983). Effect of competitive interactions between manganese and copper on cellular manganese and growth in estuarine and oceanic species of the diatom Thalassiosira. *Limnology and Oceanography, 28*(5), 924-934. doi:10.4319/lo.1983.28.5.0924

Sunda, W. G., & Huntsman, S. A. (1992). Feedback interactions between zinc and phytoplankton in seawater. *Limnology and Oceanography, 37*(1), 25-40. doi:10.4319/lo.1992.37.1.0025

Sunda, W. G., & Huntsman, S. A. (1994). Photoreduction of manganese oxides in seawater. *Marine Chemistry, 46*(1-2), 133-152. doi:10.1016/0304-4203(94)90051-5

Sunda, W. G., & Huntsman, S. A. (1995a). Cobalt and zinc interreplacement in marine phytoplankton: Biological and geochemical implications. *Limnology and Oceanography, 40*(8), 1404-1417. doi:10.4319/lo.1995.40.8.1404

Sunda, W. G., & Huntsman, S. A. (1995b). Iron uptake and growth limitation in oceanic and coastal phytoplankton. *Marine Chemistry, 50*(1-4), 189-206. doi:10.1016/0304-4203(95)00035-p

Sunda, W. G., & Huntsman, S. A. (1996). Antagonisms between cadmium and zinc toxicity and manganese limitation in a coastal diatom. *Limnology and Oceanography, 41*(3), 373-387. doi:10.4319/lo.1996.41.3.0373

Sunda, W. G., & Huntsman, S. A. (1998a). Control of Cd Concentrations in a Coastal Diatom by Interactions among Free Ionic Cd, Zn, and Mn in Seawater. *Environmental Science & Technology, 32*(19), 2961-2968. doi:10.1021/es980271y

Sunda, W. G., & Huntsman, S. A. (1998b). Interactive effects of external manganese, the toxic metals copper and zinc, and light in controlling cellular manganese and growth in a coastal diatom. *Limnology and Oceanography, 43*(7), 1467-1475. doi:10.4319/lo.1998.43.7.1467

Sunda, W. G., & Huntsman, S. A. (2000). Effect of Zn, Mn, and Fe on Cd accumulation in phytoplankton: Implications for oceanic Cd cycling. *Limnology and Oceanography, 45*(7), 1501-1516. doi:10.4319/lo.2000.45.7.1501

Tappin, A. D., Millward, G. E., Statham, P. J., Burton, J. D., & Morris, A. W. (1995). Trace Metals in the Central and Southern North Sea. *Estuarine, Coastal and Shelf Science, 41*(3), 275-323. doi:10.1006/s0272-7714(85)70068-7

Taylor, S. R. M., S. M. (1985). The Continental Crust: Its Composition and Evolution. In *Geological Magazine* (Vol. 122, pp. 673-674). Oxford, London, Edinburgh, Boston, Palo Alto, Melbourne: Blackwell Scientific.

Twining, B. S., & Baines, S. B. (2013). The trace metal composition of marine phytoplankton. *Annual Reviews of Marine Science, 5*(1), 191-215. doi:10.1146/annurev-marine-121211-172322

Twining, B. S., Baines, S. B., & Fisher, N. S. (2004). Element stoichiometries of individual plankton cells collected during the Southern Ocean Iron Experiment (SOFeX). *Limnology and Oceanography, 49*(6), 2115-2128. doi:10.4319/lo.2004.49.6.2115

Twining, B. S., Baines, S. B., Fisher, N. S., & Landry, M. R. (2004). Cellular iron contents of plankton during the Southern Ocean Iron Experiment (SOFeX). *Deep Sea Research Part I: Oceanographic Research Papers, 51*(12), 1827-1850. doi:10.1016/j.dsr.2004.08.007

Twining, B. S., Baines, S. B., Vogt, S., & Nelson, D. M. (2012). Role of diatoms in nickel biogeochemistry in the ocean. *Global Biogeochemical Cycles, 26*(4), n/a-n/a. doi:10.1029/2011gb004233

van der Merwe, P., Lannuzel, D., Nichols, C. A. M., Meiners, K., Heil, P., Norman, L. et al. (2009). Biogeochemical observations during the winter–spring transition in East Antarctic sea ice: Evidence of iron and exopolysaccharide controls. *Marine Chemistry, 115*(3-4), 163-175. doi:10.1016/j.marchem.2009.08.001

van Leeuwe, M. A., Tedesco, L., Arrigo, K. R., Assmy, P., Campbell, K., Meiners, K. M. et al. (2018). Microalgal community structure and primary production in Arctic and Antarctic sea ice: A synthesis. *Elementa: Science of the Anthropocene, 6*. doi:10.1525/elementa.267

Vega, M. & van den Berg, C. M. (1997). Determination of cobalt in seawater by catalytic adsorptive cathodic stripping voltammetry. *Analytical Chemistry*, 69, 874-81. doi:10.1021/ac960214s

Westerlund, S., & öhman, P. (1991). Cadmium, copper, cobalt, nickel, lead, and zinc in the water column of the Weddell Sea, Antarctica. *Geochimica et Cosmochimica Acta, 55*(8), 2127-2146. doi:10.1016/0016-7037(91)90092-j

Westerlund, S., & Öhman, P. (1991). Iron in the water column of the Weddell Sea. *Marine Chemistry, 35*, 199–217

Wolfe-Simon, F., Grzebyk, D., Schofield, O., & Falkowski, P. G. (2005). The Role and Evolution of Superoxide Dismutases in Algae1. *Journal of Phycology, 41*(3), 453-465. doi:10.1111/j.1529-8817.2005.00086.x

Wuttig, K., Townsend, A. T., van der Merwe, P., Gault-Ringold, M., Holmes, T., Schallenberg, C. et al. (2019). Critical evaluation of a seaFAST system for the analysis of trace metals in marine samples. *Talanta, 197*, 653-668. doi:10.1016/j.talanta.2019.01.047

Yang, T., Chen, Y., Zhou, S., & Li, H. (2019). Impacts of Aerosol Copper on Marine Phytoplankton: A Review. *Atmosphere, 10*(7). doi:10.3390/atmos10070414

Zhang, H., Davison, W., Mortimer, R. J. G., Krom, M. D., Hayes, P. J., & Davies, I. M. (2002). Localised remobilization of metals in a marine sediment. *Science of The Total Environment, 296*(1-3), 175-187. doi:10.1016/s0048-9697(02)00078-5

Appendix A

Table A1 Temperature (°C), salinity and concentration of chlorophyll-*a* (Chla [µg L^{-1}]), particulate organic carbon (POC [µM]), nitrate + nitrite (NOx [nM]), phosphate (PO_4^{-3} [nM]) and silicic acid (Si(OH) [nM]) in bulk sea ice for each section of all stations (Sample ID) encountered along the three field campaigns (Voyage).

Voyage	Sample ID	Depth (cm)	Temp (°C)	Salinity	Chl*a* (µg L^{-1})	POC (µM)	NOx (µM)	PO_4^{-3} (µM)	Si(OH) (µM)	$NH4^+$ (µM)
SIPEX-2	st2SI1	0–9	-2.5	10.1	0.3	12.2	6.42	0.39	18.3	0.79
SIPEX-2	st2SI2	9–16	-2.2	9.5	0.2	23.7	2.71	0.81	11.7	0.57
SIPEX-2	st2SI3	16–26	-2.1	8.4	1.9	10.8	1.78	0.26	9.99	0.29
SIPEX-2	st2SI4	26–33	-2.2	4.1	1.6	29.2	0.57	0.26	4.99	1.43
SIPEX-2	st2SI5	61–68	-2.1	5.0	3.9	31.6	1.07	0.45	3.33	0.36
SIPEX-2	st2SI6	68–75	-1.9	7.6	3.9	37.5	2.64	0.71	8.32	1.36
SIPEX-2	st3SI1	0–7	-8.4	18.5	0.1	5.3	3.93	0.16	8.32	0.29
SIPEX-2	st3SI2	7–15	-6.2	9.8	1.0	7.6	7.35	0.39	16.7	0.50
SIPEX-2	st3SI3	34–41	-4.6	5.1	0.7	7.5	4.28	0.36	11.7	0.50
SIPEX-2	st3SI4	92–99	-4.7	3.	0.2	18.0	5.85	0.42	11.7	0.36
SIPEX-2	st3SI5	129–136	-2.5	4.5	2.7	10.5	3.93	0.32	8.32	0.21
SIPEX-2	st3SI6	136–143	-2.2	5.7	2.7	2.0	2.07	0.19	4.99	0.29
SIPEX-2	st4SI1	0–12	-3.1	8.9	1.6	19.2	6.21	0.61	20.0	0.36
SIPEX-2	st4SI2	12–24	-4.2	9.1	0.7	9.6	0.93	0.19	8.32	0.50
SIPEX-2	st4SI3	24–34	-3.6	6.6	3.2	9.4	1.14	0.19	3.33	0.36
SIPEX-2	st4SI4	34–43.5	-3.2	4.8	1.5	7.1	1.78	0.26	4.99	0.21
SIPEX-2	st4SI5	75–83	-2.2	4.9	0.9	4.5	2.86	0.23	4.99	0.21
SIPEX-2	st4SI6	83–90	-2.0	7.1	0.8	3.7	4.07	0.23	8.32	0.43
SIPEX-2	st6SI1	0–7	-2.1	12.6	8.4	90.7	0.21	0.52	26.6	5.00
SIPEX-2	st6SI2	7–14	-2.1	7.1	1.8	32.9	0.86	0.39	11.7	3.14
SIPEX-2	st6SI3	21–28	-2.1	8.1	0.4	10.5	0.43	0.19	4.99	0.14
SIPEX-2	st6SI4	28–35	-1.4	4.6	0.0	8.8	0.50	0.19	3.33	0.29
SIPEX-2	st6SI5	56–63	-1.5	4.0	1.2	20.8	1.14	0.19	3.33	0.64
SIPEX-2	st6SI6	63–72	-1.7	4.2	2.7	36.1	1.71	0.45	6.66	1.07
SIPEX-2	st7SI1	0–7	-2.9	14.4	1.6	75.7	2.57	0.42	9.99	0.86
SIPEX-2	st7SI2	7–14	-2.8	4.3	1.0	59.7	0.29	0.13	1.66	0.64
SIPEX-2	st7SI3	14–21	-2.6	4.3	1.0	13.1	0.14	0.16		1.07
SIPEX-2	st7SI4	43–50	-2.2	3.9	4.4	87.7	1.78	0.65	1.66	0.64
SIPEX-2	st7SI5	71–77	-1.9	6.9	9.1	77.3	8.21	1.91	9.99	14.3
SIPEX-2	st7SI6	78–85	-1.9	6.6	6.4	64.2	6.57	1.36	11.7	3.93
SIPEX-2	st8SI1	0–7	-2.0	3.9	1.0	35.3	2.50	0.39	6.66	0.71
SIPEX-2	st8SI2	7–14	-1.9	4.1	1.2	18.1		0.10	1.66	0.36

SIPEX-2	st8SI3	44–51	-2.1	4.3	1.6	43.0		0.19		0.36
SIPEX-2	st8SI4	61–68	-2.4	4.6	7.8	35.4	3.00	0.61	3.33	0.71
SIPEX-2	st8SI5	81–88	-2.8	5.5	3.8	16.6	3.85	0.39	6.66	1.21
SIPEX-2	st8SI6	88–95	-2.9	7.3	4.4	20.9	6.64	0.55	9.99	11.4
Davis	st1SI1	0–20	-5.2	0.2	0.2	1.6	2.17	0.29	5.86	0.37
Davis	st1SI2	20–40	-4.8	6.8	0.4	1.8	0.78	0.19	4.43	0.61
Davis	st1SI3	40–130	-3.9	5.2	0.7	1.5	2.32	0.23	4.89	0.96
Davis	st1SI4	130–140	-2.8	3.7	1.0	1.1	0.85	0.12	3.94	<0.01
Davis	st1SI5	140–170	-2.3	4.7	0.8	1.2	0.73	0.10	2.16	0.08
Davis	st1SI6	170–175	-1.8	1.6		3.5	2.38	0.29	3.82	<0.01
Davis	st1SI7	175–180	-1.6	10.2	267	91.4	74.5	9.43	14.1	1.93
Davis	st2SI1	0–20	-5.1	0.1	0.5	2.5	3.29	0.52	5.80	1.95
Davis	st2SI2	20–40	-4.7	6.1	0.2	2.6	1.22	0.35	5.37	0.67
Davis	st2SI3	40–123	-3.5	4.3	0.2	1.6	1.54	0.56	4.63	0.90
Davis	st2SI4	123–133	-2.6	3.9	0.7	2.7	0.51	0.08	1.27	<0.01
Davis	st2SI5	133–163	-2.1	4.6	0.8	1.5	0.65	0.21	2.03	0.10
Davis	st2SI6	163–168	-1.7	6.0	2.1	5.1	2.14	0.19	3.32	0.08
Davis	st2SI7	168–173	-1.6	12.7	244	227	66.4	5.83	11.1	2.65
Davis	st3SI1	0–20	-5.6	0.2	0.1	1.8	2.65	0.25	4.49	0.91
Davis	st3SI2	20–40	-5.0	5.4	0.6	1.8	1.92	0.22	5.54	1.18
Davis	st3SI3	40–118	-3.7	5.4	1.3	1.5	2.13	0.25	5.46	1.37
Davis	st3SI4	118–128	-2.8	4.3	1.7	1.7	0.70	0.11	2.10	<0.01
Davis	st3SI5	128–158	-2.3	4.0	0.7	1.4	0.70	0.10	1.33	0.01
Davis	st3SI6	158–163	-2.0	5.0	2.8	5.7	2.72	0.25	1.44	<0.01
Davis	st3SI7	163–168	-1.9	11.1	232	169	38.8	6.34	7.60	4.74
Davis	st4SI1	0–20	-4.2	1.4		2.2	2.24	0.35	5.77	0.86
Davis	st4SI2	20–40	-4.1	5.9		2.5	0.87	0.18	4.51	0.79
Davis	st4SI3	40–128	-3.3	5.1	0.8	1.9	1.68	0.21	4.65	1.02
Davis	st4SI4	128–138	-2.5	4.3	1.1	1.6	0.59	0.08	3.50	0.12
Davis	st4SI5	138–168	-1.9	3.8	1.3	1.2	0.66	0.08	2.48	0.08
Davis	st4SI6	168–173	-1.4	4.3	11.6	4.7	3.70	0.32	2.96	0.42
Davis	st4SI7	173–178	-1.2	8.6	164	76.7	58.8	7.71	7.73	4.09
Davis	st5SI1	0–20	-3.5	0.4	0.2	2.2	1.25	0.22	4.95	0.60
Davis	st5SI2	20–40	-3.5	4.5	0.7	2.0	1.02	0.18	6.49	0.99
Davis	st5SI3	40–122	-3.2	5.6	1.5	1.7	1.29	0.18	5.32	1.24
Davis	st5SI4	122–132	-2.8	4.2	2.2	2.7	0.85	0.12	2.26	0.12
Davis	st5SI5	132–162	-2.4	4.0	0.6	1.7	1.07	0.11	2.02	0.07
Davis	st5SI6	162–167	-2.0	5.1	11.2	3.7	2.50	0.25	3.45	0.01
Davis	st5SI7	167–172	-1.9		240	273	145	10.3	36.5	1.86
Davis	st6SI1	0–20	-2.7	0.3	0.7	1.7	1.60	0.19	0.11	0.78
Davis	st6SI2	20–40	-2.8	5.9	2.6	3.0	0.47	0.13	4.57	0.78
Davis	st6SI3	40–105	-2.6	4.9	3.0	2.3	0.90	0.15	3.37	0.95
Davis	st6SI4	105–115	-2.3	4.3	1.4	1.6	0.37	0.06	1.12	0.22

Davis	st6SI5	115–145	-2.0	3.5	1.1	1.9	0.38	0.06	1.04	0.10
Davis	st6SI6	145–150	-1.7	3.6	27.7	5.3	2.96	0.15	0.83	0.10
Davis	st6SI7	150–155	-1.6	5.5	190	138	31.8	4.85	5.09	3.09
AAV2	st1SI1	0–12	-1.3	0.5	0.6	104	0.07	0.04	0.50	0.27
AAV2	st1SI2	12–20	-1.4	1.6	0.5	79.4	0.07	0.05	0.40	0.21
AAV2	st1SI3	74–84	-1.0	3.0	1.1	20.5	0.10	0.06	1.10	0.25
AAV2	st1SI4	104–114	-0.6	3.0	0.9	18.6	0.08	0.06	0.20	0.21
AAV2	st1SI5	114–124	-0.4	3.7	1.8	76.2	0.08	0.11	0.50	0.41
AAV2	st1SI6	124–132	-0.4	5.4	51.9	285	0.11	1.72	3.40	1.30
AAV2	st2SI1	0–12	-1.7	0.9	0.9	56.1	0.07	0.05	0.30	0.26
AAV2	st2SI2	12–20	-1.5	2.9	2.6	71.5	0.07	0.08	0.30	0.21
AAV2	st2SI3	74–84	-1.6	3.7	1.7	31.5	0.06	0.04	0.50	0.11
AAV2	st2SI4	104–114	-1.3	2.9	4.0	28.3	0.06	0.03	0.80	0.04
AAV2	st2SI5	118–128	-0.7	3.7	5.0	26.2	0.16	0.05	1.20	0.03
AAV2	st2SI6	128–138	-0.9	4.7	131	218	4.87	0.98	9.20	0.81
AAV2	st3SI1	0–12	-1.3	0.8	5.9	254	0.77	0.01	0.20	0.29
AAV2	st3SI2	16–26	-1.2	1.3	4.2	152	0.08	0.12	0.10	0.14
AAV2	st3SI3	41–51	-1.6	1.6	3.1	41.3	0.08	0.07	0.20	0.20
AAV2	st3SI4	105–115	-0.8	3.0	7.6	35.8	0.14	0.12	1.10	0.22
AAV2	st3SI5	115–125	-0.9	3.0	6.7	47.3	0.16	0.09	2.40	0.16
AAV2	st3SI6	125–135	-0.6	6.6	12.8	39.5	0.17	0.10	2.50	0.19
AAV2	st4SI1	0–14	-1.8	0.4	0.2	27.9	0.13	0.03	0.20	0.09
AAV2	st4SI2	14–23	-1.7	1.4	0.2	25.3	0.06	0.02	<0.01	0.21
AAV2	st4SI3	53–63	-1.1	2.3	0.7	20.6	0.06	0.06	0.60	0.07
AAV2	st4SI4	80–90	-0.7	3.7	0.4	18.7	0.32	0.24	2.70	0.16
AAV2	st4SI5	90–100	-0.7	4.1	8.3	60.5	1.14	1.04	7.20	0.61
AAV2	st4SI6	100–110	-0.5	4.6	128	259	4.74	5.60	16.0	2.50
AAV2	st5SI1	0–14	-1.4	0.4	0.3	19.0	0.13	0.01	0.10	0.19
AAV2	st5SI2	60–70	-1.7	2.6	1.5	39.0	0.08	0.09	1.10	0.17
AAV2	st5SI3	80–90	-1.6	2.9	21.3	206	0.05	0.18	1.90	0.16
AAV2	st5SI4	100–115	-1.5	2.6	22.0	98.7	0.07	0.38	1.10	0.15
AAV2	st5SI5	115–130	-0.9	3.0	48.1	124	0.18	0.62	1.50	0.26
AAV2	st5SI6	200–215	-0.5	3.1	65.7	50.3	0.23	0.22	0.40	0.10
AAV2	st6SI1	0–20	-1.8	2.2	0.8	41.4	0.52	0.17	1.30	0.43
AAV2	st6SI2	60–70	-1.7	5.9	47.2	156	4.42	1.07	1.40	0.40
AAV2	st6SI3	70–86	-1.6	7.2	79.2	171	7.88	1.78	2.70	0.28
AAV2	st6SI4	86–106	-1.6	4.1	95.8	206	7.27	1.29	3.80	0.36
AAV2	st6SI5	106–126	-1.1	3.5	47.7	84.0	9.53	1.07	7.10	0.25
AAV2	st6SI6	126–138.5	-1.1	3.4	34.1	51.8	8.32	0.97	6.30	0.20
AAV2	st6SI7	138.5-151	-1.0	3.4	27.4	38.8	7.17	0.94	3.90	0.18
AAV2	st7SI1	0–10	-1.4	0.7	3.7	92.2	0.31	0.24	3.00	0.10
AAV2	st7SI2	18–28	-1.2	4.1	0.9	30.7	0.12	0.09	2.70	0.09
AAV2	st7SI3	53–66	-1.1	3.7	3.2	66.4	0.15	0.12	2.60	0.10

AAV2	st7SI4	66–76	-1.4	4.5	2.8	37.1	0.09	0.19	2.80	0.14
AAV2	st7SI5	76–86	-1.1	4.5	2.9	38.4	0.09	0.11	1.80	0.11
AAV2	st7SI6	86–96	-1.0	4.5	17.6	101	0.33	0.18	1.80	0.23
AAV2	st8SI1	0–10	-1.5	1.1	0.2	10.4	0.30	0.03	1.80	0.25
AAV2	st8SI2	12–20	-1.4	0.8	0.7	17.0	0.07	0.09	1.40	0.09
AAV2	st8SI3	35–45	-1.4	3.6	1.7	50.1	0.09	0.08	0.70	0.10
AAV2	st8SI4	65–75	-1.6	2.5	1.2	36.6	0.04	0.09	0.30	0.08
AAV2	st8SI5	102–112	-1.4	3.4	5.9	43.8	0.10	0.11	0.90	0.08
AAV2	st8SI6	122–132	-1.1	3.2	4.5	38.9	0.09	0.13	0.70	0.11
AAV2	st8SI7	132–142	-0.9	2.9	12.0	161	0.25	0.36	1.30	0.24
AAV2	st9SI1	0–10	-1.5	1.5	0.3	4.1	0.32	0.02	0.70	0.27
AAV2	st9SI2	25–40	-1.5	10.5	54.9	270	0.22	2.03	15.1	1.13
AAV2	st9SI3	40–50	-1.7	8.4	65.6	156	0.07	0.78	14.7	0.13
AAV2	st9SI4	80–90	-1.6	5.3	6.3	17.7	1.92	0.20	6.10	0.44
AAV2	st9SI5	160–170	-1.7	3.4	4.0	10.1	1.15	0.20	3.10	0.52
AAV2	st9SI6	170–180	-1.7	3.3	5.8	19.8	0.87	0.20	2.20	0.55

Table A2 Bulk sea-ice concentration of dissolved trace metals (nM) for each section of all stations (Sample ID) encountered along the three field campaigns (Voyage).

Voyage	Sample ID	Depth (cm)	Cd (nM)	Mn (nM)	Co (nM)	Ni (nM)	Cu (nM)	Zn (nM)
SIPEX-2	st2SI1	0–9	0.44	2.87	<dl	9.9	4.6	175
SIPEX-2	st2SI2	9–16	0.47	2.44	<dl	22.3	19.7	284
SIPEX-2	st2SI3	16–26	0.83	2.79	<dl	14.7	17.0	543
SIPEX-2	st2SI4	26–33	0.55	1.42	<dl	16.3	16.0	135
SIPEX-2	st2SI5	61–68	0.46	0.47	<dl	10.0	5.7	95.9
SIPEX-2	st2SI6	68–75	0.82	0.67	<dl	10.8	2.4	60.2
SIPEX-2	st3SI1	0–7	1.90	8.70	<dl	7.1	2.4	189
SIPEX-2	st3SI2	7–15	0.67	2.01	<dl	8.0	3.3	228
SIPEX-2	st3SI3	34–41	0.37	1.10	<dl	6.3	1.8	241
SIPEX-2	st3SI4	92–99	0.39	0.60	<dl	2.3	0.3	33.3
SIPEX-2	st3SI5	129–136	0.56	1.56	<dl	4.4	3.6	31.9
SIPEX-2	st3SI6	136–143	1.57	4.63	<dl	5.7	3.0	46.5
SIPEX-2	st4SI1	0–12	0.59	2.75	<dl	533	24.8	79.5
SIPEX-2	st4SI2	12–24	0.43	2.01	<dl	338	26.6	137
SIPEX-2	st4SI3	24–34	0.47	1.61	<dl	111	12.2	39.9
SIPEX-2	st4SI4	34–43.5	0.42	1.04	<dl	200	17.3	46.2
SIPEX-2	st4SI5	75–83	0.29	1.29	<dl	82.2	15.7	82.6
SIPEX-2	st4SI6	83–90	0.34	0.90	<dl	49.1	5.1	32.7

SIPEX-2	st6SI1	0–7	0.43	1.21	<dl	104	12.0	55.6
SIPEX-2	st6SI2	7–14	0.28	0.67	<dl	19.4	5.4	61.0
SIPEX-2	st6SI3	21–28	0.35	0.81	<dl	42.8	7.0	66.6
SIPEX-2	st6SI4	28–35	0.18	0.51	<dl	16.7	4.9	30.4
SIPEX-2	st6SI5	56–63	0.46	1.36	<dl	23.2	14.4	40.2
SIPEX-2	st6SI6	63–72	0.52	0.96	<dl	11.6	3.6	23.5
SIPEX-2	st7SI1	0–7	0.61	3.40	<dl	3.4	2.7	18.2
SIPEX-2	st7SI2	7–14	0.37	1.31	<dl	2.3	1.9	14.1
SIPEX-2	st7SI3	14–21	0.35	1.48	<dl	9.5	6.0	43.7
SIPEX-2	st7SI4	43–50	0.55	1.06	<dl	4.8	2.3	28.4
SIPEX-2	st7SI5	71–77	1.11	3.02	<dl	11.2	7.5	50.9
SIPEX-2	st7SI6	78–85	0.79	2.49	<dl	8.6	7.2	53.8
SIPEX-2	st8SI1	0–7	0.38	1.77	<dl	11.4	4.5	72.2
SIPEX-2	st8SI2	7–14	0.19	1.37	<dl	27.4	12.8	160
SIPEX-2	st8SI3	44–51	0.38	1.43	<dl	13.3	4.4	71.8
SIPEX-2	st8SI4	61–68	0.56	1.62	<dl	10.5	3.8	68.1
SIPEX-2	st8SI5	81–88	0.50	1.95	<dl	24.7	8.9	280
SIPEX-2	st8SI6	88–95	0.61	3.06	<dl	20.8	6.9	313
Davis	st1SI1	0–20	0.19	5.38	0.074	2.2	1.7	37.6
Davis	st1SI2	20–40	0.24	1.89	0.064	2.0	2.8	46.9
Davis	st1SI3	40–130	0.32	1.55	0.044	2.0	1.7	64.2
Davis	st1SI4	130–140	0.24	0.90	0.034	1.5	1.0	20.7
Davis	st1SI5	140–170	0.18	1.03	0.028	1.4	0.9	22.9
Davis	st1SI6	170–175	0.43	2.78	0.063	1.9	1.7	32.1
Davis	st1SI7	175–180	2.77	8.98	0.184	6.1	3.4	44.2
Davis	st2SI1	0–20	0.29	3.46	0.077	2.7	2.2	58.0
Davis	st2SI2	20–40	0.23	2.03	0.059	2.1	1.7	77.1
Davis	st2SI3	40–123	0.29	1.30	0.040	1.9	1.2	47.0
Davis	st2SI4	123–133	0.19	0.62	0.026	1.1	0.7	13.6
Davis	st2SI5	133–163	0.14	0.91	0.037	1.3	1.0	28.4
Davis	st2SI6	163–168	0.23	1.03	0.038	1.3	0.7	20.2
Davis	st2SI7	168–173	2.05	14.1	0.131	7.0	3.7	30.2
Davis	st3SI1	0–20	0.22	2.47	0.083	2.1	1.9	62.3
Davis	st3SI2	20–40	0.27	1.61	0.057	1.9	1.4	43.5
Davis	st3SI3	40–118	0.25	1.47	0.065	1.5	1.1	42.7
Davis	st3SI4	118–128	0.15	2.09	0.053	1.0	1.1	41.3
Davis	st3SI5	128–158	0.07	1.60	0.271	1.4	7.9	41.1
Davis	st3SI6	158–163	0.30	2.29	0.070	2.0	6.5	50.1
Davis	st3SI7	163–168	3.72	23.1	0.287	11.7	19.5	97.6
Davis	st4SI1	0–20	0.20	1.48	0.068	2.0	1.8	62.7
Davis	st4SI2	20–40	0.24	1.79	0.056	1.4	2.2	36.4
Davis	st4SI3	40–128	0.19	2.42	0.051	1.7	1.9	42.9
Davis	st4SI4	128–138	0.06	1.09	0.025	0.6	1.3	37.3

Davis	st4SI5	138–168	0.11	2.50	0.086	2.3	5.2	50.8
Davis	st4SI6	168–173	0.28	2.58	0.071	1.5	3.4	62.6
Davis	st4SI7	173–178	1.88	17.4	0.265	17.3	9.2	28.5
Davis	st5SI1	0–20	0.24	1.43	0.049	1.9	1.6	42.3
Davis	st5SI2	20–40	0.23	1.00	0.029	1.5	1.2	30.8
Davis	st5SI3	40–122	0.20	1.04	0.023	1.1	0.8	26.6
Davis	st5SI4	122–132	0.12	1.18	0.018	0.8	1.3	19.1
Davis	st5SI5	132–162	0.06	0.58	0.019	0.4	1.0	15.3
Davis	st5SI6	162–167	0.32	2.72	0.088	1.7	3.8	51.0
Davis	st5SI7	167–172	3.37	16.8	0.208	8.5	7.0	74.6
Davis	st6SI1	0–20	0.17	1.52	0.031	1.2	0.9	39.3
Davis	st6SI2	20–40	0.22	2.34	0.022	1.2	0.9	32.6
Davis	st6SI3	40–105	0.21	1.09	0.032	1.2	1.1	32.3
Davis	st6SI4	105–115	0.12	0.86	0.018	0.7	0.8	23.1
Davis	st6SI5	115–145	0.07	0.58	0.040	0.6	0.7	12.6
Davis	st6SI6	145–150	0.45	2.73	0.092	2.0	1.3	26.0
Davis	st6SI7	150–155	3.43	30.0	0.369	19.3	8.3	64.1
AAV2	st1SI1	0–12	0.08	1.63	0.060	1.6	1.9	53.0
AAV2	st1SI2	12–20	0.12	1.55	0.021	3.2	2.8	26.0
AAV2	st1SI3	74–84	0.12	0.56	0.018	1.3	2.0	30.0
AAV2	st1SI4	104–114	0.16	0.43	0.013	1.7	8.4	29.1
AAV2	st1SI5	114–124	0.18	0.62	0.010	2.0	3.0	17.0
AAV2	st1SI6	124–132	1.00	1.61	0.017	3.0	5.0	16.7
AAV2	st2SI1	0–12	0.04	1.26	0.030	30.8	3.4	27.9
AAV2	st2SI2	12–20	0.08	2.74	0.112	119	18.7	50.0
AAV2	st2SI3	74–84	0.10	0.90	0.030	49.6	12.0	34.3
AAV2	st2SI4	104–114	0.07	0.31	0.009	11.1	19.3	14.5
AAV2	st2SI5	118–128	0.11	0.36	0.015	10.7	11.8	9.3
AAV2	st2SI6	128–138	0.45	0.82	0.036	7.6	8.5	6.5
AAV2	st3SI1	0–12	0.01	13.4	0.160	25.1	3.1	13.5
AAV2	st3SI2	16–26	0.20	1.95	0.051	32.4	10.7	26.9
AAV2	st3SI3	41–51	0.10	2.61	0.088	29.2	10.4	33.4
AAV2	st3SI4	105–115	0.24	1.45	0.018	5.2	4.3	12.3
AAV2	st3SI5	115–125	0.25	1.51	0.010	2.7	1.8	7.3
AAV2	st3SI6	125–135	0.30	3.53	0.057	8.1	4.3	19.5
AAV2	st4SI1	0–14	0.06	0.99	0.153	28.6	4.6	36.2
AAV2	st4SI2	14–23	0.06	2.14	0.415	28.9	6.8	64.7
AAV2	st4SI3	53–63	0.09	0.58	0.035	14.5	7.4	15.6
AAV2	st4SI4	80–90	0.15	2.53	0.036	4.7	2.3	9.2
AAV2	st4SI5	90–100	0.50	2.09	0.088	7.9	1.8	2.9
AAV2	st4SI6	100–110	2.61	6.84	0.047	5.8	4.1	8.8
AAV2	st5SI1	0–14	0.03	1.75	0.112	6.2	3.2	50.9
AAV2	st5SI2	60–70	0.14	0.80	0.037	3.3	2.5	22.7

AAV2	st5SI3	80–90	0.22	1.39	0.033	4.6	3.7	34.7
AAV2	st5SI4	100–115	0.37	2.52	0.032	5.2	6.2	62.2
AAV2	st5SI5	115–130	0.50	1.93	0.026	2.9	3.3	74.5
AAV2	st5SI6	200–215	0.29	1.08	0.008	1.9	2.4	35.9
AAV2	st6SI1	0–20	0.15	2.50	0.117	2.6	0.9	42.1
AAV2	st6SI2	60–70	0.38	0.62	0.022	2.1	1.8	7.2
AAV2	st6SI3	70–86	1.28	0.41	0.038	4.8	1.5	7.3
AAV2	st6SI4	86–106	1.93	1.60	0.066	3.4	0.9	18.5
AAV2	st6SI5	106–126	0.93	0.62	0.040	2.3	1.1	17.1
AAV2	st6SI6	126–138.5	0.95	1.90	0.060	2.0	0.8	12.4
AAV2	st6SI7	138.5-151	0.95	1.31	0.052	1.4	0.7	15.9
AAV2	st7SI1	0–10	0.36	2.06	0.033	5.5	4.4	23.1
AAV2	st7SI2	18–28	0.13	1.16	0.015	5.1	3.8	14.3
AAV2	st7SI3	53–66	0.10	0.69	0.013	1.5	0.7	2.3
AAV2	st7SI4	66–76	0.13	0.65	0.016	1.9	1.3	3.2
AAV2	st7SI5	76–86	0.12	0.68	0.014	1.6	2.0	6.3
AAV2	st7SI6	86–96	0.17	0.93	0.016	2.8	4.0	5.7
AAV2	st8SI1	0–10	0.03	0.81	0.014	2.8	0.7	39.9
AAV2	st8SI2	12–20	0.19	0.94	0.025	4.1	0.6	21.3
AAV2	st8SI3	35–45	0.16	0.65	0.018	3.5	2.7	19.4
AAV2	st8SI4	65–75	0.17	0.66	0.017	4.5	3.4	38.8
AAV2	st8SI5	102–112	0.12	0.78	0.009	9.4	2.8	8.9
AAV2	st8SI6	122–132	0.12	0.93	0.031	3.9	5.1	16.2
AAV2	st8SI7	132–142	0.26	1.83	0.009	3.8	1.5	6.7
AAV2	st9SI1	0–10	0.04	2.54	0.029	32.8	1.5	79.0
AAV2	st9SI2	25–40	0.64	2.22	0.029	16.9	1.5	16.7
AAV2	st9SI3	40–50	1.19	2.31	0.035	5.6	1.6	20.6
AAV2	st9SI4	80–90	0.13	1.17	0.013	2.7	1.3	34.1
AAV2	st9SI5	160–170	0.24	0.77	0.006	2.7	3.1	15.7
AAV2	st9SI6	170–180	0.46	1.20	0.011	2.4	3.4	17.5

Table A3. Bulk sea-ice concentration of particulate trace metals for each section of all stations (Sample ID) encountered along the three field campaigns (Voyage).

Voyage	Sample ID	Depth (cm)	Cd (nM)	Al (nM)	Mn (nM)	Co (nM)	Ni (nM)	Cu (nM)	Zn (nM)
SIPEX-2	st2SI1	0–9	0.021	196	3.78	0.232	9.24	1.56	20.3
SIPEX-2	st2SI2	9–16	0.028	68.6	2.27	0.195	4.80	2.31	25.8
SIPEX-2	st2SI3	16–26	0.009	87.0	2.23	0.157	5.47	1.76	18.7
SIPEX-2	st2SI4	26–33	0.005	10.9	1.04	0.060	2.47	0.83	12.5

SIPEX-2	st2SI5	61–68	0.009	34.5	1.53	0.108	4.29	1.27	32.2
SIPEX-2	st2SI6	68–75	0.041	52.6	2.57	0.122	4.15	2.30	136
SIPEX-2	st3SI1	0–7	0.004	116	0.49	0.028	2.09	3.53	3.07
SIPEX-2	st3SI2	7–15	0.001	44.3	0.28	0.016	1.92	1.23	1.96
SIPEX-2	st3SI3	34–41	0.001	67.3	0.39	0.047	195	2.89	8.37
SIPEX-2	st3SI4	92–99	0.000	185	1.09	0.029	1.06	1.34	0.48
SIPEX-2	st3SI5	129–136	0.003	25.3	0.38	0.020	2.57	6.49	2.19
SIPEX-2	st3SI6	136–143	0.002	109	0.37	0.020	1.41	1.02	4.65
SIPEX-2	st4SI1	0–12	0.003	75.3	0.60	0.029	14.0	21.3	19.3
SIPEX-2	st4SI2	12–24	0.010	93.3	1.30	0.073	42.3	70.4	48.3
SIPEX-2	st4SI3	24–34	0.011	43.0	0.51	0.026	10.1	8.30	9.97
SIPEX-2	st4SI4	34–43.5	0.000	0.0	<0.01	<0.001	0.01	0.01	0.01
SIPEX-2	st4SI5	75–83	0.004	36.1	0.14	0.009	5.84	10.7	7.00
SIPEX-2	st4SI6	83–90	0.003	61.5	0.18	0.011	3.29	7.32	7.00
SIPEX-2	st6SI1	0–7	0.019	57.5	1.08	0.065	6.69	0.80	24.1
SIPEX-2	st6SI2	7–14	0.003	47.8	0.25	0.020	1.99	0.96	9.02
SIPEX-2	st6SI3	21–28	0.002	21.8	0.20	0.013	1.99	2.27	14.5
SIPEX-2	st6SI4	28–35	0.005	14.4	0.11	0.010	0.94	0.43	10.6
SIPEX-2	st6SI5	56–63	0.009	18.7	0.18	0.011	1.05	1.60	9.78
SIPEX-2	st6SI6	63–72	0.253	10.8	0.70	0.087	5.78	5.42	133
SIPEX-2	st7SI1	0–7	0.004	78.3	0.35	0.021	1.27	1.00	2.56
SIPEX-2	st7SI2	7–14	0.007	47.4	0.34	0.031	3.33	1.95	5.08
SIPEX-2	st7SI3	14–21	0.006	90.6	0.39	0.032	1.51	3.09	18.0
SIPEX-2	st7SI4	43–50	0.017	181	1.18	0.077	2.25	6.30	10.4
SIPEX-2	st7SI5	71–77	0.046	213	3.92	0.326	8.01	31.5	52.6
SIPEX-2	st7SI6	78–85	0.028	286	4.44	0.335	7.28	37.7	54.0
SIPEX-2	st8SI1	0–7	0.003	66.6	0.51	0.023	1.15	1.07	2.72
SIPEX-2	st8SI2	7–14	0.002	125	0.70	0.037	27.1	15.2	12.4
SIPEX-2	st8SI3	44–51	0.019	609	5.11	0.141	4.77	9.69	114
SIPEX-2	st8SI4	61–68	0.035	406	2.77	0.116	8.26	7.50	130
SIPEX-2	st8SI5	81–88	0.007	184	0.98	0.054	6.91	8.66	90.8
SIPEX-2	st8SI6	88–95	0.010	405	1.57	0.060	4.35	10.8	158
Davis	st1SI1	0–20	<dl	11.2	0.05	0.491	0.02	<dl	<dl
Davis	st1SI2	20–40	<dl	12.4	0.04	1.18	0.05	<dl	<dl
Davis	st1SI3	40–130	<dl	12.6	0.07	0.074	0.09	<dl	<dl
Davis	st1SI4	130–140	<dl	5.4	0.01	0.101	0.02	<dl	<dl
Davis	st1SI5	140–170	<dl	7.3	0.03	0.033	<dl	<dl	<dl
Davis	st1SI6	170–175	0.004	23.2	0.11	0.494	0.07	0.04	<dl
Davis	st1SI7	175–180	0.023	46.9	0.26	0.863	0.24	0.20	<dl
Davis	st2SI1	0–20	<dl	281	1.47	2.74	0.48	0.20	<dl
Davis	st2SI2	20–40	0.008	37.1	0.15	1.08	0.11	0.06	<dl
Davis	st2SI3	40–123	<dl	27.3	0.17	0.304	0.09	0.06	<dl
Davis	st2SI4	123–133	<dl	8.2	0.04	0.426	0.02	<dl	<dl

Davis	st2SI5	133–163	<dl	32.4	0.12	0.674	0.46	0.03	<dl
Davis	st2SI6	163–168	<dl	32.3	0.12	1.37	0.10	0.07	<dl
Davis	st2SI7	168–173	0.150	119	0.54	4.46	1.01	1.11	10.3
Davis	st3SI1	0–20	<dl	28.4	0.09	0.416	0.04	0.10	<dl
Davis	st3SI2	20–40	0.008	54.0	0.12	0.718	0.32	0.25	<dl
Davis	st3SI3	40–118	<dl	3.0	0.01	0.016	0.02	<dl	<dl
Davis	st3SI4	118–128	<dl	8.3	0.04	0.138	0.04	0.03	<dl
Davis	st3SI5	128–158	<dl	106	0.12	1.47	0.07	0.36	<dl
Davis	st3SI6	158–163	<dl	578	0.43	1.93	0.19	3.88	2.83
Davis	st3SI7	163–168	0.068	724	0.61	0.777	0.46	5.90	7.54
Davis	st4SI1	0–20	0.007	351	1.38	3.17	0.40	0.47	3.35
Davis	st4SI2	20–40	0.070	1060	0.57	4.76	0.30	2.07	15.7
Davis	st4SI3	40–128	0.019	210	0.20	0.191	0.18	0.38	2.37
Davis	st4SI4	128–138	0.010	869	0.51	3.35	0.30	1.38	7.21
Davis	st4SI5	138–168	<dl	45.7	0.09	0.224	0.04	0.05	<dl
Davis	st4SI6	168–173	0.025	281	0.46	0.682	0.26	0.66	8.51
Davis	st4SI7	173–178	2.528	2490	15.6	6.62	7.46	14.2	168
Davis	st5SI1	0–20	0.006	134	0.32	0.896	0.27	0.21	<dl
Davis	st5SI2	20–40	0.041	235	0.29	1.60	0.35	0.49	6.58
Davis	st5SI3	40–122	0.022	68.2	0.12	0.162	0.10	0.14	<dl
Davis	st5SI4	122–132	<dl	465	0.33	0.598	0.18	0.92	6.83
Davis	st5SI5	132–162	<dl	14.3	0.04	0.022	<dl	<dl	<dl
Davis	st5SI6	162–167	0.017	1860	0.99	3.47	0.48	4.89	19.8
Davis	st5SI7	167–172	0.572	2010	1.29	1.53	1.33	5.45	53.5
Davis	st6SI1	0–20	0.051	147	0.48	1.04	0.19	0.15	6.38
Davis	st6SI2	20–40	0.025	162	0.29	1.64	0.17	0.32	7.03
Davis	st6SI3	40–105	0.016	121	0.14	0.099	0.11	0.26	<dl
Davis	st6SI4	105–115	<dl	49.0	0.06	0.328	0.06	0.08	<dl
Davis	st6SI5	115–145	<dl	26.0	0.04	0.118	0.02	0.04	<dl
Davis	st6SI6	145–150	0.037	165	0.35	1.31	0.40	0.85	10.3
Davis	st6SI7	150–155	1.320	1020	1.94	2.67	4.95	10.4	117
AAV2	st1SI1	0–12	0.019	566	3.55	0.077	1.37	0.82	2.49
AAV2	st1SI2	12–20	0.009	40.6	0.33	0.013	1.17	0.93	<dl
AAV2	st1SI3	74–84	0.044	279	2.24	0.041	2.03	0.69	13.3
AAV2	st1SI4	104–114	0.027	695	4.26	0.066	1.28	3.27	3.02
AAV2	st1SI5	114–124	0.044	115	0.80	0.018	0.75	0.83	<dl
AAV2	st1SI6	124–132	0.203	256	3.66	0.047	1.54	1.09	14.8
AAV2	st2SI1	0–12	0.003	88.5	0.55	0.014	0.81	0.95	<dl
AAV2	st2SI2	12–20	0.025	44.7	0.46	0.019	3.02	3.91	2.08
AAV2	st2SI3	74–84	0.012	129	1.06	0.027	4.94	4.48	2.15
AAV2	st2SI4	104–114	0.006	83.6	0.88	0.016	2.04	3.23	<dl
AAV2	st2SI5	118–128	0.022	180	1.28	0.024	3.03	2.19	5.38
AAV2	st2SI6	128–138	0.133	49.5	0.83	0.015	1.38	1.19	4.80

AAV2	st3SI1	0–12	0.001	19.7	1.19	0.004	0.57	0.13	<dl
AAV2	st3SI2	16–26	0.036	27.4	0.38	0.014	1.87	3.50	2.87
AAV2	st3SI3	41–51	0.015	22.5	0.24	0.008	1.39	1.72	1.88
AAV2	st3SI4	105–115	0.027	6.1	0.08	0.005	0.67	0.71	<dl
AAV2	st3SI5	115–125	0.032	3.5	0.08	0.003	0.28	0.29	<dl
AAV2	st3SI6	125–135	0.021	7.2	0.13	0.008	0.73	0.68	<dl
AAV2	st4SI1	0–14	0.002	204	1.20	0.120	0.75	1.26	<dl
AAV2	st4SI2	14–23	0.008	556	3.39	0.303	1.66	2.60	2.43
AAV2	st4SI3	53–63	0.017	234	1.47	0.026	0.35	0.75	<dl
AAV2	st4SI4	80–90	0.054	6280	41.8	0.625	1.39	1.76	9.32
AAV2	st4SI5	90–100	0.478	16300	91.9	1.46	4.23	2.49	31.2
AAV2	st4SI6	100–110	2.768	13100	113	1.65	6.15	4.25	73.4
AAV2	st5SI1	0–14	0.001	94.7	0.47	0.360	0.51	0.57	<dl
AAV2	st5SI2	60–70	0.024	231	0.79	0.030	0.68	0.96	<dl
AAV2	st5SI3	80–90	0.017	297	1.25	0.041	0.99	2.34	1.76
AAV2	st5SI4	100–115	0.034	344	1.54	0.061	8.46	2.97	3.29
AAV2	st5SI5	115–130	0.035	277	1.68	0.093	1.90	7.44	10.2
AAV2	st5SI6	200–215	0.031	33.7	0.16	0.007	0.81	0.55	1.28
AAV2	st6SI1	0–20	0.018	53.6	0.38	0.032	0.89	0.32	1.71
AAV2	st6SI2	60–70	0.438	367	2.81	1.90	1.65	1.15	25.6
AAV2	st6SI3	70–86	1.780	190	1.20	0.632	2.87	1.00	22.3
AAV2	st6SI4	86–106							
AAV2	st6SI5	106–126	0.394	146	0.67	0.477	0.72	0.62	9.41
AAV2	st6SI6	126–138.5	0.276	281	1.17	2.36	0.61	0.72	6.29
AAV2	st6SI7	138.5-151	0.127	40.6	0.50	0.206	4.04	0.45	3.11
AAV2	st7SI1	0–10	0.088	41.5	0.67	0.185	1.28	1.04	1.57
AAV2	st7SI2	18–28	0.022	16.2	0.23	0.006	0.32	0.75	<dl
AAV2	st7SI3	53–66	0.023	70.9	0.38	0.012	0.17	0.13	<dl
AAV2	st7SI4	66–76	0.059	115	0.79	0.021	0.41	0.26	2.48
AAV2	st7SI5	76–86	0.031	17.0	0.21	0.005	0.22	0.38	<dl
AAV2	st7SI6	86–96	0.070	43.5	0.39	0.011	0.67	1.22	2.78
AAV2	st8SI1	0–10	0.001	28.6	0.46	0.030	0.84	0.11	dl
AAV2	st8SI2	12–20	0.059	27.7	0.28	0.047	0.38	0.15	1.43
AAV2	st8SI3	35–45	0.027	32.0	0.25	0.011	0.47	0.52	<dl
AAV2	st8SI4	65–75	0.031	67.4	0.74	0.035	3.25	1.74	2.18
AAV2	st8SI5	102–112	0.046	425	2.20	0.054	1.07	1.55	3.73
AAV2	st8SI6	122–132	0.026	262	1.79	0.045	1.11	1.51	6.38
AAV2	st8SI7	132–142	0.066	1170	10.2	0.224	1.05	1.06	5.17

CHAPTER 5. GENERAL DISCUSSION AND FUTURE PERSPECTIVE

Key Points:

- The availability of inorganic silicon and nitrogen potentially controls sea-ice algae growth during spring and summer, respectively.
- A decoupling between macro and micronutrient dynamics ensures sea-ice primary production continues until macronutrient availability starts to impose sea-ice algae growth limitations.
- Future changes in sea-ice thermodynamics and physical processes are expected to impact the pace and timing of the bloom season.

5.1 Macronutrient distribution in spring and summer sea ice

In chapter 2 we reported high concentrations of sea-ice algae biomass found at the bottom of Davis fast ice during late spring. There, bottom communities receive enough irradiance, with low variability in temperature and salinity, and easy access to macronutrients from the shallow seawater below. Sea-ice macronutrients at concentrations above salinity-predicted levels for nitrate, nitrite, phosphate and ammonium but depleted in silicic acid suggest nutrient accumulation potentially fueled by remineralization processes and the dominance of diatoms. While silicic acid availability might control productivity in late-spring fast ice (Chapter 2; Lim et al., 2019), this scenario appears to change during summer. The high demand and continued consumption of silicic acid by diatoms during spring would drive a community shift during summer, potentially sustained by flagellates. This shift would explain the stronger nitrate than silicic acid depletion observed in both fast and pack ice during mid-summer (AAV2; Chapter 3). Our AAV2 summer sea-ice expedition also points to a critical stage in the sea-ice decay when inorganic nitrogen sources (i.e. nitrate, nitrite and ammonium) became exhausted, potentially to levels limiting autotrophic activity. Ammonium would be consumed shortly after being produced leading to the observed low concentrations of this N-source, despite evidence of high heterotrophic activity. During summer, enhanced ice melting exacerbates stratification within the ice, preventing convection-driven exchanges between brine and seawater, and

therefore hindering the replenishment of nutrients from seawater. Therefore, sea-ice algal communities would be particularly dependent on the microbial loop or other non-biological processes such as sea-ice-seawater interface exchanges, dynamic processes such as rafting, and sea-ice flooding as a way to obtain substrate for their survival in late summer.

5.2 Sea ice as a source of dissolved and particulate Fe

In this work, we explored the factors that influence the stocks and vertical distribution of DFe and PFe in both land-fast and pack ice across different locations and seasons. Chapter 2 emphasized the major importance of sediment resuspension as a source of DFe to the total Fe pool in fast ice during the Davis time series. It was shown that, if light and other nutrients are available, the fertilization potential of sediments to fast ice due to the enrichment of DFe could alone be responsible for 85% of the daily carbon production in Antarctic shelf waters (Arrigo et al., 2008; Chapter 2). The abundance of bioavailable DFe in fast ice combined with the extended light exposure at higher latitudes is reflected in the high biomass accumulation commonly observed in fast ice. Chapter 3 on the other hand showed that during summer background DFe levels (~3 nM) can be sustained by the mobilization of the PFe built-up during previous seasons and heterotrophic activity. We also reported higher concentrations of DFe (~7 nM) near the MUIS, likely associated with the presence of platelet ice.

The data also showed that sea ice bears a considerable amount of Fe in the particulate fraction, both biogenic and lithogenic. Windblown lithogenic Fe dominates over sedimentary sources along East Antarctica's coast due to its narrow continental shelf and lower sedimentary inputs compared to other areas such as the Ross Sea (de Jong et al., 2013). Chapter 2 highlighted the influence of continental dust to the total sea-ice PFe pool at Davis. We investigated the potential role of this source in supplying a continuous input of bioavailable soluble Fe through direct dissolution, potentially aided by a weakly acidic snow (pH ~6). This atmospheric source could be particularly important for sea-ice communities due to the rapid loss of DFe when sea ice melts in spring. Indeed, the Davis time series showed that the sea-ice thermodynamic processes, specifically changes in the ice temperature, were the major drivers of DFe transport from the upper ice layers to the bottom ice and ultimately the water column.

Chapter 3 provided new insights into the potential relationship between glacial meltwater discharge and the occurrence of PFe-rich platelet sea ice forming in the vicinity of the MUIS.

The potential fertilization of glacial ice has already been described previously (Herraiz-Borreguero et al., 2016 and references therein). Here, we brought new evidence that sea ice can play an important role by assuring this source of Fe is not lost from the pelagic system. By storing highly weathered glaciogenic material from nearby glacial systems, sea ice could potentially enhance Fe bioavailability by augmenting redox and dissolution reactions via thawing and refreezing processes (Jeong et al., 2012, 2015; Kim et al., 2010; Raiswell et al., 2018) and stabilization through organic (e.g. EPS – Fe) complexation (Genovese et al., 2018).

Whether both dust and ice shelf waters represent an important source of bioavailable Fe to phytoplankton needs further investigation. First, a spatial determination of the presence and influence of both sources is needed. In the case of continental wind-blown dust, an initial step would be achieved by constraining ice-free areas and evaluating the extent to which wind can transport Fe-rich dust. Remote sensing imagery as well as *in situ* sampling along north-south transects would complement each other for this purpose. In order to establish areas of platelet ice occurrence around major glacial systems, the deployment of remotely operated vehicles combined with optical sensors could increase observational capabilities, optimizing time and broadening the area to be assessed. Results could be then compared to available oceanographic and physical data from major glacier systems to estimate the sea-ice PFe inventory from glacial sources. In an opposite direction, the determination of the distribution of platelet ice could also prove valuable to physical oceanographers as a proxy of ice shelf dynamics as well as sub-ice cavity oceanic circulation. A second step would be evaluating the speciation and bioavailability of these sources of particles. Leaching experiments could be a cost-effective way to assess the solubility of different species of PFe under changeable physicochemical conditions. A further move would be the investigation of the main Fe species present in the snow and platelet PFe. For this purpose, spectroscopy has proved efficient to assess the abundance, morphology and valence state of PFe. Ultimately, the importance of these sources to Antarctica primary productivity will depend on a broader assessment of the likelihood of ice floes to move into Fe-limited waters.

Finally, biogenic PFe was estimated in Chapters 2 and 3. While fast ice is clearly dominated by lithogenic Fe supplied from coastal sources, pack ice is more dependent on the initial load and recycling of organic matter as the main source of Fe. The accumulation of organic matter would also favour bacterial activity and remineralization of biogenic PFe into DFe, which in turn could be stabilized by the abundance of organic ligands, particularly EPS, in the sea ice.

Therefore, recycling of the biogenic PFe can replenish sea ice with DFe, potentially extending autotrophic activity until macronutrient availability starts to impose growth limitations. As sea ice continues to melt, pelagic systems would also benefit from this input of a labile form of Fe. Closing the Fe budget could be obtained with the analysis of the contribution of the PFe pool to the DFe stock in autumn.

5.3 How EPS controls the incorporation, bioavailability and toxicity of TMs?

Research on Fe limitation in HNLC waters has spawned the awareness of the potential for other metals to limit primary production. Chapter 4 showed that sea ice is enriched in trace metals relatively to values reported for the SO surface waters. Although our results are not conclusive regarding the discriminative character of this enrichment, they suggest a preferential incorporation of some metals (Zn, Cu and Ni) at the expense of others (Co, Mn and Cd). The environmental conditions are extremely different in sea ice compared to seawater; therefore, one should expect metal speciation to also vary greatly between sea ice and seawater. Laboratory-based sea-ice growth experiments are a relatively cheap, fast and efficient way to test TMs incorporation mechanisms (Janssen et al., 2018; Kuiper et al., 2003). The design of similar experiments to evaluate the role of EPS and other naturally occurring ligands in the incorporation of TMs under controlled physical, chemical and biological conditions is encouraged.

Based on results from Chapter 4, Co and Mn are the two essential micronutrients that could potentially limit primary productivity in sea ice. The complex redox, speciation and uptake mechanism of both Co and Mn makes the assessment of their bioavailability in sea ice difficult. Eukaryotic microorganisms cannot synthetize vitamin B12 and depend on external sources to meet their demand (Bertrand et al., 2015). The availability of vitamin B12 to sea-ice algae is therefore directly controlled by the amount of this compound either incorporated into sea ice during its formation or produced *in situ* by bacteria as well as the availability of Co for its production. Ultimately, vitamin B12 production is indirectly controlled by the availability of any other substrate (macro or micronutrient) that might limit sea-ice algae, which is the main organic source for those producers to grow. Whether vitamin B12 production keeps pace with microalgae demand during different sea-ice stages remains to be demonstrated empirically. Therefore, measurements of vitamin B12 should be part of the suite of biogeochemical

parameters routinely measured in sea-ice surveys. For this purpose, HPLC or the cheaper classic bioassay method for vitamin B12 determination are available.

While Mn was not exhausted in summer sea-ice measurements, the influence of high levels of Cu and Zn in the Mn uptake has not yet been assessed. A quantitative and better qualitative characterization of sea-ice EPS and other potential ligands is needed. This would enable us to estimate the free ion activity of each metal as well as the potentially binding strength with their respective complexes. The next step would be testing the availability of these complexes to sea-ice algae. Specifically, incubation experiments designed to identify the key chemical (redox and organic complexation) and biological (remineralization) variables which control sea-ice trace metals bioavailability are mandatory. New approaches such as artificial sea-ice growth experiments where physical, chemical and biological variables can be controlled could help us to untangle and identify key processes involved in the recycling of trace metals in the sea ice. They could be run in parallel to attempts in sea-ice models. Further field sampling efforts are also encouraged to enlarge the present databases, if possible, prioritizing under-sampled sectors of Antarctica for a wider spatial resolution. These approaches will be valuable to enlarge our understanding of sea-ice biogeochemical processes.

5.4 Biogeochemistry of sea-ice macro and micronutrients in a warming planet

5.4.1 Macronutrients

Sea ice is tightly coupled to the underlying seawater and nutrient concentrations in sea ice are strongly controlled by brine circulation and exchange with seawater (Lannuzel et al., 2020). Any change in these processes could have a dramatic impact on the dynamics of macronutrients. It is not completely clear how snow accumulation rates in the Antarctic sea-ice zone will respond to future atmospheric concentrations of CO_2. The best available simulations suggest an increased transport of warmer and moister air following a net increase in snow accumulation over the sea ice of between 10 – 40% (Budd & Simmonds, 1991). Higher snow precipitation is expected to 1) increase rates of sea-ice flooding (Fischer & Lemke, 1994), and due to the thermal insulating properties of snow 2) decrease ice growth in favour of snow ice formation (Eicken et al., 1994), and 3) increase dramatically sea-ice temperature and brine volume (Eicken et al., 2017). Increased permeability and sea-ice flooding due to a thicker snowpack could offer a fresh supply of nutrients from seawater to sea ice. Higher brine volumes

also significantly reduced the ice strength (Eicken et al., 2017), which in turn could potentially enhance dynamic processes and nutrient replenishment. A gap layer observed in summer pack ice (station SR3-5 during AAV2) did exhibit particularly high macronutrient concentrations. Similarly, enhanced nutrient supply in the periphery of ice floes, ridges, and cracks could also alleviate limitations under a warmer sea-ice condition. This effect might be particularly important during summer when levels of nitrate can be significantly lowered (Duprat et al., 2020).

In the oppose direction, higher snow deposition during the early stages of sea ice might also lead to lower snow accumulation in summer since sea-ice warming increases the chances of lead formation, which in association with katabatic winds, are a major sink of snow in Antarctica (Webster et al., 2018). This scenario would reduce rates of sea-ice flooding during summer, rendering sea-ice algae even more dependent on sea ice – seawater interface exchanges and intrusions as a way of obtaining new stocks of macronutrients. This negative effect could be further intensified by a stronger brine and surface water stratification (Vancoppenolle et al., 2013). As light availability and surface water stratification increase, macronutrients could become increasingly limiting for sympagic production in the late season.

5.4.2 Micronutrients

How foreseen changes in Antarctic sea-ice properties, snow and dust deposition, biota, and surface ocean nutrients inventories will impact the sea-ice biogeochemistry and productivity is uncertain. An increase in snow accumulation during early seasons is expected to decrease sea-ice ice growth in favour of snow ice due to the snow insulating properties (Eicken et al., 1994). A thinner and warmer layer of sea ice could represent not only lower inventories of micronutrients within the ice but also a faster meltwater pulse and flushing to the water column via gravity drainage. Besides, since sea ice is enriched in micronutrients relative to seawater, any changes in the sea ice properties (e.g., permeability) and dynamics (e.g., cracks) that increase exchanges with the seawater would have a deleterious impact on the sea-ice micronutrient pool.

On the other hand, an expected increase in ice-free grounds in Antarctica (Lee et al., 2017) associated with stronger katabatic winds (Turner et al., 2009) could provide an additional input of dust and associated trace metals to sea ice. Likewise, glacial meltwater has a significant

impact on the levels of trace metals, particularly Fe, in Antarctic coastal seawater (Kim et al., 2015) and sea ice (Duprat et al., 2020). Other processes such as biological assimilation and remineralization also need to be accounted for. For example, thinner and warmer sea ice should support a greater degree of heterotrophic activity and remineralization. Greater channel connectivity and space should also facilitate the grazing of bacteria by bacterivorous protists, therefore, increasing rates of nutrient recycling (Lannuzel et al., 2020). All these processes could offset losses of micronutrients by brine flushing. The net effect of these interweaved processes on the final micronutrient availability in sea ice is unknown.

5.4.3 Future perspectives

Modelling of macro- and micronutrient dynamics for spring and summer sea ice under future projections of atmospheric warming could help us to assess the weight of each of the processes discussed above on the final nutrient availability in sea ice. A broader assessment and follow-up of sea-ice dynamics via remote sensing and continued fieldwork would complement modelling efforts. Outputs on nutrients availability could finally be coupled with other limiting resources in future models, such as projected changes in light irradiation and sea-ice liveable space to draw a more accurate scenario on future sea-ice algal biomass, perennity, and vertical distribution.

Lastly, the final fertilization potential of Antarctic sea ice to open waters will also greatly depend on a better assessment of changes Fe and other micronutrients undergo in the surface microlayer and subsurface water. Tovar-Sánchez et al. (2019) showed a clear decline in metal levels from sea ice to the top meter of the polar ocean surface water, suggesting that, when released, scavenging and/or biotic uptake dominate over remineralization and dissolution. Besides, the nutritional and/or toxic effect of trace elements on phytoplankton might also suffer significant changes due to variations in the metal's stoichiometry from sea ice to the microlayer and the subsurface water. Any future change in the residence time of different bioactive metals in the surface microlayer and water column below, such as those driven by sea salt aerosols and organic matter production, should impact phytoplankton production and dynamics (Tovar-Sánchez et al., 2019).

5.5 References

Arrigo, K. R., van Dijken, G. L., & Bushinsky, S. (2008). Primary production in the Southern Ocean, 1997-2006. *Journal of Geophysical Research-Oceans, 113*(C8). doi:Artn C0800410.1029/2007jc004551

Budd, W. F., & Simmonds, I. (1991, 11-15 Jun 1990). *The impact of global warming on the Antarctic mass balance and global sea level.* Paper presented at the International conference on the role of the polar regions in global change: Proceedings., Alaska Univ., Fairbanks, Alaska, US.

de Jong, J., Schoemann, V., Maricq, N., Mattielli, N., Langhorne, P., Haskell, T., & Tison, J.-L. (2013). Iron in land-fast sea ice of McMurdo Sound derived from sediment resuspension and wind-blown dust attributes to primary productivity in the Ross Sea, Antarctica. *Marine Chemistry, 157*, 24-40. doi:10.1016/j.marchem.2013.07.001

Duprat, L., Kanna, N., Janssens, J., Roukaerts, A., Deman, F., Townsend, A. T. et al. (2019). Enhanced Iron Flux to Antarctic Sea Ice via Dust Deposition From Ice-Free Coastal Areas. *Journal of Geophysical Research: Oceans*. doi:10.1029/2019jc015221

Duprat, L., Corkill, M., Genovese, C., Moreau, S., Townsen, A., Meiners, K., & Lannuzel, D. (2020). Nutrient distribution in East Antarctic summer sea ice: a potential Iron contribution from glacial basal melt. *Journal of Geophys Research-Oceans*.

Eicken, H., Fischer, H., & Lemke, P. (2017). Effects of the snow cover on Antarctic sea ice and potential modulation of its response to climate change. *Annals of Glaciology, 21*, 369-376. doi:10.3189/s0260305500016086

Eicken, H., Lange, M. A., & Wadhams, P. (1994). Characteristics and distribution patterns of snow and meteoric ice in the Weddell Sea and their contribution to the mass balance of sea ice. *Annales Geophysicae, 12*(1), 80-93. doi:10.1007/s00585-994-0080-x

Genovese, C., Grotti, M., Pittaluga, J., Ardini, F., Janssens, J., Wuttig, K. et al. (2018). Influence of organic complexation on dissolved iron distribution in East Antarctic pack ice. *Marine Chemistry, 203*, 28-37. doi:10.1016/j.marchem.2018.04.005

Herraiz-Borreguero, L., Lannuzel, D., van der Merwe, P., Treverrow, A., & Pedro, J. B. (2016). Large flux of iron from the Amery Ice Shelf marine ice to Prydz Bay, East Antarctica. *Journal of Geophysical Research-Oceans, 121*(8), 6009-6020. doi:10.1002/2016jc011687

Janssens, J., Meiners, K. M., Townsend, A. T., & Lannuzel, D. (2018). Organic Matter Controls of Iron Incorporation in Growing Sea Ice. *Frontiers in Earth Science, 6*. doi:UNSP 2210.3389/feart.2018.00022

Jeong, D., Kim, K., & Choi, W. (2012). Accelerated dissolution of iron oxides in ice. *Atmospheric Chemistry and Physics, 12*(22), 11125-11133. doi:10.5194/acp-12-11125-2012

Jeong, D., Kim, K., Min, D. W., & Choi, W. (2015). Freezing-Enhanced Dissolution of Iron Oxides: Effects of Inorganic Acid Anions. *Environmental Science and Technolology, 49*(21), 12816-12822. doi:10.1021/acs.est.5b04211

Kim, I., Kim, S., & Kim, G. (2010). Analytical Artifacts Associated with the Chelating Resin Extraction of Dissolved Rare Earth Elements in Natural Water Samples. *Aquatic Geochemistry, 16*(4), 611-620. doi:10.1007/s10498-010-9100-5

Kim, I., G. Kim & E. J. Choy (2015). The significant inputs of trace elements and rare earth elements from melting glaciers in Antarctic coastal waters. *Polar Research,* 34(1). https://doi.org/10.3402/polar.v34.24289

Kuiper, M. J., Lankin, C., Gauthier, S. Y., Walker, V. K., & Davies, P. L. (2003). Purification of antifreeze proteins by adsorption to ice. *Biochemical and Biophysical Research Communications, 300*(3), 645-648. doi:10.1016/s0006-291x(02)02900-5

Lannuzel, D., Tedesco, L., van Leeuwe, M., Campbell, K., Flores, H., Delille, B. et al. (2020). The future of Arctic sea-ice biogeochemistry and ice-associated ecosystems. *Nature Climate Change, 10*(11), 983-992. doi:10.1038/s41558-020-00940-4

Lee, J. R., Raymond, B., Bracegirdle, T. J., Chades, I., Fuller, R. A., Shaw, J. D., & Terauds, A. (2017). Climate change drives expansion of Antarctic ice-free habitat. *Nature, 547*(7661), 49-54. doi:10.1038/nature22996

Raiswell, R., Hawkings, J., Elsenousy, A., Death, R., Tranter, M., & Wadham, J. (2018). Iron in Glacial Systems: Speciation, Reactivity, Freezing Behavior, and Alteration During Transport. *Frontiers in Earth Science, 6*. doi:10.3389/feart.2018.00222

Saenz, B. T., & Arrigo, K. R. (2014). Annual primary production in Antarctic sea ice during 2005-2006 from a sea ice state estimate. *Journal of Geophysical Research-Oceans, 119*(6), 3645-3678. doi:10.1002/2013jc009677

Tovar-Sanchez, A., Gonzalez-Ortegon, E. & Duarte, C. M. (2019). Trace metal partitioning in the top meter of the ocean. *Science of the Total Environment*, 652, 907-914. doi:10.1016/j.scitotenv.2018.10.315

Turner, J., Chenoli, S. N., abu Samah, A., Marshall, G., Phillips, T., & Orr, A. (2009). Strong wind events in the Antarctic. *Journal of Geophysical Research, 114*(D18). doi:10.1029/2008jd011642

Vancoppenolle, M., Meiners, K. M., Michel, C., Bopp, L., Brabant, F., Carnat, G. et al. (2013). Role of sea ice in global biogeochemical cycles: emerging views and challenges. *Quaternary Science Reviews, 79*, 207-230

Webster, M., Gerland, S., Holland, M., Hunke, E., Kwok, R., Lecomte, O. et al. (2018). Snow in the changing sea-ice systems. *Nature Climate Change, 8*(11), 946-953. doi:10.1038/s41558-018-0286-7